HELMHOLTZ
Centre for Environmental Research

PHD DISSERTATION 8 | 2021

Katharina Halbach

Fate of xenobiotics inside the zebrafish embryo – mass spectrometry imaging for toxicokinetic studies

Katharina Halbach | Fate of xenobiotics inside the zebrafish embryo – mass spectrometry ...

PHD DISSERTATION 8 | 2021
Helmholtz Centre for Environmental Research – UFZ
Department of Analytical Chemistry

Fate of xenobiotics inside the zebrafish embryo – mass spectrometry imaging for toxicokinetic studies

Von der Fakultät für Chemie und Mineralogie

der Universität Leipzig

genehmigte

D I S S E R T A T I O N

zur Erlangung des akademischen Grades

DOCTOR RERUM NATURALIUM

(Dr. rer. nat.)

vorgelegt

von M. Sc. Katharina Halbach

geboren am 14.12.1990 in Remscheid

Angenommen aufgrund der Gutachten von:

Prof. Dr. Thorsten Reemtsma

Prof. Dr. Kristin Schirmer

Tag der Verleihung 12.11.2021

Vorwort

Die vorliegende Arbeit wurde im Zeitraum von September 2017 bis April 2021 am Helmholtz-Zentrum für Umweltforschung – UFZ in Leipzig im Department Analytik in der Arbeitsgruppe von Dr. Stephan Wagner und unter der Leitung von Prof. Dr. Thorsten Reemtsma angefertigt.

Grundlage dieser Dissertation sind drei Veröffentlichungen als Erstautorin in den Fachzeitschriften Analytical and Bioanalytical Chemistry und Environmental Science & Technology, ein vorbereitetes Manuskript sowie ein Kapitel mit unveröffentlichten Daten.

Halbach, K., Aulhorn, S., Lechtenfeld, O., Lecluse, M., Leippe, S., Seiwert, B., Wagner, S., Reemtsma, T., König, J., Luckenbach, T. (2021) Spatial distribution of bromoxynil in zebrafish embryos and the role of the organic anion transporting polypeptide Oatp1d1. *in preparation*

Halbach, K., Holbrook, T., Reemtsma, T., Wagner, S. (2020) Effective processing and evaluation of chemical imaging data with respect to morphological features of the zebrafish embryo. Anal. Bioanal. Chem. 413 (6), 1675–1687

Halbach, K., Ulrich, N., Goss, K.-U., Seiwert, B., Wagner, S., Scholz, S., Luckenbach, T., Bauer, C., Schweiger, N., Reemtsma, T. (2020) Yolk sac of zebrafish embryos as backpack for chemicals? Environ. Sci. Technol. 54 (16), 10159 – 10169

Halbach, K., Wagner, S., Scholz, S., Luckenbach, T., Reemtsma, T., (2019) Elemental imaging (LA-ICP-MS) of zebrafish embryos to study the toxicokinetics of the acetylcholinesterase inhibitor naled. Anal. Bioanal. Chem. 411 (3), 617 - 627

Außerdem werden Ergebnisse diskutiert von einem Manuskript mit mir als Zweitautorin, welches zur Publikation in einer Fachzeitschrift eingereicht wurde.

Muniz, M. S.; Halbach, K.; Araruna, I. C. A.; Martins, R. X.; Seiwert, B.; Lechtenfeld, O.; Reemtsma, T.; Farias, D. F. (2020) Moxidectin toxicity to zebrafish embryos: bioaccumulation and biomarker responses. *submitted*

Danksagung

Es ist vollbracht, einfach super! Viele Menschen haben mir geholfen, mich unterstützt und motiviert bis zur Verteidigung. Ich möchte besonders Prof. Reemtsma danken, für die Aufnahme als Doktorandin im Department Analytik, für die Durchsicht aller Manuskripte und die fachliche Diskussion. Vielen Dank für die Begutachtung meiner Dissertation an Herr Reemtsma und der zweiten GutachterIn. Mein herzlicher Dank gilt Stephan für die tägliche Betreuung und das konstruktive Feedback und der Arbeitsgruppe PUI.

Meine Arbeit war an die Schnittstelle dreier Departments gegliedert. Dies stellte durchaus eine Herausforderung für mich dar, weil ich die verschiedenen Erwartungen und Perspektiven zusammenzubringen hatte und hat aber auch zu einer sehr interdisziplinären Schärfung meiner Forschung geführt. Ich danke Till Luckenbach und Stefan Scholz des Department Bioanalytische Ökotoxikologie für die freundliche Unterstützung, biologisches Hintergrundwissen, Kommentare und Zusammenarbeit an den Manuskripten. Besonders möchte ich Till danken für die Idee zur Zusammenarbeit mit Jörg König und den bereichernden Austausch zu dritt. Danke auch an Nicole und Silke für die Hilfe mit den Embryoversuchen. Ich danke auch herzlich Kai-Uwe Goss und Nadin Ulrich aus dem Department Analytische Umweltchemie für das schnelle Feedback, fachliche Diskussion und die Bereitstellung der Labore für meine Studentinnen.

Ich danke ganz herzlich dem gesamten Department Analytik für die tollen 4 Jahre, besonders Oliver Lechtenfeld, Timothy Holbrook, Jan Kaesler, Coretta Bauer, Josephine Karte, Michaela Wunderlich, Steffi Schrader und Heidrun Paschke. Ich möchte auch dir, Bettina, danken für deine super schnellen Analysen und auf mich überschwappende Motivation. Ich habe während meiner Zeit einige StudentInnen betreut und möchte euch, Marion, Sanjay, Nina, Alexandra, Leonard, Sophia und Marta für die Unterstützung und Ideenreichtum danken.

Ein herzliches Dankeschön auch an euch meine lieben KollegInnen, besonders Philipp, Pietro und Kosta, meine Büro-MitbewohnerInnen Franz, Steffi, Till, Jana und Tine. Wir haben uns immer gegenseitig unterstützt, Feedback auch zu den „schwierigsten“ Fragen gegeben oder einfach nett geplauscht bei Kaffee, Schokolade, Schweineohr oder Veggie-Currywurst-Pommes. Danke auch an meine liebe WG besonders für die positive Stimmung in der Corona-Zeit und die lieben Wisente.

Zuletzt möchte ich meinen lieben Eltern und Omis für die Unterstützung während der ganzen Promotionszeit danken und den liebsten Menschen Ole, Lauri, Kathi B. und Maurits für eure Geduld, wertvolles Feedback und eine gute Portion Motivation.

Bibliographic Description

Halbach, Katharina

Fate of xenobiotics inside the zebrafish embryo – mass spectrometry imaging for toxicokinetic studies

University of Leipzig, Faculty of Chemistry and Mineralogy

Ph.D. thesis

246 Pages, 12 Figures, 2 Tables, 161 References

Abstract

The zebrafish embryo (*Danio rerio*) has developed as a popular model organism in various research fields. In the European Union, the early developmental stages are a promising alternative to animal testing, reducing ethical concerns. One important application is in the risk assessment of chemicals to aquatic organisms in ecotoxicology and drug discovery research. Understanding and predicting toxicokinetic (TK) processes is an essential step towards replacing animal tests with the zebrafish embryo. TK comprises the ADME processes of xenobiotics: absorption, distribution, metabolism, and elimination. Systematic understanding and prediction of the accumulation of xenobiotics in specific tissue and organs in the zebrafish embryo are still missing.

It was first aimed to develop a method and data analysis workflow of mass spectrometry (MS) imaging for the zebrafish embryo, taking morphological information into account and focusing on data reproducibility. Secondly, the MS imaging results should be underlined with mechanistic description of the accumulation patterns of the xenobiotics in the zebrafish embryo.

MS imaging methods were successfully applied to study TK processes of xenobiotics in the zebrafish embryo. The focus was placed on the two techniques, matrix-assisted laser desorption/ionization-MS (MALDI-MS) imaging and especially laser ablation inductively coupled plasma MS (LA-ICP-MS). For LA-ICP-MS, a workflow consisting of the ablation of whole embryos with carbon as an internal standard was developed. Reproducibility, including biological variation, was shown with Kernel density estimates. Furthermore, the workflow was advanced, presenting the software FishImager. FishImager processes MS imaging data, performs clustering of the data, and imports biological features (such as eyes, yolk) as regions of interest (ROI). The intensities and amounts are visualized in heatmaps making statistical information per ROI and

cluster easily visible. FishImager significantly reduces the data analysis time and allows objective data processing to go beyond a subjective visual inspection of the data. It will be a useful tool for zebrafish embryo research.

The spatial distribution of xenobiotics was investigated, targeting different physico-chemical and biological processes. MS imaging was combined with bulk analysis and toxicity measurements. A mechanical sample preparation separating the yolk from the rest of the zebrafish embryo (termed the embryonic body) was developed to investigate the sorption of xenobiotics to the yolk and embryonic body. By this, we could demonstrate that five selected neutral chemicals preferentially accumulated in the yolk. The extent of the accumulation increased with increasing hydrophobicity. Looking at internal concentrations in the whole embryo and relating them to toxic effects, e.g., neurotoxicity, would overestimate the target site's concentration. We could highlight this by studying the spatial distribution of a bromine-containing acetylcholinesterase (AChE) inhibitor. LA-ICP-MS was applied following the bromine distribution as a marker for the compound. The spatial distribution of bromine in the head and spine likely reflected the localization of the tissue rich in AChE. The quantitative imaging significantly correlated with the measured decline in AChE activity in the embryos.

Our studies also pointed out that processes other than simple passive diffusions such as metabolism, transporter proteins, and dynamic development are presumably affecting the distribution and steady-state establishment in the zebrafish embryo. More quantitative description is urgently needed. Biotransformation of several of the here selected compounds occurred. Different tissues were shown to likely transform the parent compounds. These are first of all the expected important organs liver and kidney but also the whole gastrointestinal tract and yolk or yolk syncytial layer.

We could localize one compound in the middle of the GI tract with MALDI-MS imaging. We confirmed that the organic anion transporter Oatp1d1 is mediating the transport of this compound. But also developmental changes might be a reason for the local accumulation.

The presented MS imaging workflows can be applied to more xenobiotics. First mechanistic understanding of tissue-specific accumulations can be extended and particular processes investigated in more depth. This can improve the knowledge and prediction of the ADME processes and increase the application of the model organism, the zebrafish embryo.

Bibliografische Beschreibung

Halbach, Katharina

Fate of xenobiotics inside the zebrafish embryo – mass spectrometry imaging for toxicokinetic studies

Universität Leipzig, Fakultät für Chemie und Mineralogie

Dissertation

246 Seiten, 12 Abbildungen, 2 Tabelle, 161 Referenzen

Kurzfassung

Der Zebrabärblingsembryo (*Danio rerio*) hat sich zu einem beliebten Modellorganismus in verschiedenen Forschungsbereichen entwickelt. In der Europäischen Union sind die embryonalen Entwicklungsstadien eine vielversprechende Alternative zu Tierversuchen, wodurch ethische Bedenken verringert werden. Eine wichtige Anwendung des Zebrabärblingsembryos liegt in der Risikobewertung von Chemikalien für aquatische Organismen in der Ökotoxikologie und Pharma-Wirkstoffforschung. Das Verständnis und die Vorhersage toxikokinetischer (TK) Prozesse ist ein wesentlicher Schritt, um Tierversuche durch den Zebrabärblingsembryo zu ersetzen. TK beinhaltet das ADME-Prinzip von Xenobiotika: Absorption, Verteilung, Metabolismus und Eliminierung. Ein systematisches Verständnis und eine Vorhersage der Akkumulation von Xenobiotika in bestimmten Geweben und Organen im Zebrabärblingsembryo fehlen noch.

Ziel war erstens die Entwicklung einer Methode und eines Datenanalyse-Workflows für die massenspektrometrische (MS) Bildgebung für den Zebrafisch-Embryo. Dies sollte unter Berücksichtigung morphologischer Informationen und mit Fokus auf die Reproduzierbarkeit der Daten erfolgen. Zweitens sollten die MS-Imaging-Ergebnisse mit einer mechanistischen Aufklärung und Quantifizierung der Anreicherung ausgewählter Xenobiotika untermauert werden.

In dieser Arbeit wurden Verfahren der MS Bildgebung für den Zebrabärblingsembryo entwickelt und erfolgreich angewendet, um TK-Prozesse von Xenobiotika zu untersuchen. Der Fokus lag dabei auf den beiden Techniken, der Matrix-unterstützten Laser-Desorptions/Ionisation-MS (MALDI-MS) Bildgebung und insbesondere der Laserablation induktiv gekoppelter Plasma-MS (LA-ICP-MS). Für die LA-ICP-MS wurde ein Arbeitsablauf entwickelt, der aus der Ablation ganzer Embryonen mit Kohlenstoff als interner Standard besteht. Die Reproduzierbarkeit,

einschließlich der biologischen Variation, wurde mit Kernel-Dichteschätzungen gezeigt. Weiterhin wurde der Workflow weiterentwickelt und die Software FishImager vorgestellt. FishImager verarbeitet MS-Bilddaten, führt ein Clustering der Daten durch und importiert biologische Merkmale (z. B. Augen, Dotter) als „regions of interest“ (ROI). Das Ergebnis wird farblich in Heatmaps visualisiert, die statistische Informationen pro ROI und Cluster leicht sichtbar machen. FishImager reduziert die Datenanalysezeit erheblich und ermöglicht eine objektive Datenverarbeitung, die über eine subjektive visuelle Inspektion der Daten hinausgeht.

Untersucht wurde die räumliche Verteilung von Xenobiotika unter Berücksichtigung verschiedener physikalisch-chemischer und biologischer Prozesse. Die MS-Bildgebung wurde mit Bulk-Analysen und Toxizitätsmessungen kombiniert. Eine mechanische Probenpräparation, die den Dotter vom Rest des Zebrabärblingsembryos (Embryonalkörper) trennt, wurde entwickelt, um die Sorption von Xenobiotika an Dotter und Embryonalkörper zu untersuchen. Dabei konnten wir zeigen, dass fünf ausgewählte neutrale Chemikalien bevorzugt im Dotter akkumulierten. Die Anreicherung nahm mit zunehmender Hydrophobizität zu. Daher würde die Betrachtung der internen Konzentrationen im gesamten Embryo, die Konzentration am Zielort z.B. Nervengewebe im Fall von Neurotoxizität überbewerten. Wir konnten dies anhand der Untersuchung der räumlichen Verteilung eines Acetylcholinesterase (AChE)-Inhibitors verdeutlichen. LA-ICP-MS wurde angewandt, um die Bromverteilung als Marker für den bromierten AChE Inhibitor zu untersuchen. Die räumliche Verteilung von Brom in Kopf und Wirbelsäule spiegelte wahrscheinlich die Lokalisation des AChE-reichen Gewebes wider. Die quantitative Bildgebung korrelierte signifikant mit dem gemessenen Rückgang der AChE-Aktivität in den Embryonen.

Unsere Untersuchungen wiesen auch darauf hin, dass vermutlich andere Prozesse als einfache passive Diffusion wie Metabolismus, Transporterproteine und dynamische Entwicklung die Verteilung und die Etablierung des Steady-State im Zebrabärblingsembryo beeinflussen. Eine genauere qualitative und quantitative Beschreibung ist dringend erforderlich. Es fand eine Biotransformation von mehreren der hier ausgewählten Verbindungen statt. Es wurde gezeigt, dass verschiedene Gewebe die Ausgangsverbindungen wahrscheinlich transformieren. Dies sind in erster Linie die erwarteten wichtigen Organe Leber und Niere, aber auch der gesamte Gastrointestinaltrakt und der Dotter bzw. die Dottersackschicht.

Weiterhin konnten wir eine Verbindung in der Mitte des GI-Trakts mit MALDI-MS lokalisieren. Wir stellten die Hypothese auf und bestätigten, dass der organische Anionentransporter Oatp1d1 den Transport dieser Verbindung vermittelt. Aber auch entwicklungsbedingte Veränderungen könnten ein Grund für die lokale Anreicherung sein.

Die vorgestellten MS Bildgebungsverfahren können auf weitere Xenobiotika angewendet werden. Das erste mechanistische Verständnis von gewebespezifischen Akkumulationen kann erweitert und bestimmte Prozesse tiefergehend untersucht werden. Diese können das Wissen und die Vorhersage der ADME-Prozesse verbessern und die Anwendung des Modellorganismus, des Zebrabärblingsembryos, erhöhen.

Table of contents

Abbreviations

9-AA	9-Aminoacridine
AChE	Acetylcholinesterase
ACS	Acyl-CoA synthetases
BCF	Bioconcentration factor
BSP	Bromosulfophthalein
CYP	Cytochrom P450
DESI	Desorption electrospray ionization
dfp	days post fertilization
EU	European Union
FT-ICR	Fourier transform ion cyclotron resonance
GC-MS	Gas chromatography-mass spectrometry
GI	Gastrointestinal
HCCA	α-Cyano-4-hydroxycinnamic acid
hpf	hours post fertilization
ICP-MS	Inductively coupled plasma-mass spectrometry
LA-ICP-MS	Laser ablation inductively coupled plasma mass spectrometry
LC-HRMS	liquid chromatography-high resolution mass spectrometry
LC-MS	liquid chromatography-mass spectrometry
MALDI	Matrix-assisted laser desorption/ionization
MS imaging	Mass spectrometry imaging
Nano-SIMS	Nano secondary ion mass spectrometry
NAT	N-acetyl transferases

Neb-ICP-MS	Nebulization-ICP-MS
Oat	Organic anion transporter
PBTK	Physiological-based toxicokinetic
pKa	Acidity constant
SFC	Supercritical fluid chromatography
REACH	Registration, Evaluation, Authorisation and Restriction of Chemicals
ROI	Regions of interest
TD	Toxicodynamic
TK	Toxicokinetic
ToF-SIMS	Time-of-Flight secondary ion mass spectrometry
YSL	Yolk syncytial layer

Chapter 1 Summary

1.1 Scientific background

1.1.1 The model organism zebrafish and its early life stages

Advancing industrialization has led to the production of many different chemicals to increase our health, facilitate and improve lifestyle. In the European Union (EU), the European Chemical Inventory has listed 106213 substances.[1] These are registered as, e.g., agricultural pesticides, pharmaceuticals, and flame retardants or corrosion inhibitors for industrial use.[2] Many of these can diffuse from the product-cycle or are intentionally introduced into the environment causing chemical pollution. Therefore, an assessment of harmful effects for humans but also other organisms inhabiting the environment is necessary.

In the EU, risk assessments are performed when new compounds are introduced. On the one hand, different scenario models calculate the potential release to various environmental compartments such as soil, river, groundwater for the assessment. On the other hand, the toxicity to model organisms is evaluated. A comparison between both results is used to assess the risk of the chemical. Model organisms cover several trophic levels, including the fish for the aquatic environment. Furthermore, these model organisms may also be used to assess the current health state of environmental compartments. However, with toxicity testing, ethical concerns arise, and alternatives to animal tests are demanded.[3]

The zebrafish (*Danio rerio*) embryo has emerged as an important model organism and alternative to animal tests over the past years.[4] The zebrafish is a freshwater fish from Asia. The popularity of the fish and its embryos in research comes from several benefits: no seasonal spawning, high fecundity, easy fish keeping, small size, a transparent chorion and embryo, and fast development of the embryo within few days. Furthermore, embryogenesis shares similarities between the zebrafish embryo and mammals[5], and essential metabolic signaling pathways are preserved[6,7], e.g., 86% of 1318 human drug targets have orthologs in the zebrafish in contrast to lower similarity with other aquatic test organisms[8]. The embryonic and early larval stages (until 120 hours post fertilization, hpf) are not protected by the EU legislation for animal welfare. During these stages, the nervous system is not fully developed, and no independent feeding has started yet.[4] In contrast to cell-based bioassays, the zebrafish embryo offers the possibility of whole organism experiments integrating different tissues and organs.[3]

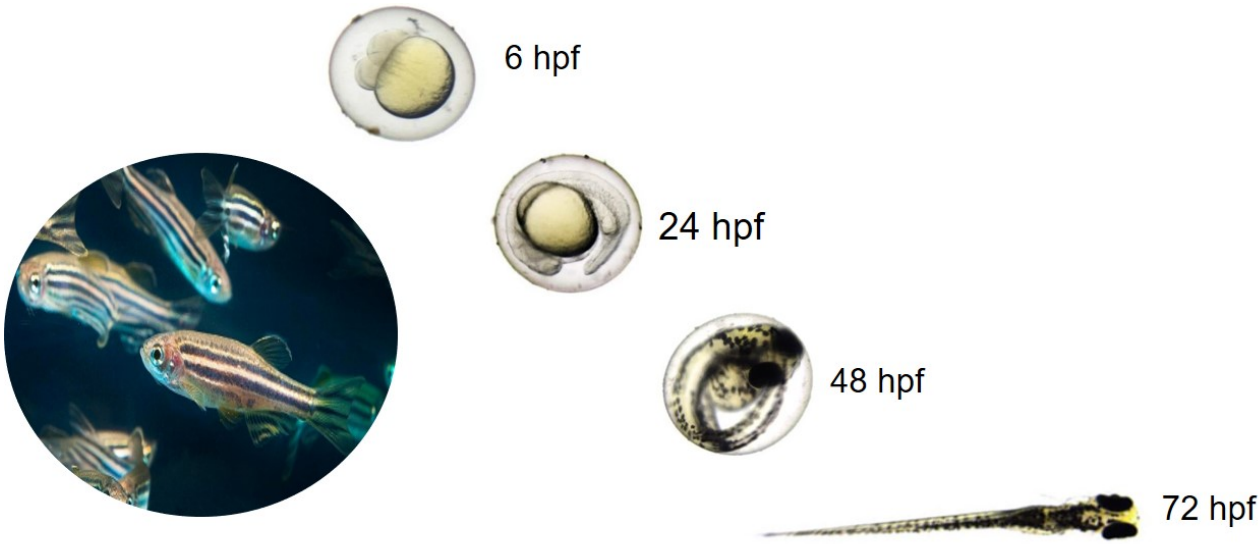

Figure 1. Zebrafish and the early developmental stages (6 to 72 hpf). hpf: hours post fertilization (Source adult zebrafish photograph: https://www.genengnews.com/resources/tutorial/assessing-phenotypic-changes-in-zebrafish-through-automated-quantitative-imaging/)

During the first 72 hpf, the embryo rapidly develops within a chorion, and tissue distinction occurs (Figure 1). The volume inside the chorion is termed the perivitelline space. The yolk (Figure 2) displays an organ containing maternally supplied nutrients, lipids, and yolk proteins (vitellogenins).[9] These phospholipo-glycoproteins can be cleaved and processed for further protein synthesis and nutrient supply. The cleavage and processing can possibly happen prior to the transport into the embryonic body or afterward.[9] The uptake process is facilitated by the yolk syncytial layer (YSL) surrounding the yolk. During the development, the yolk is constantly decreasing in volume and mass and is fully absorbed around seven days post fertilization (dfp).[10] From few cells, major tissues and organs start to differentiate, such as somites, brain, kidney (pronephros has developed between 72 and 96 hpf). The liver begins to form at 24 hpf and is functional at 72 hpf[11].[12,13] Between 24 and 48 hpf, the formation of the gastrointestinal (GI) tract starts, and a continuous lumen is established with an open mouth at 72 hpf but closed anus (opens at 98 hpf).[14] Around 72 hpf, the embryo hatches and starts to swim freely, and the larval development continues. After 120 hpf, organogenesis is mostly completed.[3] In this thesis, the term "zebrafish embryo" comprises the developmental stages until 120 hpf[11].

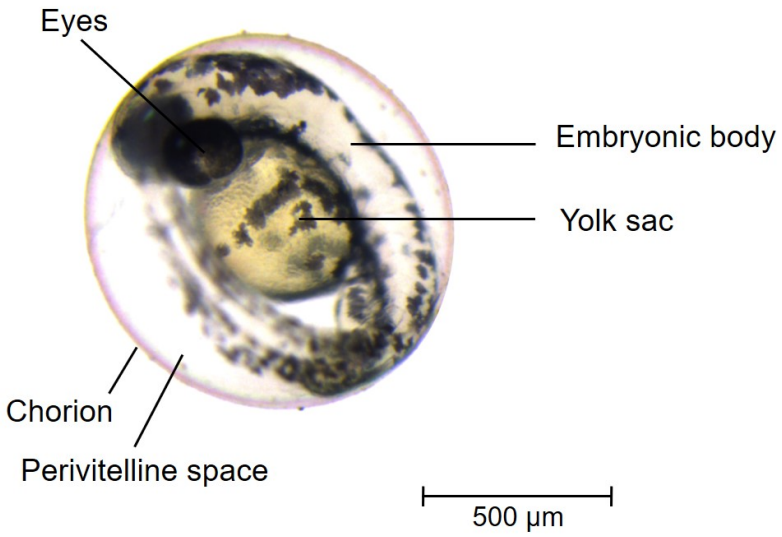

Figure 2. Zebrafish embryo at 48 hpf with assigned major body compartments.

Due to the mentioned numerous advantages of the zebrafish, the early developmental stages are used in various research fields: vertebrate development, modeling of human diseases, pharmacology, and environmental risk and hazard assessment for the aquatic environment.[6,15–17] In (eco)toxicology, the small size of the embryo enables high-throughput experiments. Embryos are placed in well plates with water containing freshwater samples, extracted solid samples, or diluted chemicals of interest. Concentration-dependent lethal or sublethal effects in the zebrafish embryo are detected over 96 h of development. Sublethal effects can be, e.g., edema, malformations of bodyparts, change of heart frequency.[17–19] These test procedures have been standardized as fish embryo toxicity test (FET) in DIN, ISO, or OECD guidelines. [17–19] Part of its application is, e.g., wastewater and effluent testing for possible toxicity. In Germany, the acute toxicity to fish test (AFT) with adult fish was replaced by the FET.[18,20] Many studies have demonstrated a comparable sensitivity to chemicals of the adult fish and the zebrafish embryo.[21] However, there are still uncertainties in the application and limitation range of the FET, e.g., for neurotoxic compounds or the zebrafish embryo's metabolism capacity.[22,23] This is also why the FET has so far not replaced the AFT in the EU for the registration, evaluation, authorization, and restriction of chemicals (REACH).

1.1.2 Toxicokinetic and -dynamic processes

The use of the zebrafish embryo in environmental risk assessment of chemicals but also by the pharmaceutical industry is highly dependent on the thorough mechanistic understanding of toxicokinetic (TK) and toxicodynamic (TD) processes of xenobiotics (chemicals naturally not present in the zebrafish embryo). TK and TD processes may explain different sensitivities during the developmental stages[24], extrapolations to adult lifestages[25], or interspecies variations[26].

Furthermore, they can help interpret and relate different exposure scenarios (membrane uptake, uptake through gills vs. application by food or syringe) between the zebrafish embryo and, e.g., rodents.[27,28] A thorough understanding of TK and TD will improve the prediction of toxicity and ultimately increase the utilization of the zebrafish embryo instead of animal tests.

TK comprises the absorption, distribution, metabolism, and elimination (ADME) processes of a chemical (Figure 3). Thus, TK processes determine the concentration of a chemical at the target site. TD describes a chemical's interaction with the target site, which is responsible for a toxic effect.

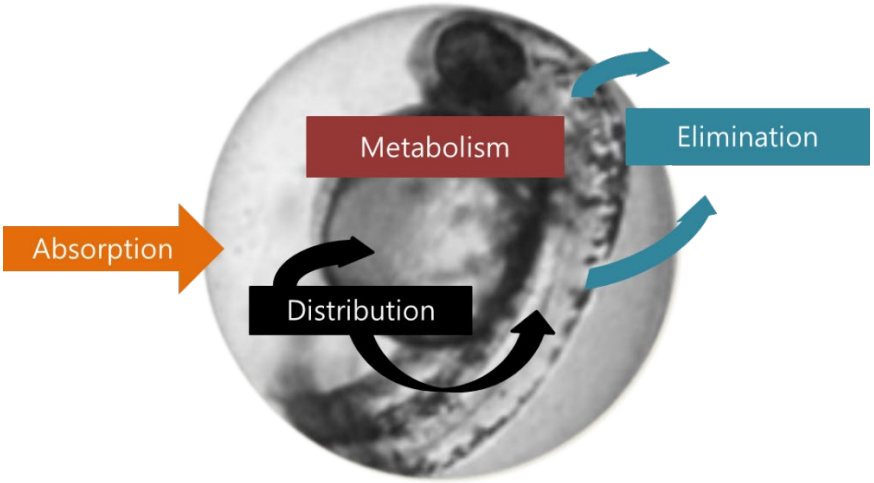

Figure 3. Toxicokinetic processes with the ADME principle for the zebrafish embryo: absorption, distribution, metabolism, and elimination of chemicals.

The rapid development from a few cell-stage to the larval stage of the zebrafish embryo, as well as the small size of the embryo (Figure 2), challenges the investigation and conversion into prediction models of the TK and TD processes. This includes, e.g., the decrease of the lipid-rich yolk, hatching from the chorion, differentiation of organs with metabolic capacity, development of the gastrointestinal tract as an elimination route.

Internal concentrations in the zebrafish embryo/larvae are one of the TK parameters reported for about 20 years in the zebrafish.[29–32] The studies on internal concentration have increased in the past years due to improved analytical sensitivities. They contribute to a better understanding of toxicological effects than only considering the nominal or measured external concentrations. The measurement of internal concentrations over several points of the exposure time may also show whether a steady-state, i.e., a stable concentration (influx and efflux rate of the chemical are the same[33]) inside the organism, has been reached. The reaching of the steady-state of chemicals within the usual timeframe of the FET (96 h) is a significant aspect for validity and its applicability. Internal concentrations also allow the calculation of steady-state partition ratios (internal

concentration/external concentration at the steady-state) and to compare these (also often referred to as bioconcentration factor, BCF) with the ones for adult fish or other vertebrates. Furthermore, the measurement of internal concentrations over time provides indications on processes such as chemicals' metabolism.[34] Partition coefficients take the sorption properties of the different tissues, e.g., lipids, water, and proteins, and physico-chemical properties of the chemical into account.[35] They can predict the equilibrium concentration, i.e., the amount of the chemical partitioning into the tissue until reaching a chemical equilibrium. The equilibrium concentration can differ from the observed steady-state concentration due to metabolism or transporter proteins.

The metabolism comprises all the biochemical reactions inside the organism, and the term "biotransformation" is more specific towards the metabolism of an anthropogenic compound or drug. Researchers have shown the expression of major metabolism enzymes already in the zebrafish embryo. These include the important cytochrome P450 (CYP) enzymes known for their role in phase I (oxidative reactions) and II (conjugation) biotransformation but also enzymes such as UDP-glucuronosyltransferase, sulfotransferase, and glutathione S-transferase.[11,36–38]

Different parameters influence the steady-state establishment, yet often the underlying quantitative description is missing. Among these are the hydrophobicity of the chemical, ionizability, biotransformation, and active transport.

It was shown that the neutral hydrophobic (log K_{OW} 3.3 to 5.8) substances naphthalene, fluorene, fluoranthene, and benz[a]anthracene reached apparent steady-state conditions in the zebrafish embryo within 72 h of exposure. Still, biotransformation decreased the internal concentration of fluoranthene and benz[a]anthracene. Other lipophilic substances were also observed not to reach a steady-state within 24 h of exposure.[31,39,40] A comprehensive study by Brox et al. investigated internal concentration time-profiles of 17 compounds over 96 h of exposure.[34] They included nonionic and ionic polar compounds (log $D \leq 2$). The main findings influencing the steady-state establishment were a slower uptake rate of ionic compounds and biotransformation for six compounds. Biotransformation products were already observed in the early developmental stages (before 28 hpf). Further factors such as low membrane permeability and efflux transporters were assumed for low-enrichment chemicals (internal concentration divided by external concentration). The authors identified several transformation products in their study and showed phase I and phase II biotransformation products.[34,38]

Calculated BCFs for antidepressants also suggested other factors than passive diffusion to be involved, e.g., the exposure medium's pH.[41] The exposure medium's pH was also affecting the internal concentration of antihistamines after 96 h of exposure.[42] A kinetic ion trap model for the

uptake was recently suggested for ionic pharmaceuticals.[43] However, the authors only assumed a steady-state after 96 h and did not prove this.

In addition, the developmental stage significantly influenced the uptake of paracetamol and diphenhydramine with higher uptake at older stages.[44,45] Reported TK of three perfluorinated alkyl acids possessed a slow or continuous uptake over 120 h of exposure. This was speculated to results from the chorion in the first 48 h of exposure functioning as a barrier.[46] Previously, the chorion was only assumed to be a barrier for large molecules (> 4000 Da).[47]

Quantitative information on biotransformation products and the influence of other uptake mechanisms such as transporter proteins and the GI tract opening are rare but urgently needed to improve TK models.

Another TK parameter that may help fill the open questions is the distribution within the zebrafish embryo. Different sorption properties of the tissues (defining the partitioning of the chemical), organic transporters, or biotransformation interact and influence tissue distribution. Furthermore, quantitative spatially resolved data allow correlating local concentrations with effects. Few studies[28,48–51] have used mass spectrometry imaging techniques as an imaging tool. One significant observation was that melanin mediates the accumulation in the embryo's eyes of cocaine and meta-chlorophenylpiperazine[50]. This affinity influenced the TK of these two compounds. The authors also suggested that organic cation transporters increase the uptake of meta-chlorophenylpiperazine. These results may give further insights to explain differences in the concentration-dependent behavioral response and tissue levels of rodents and the zebrafish embryo.[50]

In the following, analytical methods to study TK processes of organic xenobiotics are discussed.

1.1.3 Analytical tools to study TK processes

The total uptake of chemicals is usually quantified by pooling several embryos, homogenization, and solvent extraction.[29,30] Chromatographic analysis (e.g., liquid chromatography[30]- (LC), supercritical fluid chromatography (SFC), or gas chromatography[52] (GC)) coupled to a mass spectrometer (MS) for molecular or elemental detection achieve the separation of the analytes from biological tissue. In the thesis, the term bulk analysis refers to internal concentrations in homogenized embryos. Another possibility is labeling the compound such as fluorescence or radio-labeling for detection via, e.g., fluorometer and liquid scintillation counting.

Transformation products can be qualitatively determined by screening the extracts with chromatographic systems combined with high resolution-MS (e.g., LC-HRMS) using suspect and

non-target methods. Comparison based on statistical methods such as principle component analysis of extracts of embryos exposed to analytes with embryos exposed only to clean water can identify characteristic peaks of transformation products.[38] With exact mass data and fragmentation information, chemical formulas can be assigned.

The distribution and accumulation of xenobiotics in certain body parts in the zebrafish embryo can be studied using imaging techniques. Examples are quantitative whole-body autoradiography[53], micro-X-ray fluorescence spectrometry[54,55], and confocal microscopy[56], requiring labeling the compound or being restricted to metals. Another method is MS imaging. The latter includes the molecular imaging technique matrix-assisted laser desorption/ionization-MS (MALDI-MS) and the laser ablation inductively coupled plasma MS (LA-ICP-MS) for elemental information. These techniques may also give quantitative information if suitable standards are available. While other methods are often restricted to labeled compounds (fluorescent, isotope), MS imaging techniques greatly broaden the substance spectrum. LA-ICP-MS can be used to localize compounds containing a hetero-element naturally not present in the zebrafish embryo, such as bromine, iodine, arsenic, and MALDI-MS imaging allows the detection of molecules without the need for labeling. Both techniques may offer a similar spatial resolution (typically 50 – 200 µm[57]) and a sufficient mass resolution to differentiate between the exposed chemicals and the natural components. Secondary ion-MS (SIMS) imaging techniques, such as Time-of-Flight- (ToF-) SIMS or Nano-SIMS, can analyze sub-organ distributions as they have a lower spatial resolution (typically 50 nm – 1 µm[57]). In the following, LA-ICP-MS and MALDI-MS imaging are presented in more detail.

LA-ICP-MS Imaging

LA-ICP-MS offers the great potential of a quantitative imaging technique in the µm-range. It has been widely used in the past years to study distributions of natural elements[58–65] or elemental contaminants[66] in biological tissues. LA-ICP-MS can also detect molecules containing marker elements, e.g., proteins[67] or drug[62].

In principle, a pulsed laser rasters a solid sample, the sample absorbs the energy of the laser, an aerosol of fine particles is created (this process is called ablation), which is then transported via a carrier gas (e.g., argon or preferably helium[68]) into the ICP (Figure 4). In the plasma, the ablated particles are atomized and ionized. Depending on the ICP-MS device, single elements are extracted and detected (quadrupole-based ICP-MS) or simultaneously multiple elements (e.g., double-focusing sector field ICP-MS, multicollector ICP-MS, or ICP-ToF-MS). The continuous transient signal obtained in the ICP-MS can then be processed to retrieve the spatial information. A laser wavelength in the ultraviolet range is usually used due to higher fine particle production and lower

detection limits than an infrared laser[69]: Nd:YAG (213 and 266 nm) or an ArF excimer (193 nm). The spatial resolution of LA-ICP-MS can be in the range of 1 to 200 µm.[70] The spatial resolution is dependent on the diameter of the laser spot. However, super-resolution reconstruction[71] or overlapping spot sampling and deconvolution[72] can further lower (up to a factor of ten) the resolution. The sensitivity of the LA-ICP-MS is in the low µg/g range and by this superior compared to the elemental imaging techniques energy-dispersive X-ray analysis and particle-induced X-ray emission.[73]

In this work, a double-focusing sector field ICP-MS with a Mattauch-Herzog geometry[74] was used. The ions are focused by an electrostatic analyzer, separated with a magnetic field, and detected by a Direct-Charge-Detector.

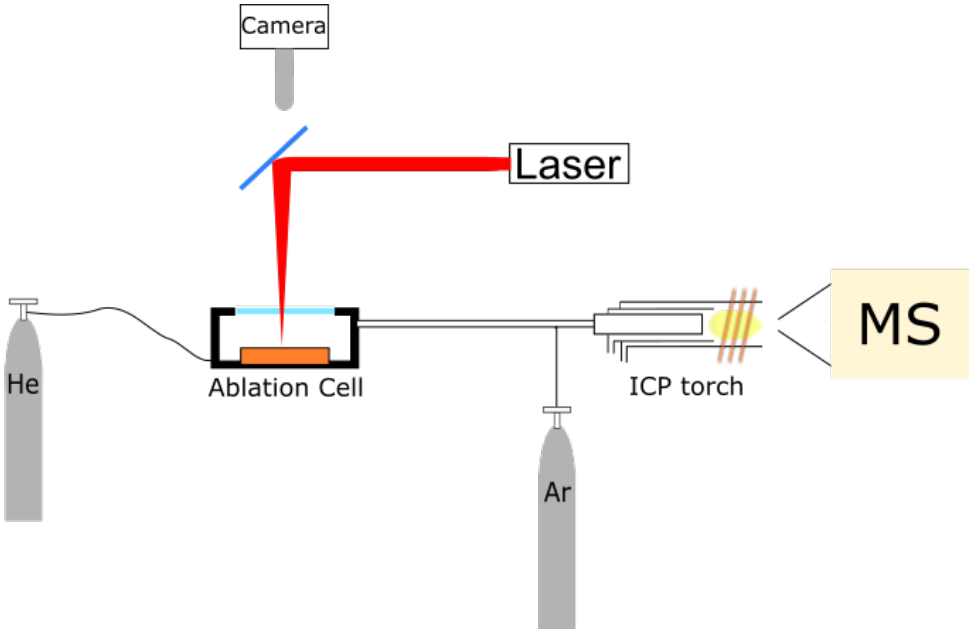

Figure 4. Example of an LA-ICP-MS system.

Instrumental developments reduced the dispersion and improved washout and aerosol transport efficiencies by implementing smaller ablation cells and tubing (e.g., the ARIS device[75]). Furthermore, the instrumental developments of ICP-ToF-MS coupled with a LA device improved the sensitivity (close to a sector field ICP-MS) for fast and simultaneous detection of multiple elements offering a mass resolving power 6000 and allows pulse-to-pulse separation.[76,77] A sector field ICP-MS restricts the analysis time due to comparatively long sampling times of the ions. Researchers use modeling approaches to optimize parameter selection (e.g., laser spot size, scan speed, fluence, repetition rate) for the experiments.[78–80]

Standards of biological matrices are usually missing and, thus, complicate quantification. In contrast, for geological samples, various standard reference materials are available by, e.g., the

National Institute of Standards and Technology[81]. Therefore, house-made standards are prepared to quantify elemental contents in biological samples and include matrix-matched calibration[82], matrix-similar substances such as gelatin[83] or agarose[48,84], dried-droplets[85], or online isotope dilution[86,87].

LA-ICP-MS data are often processed and analyzed in in-house developed workflows based on, e.g., Excel[88], Matlab[89]. The two workflows by Uerlings et al. and de Pessoa et al. are also freely available to the public.[88,89] Commercially available software solutions are, e.g., Iolite and the recently developed HDIP (based on the Hierarchical Data Format Version 5) software. An overview of available software is given by Weiskirchen et al.[90] However, software solutions should be improved for statistical analysis such as clustering and using biological information such as morphological features. Stacking different ablated tissue sections from the same specimen can also be performed to reconstruct three-dimensional images.[91,92] This strongly increases the application possibilities for LA-ICP-MS.

Concluding, LA-ICP-MS possesses the advantages of minimal sample preparation, high throughput (clinical applications are reported as fast measurements are available[93]), low limits of detection (sub µg/g), many elements are accessible, and isotopic information can be obtained.[63]

MALDI-MS imaging

In contrast to LA-ICP-MS, MALDI-MS imaging allows the detection of whole molecules from small amino acids[94,95] up to large proteins and peptides[96].

MALDI-MS imaging encompasses the following steps: cryosectioning of tissue, matrix application, and measurement. MALDI is a soft ionization technique. The principle is based on applying a small matrix molecule such as α-cyano-4-hydroxycinnamic acid (HCCA) or 9-aminoacridine (9-AA) onto the sample prior to measurement. This molecule has several purposes: (i) increasing the extraction of the analytes from the tissue, (ii) absorbing large fractions of the laser energy, thus preventing the analytes from fragmentation, and (iii) facilitating the transfer of the charge from the matrix molecule to the target molecules (better ionization). Therefore, the matrix application is a crucial sample preparation step strongly influencing the measurement's quality and reproducibility. The size of the matrix crystals defines the lower spatial resolution limit; the matrix layer's homogeneity ensures reproducible analyte extraction and ionization; the matrix's application should also prevent diffusion of the analytes within the tissue. The absorption maximum of the matrix molecule ideally is equal to the laser wavelength.

The three predominant matrix application procedures are airbrush, sublimation, and automatic spraying.[94] Airbrush applies the matrix dissolved in a solvent and is a fast and straightforward method with a manual airbrush device. Its major limitation is the manual handling, such as spray velocity and, therefore, reduced reproducibility. Sublimation usually produces smaller matrix crystals (1 to 3 µm)[97], thus, increasing the spatial resolution. The sublimation is preferably used for small and easily vaporizable molecules. No extraction occurs as the matrix molecule is applied without a solvent. However, an additional recrystallization step can also add an extraction effect on the analytes. In this case, the sample slide is placed in a humid chamber next to a disk with solvent for some minutes.[97] Automatic spraying uses the matrix dissolved in a solvent and produces a fine layer by alternating spraying and drying cycles resulting in a crystal size between 5 and 20 µm[97]. Automatic spraying devices make this method easy to handle and reproducible. However, it is rather time-consuming.

After the matrix is deposited onto the sample, the target plate with the slides is transferred to the vacuum. An electric voltage is applied, and a laser pulse desorbs matrix molecules and analytes from the tissue section and produces a gaseous plume of molecules. Due to the voltage, ionized molecules are transferred to the MS. In this work, the MALDI device was connected to a Fourier transform ion cyclotron resonance MS. This MS offers up to date the highest mass resolving power and mass accuracy.[98] The resolving power can be up to 10^6 with an accuracy < 1 ppm.[99,100] In a magnetic field, the ions are bend into circular motions (ion cyclotron). This frequency is dependent on the magnetic power and the m/z ratio. An alternating electric field perpendicular to the magnetic field is applied and accelerates the ions. The ion cyclotron creates resonance/voltage in the electric plates, which can be detected. The signal is deconvoluted by Fourier transformation, which can be converted to the m/z ratio and related to the intensity spectrum.[101]

Quantitative MALDI-MS imaging bears more difficulties than LA-ICP-MS, and few studies reported quantitative MALDI-MS imaging results of biological samples.[102] A matrix application procedure resulting in reproducible extraction efficiency is essential. Different chemical bonds between the analytes and matrix molecules also impact the extraction efficiency. Furthermore, the matrix molecules and the analytes compete for ionization.[102] Therefore, MALDI-MS imaging was applied for qualitative visualization of the xenobiotic's distribution in the thesis.

1.2 Objectives

The thesis aims to apply MS imaging for TK studies in the zebrafish embryo (Figure 5).

MS imaging can provide essential information for understanding uptake and toxicity. It can thereby increase the application domain and improve knowledge of the zebrafish embryo's limitations as a model organism. The benefits also justify the analytical effort required for MS imaging due to the specimen's small size. The concentration of xenobiotics at the target site of the toxic effect is a superior parameter than the total average internal concentration. Furthermore, biological processes influencing the distribution can be identified, such as metabolism, developmental changes, and active transport. MS imaging results can reveal tissue-specific sorption influencing uptake and elimination kinetics. These data can help to establish complex physiological-based TK (PBTK) models of the zebrafish embryo.

Therefore, a reproducible MS imaging method is required. It ideally provides reproducible qualitative or quantitative data and uses other available information such as biological features. Additionally, an automatic workflow for the data analysis can significantly reduce the time-consuming data analysis. After the developed MS imaging methods, the thesis highlights the importance of the spatial distribution for TK investigations by combining MS imaging with bulk analysis and toxicity measurements.

The thesis aims to pave the paths from single observations of spatial accumulation patterns towards an integrated process to understand and quantify magnitudes of accumulations in distinct body compartments.

In short, the objectives of the studies of this thesis are as follows:

Objective I: Method development of LA-ICP-MS analysis and MALDI-MS imaging of zebrafish embryos, including a data analysis workflow taking morphological information into account and providing statistical evidence for data reproducibility

Objective II: Identification of the mechanisms behind the accumulation patterns of xenobiotics in the zebrafish embryo

To investigate various chemical and biological processes inside the zebrafish embryo, ten chemicals for the thesis (Table 1) were selected based on their physico-chemical properties, i.e., varying hydrophobicity, different functional groups, ionizability. Three of them also contain heteroatoms (bromine, iodine), making them accessible via LA-ICP-MS. Chemicals that are

reported to enter aquatic environments have been included as well, including carbamazepine, bromoxynil, diuron, and diclofenac.[103]

The results section summarizes five different studies (Chapter 2 to Chapter 6) investigating the accumulation in various tissues inside the zebrafish embryo. After summarizing, the results are jointly discussed, and recommendations for future studies are given. Chapter 2 and Chapter 3 focus on the method development and data analysis workflow for LA-ICP-MS analysis of the zebrafish embryo. Chapter 4 investigates the different sorption of chemicals to the body compartments, yolk and embryonic body. Another part of this study was predicting the uptake kinetics of these chemicals in the zebrafish embryo. One of the selected chemicals was accumulating stronger in the embryonic body (bromoxynil). Whether it distributes evenly within this embryonic body was studied combining LA-ICP-MS with MALDI-MS imaging in the next study (Chapter 5). We hypothesized that the tissue-specific accumulation was related to organic anion transporter (Oat). Finally, the quantitative contribution of transformation products of xenobiotics and their spatial distribution in the zebrafish embryo are presented (Chapter 6).

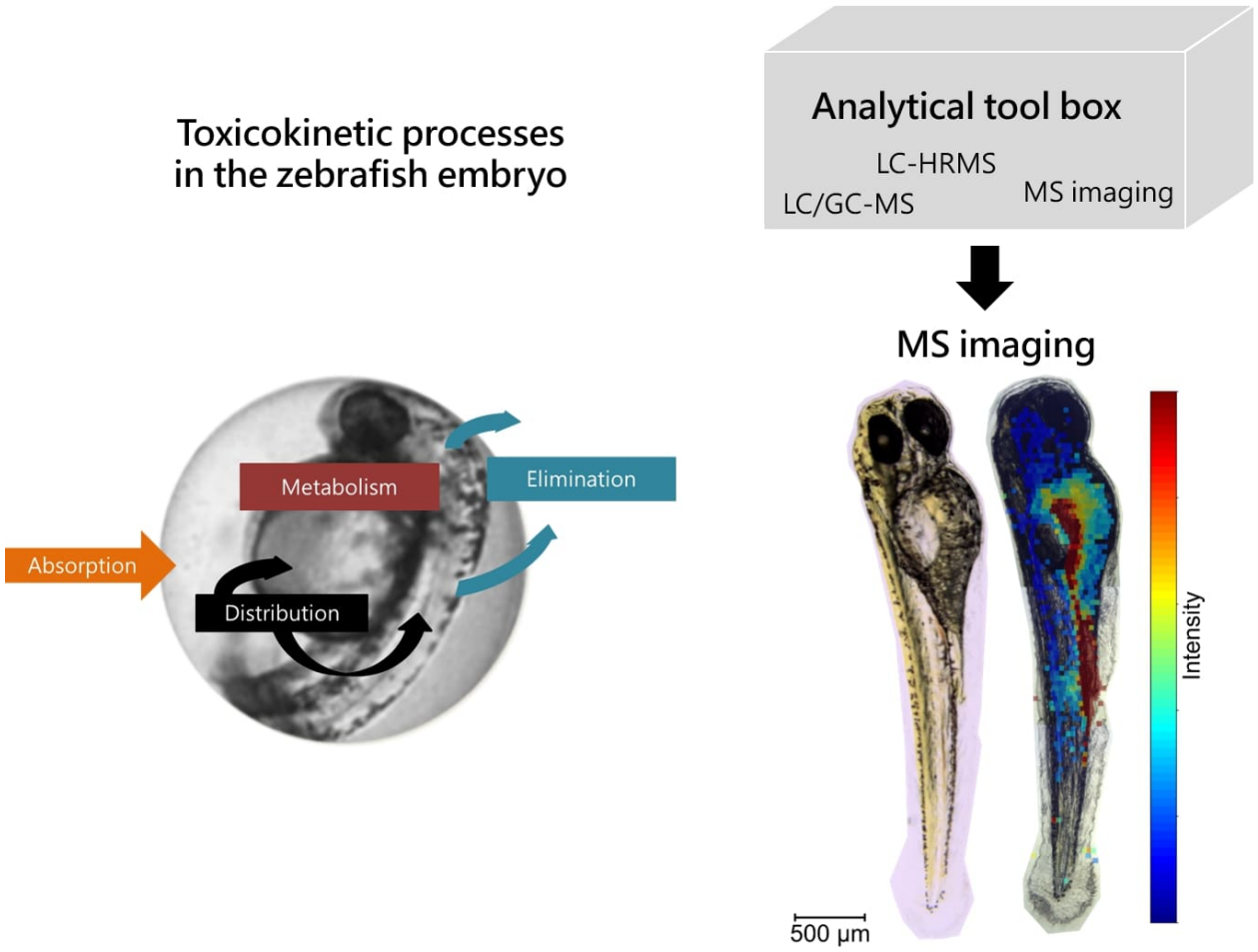

Figure 5. Toxicokinetics in the zebrafish embryo is investigated using analytical tools with a focus on MS imaging in this thesis.

Table 1. Overview of the discussed xenobiotics in this thesis with the respective chapter, their application, physicochemical parameters, and mode of toxic action. [a]Calculated with[35]; [b]calculated with[104]; [c]from[105]

Substance	**Chapter**	**Application**	**M_W (g/mol)**	**log K_{OW}[a]**	**Major species at pH=7.4[b]**	**Calculated log D at pH=7.4[b]**	**Mode of toxic action in zebrafish embryos**
Naled	2, 3	Insecticide	380.78	1.38[c]	Not ionizable	2.65	AChE inhibitor
2-Ethylpyridine	4	Industrial chemical	107.16	1.28	98.29% neutral	1.58	Unknown
Carbamazepine	4	Pharmaceutical	236.27	2.3	100% neutral	2.77	No hatching observed[106]
Diuron	4,6	Herbicide	233.09	2.89	100% neutral	2.53	Behavioral[107]
4-Iodophenol	2-4,6	Industrial chemical	220.01	2.66	98.04% neutral	2.59	Unknown
1,2,4-Tribromobenzene	4	Industrial chemical	314.80	4.62	Not ionizable	4.28	Unknown
Paroxetine	4	Pharmaceutical	329.37		99.4% cationic	0.83	Inhibitor of neuronal reuptake of serotonin[108]
Bromoxynil	4-6	Herbicide	276.92		99.98% anionic	1.19	Inhibitor of photosynthesis[109]
Diclofenac	5	Pharmaceutical	296.15		99.96% anionic	1.10	Inhibition of cyclooxygenase[110]
Clofibric acid	6	Pharmaceutical	214.65		99.99%anionic	-0.51	Unknown

1.3 Results

1.3.1 Method development of LA-ICP-MS analysis and MALDI-MS imaging of zebrafish embryos

The small size of the zebrafish embryo making the sample preparation difficult could be one reason for only a few studies using MS imaging techniques. Assuming a density equal to water, the embryo's water content calculates to 77% based on the dry weight of 57 µg/embryo and a volume of 253 nL at 96 hpf (Chapter 4). A high water content complicates freezing and cryosectioning because it increases the possibility of crystal formation during freezing, and cryosections can rip apart when structural harder parts are missing. Furthermore, a sufficient uptake of the chemical into the embryo, good ionization efficiency, and MS sensitivity contribute towards a successful MS imaging application.

To obtain unambiguous results with MS imaging, it is essential that (i) the spatial resolution provides a detailed image of the object; (ii) the method is specific towards the targeted chemicals/elements in the biological matrix; (iii) the sensitivity is sufficient for tissue concentrations; (iv) the quantification accounts for matrix effects; (v) internal standardization of imaging data include varying tissue density and composition as well as instrumental instability; (vi) for reactive toxins, both the parent chemical and possible transformation products can be detected/distinguished; and (vii) the data processing is easy to support reproducible interpretations of the color-coded images.

1.3.1.1 LA-ICP-MS

Chapter 2 demonstrates that LA-ICP-MS could determine the spatial distribution (50 µm resolution) of the neuroactive compound naled in the zebrafish embryo. The compound contains two bromine atoms. Bromine is naturally not present in the zebrafish embryo. Therefore, we used bromine as a marker for naled, which is rapidly transformed[111] in the zebrafish embryo mostly to bromide.

For this study, a method of ablating the whole zebrafish embryo was developed, increasing the amount of ablated material compared to ablated sections and thus the ions reaching the detector. Zebrafish embryos were air-dried beforehand. To account for the varying tissue density, an internal standard was needed. We compared two elements naturally present in the zebrafish embryo as candidates: ^{12}C and ^{31}P. The LA-ICP-MS intensities of these elements were compared to the height profile of the air-dried zebrafish embryo measured with a profilometer before the ablation. The

carbon intensity represented best the height of the embryo and was implemented as the internal standard. The bromine to carbon ratio of an embryo exposed to naled is displayed in Figure 6a.

We performed the calibration of the bromine signal with the matrix-similar substance agarose spiked with bromide. Here, the method by Stärk et al.[84] based on a homogenous agarose film on glass slides with different analyte concentrations was extended to the anion bromide. Anions are less homogenously distributed than cations leading to a more pronounced concentration decline close to the edges of the glass slide. We could successfully calibrate the bromine signal. We compared the summed quantitative LA-ICP-MS data over the whole embryo with nebulization- (Neb-) ICP-MS data of extracted embryos as well as ion chromatography of bromide. A good agreement of the three methods (60-150%) was obtained as soon as the internal amount is sufficient for the detection with LA-ICP-MS.

Despite the small size of the embryo, making some aspects of the MS-imaging analysis intricate (such as cryosectioning, sensitivity), its small size, as well as the classification as the non-animal approach, facilitate the evaluation of the reproducibility and biological variation of the LA-ICP-MS analysis. Often LA-ICP-MS results of single biological samples are reported, missing this evaluation.[112,113] We evaluated the reproducibility by comparing the intensity distributions of the carbon and bromine signals among three different ablations (equal to three individual embryos). Smoothed Kernel density estimates were chosen as probability density function and calculated from the intensity data. This is the first time that this approach was reported to assess reproducibility. It accounts for the distributions of the intensities per pixel of one ablation. One pixel represents the spatial resolution measured with the LA-ICP-MS analysis. However, the Kernel density estimate does not take the exact coordinates of the pixels into account. Carbon signals showed a bimodal distribution, bromine a monomodal and positively skewed distribution. The comparison of the carbon distribution of several individuals validated reproducible ablation quality. Additionally, the Kernel density estimate of the bromine intensity was calculated over different exposure times to naled. The density estimates broadened at longer exposure times towards more frequent higher intensities (Figure 6b).

In Chapter 3, we evaluated LA-ICP-MS data of different individual zebrafish embryos further. This time, we accounted for the coordinates, thus, going a step further than Chapter 2. A workflow was developed merging the LA-ICP-MS data and biological information (provided by the FishInspector[114]). This workflow is embedded in the software FishImager. It is freely available online.

The biological information is imported and assigned as regions of interest (ROIs), e.g., the yolk, swim bladder, and fish eyes. Statistical analyses such as mean, standard deviation, and the sum of the measured elements per ROI are automatically produced. More statistics such as clustering can be performed on the LA-ICP-MS data. The output of the clustering and the ROIs are visualized in heatmaps. Hence, the heatmaps provide information on intensity/quantified LA-ICP-MS data per cluster and per the biological ROIs (Figure 6c). When comparing now the heatmaps between different ablations (i.e., individuals), the information of the coordinate of the LA-ICP-MS data is included (Chapter 3) compared to before only the distribution of the intensity data (Chapter 2).

Not only the Kernel density estimates but also the heatmaps produced with FishImager confirmed reproducible LA-ICP-MS analyses of the zebrafish embryos. We could demonstrate a good agreement of the heatmaps between different ablation using Spearman's correlation coefficient, e.g., mean carbon (^{12}C) intensities in the embryonic body did not significantly deviate between three individuals (4.47±0.94, 4.61±0.73, and 4.74±0.98 x 10^5 counts per second).

Furthermore, TK experiments of the zebrafish embryo exposed to 4-iodophenol with increasing exposure times were analyzed with FishImager. A preferred accumulation of iodine in the yolk could be revealed. A shift of the yolk accumulation towards the GI tract with increasing exposure time was demonstrated (see for biological explanation 1.3.2). We quantified 37 ng iodine (50% of the total amount) in the cluster representing the GI tract, which only corresponds to 9% of the total ablation area. Thus, a remarkable amount of the iodine signal is concentrated in the GI tract (see further interpretation in 1.3.2).

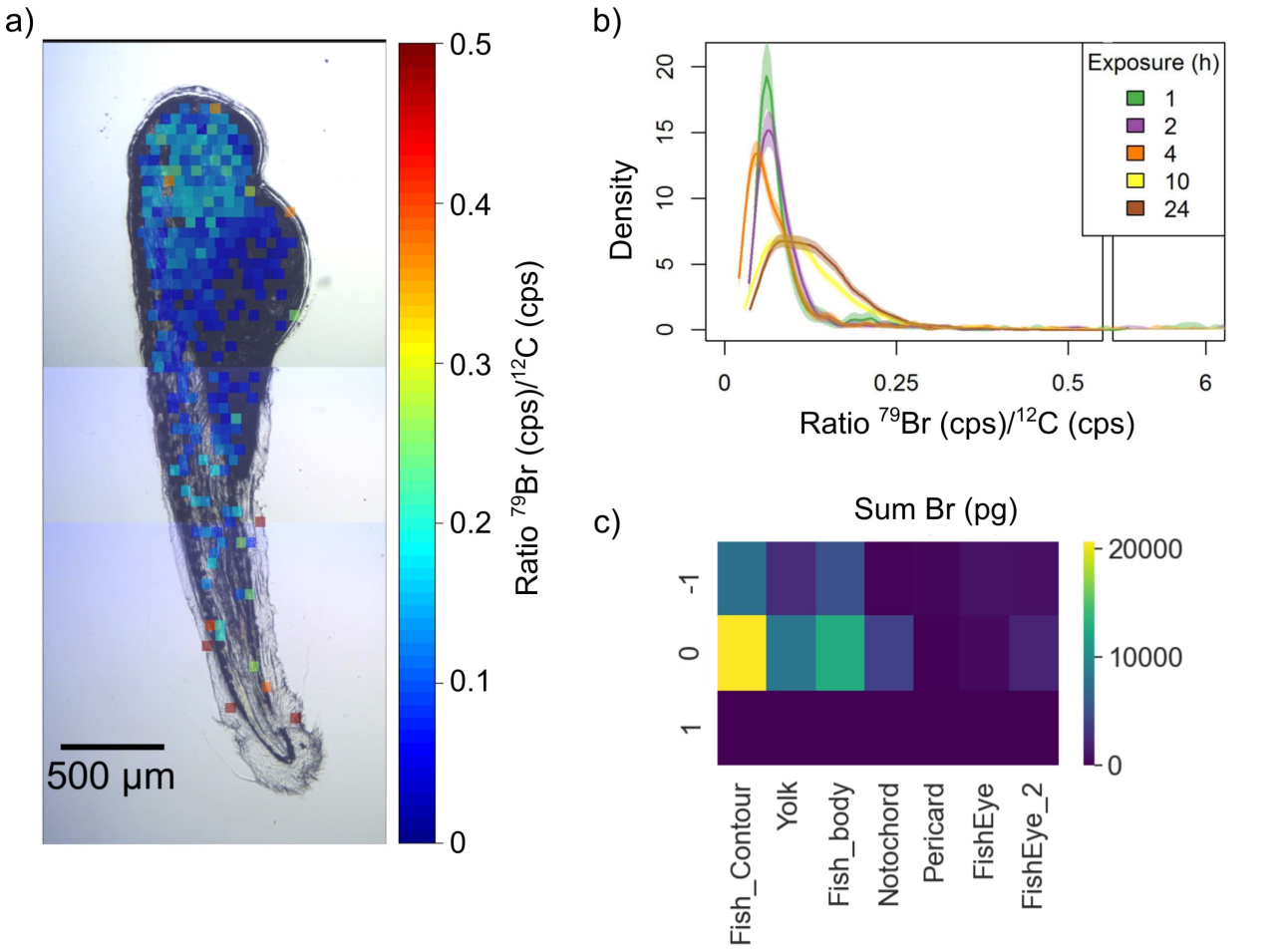

Figure 6. LA-ICP-MS results of zebrafish embryos exposed to the bromine-containing compound naled. a) Ratio of the bromine and carbon intensities in a zebrafish embryo exposed for 24 h to naled (start 72 hpf). b) Kernel density estimates of the distribution of the calculated ratio for an increased exposure time to naled (exposure end always at 96 hpf). Each density curve represents the LA-ICP-MS data of three embryos with 5% confidence interval. c) The heatmap displays the quantified bromine intensity per cluster (-1, 0, 1) and per biological region of interest (imported from FishInspector). The heatmap was produced with the FishImager software; hdbscan clustering was performed for the ablation data of the zebrafish displayed in a).

1.3.1.2 MALDI-MS imaging

To detect xenobiotics in the zebrafish embryo with LA-ICP-MS, the chemicals are required to have heteroatoms naturally not present in the organism, such as bromine, iodine, arsenic. The detection of these elements then allows tracing the parent compound and all transformation products containing the heteroatom. A distinction between the parent compound and the transformation products is not possible. Combinations with bulk analyses of zebrafish embryo extracts may add information on whether biotransformation occurs. Molecular detection methods are needed, such as MALDI-MS imaging, to measure the spatial distribution of the exact molecule.

In order to successfully use MALDI-MS imaging for the zebrafish embryo, we developed a sample preparation workflow. After exposure and washing, alive zebrafish embryos were first swiped

through a viscous frozen section medium to remove excess water and then placed in a cryomold filled with the frozen section medium. With a pipette tip, the embryo was oriented for cutting later on. Then the cryomold was placed onto dry ice to ensure rapid freezing without water crystal formation. Storage was performed at -80 °C in aluminum foil to avoid embrittling. For cryosectioning, the cryomold was placed 24 h prior to cutting into a microtome at around -17 °C. We adjusted the knife and ambient temperature for cutting smoothly through the frozen section medium. Slices were mounted onto Indium Tin Oxide-coated MALDI glass slides by placing the hand under the slide and shortly thawing the slice. Matrix selection was carried out for each analyte. Frequent matrix substances such as 9-AA, HCCA, and 2,5-dihydroxybenzoic acid were dissolved together with the analyte in a solvent, and the analyte/matrix/solvent mixture was spotted on a target. After MALDI-MS measurements, the intensities of the analyte were compared, and the best performing matrix was selected.

After pretests, we selected 9-AA as the matrix molecule for clofibric acid and bromoxynil. Both substances were measured in the negative mode in the MS. We applied the matrix by sublimation. Although the sublimation needs quite an extensive set-up, we produced an even matrix layer. Between different slides, a good reproducibility in terms of homogenous distribution and matrix amount could be achieved. Laser parameters (e.g., frequency, energy, size) and isolation windows were selected to get sufficient signal intensity. The spatial resolution was 25 µm. Biotransformation of both xenobiotics had been reported; therefore, we also scanned the MS imaging data for these.

In Chapter 5, the herbicide bromoxynil was detected with MALDI-MS imaging and accumulated in the head and especially in the gastrointestinal (GI) tract. The bromine detection by LA-ICP-MS in the GI tract center supported this result (Chapter 5). MALDI-MS imaging could confirm the bromine signal as the parent compound and reveal lower intensities of bromoxynil also in the head region. Furthermore, MALDI-MS imaging was successfully applied to detect moxidectin in the eyes.[115] Moreover, the clofibric acid taurine metabolite was measured with MALDI-MS imaging over different exposure times. The metabolite accumulated in the YSL and/or GI tract (Chapter 6). However, the MALDI-MS imaging was not suited to detect the parent compound clofibric acid in this case.

1.3.2 Identification of the mechanisms behind the accumulation patterns of xenobiotics in the zebrafish embryo

After successfully developing MS imaging for the zebrafish embryo, we investigated processes resulting in tissue-specific accumulation of xenobiotics. The thesis distinguished between physico-chemical properties, i.e., different sorption properties of the chemicals and body compartments,

mode of toxic action of the chemical, biotransformation, and other unknown parameters inside the zebrafish embryo such as transporter proteins. Understanding the internal concentration and distribution of xenobiotics is crucial for interpreting chemical effects, predicting TK parameters, and extrapolating toxic effects from the zebrafish embryo to other vertebrates.[116] Different tissue-specific accumulations of chemicals are highlighted and linked to these processes by combining MS imaging and bulk analysis after solvent extraction in the following.

Physico-chemical properties

In Chapter 4, we focused on the two major body compartments, yolk and the rest of the embryo (termed as embryonic body). These body compartments dynamically develop during the first days. The yolk supplies the embryo with micronutrients, proteins, and lipids.[9] The size of yolk decreases over the development as the embryonic body increases. As shown in Chapter 3, the xenobiotic 4-iodophenol preferentially sorbed to the yolk during the first 48 h of exposure. The yolk sac is unique to the embryonic and larval developmental, and sorption properties of yolk proteins have not been systematically investigated. The aim was to answer the following questions: (i) Is a test substance evenly distributed between the yolk and the embryonic body? (ii) Can a partition experiment with pure yolk simulate the steady-state concentrations of a substance in the yolk? (iii) Is a steady-state and within which period reached in the embryo and its two compartments, and can this be predicted by a diffusive first-order kinetic model?

Therefore, mechanical sample preparation of the zebrafish embryo was developed to remove the yolk leaving the embryonic body intact (Chapter 4). The internal concentration in the embryonic body was then determined by bulk analysis comprising of LC-MS, GC-MS, and SFC-MS depending on the compound. Subtracting the internal amount in the embryonic body from the one in the whole embryo returned the amount in the yolk. In this study, seven chemicals were selected: five neutral (log K_{OW} 1.28 to 4.62), one anionic, and one cationic. Exposure to single compounds at concentrations, where no effect on the phenotypes was observed, for 24, 48, 72, and 96 h was started around 2 hpf. We were able to compare the amount in the yolk and embryonic body for the first three exposure durations; at 98 hpf, the mechanical separation of the yolk was not possible anymore. The results of the questions introducing the study are given in the following paragraphs:

(i) After 72 h, all neutral substances had reached a steady-state in the zebrafish embryo. This was in contrast to the ionic compounds' uptake kinetics; therefore, they are not discussed in (i+ii). Partition ratios showed, first of all, higher uptake with increasing log K_{OW} in the whole embryo. Secondly, stronger sorption of the neutral substances towards the yolk compared to the embryonic body was observed, supporting the hypothesis of different

sorption properties of the two compartments. The sorption was strongest for the compounds with the highest log K_{OW}.

Consequently, internal concentrations in the embryonic body are overestimated when determining internal concentrations for whole embryos (up to a factor of 5, Figure 7a) for the selected neutral compounds. Regarding absolute internal amounts, this effect is even more pronounced. Over the development, the percentage of the total amount in the yolk shifted towards the embryonic body representing volume and compositional changes. This process was pronounced less for the most lipophilic compound 1,2,4-tribromobenzene. For this substance, the mass ratio remained constant (Figure 7b). We hypothesized that an increased exposure during yolk utilization might be possible, which needs to be confirmed in future studies.

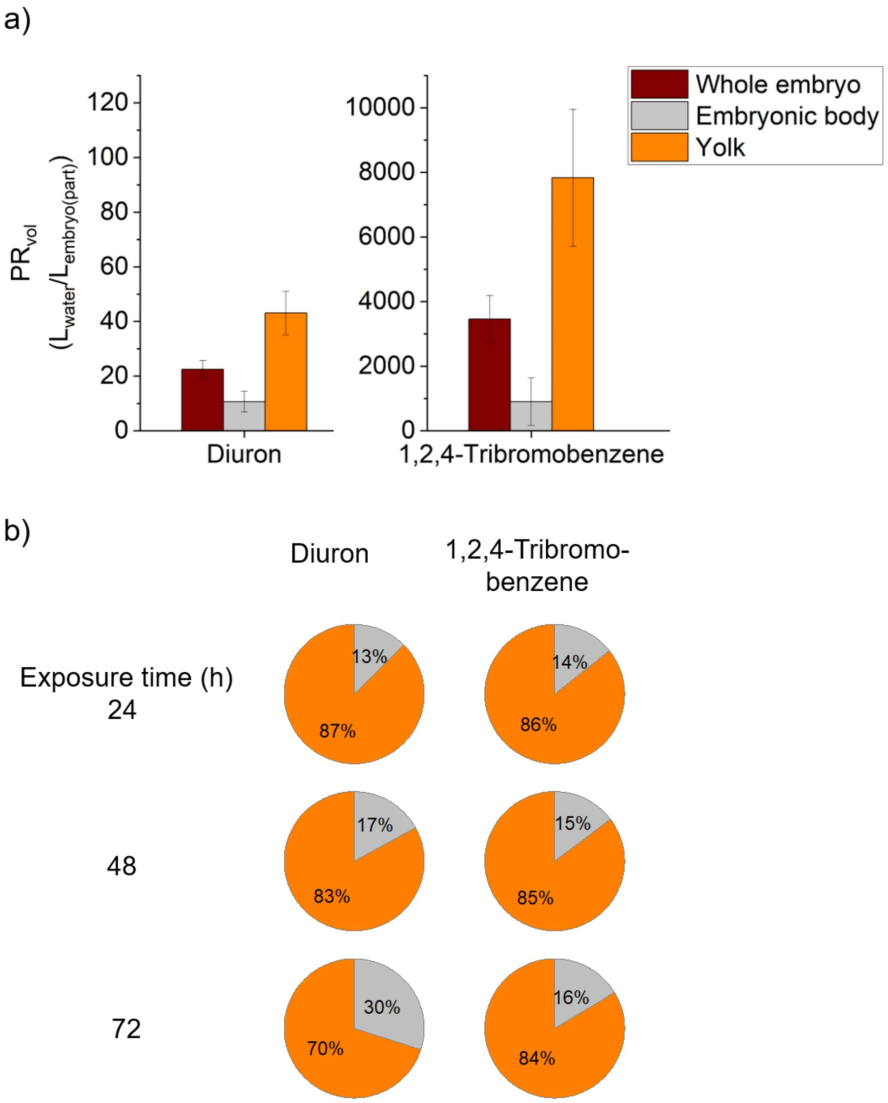

Figure 7. Partition ratios and internal amounts of diuron and 1,2,4-tribromobenzene in the whole embryo and the two body compartments, yolk and embryonic body. a) Partition ratios (Internal concentration divided by the external concentration) after 72 h of exposure at 74 hpf, n=6; b) fractions of the internal amounts in the yolk (orange) and embryonic body (grey) for 24, 48, and 72 h of exposure (start at 2 hpf), n=6.

(ii) In a dialysis approach with pure yolk (from embryos at 2 hpf), the partition coefficients of the five neutral substances were determined. This was compared to the partition coefficients of the internal measurements in the yolk at 26 hpf. The results were ambiguous: two substances possessed (circa 0.3 log units deviation) similar partition coefficients determined by the two different approaches; for the other three substances, differences up to one log unit were observed and may be related to either TK and -dynamic processes in the intact organism (quantitative contribution not known) or the noticed decomposition of the yolk in the dialysis approach. The latter might have slightly changed the sorption properties in the dialysis approach.

(iii) A first-order kinetic model was applied, accounting for an aqueous boundary layer, and diffusive transport through a single cell layer into the zebrafish embryo. For the neutral substances, good comparability was observed between predicted and measured uptake kinetics. The different sorption properties of the yolk and embryonic body did not result in different kinetics within the 24 h sampling frame. Shorter sampling times than 24 h would validate the model further.

The ionic compounds did not reach a steady-state within 96 h of exposure; however, the model predicted a steady-state within 24 h. It was shown that the even small neutral fraction (< 0.1%) should be sufficient for the steady-state establishment within 24 h. The ionic fraction itself possesses a very low membrane permeability. The reason for this discrepancy of the model and the measurements has yet to be explored. Though, we could rule out the chorion as a barrier.

Mode of toxic action

We just showed that the whole embryo's internal concentration over- and underestimates the concentration in the individual body compartments. Despite the effect of the physico-chemical properties on tissue concentration, we were interested in how a toxic effect affects the local concentrations.

LA-ICP-MS was used to investigate the uptake of the neuroactive compound naled. The bromine heteroatoms were used as a marker for naled. Naled is an acetylcholinesterase (AChE) inhibitor. As an AChE inhibitor, the compound covalently binds to the enzyme, inhibits acetylcholine's cleavage into acetate and choline, and thus causes hyperstimulation of the nerves and eventually the mortality of the embryo. The chemical bond to acetylcholinesterase results in the biotransformation of the compound.

Figure 6a shows that bromine strongly accumulated in the embryo's head and spine (Chapter 2). These are regions also rich in acetylcholinesterase. Hence, the spatial distribution presumably is a result of the mode of toxic action. The time course of the quantitative LA-ICP-MS and the colorimetric measurement of the effect significantly correlated. This further confirmed that the site where bromine accumulated represented the target site of effect. In this study, bromine was successfully used as a marker for the rapidly transformed AChE inhibitor, the site of reactive toxicity, and the quantification of the total uptake. This information would not have been accessible by bulk analysis.

In a project with Davi Farias's research group, we investigated the mode of toxic action of the veterinary antiparasitic moxidectin. Together with enzymatic analysis, MALDI-MS imaging was employed. Moxidectin accumulated in the eyes and head region of the zebrafish embryo.[115] This could induce eye damage as this was previously reported for ivermectin, also a macrocyclic lactone, and be related to the interaction with GABA receptors.

Biotransformation

While naled was transformed directly at the site of toxic action, other biotransformation sites were observed in this thesis. As mentioned earlier, LA-ICP-MS was used to investigate the spatial distribution of the iodine-containing compound 4-iodophenol (Chapter 3 and Chapter 6). This substance was described to sorb stronger to the yolk than to the embryonic body.

Furthermore, LC-HRMS also detected biotransformation products containing iodine. Quantitative LA-ICP-MS and Neb-ICP-MS of solvent extracts estimated the quantitative contribution of the metabolism (Chapter 6). After 96 h of exposure, only 11% of the total iodine was attributed to 4-iodophenol. With increasing exposure duration from 24 to 96 h, not only an accumulation in the yolk but also in the developing GI tract was measured (Chapter 3 and Chapter 6). After 96 h, 50% of the total iodine was in the GI tract. We were further interested in the elimination time of the transformation products. The elimination was investigated by placing the zebrafish embryo after exposure into clean water. While the parent compound was eliminated after 24 h, biotransformation products were still detected, and an iodine signal in the GI tract (Chapter 6). These results suggest that the GI tract likely contains high amounts of biotransformation enzymes, therefore, representing the site of biotransformation and also an elimination pathway. The accumulation in the GI tract is especially important for toxic transformation products that possess slow elimination kinetics, thus inducing a toxic effect even after exposure.

The bromine-signal of embryos exposed to bromoxynil was detected especially inside the GI tract with LA-ICP-MS (Chapter 5). As we identified several transformation products with LC-HRMS (Chapter 4), they presumably also accumulated in the GI tract.

We further explored whether the yolk is metabolically active as it was shown that the yolk processed lipids.[117] For this purpose, we used the data obtained from the yolk study (Chapter 4) of the three substances 4-iodophenol, bromoxynil, and diuron. We compared the peak areas of several transformation products in the whole embryo and the embryonic body. The major peak areas were found in the whole embryo and not the embryonic body indicating a preferential formation in the yolk. A high amount in the yolk indicates that the yolk is also active in the biotransformation of xenobiotics. However, diffusion of the transformation products into the yolk after the biotransformation in the embryonic body cannot be excluded but seems unlikely because the especially neutral lipophilic substances accumulated in the yolk in Chapter 4.

Finally, we investigated the uptake of the anionic clofibric acid. Unfortunately, the MALDI-MS imaging method was not suited to detect the parent substance. However, MALDI-MS imaging detected the taurine conjugated metabolite (Chapter 6). It is a phase II transformation product. We could measure the metabolite already after 48 h of exposure at 50 hpf. This agrees with the observations by Brox et al.[38] They detected the taurine metabolite as early as 3 h of exposure but in higher peak areas only from 48 h of exposure. With increasing exposure time, the area of the MALDI-MS imaging signal also increased. The signal was detected around the yolk, the YSL, and in the developing GI tract. Brox et al. discussed two enzymes involved in the taurine conjugation: acyl-CoA synthetases (ACS) and N-acetyl transferases (NAT).[38] While the expression in different tissues of NATs has not been reported yet, the spatial distribution of ACS[118] agrees well with the taurine metabolite's localization. This corresponding localization suggests that diffusive processes after the formation are not quantitatively relevant for this metabolite.

Our studies demonstrated that the GI tract largely biotransformed xenobiotics and indicated the yolk and the YSL might be involved in biotransformation as well.

Other parameters: transporter proteins and developmental changes

The anionic substance bromoxynil was the only substance from Chapter 4, which first showed a similar accumulation between the yolk and embryonic body and, with increasing exposure time, stronger sorption to the embryonic body. We were particularly interested in whether a specific tissue is responsible in the embryonic body for the stronger accumulation. Using LA-ICP-MS, we detected bromine in the center of the developing GI tract and with MALDI-MS imaging (Figure

8a) bromoxynil in the center of the GI tract and the head region (Chapter 5). We identified several bromine-containing transformation products of bromoxynil in embryo extracts. Therefore, LA-ICP-MS results also support the biotransformation in the GI tract.

Oats are known to be involved in the transport of chemicals from the GI lumen into the embryo. One representative is *dr*Oatp1d1 which was reported to be involved in transporting several environmental contaminants[119] and to be expressed in adult zebrafish, mainly in the liver and brain[120]. Based on the accumulation in the GI tract, we hypothesized the involvement of Oatp1d1. Thus, bromoxynil was tested as a substrate in Chapter 5. In addition to bromoxynil, diclofenac and carbamazepine were selected. Diclofenac has a similar acidity constant (pKa) as bromoxynil (3.99[110] for diclofenac and 3.75[109] for bromoxynil) and is a known substrate of Oatp1d1[119]. In contrast, carbamazepine was shown not to be transported or to a minor extent by Oatp1d1. Additionally, labeled bromosulfophthalein ([^{3}H]BSP) was included as a positive control.

We could observe that the Oatp1d1-mediated uptake into the cells of [^{3}H]BSP is increased as expected. In contrast to our expectations, Oatp1d1 was mediating the efflux of bromoxynil (Figure 8b) as well as diclofenac out of the cell. Because we directly measured the substances in the cells expressing Oatp1d1 and control cells (HEK-Co), we could show for the first time that the zebrafish embryo transporter Oatp1d1 is involved in the uptake and efflux of substances in the cells. Previous studies only indirectly measured the change of the uptake of a fluorescent substance.[119,121] Carbamazepine was not significantly transported under the chosen experimental conditions.

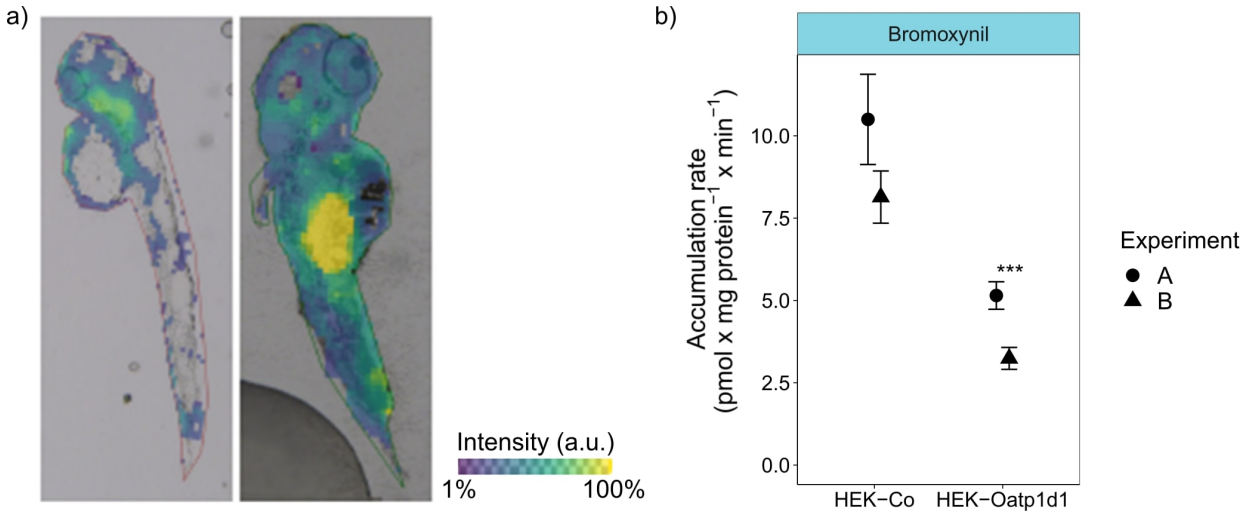

Figure 8. a) MALDI-MS imaging results of two zebrafish embryo sections (of two different individuals) after exposure to the EC5 (6.8 µM) of bromoxynil for 72 h (start at 1 hpf). Bromoxynil was measured in negative mode at 275.84671 m/z ± 0.19313 mDa. b) Uptake of bromoxynil (10 µM exposure) into control cells (HEK-CO) and cells expressing the organic anion transport Oatp1d1. Two independent experiments (A and B) are represented with three wells per concentration, respectively, mean ± SD. Net uptake values: -5.3 and -4.9; * indicates statistical significance (Manly's permutation test, *** $p < 0.001$).

We were interested in whether the addition of unlabeled BSP as a competing substrate of Oatp1d1 and thus as an inhibitor has a quantitative effect on the uptake in cell and zebrafish embryo experiments. However, BSP's effect in the cell experiments on the efflux of bromoxynil and diclofenac was ambiguous. In the zebrafish embryo experiments, the addition of BSP affected the toxicity and internal concentration. Elevated toxicities and internal concentrations of bromoxynil and diclofenac were observed. BSP may also interact with other transporter proteins, and therefore, a direct quantitative relation to Oapt1d1 could not be concluded.

Furthermore, the effect of BSP was more pronounced at the older developmental stage comparing a 24 h exposure starting at 1 hpf and 72 hpf, respectively. This indicated that the functionality of the BSP-modulated transporters is higher in the older developmental stages. This is in accordance with the reported higher expression of three Oats proteins with increasing developmental stage.[122]

Despite the effect of the BSP addition in the zebrafish embryo experiments, the uptake without the BSP addition was also higher at the older stage for bromoxynil and diclofenac (three times for diclofenac and seven times for bromoxynil). This can also be related to higher expression of transporter proteins and/or developmental characteristics such as the GI tract's opening[14]. It is exciting because the uptake kinetics of bromoxynil also attracted attention in Chapter 4. This was because the slow uptake over 96 h of exposure deviated from the predicted steady-state time of 24 h in Chapter 4. Therefore, Oats' functionality changes with the advancing development or the GI tract opening might be quantitatively involved in the uptake kinetics.

1.4 Discussion

Objective I: Method development of LA-ICP-MS analysis and MALDI-MS imaging of zebrafish embryos

The first objective was to develop imaging workflows for LA-ICP-MS and MALDI-MS to detect anthropogenic chemicals in the zebrafish embryo. With the developed workflow and software FishImager, we could produce quantitative LA-ICP-MS data and show the precision (including biological variability) between repeated measurements. This represents a significant scientific contribution because repeated measurements are often missing in clinical studies due to limited tissue samples.[61,123,124] Our approach generally provides a better quality assessment than the comparison of total internal amounts[93,125] because the applied Kernel density estimates comprised the measured intensity distribution data to assess the precision. With FishImager, we can go a step further and compare the internal amounts per body compartment to segmented LA-ICP-MS data after clustering. The user can test different cluster algorithms and modify input parameters. K-means, fuzzy, or hierarchical clustering have only singularly been applied before[73,126–129], which is why we are able to report the first comparison of different cluster algorithms with LA-ICP-MS data of biological tissues. Furthermore, the segmentation resulting from the cluster analysis has not been systematically compared with biological features. FishImager achieves this by visualizing the clustering results together with biological features in heatmaps.

We selected compounds containing bromine or iodine in the thesis, as LA-ICP-MS requires heteroatoms that are naturally not present in the zebrafish embryo. This thesis applies, for the first time, elemental imaging to study the spatial distribution of organic molecules containing heteroatoms in the zebrafish embryo. Before the distribution of natural elements[130] or nanoparticles[48] was investigated with LA-ICP-MS. While the selection of chemicals is restricted, the use of marker atoms (a marker for the organic chemical) can be useful to reveal the distribution of the parent compounds together with the transformation products. This may be especially useful when substances are rapidly transformed (Chapter 2).

In this thesis, we applied both LA-ICP-MS and MALDI-MS imaging on separate embryos due to the sensitivity of the ICP-MS. With a faster and more sensitive ICP-MS (e.g., ICP-quadrupole-MS or ICP-ToF-MS), a combination of LA-ICP-MS and MALDI-MS imaging on the same embryo section may be possible in the future. The approach has been demonstrated for a human tumor sample in 2018[129] and can achieve a distinction of the parent substance and the transformation products containing a heteroatom at the same time. In this case, MALDI-MS imaging is applied

before LA-ICP-MS. Furthermore, the developed software FishImager can also be used in the future for the MALDI-MS imaging data, and we implemented a tool for LA-ICP-ToF-MS data processing.

We combined LA-ICP-MS and MALD-MS imaging on embryos exposed under the same conditions to bromoxynil (Chapter 5). Both imaging techniques were then carried out on separate embryos to map bromine-containing compounds and bromoxynil. The results of both techniques supported each other. Furthermore, the bromine-containing transformation products are likely formed or accumulate in the GI tract, and the parent compound concentrate in the GI tract and the head. The combination of both techniques was superior to only MALDI-MS imaging because the method was not sensitive to detect single transformation products. This was likely due to the low amount formed (Chapter 4).

When analyzing zebrafish embryos exposed to clofibric acid, only the taurine metabolite was detected and not the parent substance or other transformation products (Chapter 6) with MALDI-MS imaging. We applied the matrix 9-AA via sublimation for clofibric acid. An additional recrystallization step[97] after the sublimation could further increase the substances' extraction and consequently the sensitivity of the MALDI-MS imaging method and should be considered in the future.

Apart from the localization of natural constituents such as various lipid species[49,51] and copper[130], studies also mapped anthropogenic components. Spatial distributions of nanoparticles[48,131], heavy metals[132], and psychoactive substances[50] have been reported using MS imaging. Besides the first studies by Böhme et al.[48,131] in 2015, the other studies[49–51,130,132] have been published since 2016, thus during the time the research for this thesis has been conducted.

Böhme et al.[48] presented ablated cryosections of the embryo exposed to nanoparticles with a 50 µm resolution. The chosen presentation of the results as contour plots, unfortunately, does not allow the distinction between measured data and interpolation. Additionally, the presented quantification was not satisfying compared to Neb-ICP-MS results. In contrast, the results in this thesis showed reliable quantification due to numerous ablated embryos and the approach of the ablation of the dried whole embryo instead of sections. By dividing the measured intensity with the carbon signal, we are able to normalize the signal to the tissue density. A combination of the ablation of whole embryos for quantification and of sections for better organ assignment can be used in the future, making Neb-ICP-MS measurements superfluous.

The analysis time reported by Zarco-Fernández et al.[132] in 2018 was rather time-consuming (3-8 h), also involving an additional gold metallization step compared to the measurement time of circa 20 min – 1 h per embryo in this thesis. However, the authors also ablated whole embryos resulting in a good visualization of mercury and cadmium distribution in zebrafish embryos after exposure to the metals. Their interpretation was based only on visual inspection. Hence, statistical quantification for the accumulation is not provided.

Ackerman et al.[130] studied the copper distribution (based on a quadrupole ICP-MS) in cryosections of zebrafish embryos using LA-ICP-MS. Their data analysis was based on manually drawn ROIs and quantification in the respective ROI. Due to the high sensitivity of the used ICP-MS, they reported a spatial resolution of 6 µm of the endogenous metal distribution in their study in 2018. This improves resolution by a factor of 6 (best LA-ICP-MS resolution is 35 µm in this thesis) and demonstrates that the choice of the ICP-MS instrument coupled to the laser is essential to reach the highest possible spatial resolution. In Figure 9, the result of an ablated zebrafish embryo with the LA-ICP-ToF-MS is presented to compare with the sector field instrument used throughout this thesis. The ICP-ToF-MS only became available at our facility in 2020. Due to the high-speed detection of a complete mass spectrum, the actual resolution is smaller than the spot size of the laser.

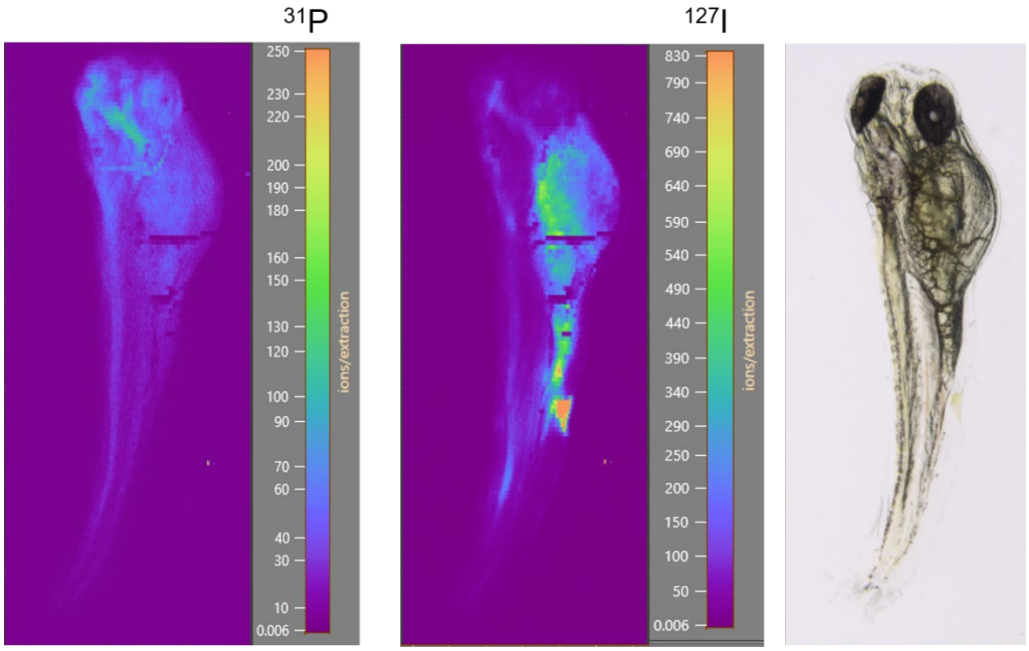

Figure 9. LA-ICP-MS intensities of ^{31}P and ^{127}I for a zebrafish embryo (microscopic image to the right) exposed for 96 h to 4-iodophenol. The spot size was 25 µm and scan speed 25 µm/s.The analysis was carried out with an LA-ICP-ToF-MS. (Measurements were conducted by Timothy Holbrook)

Overall, we provide a novel approach for the ablation of whole organisms using carbon as an internal standard resulting in good quantification. Furthermore, we show that a combination of

ablation of whole embryos and sections can make digestion and consecutive Neb-ICP-MS measurements redundant. With the developed software FishImager, we improve the time of the data analysis and support visual inspection with clustering and segmentation into morphological ROIs.

Objective II: Identification of the mechanisms behind the accumulation patterns of xenobiotics in the zebrafish embryo

The thesis integrated the spatial patterns of the xenobiotics with underlying mechanisms to tackle the second objective: improving the knowledge of TK processes in the zebrafish embryo. The spatial distribution of substances as part of the ADME concept is essential for the correct prediction of bioaccumulation and toxicity.[133,134] The increased results for the hits on Google Scholar (Figure 10) for "MS-imaging zebrafish embryo" also underline the recent focus researchers have placed on investigating distributions inside the organism.

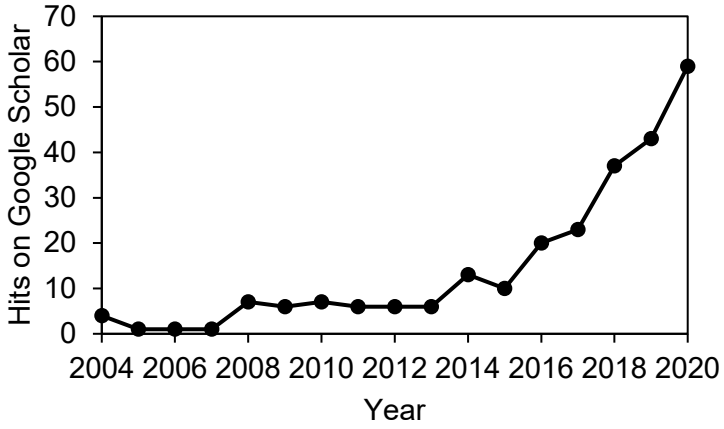

Figure 10. Hits per year on Google Scholar for "MS-imaging zebrafish embryo" (accessed 5.1.2021).

So far, only a relatively small spectrum of anthropogenic substances and their spatial accumulation inside the zebrafish embryo has been investigated, and this could be complemented by nine new anthropogenic substances (Figure 11) in our studies. We applied LA-ICP-MS, MALDI-MS imaging, and a mechanical technique separating the embryonic body from the yolk with subsequent bulk analysis. The selected compounds accumulated in the following body compartments: yolk, head, and GI tract. The assignment is made on the µm-resolution, which prohibits a further distinction of smaller body compartments, e.g., liver, kidney, and intestine.

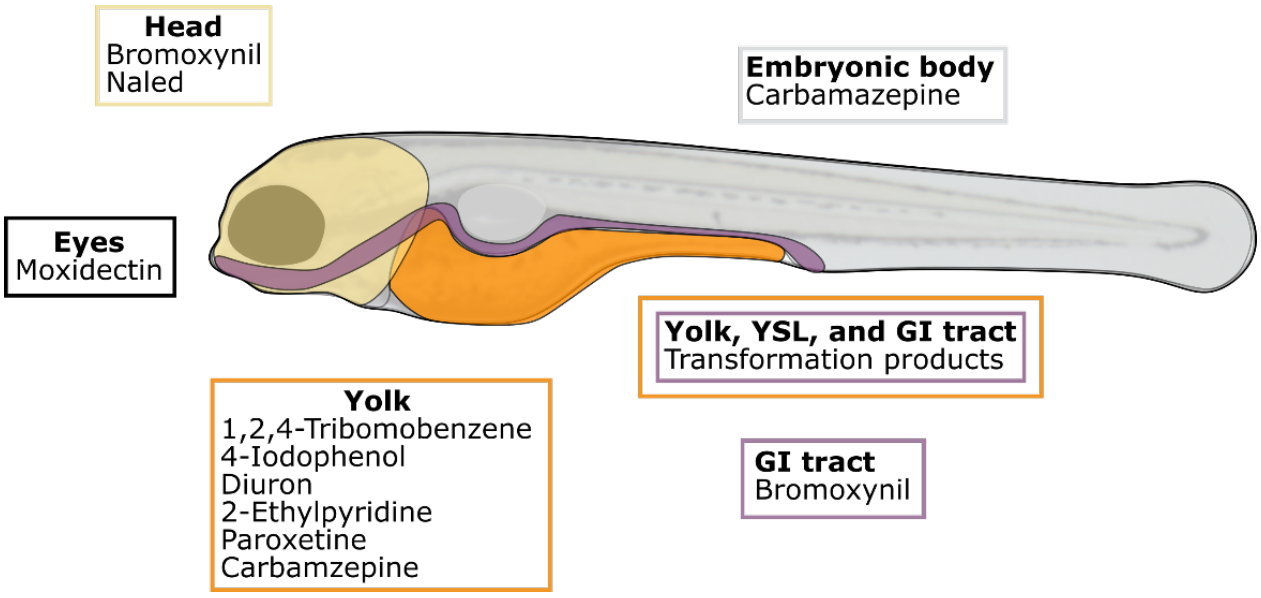

Figure 11. Overview of the body parts of the zebrafish embryo with the predominant accumulation of selected chemicals. YSL: yolk syncytial layer, GI: gastrointestinal

Yolk and yolk syncytial layer

Our study in Chapter 4 systematically investigated, for the first time, the internal concentration in the yolk for several compounds. The yolk's internal concentration was up to 5 times higher than in the embryonic body. This is in the same order of magnitude as the differences observed for the estradiol uptake into the yolk and embryonic body.[135] The sorption to the lipid-rich yolk increased with increasing log K_{OW} of the neutral substances in our study. This proportional relationship was confirmed by Ulrich et al.[136] with comprehensive research on yolk/water partition coefficients determined in the dialysis approach with pure yolk (also used for the seven compounds in Chapter 4). In their study, which was published in parallel with our study in 2020, they expanded the number of neutral substances. The authors found a correlation between the log $K_{yolk/water}$ and log K_{OW}. A polyparameter linear free energy relationship model to predict yolk-water partitioning was developed. Their model allows the prediction of the internal concentrations in the yolk for neutral substances in the future.

However, the model based on the dialysis approach by Ulrich et al.[136] neglects biotransformation and active transport. Our study demonstrates that these processes likely have a quantitative influence on the distribution of three of the five neutral compounds. Besides the accumulation potential of chemicals in the yolk, two other questions arise: 1) Does the accumulation in the yolk increase the embryo's exposure through the yolk consumption? 2) Is the yolk involved in the biotransformation?

Concerning the first question, we measured internal concentrations in the yolk and embryonic body at three different developmental stages (26, 50, and74 hpf). The experiments showed that neutral substances of low or medium hydrophobicity quickly re-established the steady-state when the yolk is depleted. In contrast, the concentration in the yolk of the most hydrophobic compound 1,2,4-tribromobenzene (log K_{OW}=4.62) increased, although a steady-state was observed in the whole embryo. This suggests that for the lipophilic substances, the re-establishment of the steady-state in the yolk while the yolk is absorbed can be slower than the absorption process itself, creating an internal concentration higher than the steady-state concentration in the yolk. This is the first time that this research question could be addressed with experimental data. For lipophilic compounds, additional exposure can be theoretically possible, and this should be investigated further in the future.

Concerning the second question, it was recently shown that the yolk is involved in lipid processing[117,118] before these are transported via the YSL into the embryonic body. Before the organs, e.g., liver and kidney with major biotransformation enzymes, are developed, the yolk may also be an important site for biotransformation of xenobiotics. Brox et al.[34] showed that even in the early developmental stages, biotransformation occurs. In our study (Chapter 6), differences between the intensities of the transformation products detected in the embryonic body and the whole embryo suggest that the yolk may be involved in the biotransformation. We also reveal that clofibric acid is transformed to the taurine conjugate in the YSL. According to Brox et al.[38], the enzymes acyl-CoA synthetase (ACS) and N-acetyl transferase (NAT) are involved in taurine formation. ACS is expressed in the YSL and GI tract, which is in agreement with our spatial data.[118,137] Spatial expression data of NATs in the zebrafish embryo are not yet available. The EROD (7-ethoxyresorufin-O-deethylase) assay provides information on receptor-mediated induction of CYP4501A1-dependant monooxygenases. Spatiotemporal patterns of the EROD activity of zebrafish embryos exposed to β-naphthoflavone also showed activity in the YSL.[138] Benzo[a]pyrene was also shown to be metabolized in the YSL of Medaka embryos.[139] The spatial distribution of the taurine metabolite provides further evidence for the biotransformation activity of the YSL and the localization of the transformed compound in the YSL.

To summarize, the yolk is a compartment with high sorption capacity, especially for neutral lipophilic compounds, thus reducing the bioavailable amount of the total internal amount. With this finding, internal concentrations of substances in the whole zebrafish embryo can be better interpreted in the future regarding their preferred body compartment. Furthermore, we present strong indications that the yolk and the YSL might also be involved in the biotransformation.

Head

The second body compartment of interest is the head. While bromoxynil was only accumulating in the head to a minor fraction compared to the GI tract, the AChE inhibitor naled strongly accumulated here. The bromine/carbon ratio was three times higher in this region than in the rest of the embryo. This enrichment is likely caused by the reactive toxicity (transforming naled) at the AChE rich regions[140,141]: the brain and the spine. In another study by Muniz et al.[115], we detected that the antiparasitic drug moxidectin accumulated in the eyes. This was related to the interaction with GABA receptors and thus also associated with the target site. Kirla et al.[50] also showed that the melanin content in the head, namely in the eyes, can result in a substantial accumulation (about three-four times higher concentration than in the brain or trunk) and slower elimination kinetics. Our main finding is that the head accumulates the xenobiotic as the cause of the neuroactive mode of toxic action. Thus, the toxicodynamic process causes the distribution.

Gastrointestinal tract

The third body compartment of interest is the GI tract. We could show that 1) biotransformation products strongly accumulated there (of 4-iodophenol, bromoxynil, and the clofibric acid taurine transformation product) and 2) bromoxynil itself.

1) Biotransformation of xenobiotics can cause an accumulation in the tissue, which predominantly expresses the respective transforming enzymes. Furthermore, redistribution of transformation products may occur for, e.g., elimination.

   Iodine signal intensities were four times higher (Chapter 3) in the GI tract than in the yolk or head, and 50% of the total iodine amount accumulated here after 96 h of exposure. The signal intensities of the clofibric acid taurine metabolite were up to one order of magnitude higher in the center of the GI tract compared to surrounding tissue (Chapter 6) after 96 h of exposure. For the taurine transformation product of clofibric acid, we revealed that as early as 48 hpf, the transformation occurs in the GI tract and in the YSL, as previously discussed. Redistribution processes (e.g., passive diffusion) inside the zebrafish embryo were not quantitatively important since the taurine transformation product accumulated from 72 to 96 hpf in the GI tract. Passive diffusion likely could have changed the distribution in the time interval of 24 h.

   The spatial distribution of transformation products in the GI tract can presumably be related to the development of organs like the liver and kidney, largely expressing enzymes that transform the xenobiotic.[13,142,143] The kidney and liver start to differentiate at 26 hpf.[144] For

many CYP genes, an increased expression with the zebrafish embryo development has been shown.[145] The CYP enzymes concentrate in the kidney or liver but are also expressed in the whole embryo until 48 hpf and later in the brain, pharynx, cardiovascular system, and GI tract.[36,143] Additionally, biotransformation activity of a CYP1-specific and a non-specific substrate was reported in the intestine[11] as well as metabolites of benzo[a]pyrene that were also detected in the GI tract in medaka embryos.[139] Furthermore, the GI tract represents an important elimination route for xenobiotics. This includes the organs pronephros and later kidney; the glomerular filtration starts around 40-48 hpf.[146]

2) In Chapter 4, bromoxynil was the only compound out of the seven tested chemicals that showed stronger uptake by the embryonic body than the yolk (67% in the embryonic body at 72 h of exposure). MALDI-MS imaging showed that bromoxynil is not equally distributed in the embryonic body but accumulated in the GI tract (up to 4 times higher intensities than in the rest of the embryo, Chapter 5). While the previously discussed localization of transformation products in the GI tract is likely linked to the transforming enzyme expression, the strong observed accumulation of bromoxynil is particularly interesting, pointing towards the involvement of transporter proteins, uptake, or the elimination via the GI tract.

   We confirmed the hypothesis of the involvement of an Oat protein for cellular transport for bromoxynil. The transporter protein Oatp1d1 exports bromoxynil out of cells expressing Oatp1d1 and is presumably located in the GI tract (only spatial distributions for adult zebrafish are available). Nano- or ToF-SIMS may further confirm the location of bromoxynil outside the cell in the GI tract and not inside the cell by their capabilities to measure single cells. This could reveal whether bromoxynil is located inside or outside the cell in the GI lumen.

   Besides the involvement of transporter proteins leading to the GI tract accumulation inside the zebrafish embryo, another explanation could be a) the mouth-opening and b) the elimination pathway.

   By 74-76 hpf, the lumen from the mouth to the anus has been developed. While the mouth has opened, the anus is still closed (until circa 102 hpf)[144], which could result in an accumulation of xenobiotics in the GI tract before this elimination route is active. Furthermore, excretion processes may be involved in eliminating the xenobiotic and hence the spatial distribution. The excretion route has been suggested to be important for some ionizable compounds.[147]

In conclusion, we show that the whole GI tract, including the intestine and liver, is an important organ for biotransformation. This is supported by the signals along the GI tract for all transformation products in this thesis and not only in the anterior of the GI tract where the liver is located. The processes driving the accumulation of bromoxynil inside the GI tract remain yet to be determined.

Prediction of uptake kinetics

Another aspect of this thesis is the prediction of uptake kinetics for the yolk and embryonic body to answer the question of whether the different sorption properties result in different uptake kinetics into the two compartments? As the usual FET is performed for 96 h, a quick steady-state establishment of the investigated chemicals is essential to predict the correct toxicity values and not to miss any toxicity possibly occurring at longer exposure times. We used an analytical solution developed by co-workers[148] for the steady-state prediction of neutral substances. The Excel file can be used by other zebrafish embryo researchers for more neutral compounds. We provided indications for the validity of the model for neutral substances; however, shorter sampling time points within the first 24 h of exposure should further confirm this. An important finding is that the different partition coefficients and the volume differences of the yolk and embryonic body do not result in large (>24 h) uptake differences into the two body compartments for the selected compounds.

Moreover, we show that for very lipophilic substances (log K_{OW} > 4.6), a steady-state within 96 h of exposure may not be reached, and reported BCF might not correspond to an established steady-state.[31,39] Our reported quick uptake kinetics for carbamazepine also explained a low sensitivity of carbamazepine for the behavioral toxicity endpoint, the spontaneous tail coiling.[149]

While we successfully demonstrated the applicability of the model for neutral compounds, a deviation of the prediction for the two ionic compounds occurred. The model predicted an equilibrium within 24 h for bromoxynil (anionic) and paroxetine (cationic), in contrast, the observed uptake curves differed: bromoxynil was slowly taken up over 96 h until reaching the steady-state concentration calculated from the dialysis approach; the concentration of paroxetine continuously increased in the zebrafish embryo over 120 h and the concentration after 120 h was higher than the steady-state concentration in the dialysis approach.

Table 2 summarizes the substances that showed a slow/continuous uptake or difference between internal amounts of developmental stages.

First, 2,4-D and the perfluorinated alkyl acids should be carefully considered as in these cases, the total anionic fraction is 100% at exposure pH, and thus, the membrane permeability may be too low to be quickly taken up by the zebrafish embryo. As the partition coefficients are not easily predictable for ionic compounds using, e.g., the LSER database[35], it is difficult to apply our kinetic model for these four compounds. The impact of the very small neutral fraction on the uptake kinetics is, therefore, demonstrated with the two ionic compounds, bromoxynil and paroxetine. For bromoxynil, a shift from 2.2 x 10^{-4} neutral fraction at pH = 7.4 to 2.2 x 10^{-7} results in a decreased membrane permeability and an equilibration time > 96 h for the zebrafish embryo; likewise, for paroxetine, a shift from 6.3x 10^{-3} to 6.3x 10^{-8} neutral fraction leads to a time for the equilibrium > 96 h (Figure 12). Thus, an exact pKa value and pH of the exposure are important to model ions' uptake kinetics.

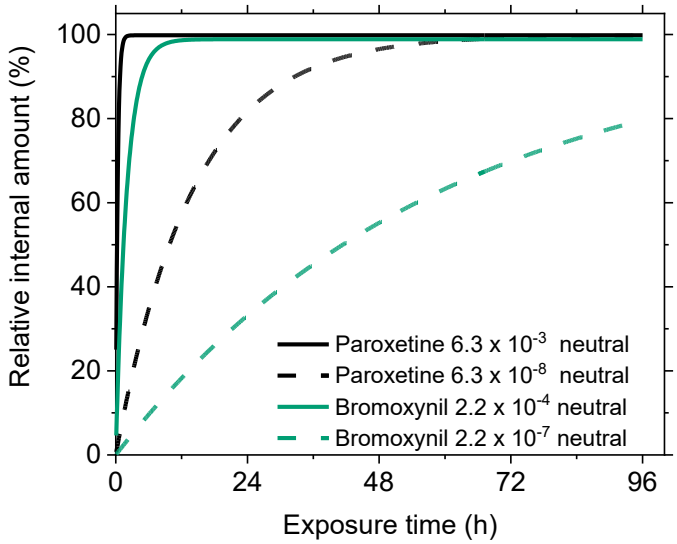

Figure 12. Modeled relative internal amount (in %) to the equilibrium concentration in the embryonic body versus exposure time, assuming first-order uptake kinetics. Black (paroxetine) and green (bromoxynil) lines display the consequence of the neutral fraction on the uptake kinetics of the ionizable compounds. Solid lines represent the actual neutral fraction at pH = 7.4 and dashed lines a theoretically smaller fraction.

Table 2. Substances with reported slow/continuous uptake or reported uptake changes with increasing developmental stage. Slow/continuous uptake refers here to a steady-state state establishment > 48 h of exposure and which cannot be explained by a high hydrophobicity. n.a.: no data available

Substance	Major species at pH=7.4[104]	Study of internal concen-trations	Slow/ continuous uptake	Higher uptake amount at older developmental stage
2,4-D	100% anionic	[34]	Yes	n.a.
Bromoxynil	99.49% anionic	Chapter 4, Chapter 5	Yes	Yes
Caffeine	100% neutral	[34]	Yes	n.a.
Clofibric acid	99.99% anionic	[34]	Yes	n.a.
Diclofenac	99.96%anionic	[150]	Yes	Yes
Diphenhydramine	96.7% cationic	[45]	Yes	Yes
Metoprolol	99.46% cationic	[34,151]	Yes	n.a.
Paracetamol	99.15% neutral	[44]	No	Yes
Perfluorooctanesulfonat, perfluorooctanoic acid, perfluorohexanesulfonic acid	100% anionic	[46]	Yes	Yes
Thiacloprid	100% neutral	[34]	Yes	n.a.
Valproic acid	99.45% anionic	[34]	Yes	n.a.

Biotransformation, active transport, and dynamic developmental changes (e.g., organ differentiation, elimination routes) are not considered in the kinetic uptake model (Chapter 4). These three factors possibly influencing uptake kinetics are discussed in the following.

1) Biotransformation would result in an even faster steady-state establishment; thus, it cannot explain the observation.

2) Active transport comprises uptake and efflux and many different transporter proteins and displays, thus a very complex process.[120,152,153] It may affect the uptake via the epidermis; additionally, spatial distributions inside the embryo (as demonstrated above for bromoxynil) can be altered, consequently resulting in an even more complex situation.

   Studies on the quantitative influence of the transporter proteins in the zebrafish embryo are rare. The few available studies on the efflux transporter demonstrated that the internal concentration of the fluorescent compound rhodamine B was changed when different Abcb4 substrates were added as an inhibitor.[154] We could present the involvement of Oatp1d1 in the export of bromoxynil out of the cell, but we could not assess how this specifically and quantitatively contributes to the uptake kinetics of bromoxynil in the zebrafish embryo. BSP as an Oatp1d1 inhibitor but also presumably inhibitor for other Oats increased the internal concentration of bromoxynil up to a factor of two. Thus, Oats likely decreased the steady-state concentration in experiments without the inhibitor. Our result contributes to the description of transporter proteins and shows that also Oats act as efflux transporters. While one can argue that bromoxynil is a single case, similar slow uptake was observed for diclofenac and clofibric acid.[34,150] All three substances are more than 99.9% anionic at the usual FET pH of 7.4. Therefore, exploring the uptake mechanisms of these three anionic substances should be targeted in future studies.

   Furthermore, our results for paroxetine also point towards an active uptake mechanism. The internal concentration of paroxetine was also higher after 96 h of exposure than the steady-state concentration obtained in the dialysis approach (Chapter 4). For the two cationic psychoactive substances, cocaine and meta-chlorophenylpiperazine, an active uptake mechanism has been suggested because the uptake was higher than predicted[50]. In this case, organic cation transporter proteins are possible candidates.

3) The dynamic development also influences uptake kinetics in the zebrafish embryo and also comprises the two before mentioned factors. The embryo rapidly develops during the 96 hpf with major organ differentiation.

For bromoxynil and diclofenac, our experiments showed that the developmental stage impacts the amount taken up (Chapter 5). Three to seven times higher internal concentrations were observed comparing the 24 h exposure for the embryonic (start at 1 hpf) and the larval stage (start at 72 hpf). The slope of the uptake curve for paroxetine (Chapter 4) could suggest that a stronger absorption at the older stage is also occurring for this cationic compound. We could exclude influences of the chorion for bromoxynil and paroxetine. This agrees with previous studies suggesting the chorion as a barrier only for large compounds (> 4000 Da).[45,47,155] In literature, the developmental stage of the early life stage of the zebrafish also had a lower sorption capacity for the neutral paracetamol and cationic diphenhydramine.[44,45]

These observations may be linked to the dynamic development of the zebrafish embryo affecting the sorption properties of the tissues. Sorption properties determine the partition coefficient, i.e., the thermodynamic equilibrium situation, and, therefore, also the required time to reach a steady-state. A sorption capacity increase for paracetamol was hypothesized by van Wijk et al.[44] to be related to the opening of the GI tract. Furthermore, developmental changes also include the expression of the above-discussed transporter proteins. Many of these show an increased expression with development.[121,156] Additionally, Kristofco et al.[45] mentioned gill functional shifts, and Kirla et al.[157] showed that melanin-binding influences the TK, and melanin-pigmentation increases with embryonic development[158]. The net charge and thickness of the mucus hydrogel surrounding the embryo might also reduce the uptake kinetics.[147]

To summarize, the provided kinetic model and prediction tools of partition coefficients, such as the LSER database, were proven to reliably calculate uptake kinetics of neutral substances. The sorption differences between the yolk and embryonic body do not drastically deviate for the selected compounds, and thus uptake kinetics are similar between the two compartments. The factors explaining the uptake kinetics of ions and developmental differences should be systematically investigated in the future.

1.5 Future perspectives

Considering the open questions remaining after the study of the TK processes of ten xenobiotics, I recommend a close investigation of bromoxynil, diclofenac, and clofibric acid because these three compounds possess uptake kinetics and similar pKa values. Future studies should elucidate the GI tract accumulation in relation to transporter proteins, elimination pathway, or sorption. Thereby, a systematic understanding of the anionic compounds may be achieved.

This work indicated that the GI tract is likely involved in the biotransformation, accumulation, and elimination, thus accumulating high amounts of xenobiotics and their transformation products. The zebrafish embryo has also been proposed as a model organism to study xenobiotic - microbiota interactions.[159] Therefore, changes in the microbiota (colonizing starts around 3 dpf[159]) after exposure to, e.g., 4-iodophenol and bromoxynil should be tested. Research should explore how xenobiotic exposure and microbiota interact and in relation to the zebrafish embryo's development.

We found several accumulation sites of biotransformation products, indicating a co-localization of the transforming enzyme and transformation product. The site of the transforming enzyme can be directly linked to the accumulation of transformation products combining changes in gene regulation with time-profiles of internal concentrations. Enzymatic biotransformation is then detected via gene upregulation and may further correlate with internal concentration kinetics. MS imaging may complement information about the localization of the biotransformation. This would be particularly interesting when the transformation product is more toxic than the parent, e.g., acridine and carbamazepine.

To further enhance the understanding of uptake kinetics of toxic substances, the substances listed in Table 2 should be further explored. These showed particular slow or continuous uptake kinetics and differences between the developmental stages. MS imaging can certainly contribute to identifying underlying processes. A thorough understanding of the uptake kinetics is essential for toxicity prediction.

A focus was placed on the two MS imaging techniques LA-ICP-MS and MALDI-MS imaging, because they reveal accumulation sites in the µm-range with an acceptable measurement time. Other imaging techniques can complement information on TKTD processes. ToF-SIMS[160] or Nano-SIMS can map organic components in the nm scale and thus add information on sub-organ-distributions. Xenobiotics could be spatially mapped using these imaging techniques, but also, the dynamic changes of biological constituents during the exposure could be assessed. Confocal Raman spectroscopy imaging was recently used to map proteins, lipids, and carotenoids and

regions rich in collagen, DNA, cytochrome in zebrafish embryos.[161] Desorption electrospray ionization (DESI) MS imaging also exhibited lipid dynamics during embryonic development.[49] Furthermore, changes of natural components during exposures with toxic components can be imaged. This could be relevant for the compounds highly accumulating in a body compartment leading to tissue changes. Pirro et al.[49] were able to identify changes in the lipid profile after trichloroethylene exposure. Their study using Raman imaging demonstrated tissue changes due to wound response and after mycobacterial infections.[161] LA-ICP-MS combined with Nano-SIMS showed changes in the copper distribution, mainly in the retina in the zebrafish larva induced by the Menkes disease.[130]

1.6 Conclusions

The research results demonstrate that tissue-specific distributions are quantitatively important and advance the understanding of TK processes in the zebrafish embryo by the following achievements:

- FishImager promotes the study of the spatial distribution of xenobiotics using LA-ICP-MS and MALDI-MS imaging. FishImager combines imaging data analysis with biological features and statistical methods such as clustering.

- LA-ICP-MS and MALDI-MS imaging are sufficiently sensitive to detect dynamic changes in the distribution with exposure time and development of the specimen. Both methods can be applied throughout the development of the zebrafish embryo. This makes them superior to mechanical organ separation, which is often restricted to specific developmental stages.

- Quantitative LA-ICP-MS can trace marker atoms for reactive toxicants and supersede digestion and subsequent Neb-ICP-MS.

- Reasons for accumulation patterns depend on physico-chemical properties, the mode of toxic action, metabolism, and presumably active transport. The dynamic development of the zebrafish embryo influences the magnitude of these parameters. Compound concentrations varied between different tissues within one order of magnitude. Thus, internal concentrations in whole embryos under- or overestimate organ concentrations.

- It was shown for the first time that neutral substances with increasing hydrophobicity are taken up stronger by the yolk.

- Reactive toxicity can cause an accumulation at the site of effect. Quantitative spatial data can be representative of the time course of the effect.

- It was revealed that transformation products were especially located inside the GI tract. The GI tract, the yolk, and YSL may be involved in the biotransformation of xenobiotics.

- Transporter proteins had a quantitative effect on the steady-state concentration of three compounds.

- The diffusive first-order kinetic model can be used to predict uptake kinetics for neutral compounds into the zebrafish embryo.

References

(1) EC Inventory - ECHA https://www.echa.europa.eu/information-on-chemicals/ec-inventory (accessed Dec 3, 2020).

(2) Loos, R.; Carvalho, R.; António, D. C.; Comero, S.; Locoro, G.; Tavazzi, S.; Paracchini, B.; Ghiani, M.; Lettieri, T.; Blaha, L.; et al. EU-Wide Monitoring Survey on Emerging Polar Organic Contaminants in Wastewater Treatment Plant Effluents. *Water Res.* **2013**. https://doi.org/10.1016/j.watres.2013.08.024.

(3) Scholz, S.; Fischer, S.; Gündel, U.; Küster, E.; Luckenbach, T.; Voelker, D. The Zebrafish Embryo Model in Environmental Risk Assessment - Applications beyond Acute Toxicity Testing. *Environ. Sci. Pollut. Res.* **2008**, *15* (5), 394–404. https://doi.org/10.1007/s11356-008-0018-z.

(4) Strähle, U.; Scholz, S.; Geisler, R.; Greiner, P.; Hollert, H.; Rastegar, S.; Schumacher, A.; Selderslaghs, I.; Weiss, C.; Witters, H.; et al. Zebrafish Embryos as an Alternative to Animal Experiments-A Commentary on the Definition of the Onset of Protected Life Stages in Animal Welfare Regulations. *Reprod. Toxicol.* **2012**, *33* (2), 128–132. https://doi.org/10.1016/j.reprotox.2011.06.121.

(5) Weigt, S.; Huebler, N.; Strecker, R.; Braunbeck, T.; Broschard, T. H. Zebrafish (Danio Rerio) Embryos as a Model for Testing Proteratogens. *Toxicology* **2011**, *281* (1–3), 25–36. https://doi.org/10.1016/j.tox.2011.01.004.

(6) Sipes, N. S.; Padilla, S.; Knudsen, T. B. Zebrafish-As an Integrative Model for Twenty-First Century Toxicity Testing. *Birth Defects Research Part C - Embryo Today: Reviews*. September 2011, pp 256–267. https://doi.org/10.1002/bdrc.20214.

(7) Weigt, S.; Huebler, N.; Strecker, R.; Braunbeck, T.; Broschard, T. H. Zebrafish (Danio Rerio) Embryos as a Model for Testing Proteratogens. *Toxicology* **2011**, *281* (1–3), 25–36. https://doi.org/10.1016/j.tox.2011.01.004.

(8) Gunnarsson, L.; Jauhiainen, A.; Kristiansson, E.; Nerman, O.; Larsson, D. G. J. Evolutionary Conservation of Human Drug Targets in Organisms Used for Environmental Risk Assessments. *Environ. Sci. Technol.* **2008**, *42* (15), 5807–5813. https://doi.org/10.1021/es8005173.

(9) Sant, K. E.; Timme-Laragy, A. R. Zebrafish as a Model for Toxicological Perturbation of Yolk and Nutrition in the Early Embryo. *Curr. Environ. Heal. reports* **2018**, *5* (1), 125–133. https://doi.org/10.1007/s40572-018-0183-2.

(10) Wilson, C. Aspects of Larval Rearing Carole. *ILAR J.* **2012**, *53* (2), 169–178.

(11) Verbueken, E.; Bars, C.; Ball, J. S.; Periz-Stanacev, J.; Marei, W. F. A.; Tochwin, A.; Gabriëls, I. J.; Michiels, E. D. G.; Stinckens, E.; Vergauwen, L.; et al. From MRNA Expression of Drug Disposition Genes to in Vivo Assessment of CYP-Mediated Biotransformation during Zebrafish Embryonic and Larval Development. *Int. J. Mol. Sci.* **2018**, *19* (12), 1–30. https://doi.org/10.3390/ijms19123976.

(12) Kimmel, C. B.; Ballard, W. W.; Kimmel, S. R.; Ullmann, B.; Schilling, T. F. Stages of Embryonic Development of the Zebrafish. *Dev. Dyn.* **1995**, *203*, 253–310.

(13) Tao, T.; Peng, J. Liver Development in Zebrafish (Danio Rerio). *J. Genet. Genomics* **2009**, *36* (6), 325–334. https://doi.org/10.1016/S1673-8527(08)60121-6.

(14) Ng, A. N. Y.; De Jong-Curtain, T. A.; Mawdsley, D. J.; White, S. J.; Shin, J.; Appel, B.; Dong, P. D. S.; Stainier, D. Y. R.; Heath, J. K. Formation of the Digestive System in Zebrafish: III. Intestinal Epithelium Morphogenesis. *Dev. Biol.* **2005**, *286* (1), 114–135. https://doi.org/10.1016/j.ydbio.2005.07.013.

(15) Lieschke, G. J.; Currie, P. D. Animal Models of Human Disease: Zebrafish Swim into View. *Nat. Rev. Genet.* **2007**, *8* (5), 353–367. https://doi.org/10.1038/nrg2091.

(16) Embry, M. R.; Belanger, S. E.; Braunbeck, T. A.; Galay-burgos, M.; Halder, M.; Hinton, D. E.; Léonard, M. A.; Lillicrap, A.; Norberg-king, T.; Whale, G. The Fish Embryo Toxicity Test as an Animal Alternative Method in Hazard and Risk Assessment and Scientific Research. *Aquat. Toxicol.* **2010**, *97* (0349), 79–87. https://doi.org/10.1016/j.aquatox.2009.12.008.

(17) OECD Guidelines for the Testing of Chemicals - Fish Embryo Acute Toxicity (FET) Test. *OECD 236* **2013**.

(18) ISO. Water Quality — Determination of the Acute Toxicity of Waste Water to Zebrafish Eggs (Danio Rerio). *ISO 150882007* **2007**.

(19) DIN. German Standard Methods for the Examination of Water, Waste Water and Sludge – Subanimal Testing (Group T) – Part 6: Toxicity to Fish. Determination of the Non-Acute-Poisonous Effect of Waste Water to Fish Eggs by Dilution Limits (T 6). *German Standardization Organization. DIN 38415-6*. 2003.

(20) ISO. Water Quality - Determination of the Acute Lethal Toxicity of Substances to a Freshwater Fish. *ISO 7346-1* **1996**.

(21) Belanger, S. E.; Rawlings, J. M.; Carr, G. J. Use of Fish Embryo Toxicity Tests for the Prediction of Acute Fish Toxicity to Chemicals. *Environ. Toxicol. Chem.* **2013**, *32* (8), 1768–1783. https://doi.org/10.1002/etc.2244.

(22) Joint Report ECHA and UBA: Expert Workshop on the Potential Regulatory Application of the Fish Embryo Acute Toxicity (FET) Test under REACH, CLP and the BPR; European Chemical Agency, Umweltbundesamt: Helsinki, 2017.

(23) Sobanska, M.; Scholz, S.; Nyman, A. M.; Cesnaitis, R.; Gutierrez Alonso, S.; Klüver, N.; Kühne, R.; Tyle, H.; de Knecht, J.; Dang, Z.; et al. Applicability of the Fish Embryo Acute Toxicity (FET) Test (OECD 236) in the Regulatory Context of Registration, Evaluation, Authorisation, and Restriction of Chemicals (REACH). *Environmental Toxicology and Chemistry*. Wiley Blackwell March 1, 2018, pp 657–670. https://doi.org/10.1002/etc.4055.

(24) Massei, R.; Vogs, C.; Renner, P.; Altenburger, R.; Scholz, S. Differential Sensitivity in Embryonic Stages of the Zebrafish (Danio Rerio): The Role of Toxicokinetics for Stage-Specific Susceptibility for Azinphos-Methyl Lethal Effects. *Aquat. Toxicol.* **2015**, *166*, 36–41. https://doi.org/10.1016/j.aquatox.2015.06.011.

(25) Klüver, N.; König, M.; Ortmann, J.; Massei, R.; Paschke, A.; Kühne, R.; Scholz, S. Fish Embryo Toxicity Test: Identification of Compounds with Weak Toxicity and Analysis of Behavioral Effects to Improve Prediction of Acute Toxicity for Neurotoxic Compounds. *Environ. Sci. Technol.* **2015**, *49* (11), 7002–7011. https://doi.org/10.1021/acs.est.5b01910.

(26) Nyman, A. M.; Schirmer, K.; Ashauer, R. Importance of Toxicokinetics for Interspecies Variation in Sensitivity to Chemicals. *Environ. Sci. Technol.* **2014**, *48* (10), 5946–5954. https://doi.org/10.1021/es5005126.

(27) Ducharme, N. A.; Peterson, L. E.; Benfenati, E.; Reif, D.; McCollum, C. W.; Gustafsson, J. Å.; Bondesson, M. Meta-Analysis of Toxicity and Teratogenicity of 133 Chemicals from Zebrafish Developmental Toxicity Studies. *Reprod. Toxicol.* **2013**, *41*, 98–108. https://doi.org/10.1016/j.reprotox.2013.06.070.

(28) Kirla, K. T.; Groh, K. J.; Steuer, A. E.; Poetzsch, M.; Banote, R. K.; Stadnicka-Michalak, J.; Eggen, R. I. L.; Schirmer, K.; Kraemer, T. Zebrafish Larvae Are Insensitive to Stimulation by Cocaine: Importance of Exposure Route and Toxicokinetics. *Toxicol. Sci.* **2016**, *154* (1), 183–193. https://doi.org/10.1093/toxsci/kfw156.

(29) Kühnert, A.; Vogs, C.; Altenburger, R.; Küster, E. The Internal Concentration of Organic Substances in Fish Embryos-A Toxicokinetic Approach. *Environ. Toxicol. Chem.* **2013**, *32* (8), 1819–1827. https://doi.org/10.1002/etc.2239.

(30) Brox, S.; Ritter, A. P.; Küster, E.; Reemtsma, T. A Quantitative HPLC-MS/MS Method for Studying Internal Concentrations and Toxicokinetics of 34 Polar Analytes in Zebrafish (Danio Rerio) Embryos. *Anal. Bioanal. Chem.* **2014**, *406* (20), 4831–4840. https://doi.org/10.1007/s00216-014-7929-y.

(31) El-Amrani, S.; Pena-Abaurrea, M.; Sanz-Landaluze, J.; Ramos, L.; Guinea, J.; Cámara, C. Bioconcentration of Pesticides in Zebrafish Eleutheroembryos (Danio Rerio). *Sci. Total Environ.* **2012**, *425*, 184–190. https://doi.org/10.1016/j.scitotenv.2012.02.065.

(32) Petersen, G. I.; Kristensen, P. Bioaccumulation of Lipophilic Substances in Fish Early Life Stages. *Environ. Toxicol. Chem.* **1998**, *17* (7), 1385–1395. https://doi.org/10.1002/etc.5620170724.

(33) Burton, A. C. The Properties of the Steady State Compared to Those of Equilibrium as Shown in Characteristic Biological Behavior. *J. Cell. Comp. Physiol.* **1939**, *14* (3), 327–349. https://doi.org/10.1002/jcp.1030140309.

(34) Brox, S.; Seiwert, B.; Küster, E.; Reemtsma, T. Toxicokinetics of Polar Chemicals in Zebrafish Embryo (Danio Rerio): Influence of Physicochemical Properties and of Biological Processes. *Environ. Sci. Technol.* **2016**, *50* (18), 10264–10272. https://doi.org/10.1021/acs.est.6b04325.

(35) Ulrich, N.; Endo, S.; Brown, T. N.; Watanabe, N.; Bronner, G.; Abraham, M. H.; Goss, K.-U. UFZ-LSER database v 3.2.1 [Internet], Leipzig, Germany, Helmholtz Centre for Environmental Research-UFZ http://www.ufz.de/lserd (accessed Aug 10, 2019).

(36) Saad, M.; Cavanaugh, K.; Verbueken, E.; Pype, C.; Casteleyn, C.; Van Ginneken, C.; Van Cruchten, S. Xenobiotic Metabolism in the Zebrafish: A Review of the Spatiotemporal Distribution, Modulation and Activity of Cytochrome P450 Families 1 to 3. *J. Toxicol. Sci.* **2016**, *41* (1), 1–11. https://doi.org/10.2131/jts.41.1.

(37) Jones, H. S.; Panter, G. H.; Hutchinson, T. H.; Chipman, J. K. Oxidative and Conjugative Xenobiotic Metabolism in Zebrafish Larvae in Vivo. *Zebrafish* **2010**, *7* (1), 23–30. https://doi.org/10.1089/zeb.2009.0630.

(38) Brox, S.; Seiwert, B.; Haase, N.; Küster, E.; Reemtsma, T. Metabolism of Clofibric Acid in

Zebrafish Embryos (Danio Rerio) as Determined by Liquid Chromatography-High Resolution-Mass Spectrometry. *Comp. Biochem. Physiol. Part - C Toxicol. Pharmacol.* **2016**, *185–186*, 20–28. https://doi.org/10.1016/j.cbpc.2016.02.007.

(39) Di Paolo, C.; Groh, K. J.; Zennegg, M.; Vermeirssen, E. L. M.; Murk, A. J.; Eggen, R. I. L.; Hollert, H.; Werner, I.; Schirmer, K. Early Life Exposure to PCB126 Results in Delayed Mortality and Growth Impairment in the Zebrafish Larvae. *Aquat. Toxicol.* **2015**, *169*, 168–178. https://doi.org/10.1016/j.aquatox.2015.10.014.

(40) Tu, W.; Lu, B.; Niu, L.; Xu, C.; Lin, C.; Liu, W. Dynamics of Uptake and Elimination of Pyrethroid Insecticides in Zebrafish (Danio Rerio) Eleutheroembryos. *Ecotoxicol. Environ. Saf.* **2014**, *107*, 186–191. https://doi.org/10.1016/j.ecoenv.2014.05.013.

(41) Nowakowska, K.; Giebułtowicz, J.; Kamaszewski, M.; Adamski, A.; Szudrowicz, H.; Ostaszewska, T.; Solarska-Dzięciołowska, U.; Nałęcz-Jawecki, G.; Wroczyński, P.; Drobniewska, A. Acute Exposure of Zebrafish (Danio Rerio) Larvae to Environmental Concentrations of Selected Antidepressants: Bioaccumulation, Physiological and Histological Changes. *Comp. Biochem. Physiol. Part - C Toxicol. Pharmacol.* **2020**, *229*, 108670. https://doi.org/10.1016/j.cbpc.2019.108670.

(42) Bittner, L.; Teixidó, E.; Keddi, I.; Escher, B. I.; Klüver, N. PH-Dependent Uptake and Sublethal Effects of Antihistamines in Zebrafish (Danio Rerio) Embryos. *Environ. Toxicol. Chem.* **2019**, 1–37. https://doi.org/10.1002/etc.4395.

(43) Bittner, L.; Klüver, N.; Henneberger, L.; Mühlenbrink, M.; Zarfl, C.; Escher, B. I. Combined Ion-Trapping and Mass Balance Models To Describe the PH-Dependent Uptake and Toxicity of Acidic and Basic Pharmaceuticals in Zebrafish Embryos (Danio Rerio). *Environ. Sci. Technol.* **2019**, acs.est.9b02563. https://doi.org/10.1021/acs.est.9b02563.

(44) van Wijk, R. C.; Krekels, E. H. J.; Kantae, V.; Harms, A. C.; Hankemeier, T.; van der Graaf, P. H.; Spaink, H. P. Impact of Post-Hatching Maturation on the Pharmacokinetics of Paracetamol in Zebrafish Larvae. *Sci. Rep.* **2019**, *9* (1), 2149. https://doi.org/10.1038/s41598-019-38530-w.

(45) Kristofco, L. A.; Haddad, S. P.; Chambliss, C. K.; Brooks, B. W. Differential Uptake of and Sensitivity to Diphenhydramine in Embryonic and Larval Zebrafish. *Environ. Toxicol. Chem.* **2018**, *37* (4), 1175–1181. https://doi.org/10.1002/etc.4068.

(46) Vogs, C.; Johanson, G.; Näslund, M.; Wulff, S.; Sjödin, M.; Hellstrandh, M.; Lindberg, J.; Wincent, E. Toxicokinetics of Perfluorinated Alkyl Acids Influences Their Toxic Potency in the Zebrafish Embryo (Danio Rerio). *Environ. Sci. Technol.* **2019**, *53* (7), 3898–3907. https://doi.org/10.1021/acs.est.8b07188.

(47) Pelka, K. E.; Henn, K.; Keck, A.; Sapel, B.; Braunbeck, T. Size Does Matter – Determination of the Critical Molecular Size for the Uptake of Chemicals across the Chorion of Zebrafish (Danio Rerio) Embryos. *Aquat. Toxicol.* **2017**, *185*, 1–10. https://doi.org/10.1016/j.aquatox.2016.12.015.

(48) Böhme, S.; Stärk, H.-J.; Kühnel, D.; Reemtsma, T. Exploring LA-ICP-MS as a Quantitative Imaging Technique to Study Nanoparticle Uptake in Daphnia Magna and Zebrafish (Danio Rerio) Embryos. *Anal Bioanal Chem* **2015**, *407*, 5477–5485.

(49) Pirro, V.; Guffey, S. C.; Sepúlveda, M. S.; Mahapatra, C. T.; Ferreira, C. R.; Jarmusch, A. K.; Cooks, R. G. Lipid Dynamics in Zebrafish Embryonic Development Observed by DESI-

MS Imaging and Nanoelectrospray-MS. *Mol. BioSyst.* **2016**, *12* (7), 2069–2079. https://doi.org/10.1039/C6MB00168H.

(50) Kirla, K. T.; Groh, K. J.; Poetzsch, M.; Banote, R. K.; Stadnicka-Michalak, J.; Eggen, R. I. L.; Schirmer, K.; Kraemer, T. Importance of Toxicokinetics to Assess the Utility of Zebrafish Larvae as Model for Psychoactive Drug Screening Using Meta-Chlorophenylpiperazine (MCPP) as Example. *Front. Pharmacol.* **2018**, *9*, 414. https://doi.org/10.3389/fphar.2018.00414.

(51) Dueñas, M. E.; Essner, J. J.; Lee, Y. J. 3D MALDI Mass Spectrometry Imaging of a Single Cell: Spatial Mapping of Lipids in the Embryonic Development of Zebrafish. *Sci. Rep.* **2017**, *7* (1). https://doi.org/10.1038/s41598-017-14949-x.

(52) Foekema, E. M.; Lopez Parron, M.; Mergia, M. T.; Carolus, E. R. M.; vd Berg, J. H. J.; Kwadijk, C.; Dao, Q.; Murk, A. T. J. Internal Effect Concentrations of Organic Substances for Early Life Development of Egg-Exposed Fish. *Ecotoxicol. Environ. Saf.* **2014**, *101* (1), 14–22. https://doi.org/10.1016/j.ecoenv.2013.12.006.

(53) McEwen, A.; Henson, Cl. Quantitative Whole-Body Autoradiography: Past, Present and Future. *Bioanalysis* **2015**, *7* (5), 557–568. https://doi.org/10.4155/BIO.15.9.

(54) Gholap, D. S.; Izmer, A.; De Samber, B.; van Elteren, J. T.; Šelih, V. S.; Evens, R.; De Schamphelaere, K.; Janssen, C.; Balcaen, L.; Lindemann, I.; et al. Comparison of Laser Ablation-Inductively Coupled Plasma-Mass Spectrometry and Micro-X-Ray Fluorescence Spectrometry for Elemental Imaging in Daphnia Magna. *Anal. Chim. Acta* **2010**, *664*, 19–26. https://doi.org/10.1016/j.aca.2010.01.052.

(55) Bourassa, D.; Gleber, S.-C.; Vogt, S.; Yi, H.; Will, F.; Richter, H.; Shin, C. H.; Fahrni, C. J. 3D Imaging of Transition Metals in the Zebrafish Embryo by X- Ray Fluorescence Microtomography. *Metallomics* **2014**, *6* (9), 1648–1655. https://doi.org/10.1039/c4mt00121d.

(56) Guan, P.; Liu, Y.; Yang, B.; Wu, Y.; Chai, J.; Wen, G. Fluorometric Probe for the Lipase Level : Design , Mechanism and Biological Imaging Application. *Talanta* **2021**, *225* (1 April 2021).

(57) Senoner, M.; Unger, W. E. S. SIMS Imaging of the Nanoworld: Applications in Science and Technology. *Journal of Analytical Atomic Spectrometry*. The Royal Society of Chemistry July 1, 2012, pp 1050–1068. https://doi.org/10.1039/c2ja30015j.

(58) Becker, J. S.; Zoriy, M.; Matusch, A.; Wu, B.; Salber, D.; Palm, C.; Becker, J. S. Bioimaging of Metals by Laser Ablation Inductively Coupled Plasma Mass Spectrometry (LA-ICP-MS). *Mass Spectrom. Rev.* **2010**, *29*, 156–175. https://doi.org/10.1002/mas.20239.

(59) Hare, D.; Austin, C.; Doble, P. Quantification Strategies for Elemental Imaging of Biological Samples Using Laser Ablation-Inductively Coupled Plasma-Mass Spectrometry. *Analyst* **2012**, *137*, 1527–1537. https://doi.org/10.1039/c2an15792f.

(60) Urgast, D. S.; Beattie, J. H.; Feldmann, J. Imaging of Trace Elements in Tissues: With a Focus on Laser Ablation Inductively Coupled Plasma Mass Spectrometry. *Current Opinion in Clinical Nutrition and Metabolic Care*. 2014, pp 431–439. https://doi.org/10.1097/MCO.0000000000000087.

(61) Reifschneider, O.; Schütz, C. L.; Brochhausen, C.; Hampel, G.; Ross, T.; Sperling, M.;

Karst, U. Quantitative Bioimaging of P-Boronophenylalanine in Thin Liver Tissue Sections as a Tool for Treatment Planning in Boron Neutron Capture Therapy. *Anal Bioanal Chem* **2015**, *407*, 2365–2371. https://doi.org/10.1007/s00216-014-8012-4.

(62) Theiner, S.; Van Malderen, S. J. M.; Van Acker, T.; Legin, A. A.; Keppler, B. K.; Vanhaecke, F.; Koellensperger, G. Fast High-Resolution LA-ICP-MS Imaging of the Distribution of Platinum-Based Anti-Cancer Compounds in Multicellular Tumor Spheroids. *Anal. Chem.* **2017**, *89* (23), 12641–12645. https://doi.org/10.1021/acs.analchem.7b02681.

(63) Limbeck, A.; Galler, P.; Bonta, M.; Bauer, G.; Nischkauer, W.; Vanhaecke, F. Recent Advances in Quantitative LA-ICP-MS Analysis: Challenges and Solutions in the Life Sciences and Environmental Chemistry ABC Highlights: Authored by Rising Stars and Top Experts. *Anal. Bioanal. Chem.* **2015**, *407* (22), 6593–6617. https://doi.org/10.1007/s00216-015-8858-0.

(64) Konz, I.; Fernández, B.; Fernández, M. L.; Pereiro, R.; González-Iglesias, H.; Coca-Prados, M.; Sanz-Medel, A. Quantitative Bioimaging of Trace Elements in the Human Lens by LA-ICP-MS. *Anal. Bioanal. Chem.* **2014**, *406* (9–10), 2343–2348. https://doi.org/10.1007/s00216-014-7617-y.

(65) Becker, J. S.; Matusch, A.; Wu, B. Bioimaging Mass Spectrometry of Trace Elements - Recent Advance and Application of LA-ICP-MS: A Review. *Anal. Chim. Acta* **2014**, *835*, 1–18.

(66) Barst, B. D.; Gevertz, A. K.; Chumchal, M. M.; Smith, J. D.; Rainwater, T. R.; Drevnick, P. E.; Hudelson, K. E.; Hart, A.; Verbeck, G. F.; Roberts, A. P. Laser Ablation ICP-MS Co-Localization of Mercury and Immune Response in Fish. *Environ. Sci. Technol.* **2011**, *45* (20), 8982–8988. https://doi.org/10.1021/es201641x.

(67) Waentig, L.; Jakubowski, N.; Hayen, H.; Roos, P. H. Iodination of Proteins, Proteomes and Antibodies with Potassium Triodide for LA-ICP-MS Based Proteomic Analyses. *J. Anal. At. Spectrom.* **2011**, *26*, 1610–1618. https://doi.org/10.1039/c1ja10090d.

(68) Guillong, M.; Günther, D. Effect of Particle Size Distribution on ICP-Induced Elemental Fractionation in Laser Ablation-Inductively Coupled Plasma-Mass Spectrometry. *J. Anal. At. Spectrom.* **2002**, *17*, 831–837. https://doi.org/10.1039/b202988j.

(69) Jeffries, T. E.; Perkins, W. T.; Pearce, N. J. G. Comparisons of Infrared and Ultraviolet Laser Probe Microanalysis Inductively Coupled Plasma Mass Spectrometry in Mineral Analysis. *Analyst* **1995**, *120* (5), 1365–1371. https://doi.org/10.1039/AN9952001365.

(70) What is Laser Ablation ICP-MS Imaging? - TOFWERK https://www.tofwerk.com/laser-ablation-icp-ms-imaging/ (accessed Dec 21, 2020).

(71) Westerhausen, M. T.; Bishop, D. P.; Dowd, A.; Wanagat, J.; Cole, N.; Doble, P. A. Super-Resolution Reconstruction for Two-and Three-Dimensional LA-ICP-MS Bioimaging. *Anal. Chem.* **2019**, *91*, 14879–14886. https://doi.org/10.1021/acs.analchem.9b02380.

(72) Van Malderen, S. J. M.; Van Elteren, J. T.; Vanhaecke, F. Submicrometer Imaging by Laser Ablation-Inductively Coupled Plasma Mass Spectrometry via Signal and Image Deconvolution Approaches. *Anal. Chem.* **2015**, *87*, 6125–6132. https://doi.org/10.1021/acs.analchem.5b00700.

(73) Castellanos-García, L. J.; Gokhan Elci, S.; Vachet, R. W. Reconstruction, Analysis, and

Segmentation of LA-ICP-MS Imaging Data Using Python for the Identification of Sub-Organ Regions in Tissues. *Analyst* **2020**, *145* (10), 3705–3712. https://doi.org/10.1039/c9an02472g.

(74) Ardelt, D.; Polatajko, A.; Primm, O.; Reijnen, M. Isotope Ratio Measurements with a Fully Simultaneous Mattauch-Herzog ICP-MS. *Anal. Bioanal. Chem.* **2013**, *405* (9), 2987–2994. https://doi.org/10.1007/s00216-012-6543-0.

(75) Van Malderen, S. J. M.; Van Elteren, J. T.; Vanhaecke, F. Development of a Fast Laser Ablation-Inductively Coupled Plasma-Mass Spectrometry Cell for Sub-Mm Scanning of Layered Materials †. **2015**, *30*, 1–316. https://doi.org/10.1039/c4ja00137k.

(76) icpTOF - Detection for Nanoparticles and Laser Ablation Imaging https://www.tofwerk.com/products/icptof/ (accessed Dec 21, 2020).

(77) Van Malderen, S. J. M.; Managh, A. J.; Sharp, B. L.; Vanhaecke, F. Recent Developments in the Design of Rapid Response Cells for Laser Ablation-Inductively Coupled Plasma-Mass Spectrometry and Their Impact on Bioimaging Applications. *Journal of Analytical Atomic Spectrometry*. 2016, pp 423–439. https://doi.org/10.1039/c5ja00430f.

(78) Triglav, J.; Van Elteren, J. T.; Elih, V. S. Š. Basic Modeling Approach To Optimize Elemental Imaging by Laser Ablation ICPMS. *Anal. Chem.* **2010**, *82*, 8153–8160. https://doi.org/10.1021/ac1014832.

(79) Van Elteren, J. T.; Izmer, A.; Šelih, V. S.; Vanhaecke, F. Novel Image Metrics for Retrieval of the Lateral Resolution in Line Scan-Based 2D LA-ICPMS Imaging via an Experimental-Modeling Approach. *Anal. Chem.* **2016**, *88* (14), 7413–7420. https://doi.org/10.1021/acs.analchem.6b02052.

(80) Van Elteren, J. T.; Vanhaecke, F. Angular Resolution Dependency in 2D LA-ICP-MS Mapping – the Case for Low-Dispersion Laser Ablation Cells. *J. Anal. At. Spectrom.* **2016**. https://doi.org/10.1039/c6ja00234j.

(81) National Institute of Standards and Technology | NIST https://www.nist.gov/ (accessed Jan 28, 2021).

(82) Elci, S. G.; Yan, B.; Kim, S. T.; Saha, K.; Jiang, Y.; Klemmer, G. A.; Moyano, D. F.; Tonga, G. Y.; Rotello, V. M.; Vachet, R. W. Quantitative Imaging of 2 Nm Monolayer-Protected Gold Nanoparticle Distributions in Tissues Using Laser Ablation Inductively-Coupled Plasma Mass Spectrometry (LA-ICP-MS). *Analyst* **2016**, *141* (8), 2418–2425. https://doi.org/10.1039/c6an00123h.

(83) Šala, M.; Šelih, V. S.; Van Elteren, J. T. Gelatin Gels as Multi-Element Calibration Standards in LA-ICP-MS Bioimaging: Fabrication of Homogeneous Standards and Microhomogeneity Testing. *Analyst* **2017**, *142* (18), 3356–3359. https://doi.org/10.1039/c7an01361b.

(84) Stärk, H.-J.; Wennrich, R. A New Approach for Calibration of Laser Ablation Inductively Coupled Plasma Mass Spectrometry Using Thin Layers of Spiked Agarose Gels as References. *Anal Bioanal Chem* **2011**, *399*, 2211–2217. https://doi.org/10.1007/s00216-010-4413-1.

(85) Bonta, M.; Hegedus, B.; Limbeck, A. Application of Dried-Droplets Deposited on Pre-Cut Filter Paper Disks for Quantitative LA-ICP-MS Imaging of Biologically Relevant Minor

and Trace Elements in Tissue Samples. *Anal. Chim. Acta* **2016**, *908*, 54–62. https://doi.org/10.1016/j.aca.2015.12.048.

(86) Douglas, D. N.; O'Reilly, J.; O'Connor, C.; Sharp, B. L.; Goenaga-Infante, H. Quantitation of the Fe Spatial Distribution in Biological Tissue by Online Double Isotope Dilution Analysis with LA-ICP-MS: A Strategy for Estimating Measurement Uncertainty. *J. Anal. At. Spectrom.* **2016**, *31* (1), 270–279. https://doi.org/10.1039/c5ja00351b.

(87) Bauer, O. B.; Köppen, C.; Sperling, M.; Schurek, H. J.; Ciarimboli, G.; Karst, U. Quantitative Bioimaging of Platinum via Online Isotope Dilution-Laser Ablation-Inductively Coupled Plasma Mass Spectrometry. *Anal. Chem.* **2018**, *90* (11), 7033–7039. https://doi.org/10.1021/acs.analchem.8b01429.

(88) Uerlings, R.; Matusch, A.; Weiskirchen, R. Reconstruction of Laser Ablation Inductively Coupled Plasma Mass Spectrometry (LA-ICP-MS) Spatial Distribution Images in Microsoft Excel 2007. *Int. J. Mass Spectrom.* **2016**, *395*, 27–35. https://doi.org/10.1016/j.ijms.2015.11.010.

(89) de Pessoa, G. S.; Capelo-Martinez, J. L.; Fdez-Riverola, F.; Lopez-Fernandez, H.; Glez-Pena, D.; Reboiro-Jato, M.; Arruda, M. A. Z. Laser Ablation and Inductively Coupled Plasma Mass Spectrometry Focusing on Bioimaging from Elemental Distribution Using MatLab Software: A Practical Guide. *J. Anal. At. Spectrom.* **2016**, *31*, 832–840. https://doi.org/10.1039/c5ja00451a.

(90) Weiskirchen, R.; Weiskirchen, S.; Kim, P.; Winkler, R. Software Solutions for Evaluation and Visualization of Laser Ablation Inductively Coupled Plasma Mass Spectrometry Imaging (LA-ICP-MSI) Data: A Short Overview. *Journal of Cheminformatics*. Springer International Publishing December 18, 2019, p 16. https://doi.org/10.1186/s13321-019-0338-7.

(91) Van Malderen, S. J. M.; Laforce, B.; Van Acker, T.; Nys, C.; De Rijcke, M.; De Rycke, R.; De Bruyne, M.; Boone, M. N.; De Schamphelaere, K.; Borovinskaya, O.; et al. Three-Dimensional Reconstruction of the Tissue-Specific Multielemental Distribution within Ceriodaphnia Dubia via Multimodal Registration Using Laser Ablation ICP-Mass Spectrometry and X-Ray Spectroscopic Techniques. *Anal. Chem.* **2017**, *89* (7), 4161–4168. https://doi.org/10.1021/acs.analchem.7b00111.

(92) Bishop, D. P.; Grossgarten, M.; Dietrich, D.; Vennemann, A.; Cole, N.; Sperling, M.; Wiemann, M.; Doble, P. A.; Karst, U. Quantitative Imaging of Translocated Silver Following Nanoparticle Exposure by Laser Ablation-Inductively Coupled Plasma-Mass Spectrometry. *Anal. Methods* **2018**, *10* (8), 836–840. https://doi.org/10.1039/c7ay02294h.

(93) Doble, P. A.; Miklos, G. L. G. Distributions of Manganese in Diverse Human Cancers Provide Insights into Tumour Radioresistance. *Metallomics* **2018**, *10* (9), 1191–1210. https://doi.org/10.1039/c8mt00110c.

(94) Gemperline, E.; Rawson, S.; Li, L. Optimization and Comparison of Multiple MALDI Matrix Application Methods for Small Molecule Mass Spectrometric Imaging. *Anal. Chem.* **2014**. https://doi.org/10.1021/ac5028534.

(95) Gobey, J.; Cole, M.; Janiszewski, J.; Covey, T.; Chau, T.; Kovarik, P.; Corr, J. Characterization and Performance of MALDI on a Triple Quadrupole Mass Spectrometer for Analysis and Quantification of Small Molecules. *Anal. Chem.* **2005**, *77*, 5641–5654.

https://doi.org/10.1021/ac0506130.

(96) Burnum, K. E.; Frappier, S. L.; Caprioli, R. M. Matrix-Assisted Laser Desorption/Ionization Imaging Mass Spectrometry for the Investigation of Proteins and Peptides. *Annu. Rev. Anal. Chem* **2008**, *1*, 689–705. https://doi.org/10.1146/annurev.anchem.1.031207.112841.

(97) Phan, N. T. N.; Mohammadi, A. S.; Dowlatshahi Pour, M.; Ewing, A. G. Laser Desorption Ionization Mass Spectrometry Imaging of Drosophila Brain Using Matrix Sublimation versus Modification with Nanoparticles. *Anal. Chem.* **2016**, *88* (3), 1734–1741. https://doi.org/10.1021/acs.analchem.5b03942.

(98) Smith, D. F.; Kharchenko, A.; Konijnenburg, M.; Klinkert, I.; Pasa-Tolic, L.; Heeren, R. M. A. Advanced Mass Calibration and Visualization for FT-ICR Mass Spectrometry Imaging. *J. Am. Soc. Mass Spectrom.* **2012**. https://doi.org/10.1007/s13361-012-0464-1.

(99) Norris, J. L.; Caprioli, R. M. Analysis of Tissue Specimens by Matrix-Assisted Laser Desorption/Ionization Imaging Mass Spectrometry in Biological and Clinical Research. *Chemical Reviews*. 2013, pp 2309–2342. https://doi.org/10.1021/cr3004295.

(100) Adams, F.; Barbante, C. History and Present Status of Micro- and Nano-Imaging Analysis. In *Comprehensive Analytical Chemistry*; Elsevier, 2015; Vol. 69, pp 67–124. https://doi.org/10.1016/B978-0-444-63439-9.00003-7.

(101) Mass Spectrometry Facility | FTICRMS http://www.chm.bris.ac.uk/ms/fticrms.xhtml (accessed Dec 29, 2020).

(102) Porta, T.; Lesur, A.; Varesio, E.; Hopfgartner, G. Quantification in MALDI-MS Imaging: What Can We Learn from MALDI-Selected Reaction Monitoring and What Can We Expect for Imaging? *Anal. Bioanal. Chem.* **2015**, *407* (8), 2177–2187. https://doi.org/10.1007/s00216-014-8315-5.

(103) Busch, W.; Schmidt, S.; Kühne, R.; Schulze, T.; Krauss, M.; Altenburger, R. Micropollutants in European Rivers: A Mode of Action Survey to Support the Development of Effect-Based Tools for Water Monitoring. *Environ. Toxicol. Chem.* **2016**, *35* (8), 1887–1899. https://doi.org/10.1002/etc.3460.

(104) Chemicalize - Instant Cheminformatics Solutions https://chemicalize.com/#/calculation (accessed Jul 12, 2019).

(105) Hansch, C; Leo, A; Hoekman, D. *Exploring QSAR: Hydrophobic, Electronic, and Steric Constants*, ACS Profes.; American Chemical Society: Washington, DC, 1995.

(106) Schmidt, S. Bewertung Der Mischungstoxizität von Gentoxischen Substanzen Auf Embryonen Des Zebrabärblings (Danio Rerio) Unter Berücksichtigung Der Spezifischen Wirkweisen Und Reaktionen Auf, Masterarbeit, Martin-Luther-Universität Halle-Wittenberg, 2013.

(107) Velki, M.; Di Paolo, C.; Nelles, J.; Seiler, T.-B.; Hollert, H. Diuron and Diazinon Alter the Behavior of Zebrafish Embryos and Larvae in the Absence of Acute Toxicity. *Chemosphere* **2017**, *180*, 65–76. https://doi.org/10.1016/j.chemosphere.2017.04.017.

(108) Cunningham, V. L.; Constable, D. J. C.; Hannah, R. E. Environmental Risk Assessment of Paroxetine. *Environ. Sci. Technol.* **2004**, *38* (12), 3351–3359. https://doi.org/10.1021/es035119x.

(109) Machado, F.; Collin, L.; Boule, P. Photolysis of Bromoxynil (3,5-dibromo-4-hydroxybenzonitrile) in Aqueous Solution. *Pesticide Science*. 1995, pp 107–110. https://doi.org/10.1002/ps.2780450203.

(110) Klüver, N.; Bittermann, K.; Escher, B. I. QSAR for Baseline Toxicity and Classification of Specific Modes of Action of Ionizable Organic Chemicals in the Zebrafish Embryo Toxicity Test. *Aquat. Toxicol.* **2019**, *207* (December 2018), 110–119. https://doi.org/10.1016/j.aquatox.2018.12.003.

(111) Helliker, P. E. Naled - Risk Characterization Document (RCD 99-03), California Environmental Protection Agency - Department of Pesticide Regulation, 1999.

(112) Portbury, S. D.; Hare, D. J.; Bishop, D. P.; Finkelstein, D. I.; Doble, P. A.; Adlard, P. A. Trehalose Elevates Brain Zinc Levels Following Controlled Cortical Impact in a Mouse Model of Traumatic Brain Injury. *Metallomics* **2018**, *10* (6), 846–853. https://doi.org/10.1039/c8mt00068a.

(113) Hare, D. J.; Raven, E. P.; Roberts, B. R.; Bogeski, M.; Portbury, S. D.; McLean, C. A.; Masters, C. L.; Connor, J. R.; Bush, A. I.; Crouch, P. J.; et al. Laser Ablation-Inductively Coupled Plasma-Mass Spectrometry Imaging of White and Gray Matter Iron Distribution in Alzheimer's Disease Frontal Cortex. *Neuroimage* **2016**, *137*, 124–131. https://doi.org/10.1016/j.neuroimage.2016.05.057.

(114) Teixidó, E.; Kießling, T. R.; Krupp, E.; Quevedo, C.; Muriana, A.; Scholz, S. Automated Morphological Feature Assessment for Zebrafish Embryo Developmental Toxicity Screens. *Toxicol. Sci.* **2019**, *167* (2), 438–449. https://doi.org/10.1093/toxsci/kfy250.

(115) Muniz, M. S.; Halbach, K.; Araruna, I. C. A.; Martins, R. X.; Seiwert, B.; Lechtenfeld, O.; Reemtsma, T.; Farias, D. F. Moxidectin Toxicity to Zebrafish Embryos: Bioaccumulation and Biomarker Responses. *submitted* **2020**.

(116) Escher, B.; Hermens, J.; Schwarzenbach, R. International Workshop: Internal Exposure - Linking Bioavailability to Effects. In *Environmental Science and Pollution Research*; 2005; Vol. 12, pp 57–60. https://doi.org/10.1065/espr2005.01.004.

(117) Fraher, D.; Sanigorski, A.; Mellett, N. A.; Meikle, P. J.; Sinclair, A. J.; Gibert, Y. Zebrafish Embryonic Lipidomic Analysis Reveals That the Yolk Cell Is Metabolically Active in Processing Lipid. *Cell Rep.* **2016**, *14* (6), 1317–1329. https://doi.org/10.1016/j.celrep.2016.01.016.

(118) Quinlivan, V. H.; Farber, S. A. Lipid Uptake, Metabolism, and Transport in the Larval Zebrafish. *Front. Endocrinol. (Lausanne).* **2017**, *8* (NOV), 1–11. https://doi.org/10.3389/fendo.2017.00319.

(119) Popovic, M.; Zaja, R.; Fent, K.; Smital, T. Interaction of Environmental Contaminants with Zebrafish Organic Anion Transporting Polypeptide, Oatp1d1 (Slco1d1). *Toxicol. Appl. Pharmacol.* **2014**, *280* (1), 149–158. https://doi.org/10.1016/j.taap.2014.07.015.

(120) Popovic, M.; Zaja, R.; Smital, T. Organic Anion Transporting Polypeptides (OATP) in Zebrafish (Danio Rerio): Phylogenetic Analysis and Tissue Distribution. *Comp. Biochem. Physiol. - A Mol. Integr. Physiol.* **2010**, *155* (3), 327–335. https://doi.org/10.1016/j.cbpa.2009.11.011.

(121) Faltermann, S.; Grundler, V.; Gademann, K.; Pernthaler, J.; Fent, K. Comparative Effects

of Nodularin and Microcystin-LR in Zebrafish: 2. Uptake and Molecular Effects in Eleuthero-Embryos and Adult Liver with Focus on Endoplasmic Reticulum Stress. *Aquat. Toxicol.* **2016**, *171*, 77–87. https://doi.org/10.1016/j.aquatox.2015.12.001.

(122) Faltermann, S.; Prétôt, R.; Pernthaler, J.; Fent, K. Comparative Effects of Nodularin and Microcystin-LR in Zebrafish: 1. Uptake by Organic Anion Transporting Polypeptide Oatp1d1 (Slco1d1). *Aquat. Toxicol.* **2016**, *171*, 69–76. https://doi.org/10.1016/j.aquatox.2015.11.016.

(123) van der Bent, S. A. S.; Berg, T.; Karst, U.; Sperling, M.; Rustemeyer, T. Allergic Reaction to a Green Tattoo with Nickel as a Possible Allergen. *Contact Dermatitis* **2019**, *81* (1), 64–66. https://doi.org/10.1111/cod.13226.

(124) Becker, J. S.; Zoriy, M. V.; Pickhardt, C.; Palomero-Gallagher, N.; Zilles, K. Imaging of Copper, Zinc, and Other Elements in Thin Section of Human Brain Samples (Hippocampus) by Laser Ablation Inductively Coupled Plasma Mass Spectrometry. *Anal. Chem.* **2005**. https://doi.org/10.1021/ac040184q.

(125) Drescher, D.; Giesen, C.; Traub, H.; Panne, U.; Kneipp, J.; Jakubowski, N. Quantitative Imaging of Gold and Silver Nanoparticles in Single Eukaryotic Cells by Laser Ablation ICP-MS. *Anal. Chem.* **2012**, *84* (22), 9684–9688. https://doi.org/10.1021/ac302639c.

(126) Oros-Peusquens, A. M.; Matusch, A.; Becker, J. S.; Shah, N. J. Automatic Segmentation of Tissue Sections Using the Multielement Information Provided by LA-ICP-MS Imaging and k-Means Cluster Analysis. *Int. J. Mass Spectrom.* **2011**, *307* (1–3), 245–252. https://doi.org/10.1016/j.ijms.2011.03.014.

(127) Paul, B.; Hare, D. J.; Bishop, D. P.; Paton, C.; Nguyen, V. T.; Cole, N.; Niedwiecki, M. M.; Andreozzi, E.; Vais, A.; Billings, J. L.; et al. Chemical Science Visualising Mouse Neuroanatomy and Function by Metal Distribution Using Laser Ablation-Inductively Coupled Plasma-Mass Spectrometry Imaging. *Chem. Sci.* **2015**, *6*, 5383–5393.

(128) Theiner, S.; Schweikert, A.; Van Malderen, S. J. M.; Schoeberl, A.; Neumayer, S.; Jilma, P.; Peyrl, A.; Koellensperger, G. Laser Ablation-Inductively Coupled Plasma Time-of-Flight Mass Spectrometry Imaging of Trace Elements at the Single-Cell Level for Clinical Practice. *Anal. Chem.* **2019**, *91* (13), 8207–8212. https://doi.org/10.1021/acs.analchem.9b00698.

(129) Holzlechner, M.; Bonta, M.; Lohninger, H.; Limbeck, A.; Marchetti-Deschmann, M. Multisensor Imaging - From Sample Preparation to Integrated Multimodal Interpretation of LA-ICPMS and MALDI MS Imaging Data. *Anal. Chem.* **2018**, *90* (15), 8831–8837. https://doi.org/10.1021/acs.analchem.8b00816.

(130) Ackerman, C. M.; Weber, P. K.; Xiao, T.; Thai, B.; Kuo, T. J.; Zhang, E.; Pett-Ridge, J.; Chang, C. J. Multimodal LA-ICP-MS and NanoSIMS Imaging Enables Copper Mapping within Photoreceptor Megamitochondria in a Zebrafish Model of Menkes Disease. *Metallomics* **2018**, *10* (3), 474–485. https://doi.org/10.1039/c7mt00349h.

(131) Böhme, S.; Stärk, H.-J.; Reemtsma, T.; Kühnel, D. Effect Propagation after Silver Nanoparticle Exposure in Zebrafish (Danio Rerio) Embryos: A Correlation to Internal Concentration and Distribution Patterns. *Environ. Sci. Nano* **2015**, *2*, 603–614. https://doi.org/10.1039/c5en00118h.

(132) Zarco-Fernández, S.; García-García, A.; Sanz-Landaluze, J.; Pecheyran, C.; Muñoz-Olivas,

R. In Vivo Bioconcentration of a Metal Mixture by Danio Rerio Eleutheroembryos. *Chemosphere* **2018**, *196*, 87–94. https://doi.org/10.1016/j.chemosphere.2017.12.141.

(133) Verwei, M.; van Burgsteden, J. A.; Krul, C. A. M.; van de Sandt, J. J. M.; Freidig, A. P. Prediction of in Vivo Embryotoxic Effect Levels with a Combination of in Vitro Studies and PBPK Modelling. *Toxicol. Lett.* **2006**, *165* (1), 79–87. https://doi.org/10.1016/j.toxlet.2006.01.017.

(134) Louisse, J.; de Jong, E.; van de Sandt, J. J. M.; Blaauboer, B. J.; Woutersen, R. A.; Piersma, A. H.; Rietjens, I. M. C. M.; Verwei, M. The Use of In Vitro Toxicity Data and Physiologically Based Kinetic Modeling to Predict Dose-Response Curves for In Vivo Developmental Toxicity of Glycol Ethers in Rat and Man. *Toxicol. Sci.* **2010**, *118* (2), 470–484. https://doi.org/10.1093/toxsci/kfq270.

(135) Souder, J. P.; Gorelick, D. A. Quantification of Estradiol Uptake in Zebrafish Embryos and Larvae. *Toxicol. Sci.* **2017**, *158* (2), 465–474. https://doi.org/10.1093/toxsci/kfx107.

(136) Ulrich, N.; Schweiger, N.; Pfennigsdorff, A.; Scholz, S.; Goss, K. U. Yolk–Water Partitioning of Neutral Organic Compounds in the Model Organism Danio Rerio. *Environ. Toxicol. Chem.* **2020**, *39* (8), 1506–1516. https://doi.org/10.1002/etc.4744.

(137) Miyares, R. L.; Stein, C.; Renisch, B.; Anderson, J. L.; Hammerschmidt, M.; Farber, S. A. Long-Chain Acyl-CoA Synthetase 4A Regulates Smad Activity and Dorsoventral Patterning in the Zebrafish Embryo. *Dev. Cell* **2013**, *27* (6), 635–647. https://doi.org/10.1016/j.devcel.2013.11.011.

(138) Otte, J. C.; Schmidt, A. D.; Hollert, H.; Braunbeck, T. Spatio-Temporal Development of CYP1 Activity in Early Life-Stages of Zebrafish (Danio Rerio). *Aquat. Toxicol.* **2010**, *100* (1), 38–50. https://doi.org/10.1016/j.aquatox.2010.07.006.

(139) Hornung, M. W.; Cook, P. M.; Fitzsimmons, P. N.; Kuehl, D. W.; Nichols, J. W. Tissue Distribution and Metabolism of Benzo[a]Pyrene in Embryonic and Larval Medaka (Oryzias Latipes). *Toxicol. Sci.* **2007**, *100* (2), 393–405. https://doi.org/10.1093/toxsci/kfm231.

(140) Downes, G. B.; Granato, M. Acetylcholinesterase Function Is Dispensable for Sensory Neurite Growth but Is Critical for Neuromuscular Synapse Stability. *Dev. Biol.* **2004**, *270*, 232–245. https://doi.org/10.1016/j.ydbio.2004.02.027.

(141) Behra, M.; Cousin, X.; Bertrand, C.; Vonesch, J.-L.; Biellmann, D.; Chatonnet, A.; Strähle, U. Acetylcholinesterase Is Required for Neuronal and Muscular Development in the Zebrafish Embryo. *Nat. Neurosci.* **2002**, *5* (2), 111–118. https://doi.org/10.1038/nn788.

(142) Vliegenthart, A. D. B.; Tucker, C. S.; Del Pozo, J.; Dear, J. W. Zebrafish as Model Organisms for Studying Drug-Induced Liver Injury. *Br. J. Clin. Pharmacol.* **2014**, *78* (6), 1217–1227. https://doi.org/10.1111/bcp.12408.

(143) Loerracher, A. K.; Grethlein, M.; Braunbeck, T. In Vivo Fluorescence-Based Characterization of Cytochrome P450 Activity during Embryonic Development of Zebrafish (Danio Rerio). *Ecotoxicol. Environ. Saf.* **2020**, *192* (November 2019), 110330. https://doi.org/10.1016/j.ecoenv.2020.110330.

(144) Ng, A. N. Y.; De Jong-Curtain, T. A.; Mawdsley, D. J.; White, S. J.; Shin, J.; Appel, B.; Dong, P. D. S.; Stainier, D. Y. R.; Heath, J. K. Formation of the Digestive System in Zebrafish: III. Intestinal Epithelium Morphogenesis. *Dev. Biol.* **2005**, *286* (1), 114–135.

https://doi.org/10.1016/j.ydbio.2005.07.013.

(145) Kühnert, A.; Vogs, C.; Aulhorn, S.; Altenburger, R.; Küster, E.; Busch, W.; Kühnert, A.; Vogs, C.; Altenburger, R.; Hollert, H.; et al. Biotransformation in the Zebrafish Embryo – Temporal Gene Transcription Changes of Cytochrome P450 Enzymes and Internal Exposure Dynamics of the AhR Binding Xenobiotic Benz[a]Anthracene. *Environ. Pollut.* **2017**, *230*, 1–11. https://doi.org/10.1016/j.envpol.2017.04.083.

(146) Drummond, I. A.; Majumdar, A.; Hentschel, H.; Elger, M.; Solnica-Krezel, L.; Schier, A. F.; Neuhauss, S. C. F.; Stemple, D. L.; Zwartkruis, F.; Rangini, Z.; et al. Early Development of the Zebrafish Pronephros and Analysis of Mutations Affecting Pronephric Function. *Development* **1998**, *125* (23), 4655–4667. https://doi.org/10.5167/uzh-216.

(147) Armitage, J. M.; Erickson, R. J.; Luckenbach, T.; Ng, C. A.; Prosser, R. S.; Arnot, J. A.; Schirmer, K.; Nichols, J. W. Assessing the Bioaccumulation Potential of Ionizable Organic Compounds: Current Knowledge and Research Priorities. *Environmental Toxicology and Chemistry*. 2017, pp 882–897. https://doi.org/10.1002/etc.3680.

(148) Larisch, W.; Goss, K. U. Calculating the First-Order Kinetics of Three Coupled, Reversible Processes. *SAR QSAR Environ. Res.* **2017**, *28* (8), 651–659. https://doi.org/10.1080/1062936X.2017.1365763.

(149) Ogungbemi, A. O.; Teixido, E.; Massei, R.; Scholz, S.; Küster, E. Optimization of the Spontaneous Tail Coiling Test for Fast Assessment of Neurotoxic Effects in the Zebrafish Embryo Using an Automated Workflow in KNIME®. *Neurotoxicol. Teratol.* **2020**, *81* (April). https://doi.org/10.1016/j.ntt.2020.106918.

(150) Nawaji, T.; Yamashita, N.; Umeda, H.; Zhang, S. Cytochrome P450 Expression and Chemical Metabolic Activity before Full Liver Development in Zebrafish. **2020**, 1–17.

(151) Dürkop, K. Einflussfaktoren Auf Die Biotransformation von Metoprolol Im Zebrabärblingsembryo – Untersucht Mittels LC-MS, University Leipzig, 2016.

(152) Luckenbach, T.; Fischer, S.; Sturm, A. Current Advances on ABC Drug Transporters in Fish. *Comparative Biochemistry and Physiology Part - C: Toxicology and Pharmacology*. 2014. https://doi.org/10.1016/j.cbpc.2014.05.002.

(153) Gordon, W. E.; Espinoza, J. A.; Leerberg, D. M.; Yelon, D.; Hamdoun, A. Uptake and Efflux of Xenobiotic Transporter Substrates in Zebrafish Embryo Ionocytes. *Aquat. Toxicol.* **2019**, 88–97. https://doi.org/10.1016/j.aquatox.2019.04.013.

(154) Bieczynski, F.; Burkhardt-Medicke, K.; Luquet, C. M.; Scholz, S.; Luckenbach, T. Chemical Effects on Dye Efflux Activity in Live Zebrafish Embryos and on Zebrafish Abcb4 ATPase Activity. *FEBS Lett.* **2020**, 1873-3468.14015. https://doi.org/10.1002/1873-3468.14015.

(155) Brox, S.; Ritter, A. P.; Küster, E.; Reemtsma, T. Influence of the Perivitelline Space on the Quantification of Internal Concentrations of Chemicals in Eggs of Zebrafish Embryos (Danio Rerio). *Aquat. Toxicol.* **2014**. https://doi.org/10.1016/j.aquatox.2014.10.008.

(156) Luckenbach, T.; Fischer, S.; Sturm, A. Current Advances on ABC Drug Transporters in Fish. *Comparative Biochemistry and Physiology Part - C: Toxicology and Pharmacology*. 2014, pp 28–52. https://doi.org/10.1016/j.cbpc.2014.05.002.

(157) Kirla, K. T.; Poetzsch, M.; Banote, R. K.; Eggen, R. I. L.; Schirmer, K.; Stadnicka-Michalak,

J.; Groh, K. J.; Kraemer, T. SI: Importance of Toxicokinetics to Assess the Utility of Zebrafish Larvae as Model for Psychoactive Drug Screening Using Meta-Chlorophenylpiperazine (MCPP) as Example. *Front. Pharmacol.* **2018**, *9* (April), 1–12. https://doi.org/10.3389/fphar.2018.00414.

(158) Fernandes, B.; Matamá, T.; Guimarães, D.; Gomes, A.; Cavaco-Paulo, A. Fluorescent Quantification of Melanin. *Pigment Cell Melanoma Res.* **2016**, *29* (6), 707–712. https://doi.org/10.1111/pcmr.12535.

(159) Catron, T. R.; Gaballah, S.; Tal, T. Using Zebrafish to Investigate Interactions Between Xenobiotics and Microbiota. *Curr. Pharmacol. Reports* **2019**, *5*, 468–480. https://doi.org/10.1007/s40495-019-00203-7.

(160) Benabdellah, F.; Seyer, A.; Quinton, L.; Touboul, D.; Brunelle, A.; Laprévote, O. Mass Spectrometry Imaging of Rat Brain Sections: Nanomolar Sensitivity with MALDI versus Nanometer Resolution by TOF-SIMS. *Anal. Bioanal. Chem.* **2010**. https://doi.org/10.1007/s00216-009-3031-2.

(161) Hogset, H.; Horgan, C.; Bergholt, M.; Armstrong, J.; Torraca, V.; Chen, Q.; Keane, T.; Bugeon, L.; Dallman, M.; Mostowy, S.; et al. In Vivo Biomolecular Imaging of Zebrafish Embryos Using Confocal Raman Spectroscopy. *Nat. Commun.* **2020**, No. 2020, 1–12. https://doi.org/10.1038/s41467-020-19827-1.

Chapter 2 Elemental imaging (LA-ICP-MS) of zebrafish embryos to study the toxicokinetics of the acetylcholinesterase inhibitor naled

Halbach, K.; Wagner, S.; Scholz, S.; Luckenbach, T.; Reemtsma, T. *Anal. Bioanal. Chem.* **2019**, *411* (3), 617–627.

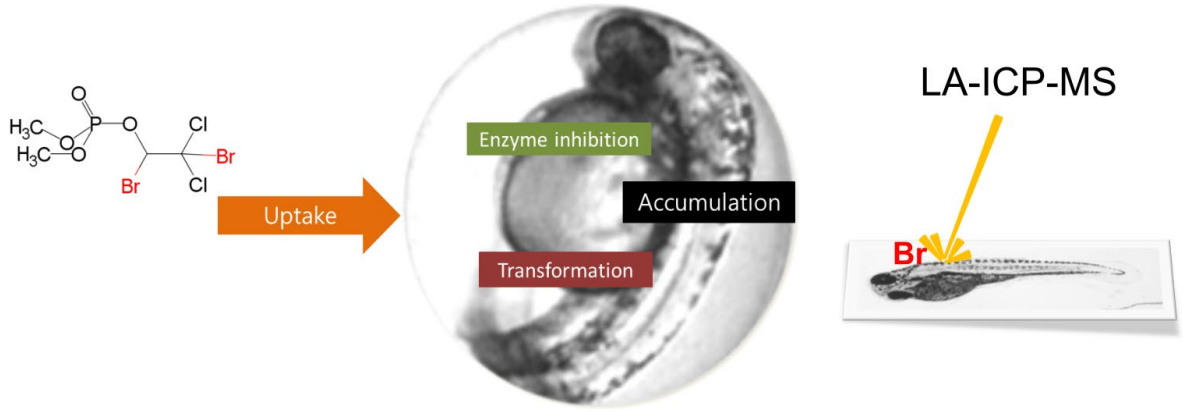

Link to the publication:

https://link.springer.com/article/10.1007/s00216-018-1471-2

Author's contribution:

I am the first author of this publication. The idea of the localization of a neuroactive compound was developed by the co-authors. I performed the exposure experiments, developed an LA-ICP-MS method and data analysis workflow. The acetylcholinesterase activity tests were performed together by Nicole Schweiger and me. The discussion and structure of the manuscript were developed together with the co-authors. I wrote the manuscript.

Analytical and Bioanalytical Chemistry (2019) 411:617–627
https://doi.org/10.1007/s00216-018-1471-2

RESEARCH PAPER

Elemental imaging (LA-ICP-MS) of zebrafish embryos to study the toxicokinetics of the acetylcholinesterase inhibitor naled

Katharina Halbach[1] · Stephan Wagner[1] · Stefan Scholz[2] · Till Luckenbach[2] · Thorsten Reemtsma[1,3]

Received: 4 September 2018 / Revised: 25 October 2018 / Accepted: 2 November 2018 / Published online: 16 November 2018

Abstract

The zebrafish embryo is an important model in ecotoxicology but the spatial distribution of chemicals and the relation to observed effects is not well understood. Quantitative imaging can help to gain insights into the distribution of chemicals in the zebrafish embryo. Laser ablation inductively coupled plasma-mass spectrometry (LA-ICP-MS) is used to quantify the uptake and the uptake kinetics of the bromine (Br) containing organophosphate naled (Dibrom®, dimethyl-1,2-dibromo-2,2-dichloroethylphosphate) and its distribution in zebrafish embryos using Br as the marker element. During exposure, the Br amounts increase in the embryos parallel to the irreversible inhibition of the acetylcholinesterase (AChE). The final amount of Br in the embryo (545 pmol/embryo) corresponds to a 280-fold enrichment of naled from the exposure solution. However, LC-MS/MS analyses showed that the internal concentration of naled remained below the LOD (7.8 fmol/embryo); also the concentration of its known transformation product dichlorvos remained low (0.85 to 2.8 pmol/embryo). These findings indicate the high reactivity and high transformation rate of naled to other products than dichlorvos. ^{12}C normalized intensity distributions of Br in the zebrafish embryo showed an enrichment of Br in its head region. Kernel density estimates of the LA-ICP-MS data were calculated and outline the high reproducibility between replicated and the shift in the Br distribution during exposure. The Br enrichment indicates a preferential debromination or direct covalent reaction of naled with AChE in this region.

Keywords Elemental distribution · Enzyme inhibition · Quantitative bioimaging · Biotransformation · Bioaccumulation · Reactive toxicity

Introduction

Zebrafish (*Danio rerio*) early life stages (0–ca. 120 h post fertilization (hpf)) represent an attractive small scale in vivo experimental and alternative model to adult animals [1] used in various research fields, such as pharmacology, (eco)toxicology, and genetics [2–4]. Toxicokinetic studies are of essential importance for the understanding of how the external exposure concentration of a toxicant translates into the internal concentration and, possibly, into an adverse outcome [5]. For example, the uptake of some compounds into the tissue depends on the pH of the exposure solution resulting in a seemingly pH-dependent toxicity of these compounds [6]. Furthermore, for compounds with a specific toxic action the effect relates to the concentration at the target site, which is either the receptor with which the toxicant interacts or the reactive site to which it binds, rather than to the average internal concentration of the organism/organ.

Published in the topical collection *Elemental and Molecular Imaging by LA-ICP-MS* with guest editor Beatriz Fernández García.

Electronic supplementary material The online version of this article (https://doi.org/10.1007/s00216-018-1471-2) contains supplementary material, which is available to authorized users.

✉ Thorsten Reemtsma
thorsten.reemtsma@ufz.de

[1] Department of Analytical Chemistry, Helmholtz Centre for Environmental Research - UFZ, Permoserstraße 15, 04318 Leipzig, Germany

[2] Department of Bioanalytical Ecotoxicology, Helmholtz Centre for Environmental Research - UFZ, Permoserstraße 15, 04318 Leipzig, Germany

[3] Institute of Analytical Chemistry, University of Leipzig, Johannisallee 29, 04103 Leipzig, Germany

Total internal concentrations in zebrafish embryos are typically determined from whole body homogenates, by extraction of the analyzed chemical and subsequent analysis with inductively coupled plasma-mass spectrometry (ICP-MS), liquid chromatography- (LC) or gas chromatography-MS [7–12]. However, the small size of the zebrafish embryo hampers the analysis of a chemical's spatial distribution given that it is not possible or difficult to dissect organs or tissues. The spatial distribution of chemicals in zebrafish embryos may, instead, be studied by quantitative imaging of molecular or elemental constituents. Chemical imaging could substantially contribute to a better understanding of toxicokinetics in zebrafish embryos, as it would show how chemicals distribute in the zebrafish embryo and whether or not they enrich in specific regions/organs. Such information would be essential to associate biological effects of chemicals with the local concentration at their site of effect.

Mass spectrometry imaging for localizing chemicals in the zebrafish embryo has been performed only recently in a few studies with lipids and exogenous compounds (e.g., cocaine, copper) and nanoparticles [10, 13–15]. The most reproducible quantitative results in MS bioimaging can be obtained with laser ablation (LA) ICP-MS [16] which was applied in the past years to study distributions of natural elements [17–21] or elemental contaminants [22] in biological matrices and to quantify local chemical concentrations [17, 23–25]. The technique determines the elemental composition of a biological sample; it thus can be applied in analyses using elemental constituents as markers, e.g., for the presence of certain proteins, for disease diagnosis, for the mode and potential of biotransformation of a compound, and/or for occurrence of reactive toxicity [26, 27]. The quantification of elements is usually performed either with matrix-matched calibration [28] or with matrix-similar substances such as gelatin [29] or agarose [13, 30].

For obtaining unambiguous results when imaging a biological sample with mass spectrometry, such as LA-ICP-MS, it is crucial that (i) the spatial resolution of the method is adequate to provide a sufficiently detailed image of the object under study. Thus, requirements in spatial resolution increase with decreasing size of this object, e.g., from a fish to a fish embryo; (ii) the specificity of the method is sufficient to detect the chemical in the complex biological matrix; (iii) the sensitivity is sufficient for tissue concentrations that can be low; (iv) quantification is possible, also taking into account matrix effects from the biological sample; (v) internal standardization of the imaging data is possible to account for varying tissue density and composition and for instrumental instability; and (vi) for reactive toxicants, both the primary chemical and the transformation product formed by the reaction with the biogenic target can be detected.

This study shows how quantitative LA-ICP-MS imaging combined with complementary techniques such as LC-MS/MS, nebulization- (neb) ICP-MS and ion chromatography (IC) can be used to study the toxicokinetics of a reactive toxicant in the zebrafish embryo. The study was performed with naled (1,2-dibromo-2,2-dichloroethyl) dimethyl phosphate, Dibrom®), as an organophosphate model insecticide containing the heteroatom bromine (Br) and thus enabling the detection of the compound by ICP-MS. The analytical results on tissue concentrations and localization were combined with the determination of its biological effect, the inhibition of the acetylcholinesterase (AChE). We aimed to (i) quantify the exposure time-dependent naled tissue concentration in relation to its AChE inhibition and transformation, (ii) determine the site (tissue/organ) of transformation, and (iii) statistically compare the LA-ICP-MS results for different individuals exposed to naled for different durations by calculating Kernel densities of the frequencies of pixel intensities. We also tested the hypothesis that Br serves as a marker for naled, i.e., whether the analysis of Br may inform about naled tissue levels.

Material and methods

Culture of zebrafish, collection of eggs, and culture of embryos

Zebrafish (*Danio rerio*, Hamilton-Buchanan, 1822), descendents from fish obtained from a local hardware store (generation F13 and F14 from the strain "UFZ-OBI") were cultured and used for the production of embryos as described previously [31]. Husbandry and experimental procedures were performed in accordance with the German animal protection standards and were approved by the Government of Saxony, Landesdirektion Leipzig, Germany (DD24-5131/25/7).

Exposure experiments

Naled ((1,2-dibromo-2,2-dichloroethyl) dimethyl phosphate, CAS no. 300-76-5) was dissolved in dimethyl sulfoxide (DMSO) and then diluted with ISO standard dilution water [32] (ISO-water) to the intended exposure concentration (DMSO concentration was 0.02% (*v*/*v*) in all treatments). Concentrations were selected to determine the effect concentrations for AChE inhibition. Based on the results (see the Electronic Supplementary Material (ESM) Fig. S1), a concentration of 3.7 μmol/L naled (corresponding to an AChE inhibition of ca. 45% and approximately 25% of the LC50 [33]) was chosen for subsequent time-resolved effect and spatial analysis. Exposure times of zebrafish embryos were varied from 0.5 to 24 h, with the termination of exposure at 96 hpf to enable measurements at the same developmental stage: 72–96, 86–96, 92–96, 94–96, 95–96, and 95.5–96 hpf. Exposure experiments were performed with 50 zebrafish embryos in a volume of 100 mL exposure solution in three replicates; three

negative control experiments were conducted by placing 50 zebrafish embryos in 100 mL ISO-water, respectively. Depuration of naled from the embryo was analyzed by transferring the embryo to control medium [32] after an exposure of 24 h and measurement of naled concentration after 1 and 24 h incubation.

Measurements of the AChE activity

The AChE enzyme activity in zebrafish embryos tissue extracts was colorimetrically determined [34]. The total amount of protein in tissue extracts was quantified according to Lowry et al. [35]. Twenty zebrafish embryos were placed in FastPrep tubes, washed with 1 mL Milli-Q water, flash frozen in liquid N_2 and stored at − 20 °C until analysis. Prior to the measurement, 400 μL cold phosphate-buffered saline (PBS, pH 7.7, 0.1 M containing 0.1% *v*/*v* Triton X-100) were added to the embryos, and the embryos were homogenized in a FastPrep®-24 (MP Biomedicals, 6 UxS^{-1}, 30 s) and centrifuged at 4 °C for 15 min (13,200 rpm). The supernatant was taken for the enzyme assay and the protein determination. For the enzyme assay, 50 μL of the sample, 50 μL PBS buffer, 100 μL 5,5′-dithiobis-(2-nitrobenzoic acid), and 100 μL acetylthiocholine iodide were added onto a 96-well plate. The absorbance was measured at 412 nm, 22 °C for 10 min. For the protein assay (Bio-Rad *DC*), 5 μL buffer, standard (bovine serum albumin in PBS buffer) or sample was pipetted into a 96-well plate, 25 μL reagent A' (0.02% *v*/*v* reagent surfactant solution in alkaline copper tartrate solution) and 200 μL Folin reagent were added. After 20 min, the absorbance was measured at 750 nm. In the results, the specific AChE activity was normalized to the mean of the negative controls.

Sample preparation for LA-ICP-MS and internal concentration analysis

For LA-ICP-MS, zebrafish embryos were washed once with 1 mL Milli-Q water, placed on glass slides and dried at room temperature (RT) for a minimum of 72 h up to a maximum of 144 h. Dried embryos were up to 150 μm in height.

For determining the internal concentration of naled and dichlorvos, 18 zebrafish embryos were placed in FastPrep tubes with glass beads, washed with Milli-Q water, and then frozen in liquid N_2. For extraction of the chemicals from the embryos, 540 μL methanol (MeOH) were added to each tube. Zebrafish embryos were homogenized in a FastPrep®-24 (MP Biomedicals, 6 m/s, 20 s), placed in an ultrasonic bath (15 min, RT) and centrifuged (13,000 rpm, 15 min, RT). The supernatant was placed in HPLC glass vials and stored at − 20 °C until analysis with LC-MS/MS. For IC measurements of bromide, 200 μL of the supernatant was transferred into a vial and placed for 2 h under a N_2 gas stream to evaporate the solvent. Afterwards, 200 μL of Milli-Q water was added. For the independent analysis of total bromine with Neb-ICP-MS, 200 μL of the supernatant was taken and diluted with 4 mL of Milli-Q water.

Instrumentation

LA-ICP-MS

LA-ICP-MS measurements were conducted with an Analyte G2 (Teledyne CETAC Technologies Inc., Bozeman, MT, USA) coupled to a double-focusing sector field ICP-MS (Spectro, Ametek, Kleve, Germany) with a Mattauch-Herzog geometry. It allows the simultaneous measurement of the mass range of *m*/*z* 6 to 238. Daily performance and fine tuning of the ICP-MS was performed with a NIST610 glass reference material (SRM-610, LGC Ltd., Middlesex, UK). ^{12}C, ^{13}C ^{31}P, ^{34}S, ^{39}K, ^{79}Br, and ^{81}Br were the measured isotopes. Determination of both Br isotopes can have contributions from polyatomic interferences, especially the ^{81}Br isotope by an abundant argon polyatomic ion [36]. Therefore, only the ^{79}Br is shown in the results part. Zebrafish embryos were ablated in line scan mode with a chosen 50 μm spotsize (square shape) in order to be able to quantify Br at different exposure durations and to have sufficient spatial resolution. A second ablation was performed to ensure the completeness of the ablation of embryo. A mean of 4 ± 3% of the total ^{12}C intensity was ablated during the second run. Furthermore, the ^{28}Si signal was analyzed as marker for complete ablation. Parameters for the measurements are listed in Table S1 (see the ESM). The acquisition time of the ICP-MS together with the spotsize and scan speed of the laser allow the calculation of a calibration range per spot (50 × 50 μm). Data analysis was performed with Iolite 3.6 in Igor Pro 7.04. Exported data were overlaid with the optical photograph in MATLAB R2015b.

Neb-ICP-MS and IC

Parameters for neb-ICP-MS can be seen in Table S1 (see the ESM). Matrix-matched calibration (range from 10 to 100 μg/L bromide) was performed by taking 200 μL of MeOH extracts from negative control zebrafish embryos, adding a bromide standard solution and diluting to 4.2 mL with Milli-Q water (LOD 1.2 μg/L; LOQ 4.0 μg/L).

The IC experiments were performed with an ICS-2000 (Dionex, ThermoFisher Scientific) and an IonPac AS18, AG18, 4 mm column (Dionex, ThermoFisher Scientific). The eluent was 21–40 mM KOH in an eluent generator cartridge, a flow rate of 1 mL/min was applied and an injection volume of 5 μL. The temperature of the column was 30 °C. Before entering the conductivity detector, a suppressor (ASRS 300 4 mm) was used.

LC-MS/MS

LC-MS/MS measurements were performed with a 1260 Infinity HPLC system (Agilent Technologies, Böblingen. Germany) and a QTrap 5500 mass spectrometer (AB Sciex, Darmstadt, Germany, TurbolonSpray interface). An Ascentis® Express C18-column (10 cm × 3.0 mm; 2.7 μm; Sigma-Aldrich) was used and Milli-Q water with 10 mM NH_4Ac as solvent A and MeOH with 10 mM NH_4Ac as solvent B. The following gradient was applied: 0 min, 95% solvent A; 3 min, 5% solvent A; 6.1 min, 95% solvent A. The flow rate was 300 μL/min and 5 μL were injected. The calibration was performed by diluting naled and dichlorvos with MeOH (LOD: dichlorvos 2 nmol/L, naled 0.3 nmol/L; corresponds to dichlorvos 7×10^{-2} pmol/embryo, naled 8×10^{-3} pmol/embryo). The transitions for naled (398–127, 382–128) and dichlorvos (221–109, 221–127) were acquired in multiple reaction monitoring. Reported data for the extracts were not corrected for matrix effects and recovery after sample preparation (matrix effects naled < 45%, recovery naled < 5%; matrix effects dichlorvos < 10%, recovery dichlorvos > 90%).

Profilometer

Measurements were performed with a S neox non-contact 3D surface profiler (Sensofar, Barcelona, Spain). Data were analyzed with the software SensoScan 5.3 and SensoMap 7.0. Two profiles of two ablations, respectively, are depicted in Fig. S2 (see the ESM).

Bromine quantification

The internal amount of Br was determined in three independent ways: (i) by summation of the calibrated ^{79}Br-signal of the imaging data (LA-ICP-MS), (ii) in the extract of the homogenized embryos by Neb-ICP-MS, and (iii) in the extracts by IC as bromide. For LA-ICP-MS, the quantification was performed with agarose gels spiked with a bromide ICP-MS standard solution [30]. The standards were ablated under the same measurement parameters as the zebrafish embryos. The homogeneity of the standards was determined by ablating the total length and width of the glass slide: a decrease in the Br intensity was observed at the edges of the slide leading to a higher concentration in the middle. Therefore, a factor of 1.32 was applied during Br quantification to correct for this concentration gradient [30]. The workflow in Iolite 3.6 included a baseline subtraction, a correction of peak drift over time measured with the agarose standards, and the quantification of counts per second to mass. The calibration range was 37 to 598 ng Br/spot (two calibration curves are shown in ESM Fig. S3). After ablation of 4 embryos, a calibration was performed. This was necessary because the intensity of one agarose standard showed a high variation between different ablation cycles (incl. different days of ablation), e.g., 30,900–57,500 cps (RSD of 21%) for the agarose standard 62 pg Br/spot and 46,800–122,600 cps (RSD of 28%) for the agarose standard 108 pg Br/spot. A range for the LOQ was obtained of 38 pg Br/spot (calculated out of a signal to noise ratio of 10 in a blank agarose standard). In order to account for the varying ablated mass of the dried embryo, the intensity ratio of ^{79}Br to ^{12}C was calculated.

Results and discussion

Time course of uptake and effect during exposure of zebrafish embryos to naled

Naled as a phosphoric acid triester is an electrophile that reacts with AChE or with other nucleophiles including water (Fig. 1). Moreover, naled has been reported to undergo non-enzymatic reductive debromination in biological tissues to form dichlorvos, which can also act as AChE inhibitor [37–39]. Dichlorvos may be further transformed to non-toxic and non-brominated products. It should be noted that during the time of exposure the external concentration of naled decreased from 3.7 to 1.0 μmol/L (ESM Fig. S4), likely due to hydrolysis [37]. The hydrolysis products of naled do not act as AChE inhibitors and are more hydrophilic. Hence, they are possibly taken up more slowly than the parent compound [40]. Because naled is highly reactive, its uptake and distribution in the embryo may not be determined by analyzing naled itself. Indeed, naled could not be detected in embryo extracts by LC-MS/MS (LOD: 8 fmol/embryo) at any time during exposure to 3.7 μmol/L naled.

However, it was hypothesized that the amount of Br in the embryo reflects the amount of naled taken up. Indeed, the internal Br amount rapidly increased within the first 10 h of exposure to naled and reached 545 pmol/individual after 24 h exposure (Fig. 2a). Based on a volume of 250 nL for the zebrafish embryo at 96 hpf (ESM Fig. S6), this Br amount would correspond to a 280-fold enrichment of naled in the embryo compared to the exposure solution, provided that all Br in the embryo originates from naled. This would be two orders of magnitude higher compared to the bioconcentration factor in zebrafish embryos reported by Brox et al. for compounds with a similar octanol-water partition coefficient (e.g., phenacetin (log $D = 1.41$), colchicine (log $D = 1.46$)) [12]. Thus, the transformation of the parent compound to the bromine-containing transformation product results in an accumulation of Br. No significant decrease of the Br signal was visible over 24 h of depuration (t test: $p = 0.22$ for 1 h depuration and $p = 0.55$ for 24 h depuration, respectively) (ESM Fig. S8).

AChE activity in the embryos decreased with increase in Br amount and after 24 h exposure was at 30% compared to the non-exposed control (Fig. 2a). Given that AChE inhibition quickly proceeds [41], the inverse time course of the internal

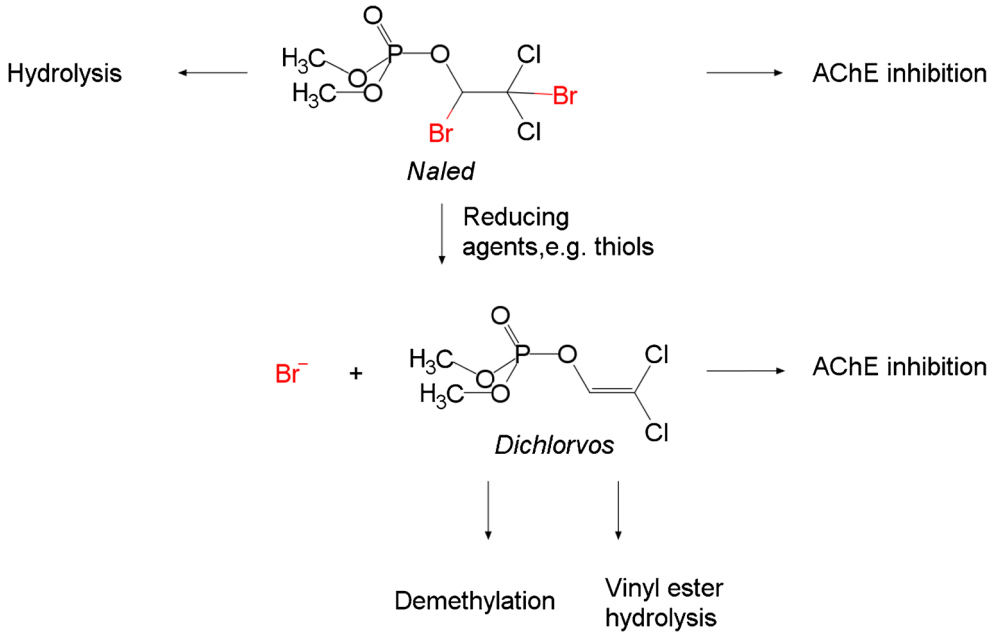

Fig. 1 Transformation products and biological effects of naled. Naled may be hydrolyzed (mainly in the exposure solution) or reduced to dichlorvos (in biological systems). Total Br in the tissue was quantified with LA-ICP-MS and in extracts by neb-ICP-MS, naled and dichlorvos were determined in extracts by LC-MS/MS, bromide by ion chromatography. AChE activity was determined in an enzyme assay

Br amount and AChE activity suggests a rapid distribution of naled or of its transformation product to the target site AChE. As there is no apparent time delay between the acquirements of measurable tissue levels and the AChE inhibiting effect of naled in the organism, the internal Br amount may, therefore, be a suitable measure for the biological effect amplitude.

LC-high-resolution MS (LC-HRMS) analysis of the embryo extracts (ESM Table S2) was performed and the data were searched for signals of other brominated or chlorinated transformation products of naled. However, there were no indications for the presence of other brominated compounds. Additionally, the bromide amount in embryo extracts was analyzed by IC, showing that the Br detected by LA-ICP-MS, indeed, occurred as bromide (Table 1). With respect to toxicokinetics, these findings consistently suggest that the entire naled that initially was taken up by the embryo was quantitatively transformed to non-brominated products, among them dichlorvos and bromide. The Br amounts were well above the sum of internal amounts of naled and dichlorvos, e.g., 2 times as high at 0.5 h exposure and 326 times higher at 24 h.

The time course of the internal amount of dichlorvos is not correlated to the AChE inhibition, whereas the internal Br amounts significantly correlate with the AChE inhibition (Fig. 2b; Spearman correlation $p = 0.18$ and 0.0028, respectively). This may indicate that irreversible binding of naled to AChE proceeds more quickly than the transformation of naled to dichlorvos, so that the internal dichlorvos amount is not relevant for the biological effect. This would contradict the earlier assumption from a rat and mouse study that indeed dichlorvos is the biologically effective form of naled [39, 42]. Since the inhibition of AChE is due to binding to the AChE and transesterification of the toxicant, either naled or dichlorvos, the time course of the internal amount of dichlorvos may not be expected to represent the time course of the inhibition. In addition, the concentration gradient of dichlorvos to the exposure solution may also affect a possible correlation with the AChE inhibition. Hence, internal Br amount can be used as an indicator of the uptake of naled but does not help to clarify the mechanism of the subsequent inhibition of AChE.

The internal amounts of Br were also determined from ZFE extracts by neb-ICP-MS. For most sampling time points, they were higher than those calculated from the spatially resolved LA-ICP-MS results (Table 1). The internal Br amounts were particularly underestimated by LA-ICP-MS after short exposure periods when internal concentrations are lowest: e.g., at 0.5 h of exposure only 23% of the amount determined in the extract by neb-ICP-MS was found by LA-ICP-MS. If tissue concentrations are low, the signal intensity of most spots analyzed by LA-ICP-MS is below the LOQ, whereas the total concentration is well measurable from the extract by neb-ICP-MS. At Br levels of 100 pmol/individual, the agreement of Br quantities is acceptable (66–110%): this confirms previous findings that LA-ICP-MS imaging can be performed quantitatively if combined with external calibration using spiked agarose gels [30]. The bromide data in Table 1 support the validity of both quantitative approaches, one consisting of air-drying of the embryos followed by LA-ICP-MS, the other one of extraction of the embryos, solvent change, and IC analysis.

Validation of the LA-ICP-MS measurements for the ablation of biological tissue of varying thickness

In this study, the entire air-dried embryo was ablated rather than a slice of constant thickness as would be obtained by

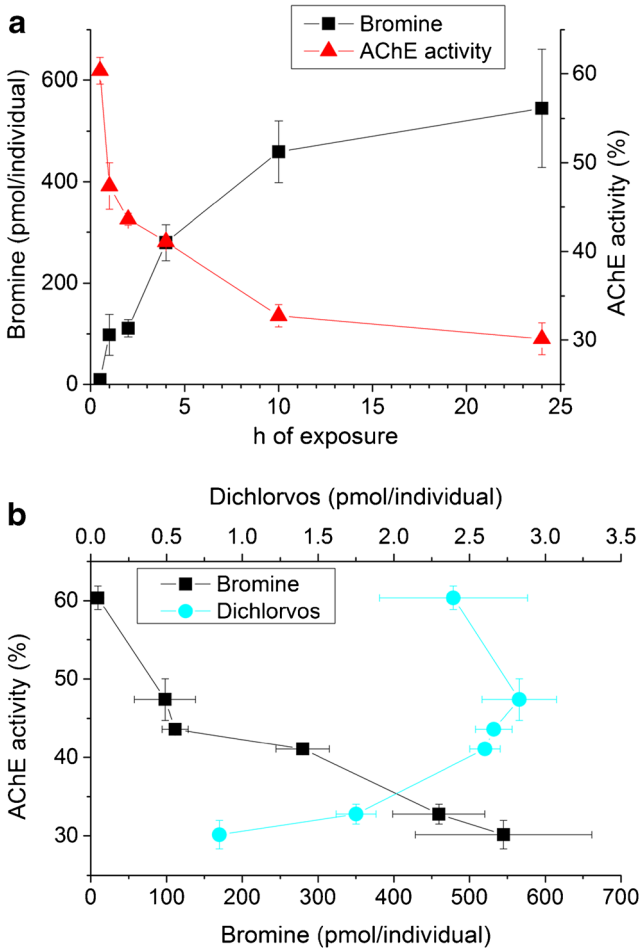

Fig. 2 **a** AChE inhibition ($n = 3$) normalized to the specific activity in the negative control and integrated Br amount in the zebrafish embryo ($n = 4$, in the case of 24 h $n = 5$) determined with LA-ICP-MS. **b** AChE activity plotted against the internal dichlorvos (LC-MS/MS, $n = 3$) and Br amounts (measured with LA-ICP-MS) (see also ESM Fig. S5). Endpoint of the exposures was 96 hpf

sectioning. On the one hand, this may have several disadvantages. (i) The visual image of the signal intensity of an element does not represent its (variable) concentration as the mass of the biological material ablated per spot is not constant but varies with the thickness of the object at that site. However, the completeness of the ablation was ensured by a second ablation (see the "Material and methods" section). (ii) Also, the amount of matrix may increase with increasing thickness of the object. However, this was found to be negligible when validating the quantification with the neb-ICP-MS. (iii) Smaller organs of the embryo, e.g., its liver or heart may be less clearly visible if they are superimposed by other body compartments. On the other hand, LA-ICP-MS imaging of the whole air-dried embryo provides advantages: it provides higher sensitivity as the whole organism is available for analysis rather than a slim tissue section, only, it excludes the uncertainty of extrapolating quantitative data obtained from a limited number of cryosections to the whole body and it requires less sample preparation.

Due to the variable thickness and tissue density of the embryo, the Br intensity images need to be normalized to the amount of biogenic organic matter ablated at each spot to obtain Br concentration images. Here, ^{12}C was used for this purpose, as its concentration should be fairly uniform among the different biological tissues [43].

The ^{12}C signal intensities were partly comparable with the thickness profile recorded for three embryos before the laser ablation process by a profilometer (ESM Fig. S2). The ^{12}C to thickness ratio of the data normalized to a range from 0 to 1 was in average 1.1 with a rsd of 51% (for 269 spots from 9 transects of three ablations). The element ^{31}P signal exhibited a similar ratio and could be used for the normalization as well (ESM Fig. S2) [18, 24, 44]. In the region of the swim bladder, the ^{12}C signal intensity and the thickness were deviating. Since the swim bladder represents a gas-filled organ, the thickness does not correlate to the tissue amount. Moreover, from the head of the embryo the intensity of ^{12}C increases to the tail (see an example for both observations in ESM Fig. S2i). The latter may be related to the higher tissue density in the yolk of

Table 1 Comparison of internal amounts of Br determined by LA-ICP-MS ($n = 4$, in the case of 24 h $n = 5$), neb-ICP-MS ($n = 3$), and of bromide measured with IC ($n = 3$) (mean in pmol/individual and %rsd)

h of exposure Endpoint: 96 hpf	Br LA-ICP-MS		Br in extracts neb-ICP-MS		Bromide in extracts IC		Br: LA-ICP-MS/ neb-ICP-MS	Br vs. bromide: LA-ICP-MS/IC
	pmol/individual	%rsd	pmol/individual	%rsd	pmol/individual	%rsd		
0.5	9.3	24	41	50	< LOQ		0.23	< LOQ IC
1	98	38	90	11	58	30	1.1	1.7
2	111	15	167	2	106	11	0.66	1.0
4	280	13	342	5	232	10	0.82*	1.2
10	459	13	507	6	398	6	0.91	1.2
24	545	21	713	7	462	16	0.76*	1.2

* Labeled ratios indicate that the mean of the two methods are significantly (Welch's t test or Mann-Whitney U test, $p < 0.05$) different

the embryo which may lead to larger particle sizes generated by the laser ablation, a diminished particle transport efficacy to the plasma, and, therefore, a lower sensitivity of the ICP-MS [45]. This may also contribute to the deviation of the LA-ICP-MS and neb-ICP-MS results. A further advantage of normalization to the intensity of ^{12}C is the possibility to compensate for instrumental fluctuations during LA-ICP-MS.

Spatial distribution of Br in the zebrafish embryo investigated with LA-ICP-MS

The total internal amount of a compound does not provide information on its spatial distribution in the organism and how much of the compound is present in the tissue areas with the biological target site. Therefore, the distribution of Br in the zebrafish embryo was determined by quantitative LA-ICP-MS analysis, after different durations of exposure (Fig. 3b, f, j). The color-coded visual images of the Br distribution showed the most intensive Br signal in the head region already after 2 h of exposure (Fig. 3b). This distribution appears to remain stable or to become even more pronounced until the end of the exposure (24 h, Fig. 3f) and remains also after 24 h of depuration (Fig. 3j). The portion of Br in the head region corresponds to approximately 40% of the total Br (calculated by defining regions of interest with "Monocle" in Iolite, Tables 1 and 2) [46]. This is consistent over the different exposure duration. An enrichment of Br is not seen for the yolk, although this compartment accounts for a similar portion of the body mass (29% of the total carbon as mean of the different exposure durations, in contrast the head accounts for 26% of the total carbon).

The mean $^{79}Br/^{12}C$ ratio confirms the enrichment of Br in the head region, exhibiting levels between 2.6 and 4.7 times higher than in the yolk (Fig. 3d, h, l) (Table 2). However, Br amounts were often below the LOQ of the LA-ICP-MS approach, namely for the thin tail and also partly for the yolk. Therefore, $^{79}Br/^{12}C$ ratios could only be calculated for 30% of the spots.

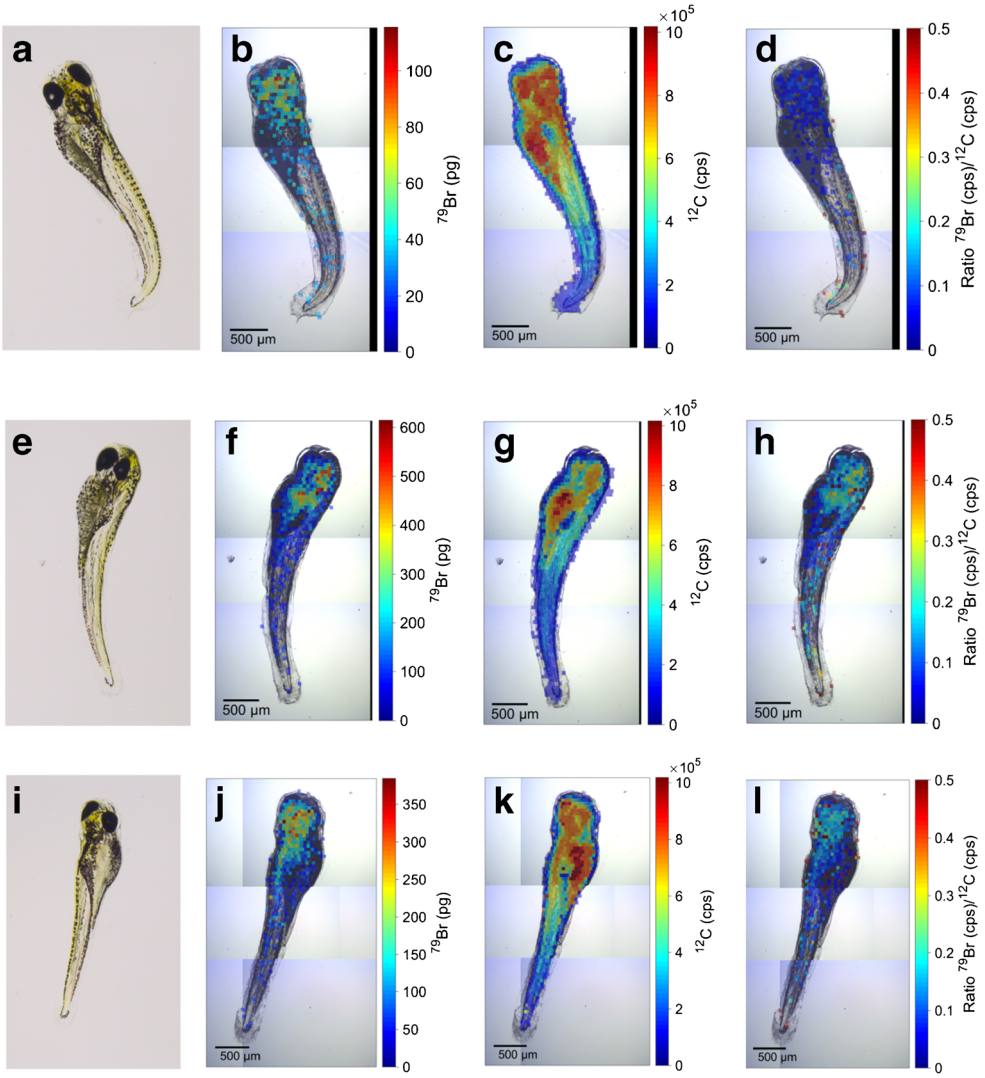

Fig. 3 Microscopic images of the zebrafish embryo (**a**, **e**, **i**) and spatially resolved images obtained by LA-ICP-MS for ^{79}Br (**b**, **f**, **j**), ^{12}C (**c**, **g**, **k**), and the ratio of intensities (cps) of ^{79}Br to ^{12}C (**d**, **h**, **l**). A spotsize of 50 µm was used for ablation. Intensities that were below the LOQ were not color coded. Zebrafish embryos were exposed for 2 h (**a**–**d**) and 24 h (**e**–**h**); endpoint was 96 hpf. Zebrafish embryos in **i**–**l** were exposed for 24 h with 24 h depuration (endpoint was 120 hpf)

Table 2 Total Br amounts and mean $^{79}Br/^{12}C$ ratios in the regions of interest head and yolk measure with LA-ICP-MS (an example for the definition can be found in ESM Fig. S7). Endpoint of exposure was 96 hpf. (0.5 h exposure are not displayed because of the low Br amount)

h of exposure	Br head pmol/individual	%rsd	Br yolk pmol/individual	%rsd	$^{79}Br/^{12}C$ head	%rsd	$^{79}Br/^{12}C$ yolk	%rsd
1	32	14	5.4	36	0.019	11	0.0048	40
2	54	17	12	35	0.042	8.1	0.0088	24
4	102	9.3	45	21	0.048	20	0.015	27
10	168	12	75	34	0.10	18	0.036	20
24	216	25	117	25	0.12	15	0.047	18

Evaluation of the uncertainty of the LA-ICP-MS measurements and biological variation

Independent from the normalization, a visual inspection and comparison of images could be subjective and prone to misinterpretation. A visual inspection does neither provide a measure for the similarity of the elemental distribution of individuals in one experiment (i.e., the precision) nor for the differences between the mean distributions of different exposures.

Obviously, a quantitative measure is needed to describe the degree of homogeneity in the spatial distribution of an analyte in imaging mass spectrometry. This measure would allow comparing both the similarity in the distribution of an analyte in biological replicates as well as the dissimilarity in the distribution between organisms exposed under different conditions. On this basis, it would be possible to judge as to whether differences in the spatial distribution between groups of organisms are statistically significant.

For this purpose, Kernel density estimates of the intensities per pixel were calculated from the LA-ICP-MS data of the zebrafish embryos (Fig. 4). Kernel density estimates have been conducted previously for an experimental-modeling-approach in LA-ICP-MS and as a first visual inspection tool [46, 47]. However, to our knowledge Kernel density estimates have not yet been used for a comprehensive comparison of the distribution of toxicants between biological objects.

In the Kernel density estimates, the width of the confidence interval of the density estimates, i.e., the width of the lines in Fig. 4, are influenced by the measurement uncertainty as well as by biological variability between individual organism and is, thus, a measure of the total precision. For ^{79}Br, the lines are very narrow and significant differences between the different times of exposure are visible (Fig. 4a). For ^{12}C, the lines are wider and less distinct, indicating a higher variability in the ^{12}C distribution of individuals (Fig. 4b).

The distribution of ^{79}Br in the zebrafish embryos is monomodal and positively skewed (Fig. 4a). In contrast, Kernel density estimates of the ^{12}C intensities are bimodal (Fig.4b). The thicker parts of the embryo (head and yolk) are represented by the maximum at higher and thinner parts of the embryo by the maximum at lower intensities. By comparing Fig. 4a and Fig. 4b, it becomes clear that ^{79}Br and ^{12}C are distributed differently. Theoretically, an even distribution of ^{79}Br and ^{12}C would be represented by a vertical line in the graph for the $^{79}Br/^{12}C$ ratio, while real, measured data of the even distribution would translate into a (narrow) Gaussian curve due to measurement uncertainty. The difference between biological replicates would broaden this Gaussian curve further. Individual density curves for the replicates can be seen in Figs. S9 and S10 (see the ESM).

The density curves of $^{79}Br/^{12}C$ in Fig. 4c show a change in distribution from a narrow (more homogenous) distribution at 1 h (green line in Fig. 4c) towards a broader distribution with increasing frequency of spots with higher $^{79}Br/^{12}C$ ratios after 10 h (yellow line). The 24 h density (brown line) is comparable to the 10 h. This is consistent with the stable total internal Br amount in this period of exposure (Fig. 2a). The effect of the exposure duration is particularly visible in the density curves of $^{79}Br/^{12}C$ in Fig. 4c stressing the importance of the normalization.

The Kernel density estimates turn out to be a useful tool to exploit the data on Br concentrations resolved in space and time.

Toxicokinetics of naled based on time-resolved imaging data

The LA-ICP-MS imaging of zebrafish embryos after different durations of exposure to naled combined with a suite of complementary analytical techniques allows drawing the following picture of the toxicokinetics of naled:

The internal amounts of Br (Fig. 2 and Table 2) show that naled is taken up and rapidly quantitatively transformed to bromide and smaller amounts of dichlorvos and other possible transformation products. This transformation possibly increased the uptake and lead to a strong enrichment of Br in the embryo. After 10 h of exposure, the internal Br amount was stable for the rest of the exposure duration. The AChE inhibition correlates with the internal Br amount (Fig. 2a). Br in the embryo occurred as bromide, as shown by IC.

LA-ICP-MS imaging confirmed an enrichment of Br in the head compared to the yolk of the embryos (Fig. 3). Bromide

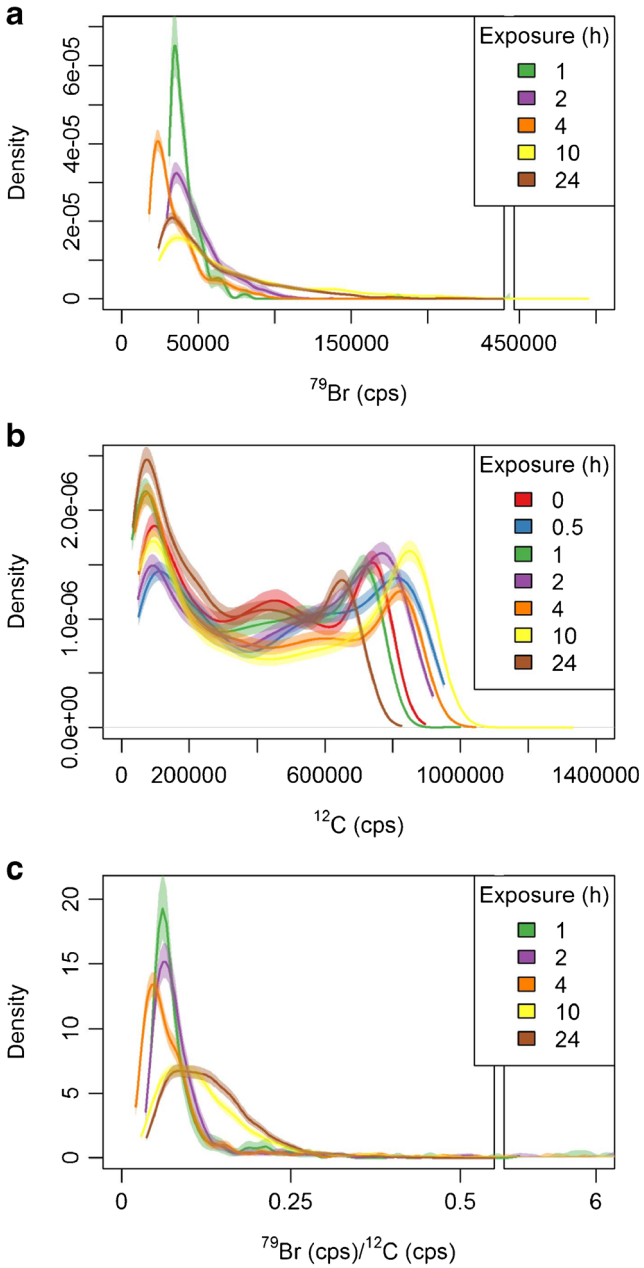

Fig. 4 Kernel density estimates with 5% confidence interval (using the density function in R3.3.2 with default smoothing settings, confidence intervals were calculated with 1000 bootstrap iterations) for **a** ^{79}Br, **b** ^{12}C, and **c** ^{79}Br/^{12}C; $n = 4$ for each exposure duration (except 24 h exposure $n = 5$). At 0 and 0.5 of exposure to naled, only few pixels contained Br intensities above the LOQ restricting the calculation of Kernel densities

may have been released from naled at the target site before or after covalent binding to and inhibition of the AChE. However, the Br enrichment in regions rich in nervous tissue and, hence, in cholinergic synapses, suggests that naled was accumulated and reacted with its target, possibly releasing dibromdichloroethanol which was eventually debrominated. The local accumulation may be explained partially by affinity to the target site. This hypothesis is supported by literature. Firstly, it has been shown for AChE in other fish (electric eel) that naled is more reactive towards AChE than dichlorvos, with a bimolecular rate constant being 17 times higher [41]. Secondly, it has been shown by staining that AChE is located in the brain and heart of zebrafish embryos [48, 49].

Alternatively, bromide may have been released at the target site prior to binding of a transformation process such as dichlorvos to the AChE. Then the distribution of Br would indicate higher frequencies of the reducing agents that transform naled to dichlorvos (e.g., thiols) in these regions. Subsequently, dichlorvos rather than naled reacts with and thereby inhibits the AChE. This was suggested by Casida (1972). However, in this case one may not expect an accumulation of Br in regions rich of the AChE target. The rapid transformation could be tested by detection of thiols representing major reductants of naled. It could be expected that thiols or sulfur is enriched in the same region as bromide. However, the ^{34}S signal obtained by our LA-ICP-MS analyses was too weak to generate a meaningful image of its distribution in the embryo. Also, a parallel occurrence of both processes—covalent binding of naled and its transformation products—may be possible.

Conclusion

This study demonstrated that the combined time-resolved analysis of biological activity, of total internal concentrations and of the tissue distribution of naled in zebrafish embryos by LA-ICP-MS, in combination with additional analytical techniques allows to elucidate the toxicokinetic and initial steps of the toxicodynamics of this reactive toxicants. It was demonstrated for the AChE inhibitor naled that these processes can be quite complex. Quantitative imaging by LA-ICP-MS is attractive to determine the spatial distribution of toxic compounds with a suitable elemental signature and to detect their enrichment in certain regions of the zebrafish embryo. Beyond Br also other heteroatoms such as iodine, arsenic, platinum, or gadolinium can be found in chemicals released by human activity to the environment. For these compounds, LA-ICP-MS represents a suitable method to study uptake and distributions in the zebrafish embryo model.

Compared to the imaging of sections of zebrafish embryos, the analysis of air-dried whole embryos is much easier. If combined with normalization to ^{12}C, it allows for quantitative imaging and the determination of concentrations in selected regions of the embryo. Kernel density estimates are helpful tools to assess the homogeneity of the distribution for elements or molecules determined by MS imaging in the zebrafish embryo and to assess its variability between individuals. They are essential also to determine differences in the internal distribution over time. This may be further developed, e.g. by parametrization of the density estimates, in order to

statistically show the significance of the exposure time or distribution of different elements.

Acknowledgements This work is part of the Integrated Project "Exposome "of the topic "Chemicals in the Environment" at the Helmholtz Centre for Environmental Research. LA-ICP-MS measurements were conducted in the ProVIS Centre for Chemical Microscopy at UFZ. We thank Nicole Schweiger for the support with the zebrafish embryo exposure experiments and AChE activity test. We acknowledge Dr. Bettina Seiwert for the Xevo-Tof and Michaela Wunderlich for the ion chromatography measurements. We acknowledge the help of Teresa Split for generating zebrafish images and calculating volumes of embryos.

Compliance with ethical standards

Conflict of interest The authors declare that they have no conflict of interest.

References

1. Strähle U, Geisler R, Greiner P, Hollert H, Rastegar S, Schumacher A, et al. Zebrafish embryos as an alternative to animal experiments—a commentary on the definition of the onset of protected life stages in animal welfare regulations. Reprod Toxicol. 2012;33:128–32. https://doi.org/10.1016/J.REPROTOX.2011.06.121.
2. Lieschke GJ, Currie PD. Animal models of human disease: zebrafish swim into view. Nat Rev Genet. 2007;8:353–67. https://doi.org/10.1038/nrg2091.
3. Grunwald DJ, Eisen JS. Headwaters of the zebrafish—emergence of a new model vertebrate. Nat Rev Genet. 2002;3:717–24. https://doi.org/10.1038/nrg892.
4. Saad M, Cavanaugh K, Verbueken E, Pype C, Casteleyn C, Van Ginneken C, et al. Xenobiotic metabolism in the zebrafish: a review of the spatiotemporal distribution, modulation and activity of Cytochrome P450 families 1 to 3. J Toxicol Sci. 2016;41:1–11. https://doi.org/10.2131/jts.41.1.
5. Escher B, Hermens J, Schwarzenbach R. International workshop: internal exposure—linking bioavailability to effects. Environ Sci Pollut Res. 2005:57–60.
6. Bittner L, Teixido E, Seiwert B, Escher BI, Klüver N. Influence of pH on the uptake and toxicity of B-blockers in embryos of zebrafish, Danio rerio. Aquat Toxicol. 2018;201:129–37. https://doi.org/10.1016/j.aquatox.2018.05.020.
7. Costas-Rodríguez M, Van Acker T, Hastuti AAMB, Devisscher L, Van Campenhout S, Van Vlierberghe H, et al. Laser ablation-inductively coupled plasma-mass spectrometry for quantitative mapping of the copper distribution in liver tissue sections from mice with liver disease induced by common bile duct ligation. J Anal At Spectrom. 2017;32:1805–12. https://doi.org/10.1039/C7JA00134G.
8. Kühnert A, Vogs C, Altenburger R, Küster E. The internal concentration of organic substances in fish embryos—a toxicokinetic approach. Environ Toxicol Chem. 2013;32:1819–27. https://doi.org/10.1002/etc.2239.
9. Brox S, Ritter AP, Küster E, Reemtsma T. A quantitative HPLC-MS/MS method for studying internal concentrations and toxicokinetics of 34 polar analytes in zebrafish (Danio rerio) embryos. Anal Bioanal Chem. 2014;406:4831–40. https://doi.org/10.1007/s00216-014-7929-y.
10. Kirla KT, Groh KJ, Steuer AE, Poetzsch M, Banote RK, Stadnicka-Michalak J, et al. Zebrafish larvae are insensitive to stimulation by cocaine: importance of exposure route and toxicokinetics. Toxicol Sci. 2016;154:183–93. https://doi.org/10.1093/toxsci/kfw156.
11. Wang G, Shi H, Du Z, Chen H, Peng J, Gao S. Bioaccumulation mechanism of organophosphate esters in adult zebrafish (Danio rerio). Environ Pollut. 2017;229:177–87. https://doi.org/10.1016/j.envpol.2017.05.075.
12. Brox S, Seiwert B, Küster E, Reemtsma T. Toxicokinetics of polar chemicals in zebrafish embryo (Danio rerio): influence of physicochemical properties and of biological processes. Environ Sci Technol. 2016;50:10264–72. https://doi.org/10.1021/acs.est.6b04325.
13. Böhme S, Stärk H-J, Kühnel D, Reemtsma T. Exploring LA-ICP-MS as a quantitative imaging technique to study nanoparticle uptake in Daphnia magna and zebrafish (Danio rerio) embryos. Anal Bioanal Chem. 2015;407:5477–85.
14. Pirro V, Guffey SC, Sepúlveda MS, Mahapatra CT, Ferreira CR, Jarmusch AK, et al. Lipid dynamics in zebrafish embryonic development observed by DESI-MS imaging and nanoelectrospray-MS. Mol BioSyst. 2016;12:2069–79. https://doi.org/10.1039/C6MB00168H.
15. Ackerman CM, Weber PK, Xiao T, Thai B, Kuo TJ, Zhang E, et al. Multimodal LA-ICP-MS and nanoSIMS imaging enables copper mapping within photoreceptor megamitochondria in a zebrafish model of Menkes disease. Metallomics. 2018;10:474–85. https://doi.org/10.1039/C7MT00349H.
16. Ellis SR, Bruinen AL, Heeren RMA. A critical evaluation of the current state-of-the-art in quantitative imaging mass spectrometry. Anal Bioanal Chem. 2014;406:1275–89. https://doi.org/10.1007/s00216-013-7478-9.
17. Becker JS, Zoriy M, Matusch A, Wu B, Salber D, Palm C, et al. Bioimaging of metals by laser ablation inductively coupled plasma mass spectrometry (LA-ICP-MS). Mass Spectrom Rev. 2010;29:156–75. https://doi.org/10.1002/mas.20239.
18. Hare D, Austin C, Doble P. Quantification strategies for elemental imaging of biological samples using laser ablation-inductively coupled plasma-mass spectrometry. Analyst. 2012;137:1527–37. https://doi.org/10.1039/c2an15792f.
19. Urgast DS, Beattie JH, Feldmann J. Imaging of trace elements in tissues: with a focus on laser ablation inductively coupled plasma mass spectrometry. Curr Opin Clin Nutr Metab Care. 2014;17:432–9. https://doi.org/10.1097/MCO.0000000000000087.
20. Reifschneider O, Schütz CL, Brochhausen C, Hampel G, Ross T, Sperling M, et al. Quantitative bioimaging of p-boronophenylalanine in thin liver tissue sections as a tool for treatment planning in boron neutron capture therapy. Anal Bioanal Chem. 2015;407:2365–71. https://doi.org/10.1007/s00216-014-8012-4.
21. Theiner S, Van Malderen SJM, Van Acker T, Legin AA, Keppler BK, Vanhaecke F, et al. Fast high-resolution LA-ICP-MS imaging of the distribution of platinum-based anti-cancer compounds in multicellular tumor spheroids. Anal Chem. 2017;89:12641–5. https://doi.org/10.1021/acs.analchem.7b02681.
22. Barst BD, Gevertz AK, Chumchal MM, Smith JD, Rainwater TR, Drevnick PE, et al. Laser ablation ICP-MS co-localization of mercury and immune response in fish. Environ Sci Technol. 2011;45:8982–8. https://doi.org/10.1021/es201641x.
23. Limbeck A, Galler P, Bonta M, Bauer G, Nischkauer W, Vanhaecke F. Recent advances in quantitative LA-ICP-MS analysis: challenges and solutions in the life sciences and environmental chemistry. Anal

Bioanal Chem. 2015;407:6593–617. https://doi.org/10.1007/s00216-015-8858-0.
24. Konz I, Fernández B, Fernández ML, Pereiro R, González-Iglesias H, Coca-Prados M, et al. Quantitative bioimaging of trace elements in the human lens by LA-ICP-MS. Anal Bioanal Chem. 2014;406:2343–8. https://doi.org/10.1007/s00216-014-7617-y.
25. Becker JS, Matusch A, Wu B. Bioimaging mass spectrometry of trace elements - recent advance and application of LA-ICP-MS: a review. Anal Chim Acta. 2014;835:1–18.
26. Waentig L, Jakubowski N, Hayen H, Roos PH. Iodination of proteins, proteomes and antibodies with potassium triodide for LA-ICP-MS based proteomic analyses. J Anal At Spectrom. 2011;26:1610–8. https://doi.org/10.1039/c1ja10090d.
27. Matusch A, Depboylu C, Palm C, Wu B, Höglinger GU, Schäfer MKH, et al. Cerebral bioimaging of Cu, Fe, Zn, and Mn in the MPTP mouse model of Parkinson's disease using laser ablation inductively coupled plasma mass spectrometry (LA-ICP-MS). J Am Soc Mass Spectrom. 2010;21:161–71. https://doi.org/10.1016/j.jasms.2009.09.022.
28. Gokhan Elci S, Yan B, Tae Kim S, Saha K, Jiang Y, Klemmer GA, et al. Quantitative imaging of 2 nm monolayer-protected gold nanoparticle distributions in tissues using laser ablation inductively-coupled plasma mass spectrometry (LA-ICP-MS). Analyst. 2016;141:2418–25.
29. Šala M, Šelih VS, van Elteren J. Gelatin gels as multi-element calibration standards in LA-ICP-MS bioimaging: fabrication of homogeneous standards and micro-homogeneity testing. Analyst. 2017;142:3356–9. https://doi.org/10.1039/C7AN01361B.
30. Stärk H-J, Wennrich R. A new approach for calibration of laser ablation inductively coupled plasma mass spectrometry using thin layers of spiked agarose gels as references. Anal Bioanal Chem. 2011;399:2211–7. https://doi.org/10.1007/s00216-010-4413-1.
31. Fetter E, Baldauf L, Lidzba A, Altenburger R, Schu A, Scholz S. Identification and characterization of androgen-responsive genes in zebrafish embryos. Environ Sci Technol. 2015;49:11789–98. https://doi.org/10.1021/acs.est.5b01034.
32. ISO. Water quality—determination of the acute lethal toxicity of substances to a freshwater fish. ISO. 1996:7346–1.
33. Padilla S, Corum D, Padnos B, Hunter DL, Beam A, Houck KA, et al. Zebrafish developmental screening of the ToxCast (TM) phase I chemical library. Reprod Toxicol. 2012;33:174–87. https://doi.org/10.1016/j.reprotox.2011.10.018.
34. Küster E. Cholin- and carboxylesterase activities in developing zebrafish embryos (Danio rerio) and their potential use for insecticide hazard assessment. Aquat Toxicol. 2005. https://doi.org/10.1016/j.aquatox.2005.07.005.
35. Lowry OH, Rosenbrough NJ, Farr AL, Randall RJ. Protein measurement with the folin. J Biol Chem. 1951;193:265–75. https://doi.org/10.1016/0304-3894(92)87011-4.
36. May TW, Wiedmeyer RH. A table of polyatomic interferences. At Spectrosc. 1998;19:150–5.
37. Helliker PE. Naled—risk characterization document (RCD 99-03). California Environmental Protection Agency - Department of Pesticide Regulation. 1999
38. Eto M. Organophosphorus pesticides: organic and biological chemistry. Boca Raton: CRC Press; 1976.
39. Casida JE. Chemistry and metabolism of terminal residues of organophosphorus compounds and carbamates. In: Tahori AS, editor. Pesticide chemistry, Proceedings of the Second International IUPAC Congress, vol. VI. London: Gordon & Breach; 1972. p. 295–315.
40. Escher BI, Hermens JLM. Modes of action in ecotoxicology: their role in body burdens, species sensitivity, QSARs, and mixture effects. Environ Sci Technol. 2002;36:4201–17.
41. Herzsprung P, Weil L, Niessner R. Measurement of bimolecular rate constants ki of the cholinesterase inactivation reaction by 55 insecticides and of the influence of various pyridiniumoximes on ki. Int J Environ Anal Chem. 1992;47:181–200. https://doi.org/10.1080/03067319208027028.
42. Quistad GB, Klintenberg R, Casida JE. Blood acylpeptide hydrolase activity is a sensitive marker for exposure to some organophosphate toxicants. Toxicol Sci. 2005;86:291–9. https://doi.org/10.1093/toxsci/kfi195.
43. Feldmann J, Kindness A, Ek P. Laser ablation of soft tissue using a cryogenically cooled ablation cell. J Anal At Spectrom. 2002;17:813–8. https://doi.org/10.1039/b201960d.
44. Austin C, Fryer F, Lear J, Bishop D, Hare D, Rawling T, et al. Factors affecting internal standard selection for quantitative elemental bio-imaging of soft tissues by LA-ICP-MS. J Anal At Spectrom. 2011;26:1494–501.
45. Jeong SH, Borisov OV, Yoo JH, Mao XL, Russo RE. Effects of particle size distribution on inductively coupled plasma mass spectrometry signal intensity during laser ablation of glass samples. Anal Chem. 1999;71:5123–30. https://doi.org/10.1021/ac990455a.
46. Petrus JA, Chew DM, Leybourne MI, Kamber BS. A new approach to laser-ablation inductively-coupled-plasma mass-spectrometry (LA-ICP-MS) using the flexible map interrogation tool 'Monocle'. Chem Geol. 2017;463:76–93. https://doi.org/10.1016/j.chemgeo.2017.04.027.
47. Van Elteren JT, Izmer A, Šelih VS, Vanhaecke F. Novel image metrics for retrieval of the lateral resolution in line scan-based 2D LA-ICPMS imaging via an experimental-modeling approach. Anal Chem. 2016;88:7413–20. https://doi.org/10.1021/acs.analchem.6b02052.
48. Downes GB, Granato M. Acetylcholinesterase function is dispensable for sensory neurite growth but is critical for neuromuscular synapse stability. Dev Biol. 2004;270:232–45. https://doi.org/10.1016/j.ydbio.2004.02.027.
49. Behra M, Cousin X, Bertrand C, Vonesch J-L, Biellmann D, Chatonnet A, et al. Acetylcholinesterase is required for neuronal and muscular development in the zebrafish embryo. Nat Neurosci. 2002;5:111–8. https://doi.org/10.1038/nn788.

Analytical and Bioanalytical Chemistry

Electronic Supplementary Material

Elemental imaging (LA-ICP-MS) of zebrafish embryos to study the toxicokinetics of the acetylcholinesterase inhibitor naled

Katharina Halbach, Stephan Wagner, Stefan Scholz, Till Luckenbach, Thorsten Reemtsma

AChE activity measurements at different naled concentrations

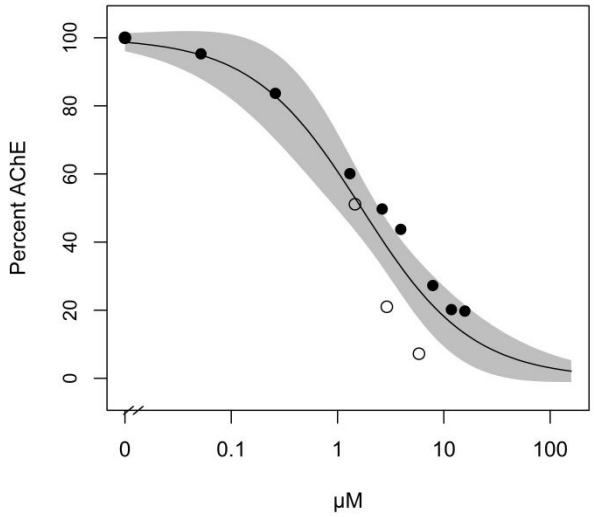

Fig. S1 AChE activity presented as percentage of the activity of the control measured in zebrafish embryos exposed to different concentrations of naled from 72 to 96 hpf. (Data points are the mean of three technical replicates; filled and open symbols represent two independent exposure experiments). The line represents the modelled concentration-response-curve obtained using a sigmoidal model and using the R package drc. EC50=1.68 (0.961-2.4 confidence interval); slope= -0.843

Instrumental parameters of LA-ICP-MS and neb-ICP-MS measurements

Table S1 LA-ICP-MS and nebulization-ICP-MS parameters

		Neb-ICP-MS	LA-ICP-MS
ICP-MS			
RF power	[W]	1550	1300
Cooling gas flow rate, Argon	[L/min]	12	13.50
Auxiliary gas flow rate, Argon	[L/min]	2.30	2.6
Nebulizer gas flow rate, Argon	[L/min]	0.88	/
Carrier gas flow rate, Helium	[L/min]	/	0.8
Integration time	[s]	10	1
Baseinterval	[ms]	1000	100
Laser ablation system			
Wavelength of ArF laser	[nm]		193
Laser beam diameter	[µm]		50
Laser scan speed	[µm/s]		50
Repetition frequency	[Hz]		100
Laser fluence	[J/cm^2]		1.79 (25% laser output at 4 mJ)

Profilometer data

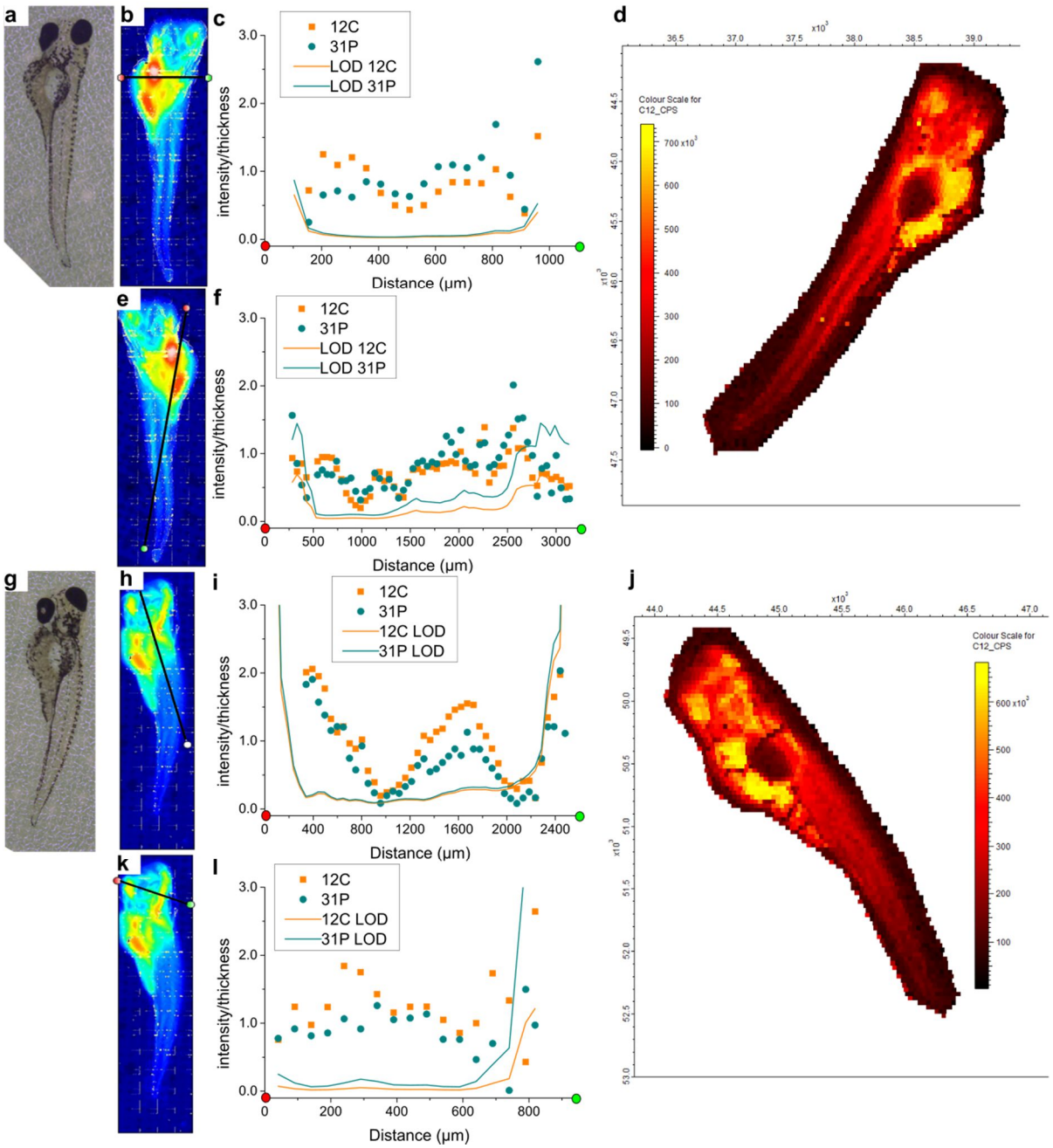

Fig. S2 Profilometer data before ablation and corresponding intensities of ^{12}C, ^{31}P, ^{39}K after ablation with LA-ICP-MS of 96 hpf zebrafish embryos. **a**, **g:** Microscopic image; **b**, **e**, **h**, **k**: Heat map of thickness measurement, line indicates the linear profile (red is the starting point, green the end point); **c**, **f**, **i**, **l**: Scatter graph of the ratio of the intensities (counts per second) of LA-ICP-MS measurement (spot size 50 µm) and the thickness (µm) of the profile; lines, respectively, indicate the ratio (intensity/thickness) belonging to the LOQ ($32.5 \cdot 10^3$, $22.3 \cdot 10^3$cps for ^{12}C, ^{31}P, respectively) of the elements; **d, j**:intensity (cps) map of the ^{12}C signal measured with LA-ICP-MS. The intensity and thickness data were scaled to a 0-1 range in order to calculate the ratio

Calibration with agarose gels for LA-ICP-MS

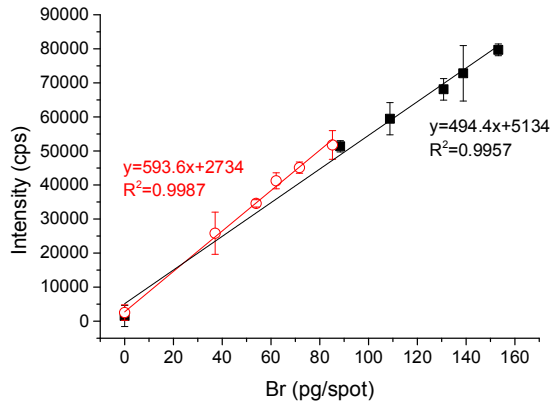

Fig. S3 Two examples for measured calibration curves in different concentration ranges, spotsize: 50 µm. Calibration curves conducted for experiments with embryos exposed from 86 to 96 hpf (black square) and from 95 to 96 hpf (red circle)

LC-MS/MS of aliquots from exposure solution

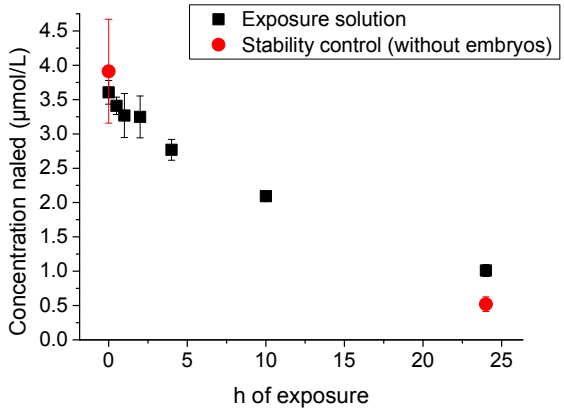

Fig. S4 Concentration of naled in the exposure medium (n=3) decreased with exposure time due to hydrolysis

Time course of dichlorvos internal concentration

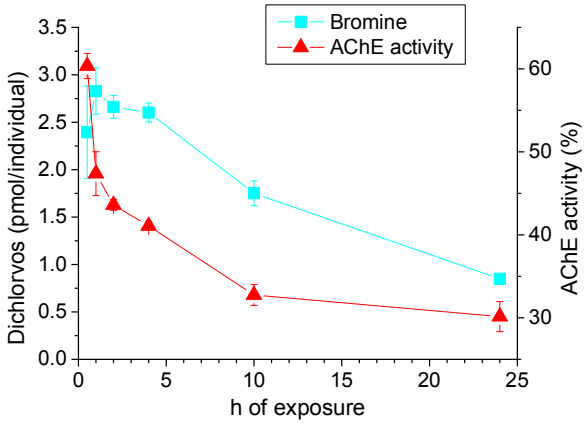

Fig. S5 AChE inhibition (n=3) normalized to the specific activity in the negative control and internal dichlorvos amount in the zebrafish embryo (n=3) determined with LC-MS/MS

Zebrafish embryo and embryo volumes

Zebrafish embryo volumes of different stages were estimated using the VAST Bioimager (Union Biometrica, Holliston, MA, USA). For each stage images of 10 embryos were taken in dorsal, ventral and lateral (left, right) position. Images were loaded into a KNIME workflow with appropriate image processing nodes [1]. On each image the trunk, yolk and pericardium were labelled manually using the KNIME interactive image annotator. Subsequently, images were sliced virtually in 10 µm sections. Each section was considered as an ellipsoid cylinder for which the volume was estimated based on the lateral and dorsoventral diameter. The total volume was calculated by summing up the slice volumes. Volume for 96 hpf stages were obtained by interpolation from mean volumes of stages used to estimate the volume (Fig. S6).

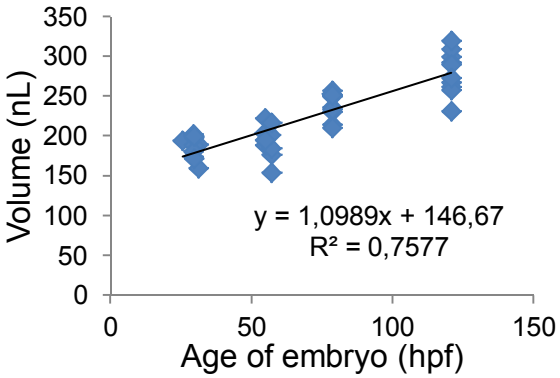

Fig. S6 Volumes of zebrafish embryos (incubated at 26 °C)

LC-HRMS measurements

A Xevo G2-XS Quadrupole-Time-of-flight (Waters, Milford, USA) coupled to a UPLC Acquity I-Class System (Waters, Milford, USA) equipped with an electrospray interface was used for the non-target screening. Separation was performed on a Waters Acquity UPLC HSS T3 (2.1x100 mm, 1.8 µm) at a column temperature of 45 °C. Water (A, pH 5, 10 mM ammonium acetate) and MeOH (B, 10 mM ammonium acetate) were used as eluents. 10 µL of the sample was injected and a total flow rate of 450 µL was applied. The gradient was as follows: 0.0 min, 2 % B; 0.25 min, 2 % B; 12.5 min, 99 % B; 13.0 min 99 % B; 13.01 min, 2 % B; 17.0 min, 2 % B. Further parameters for the ionization can be found in Table S2. Leucine enkephaline was used as lock spray reference. The mass range from m/z 50-1200 was scanned in positive and negative mode. The data was acquired with a low (4 eV) and a high collision energy (15-40 eV), in parallel. The data were analyzed with UNIFI (version 1.7; Waters).

Table S2 Parameters of the electrospray ionization for the UPLC-Tof measurements

Capillary voltage (kV)	0.8;-0.8
Source temperature (°C)	140
Desolvation temperature (°C)	600
Sampling cone voltage (V)	20
Source offset voltage (V)	80
Cone gas	Nitrogen
Collision gas	Argon

Definition of areas of interest with “Monocle” in Iolite

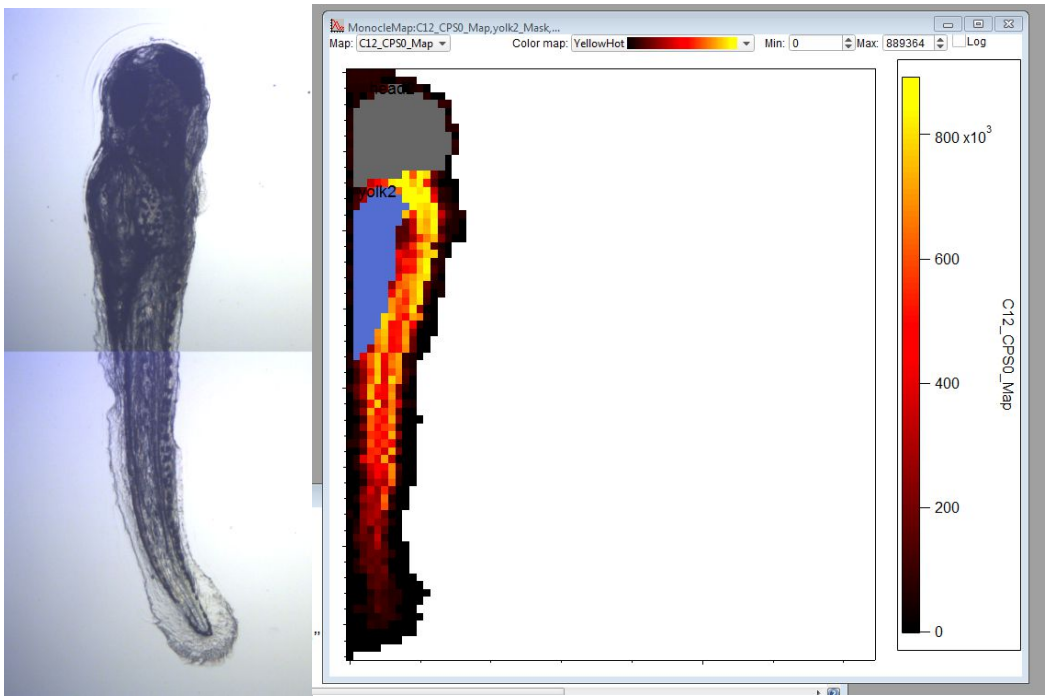

Fig. S7 Microscopic image and defined areas of interest in Iolite with “Monocle” [2] (grey: head; blue:yolk). Displayed is the ^{12}C distribution but the same defined areas of interest applies also for other measured elements or the calculated ratio (by simply changing the channel)

Depuration experiments

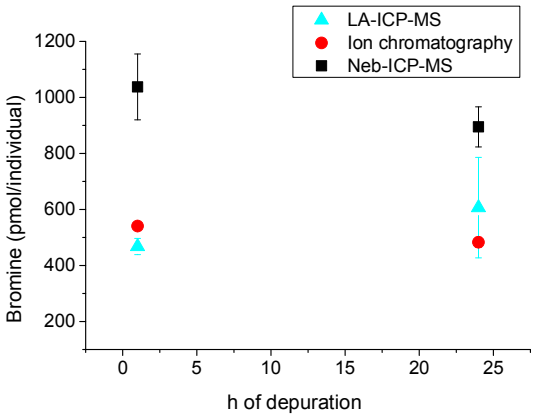

Fig. S8 Br and bromide (in case of ion chromatography) internal amounts after 1 and 24 h of depuration (exposure from 72 to 96 hpf)

Frequency distribution of LA-ICP-MS measurements

The Kernel density estimates of two individuals of an exposure duration of 4 h may contain outliers leading to the local maximum around and above 300000 cps (Fig. S10c). In order to identify these pixels as outliers one would also need to take the spatial distribution and the size of body compartments into account. Since it is reasonable that body compartment smaller than the spot size are present, these pixels were not excluded from the data analysis. Otherwise, the variation between biological replicates is comparatively narrow (rsd of the densities at the maxima are <23% except for the ^{79}Br signal at 1 h exposure, Table S3) which proves that the precision of the whole approach is high (Fig. S9 and Fig. S10).

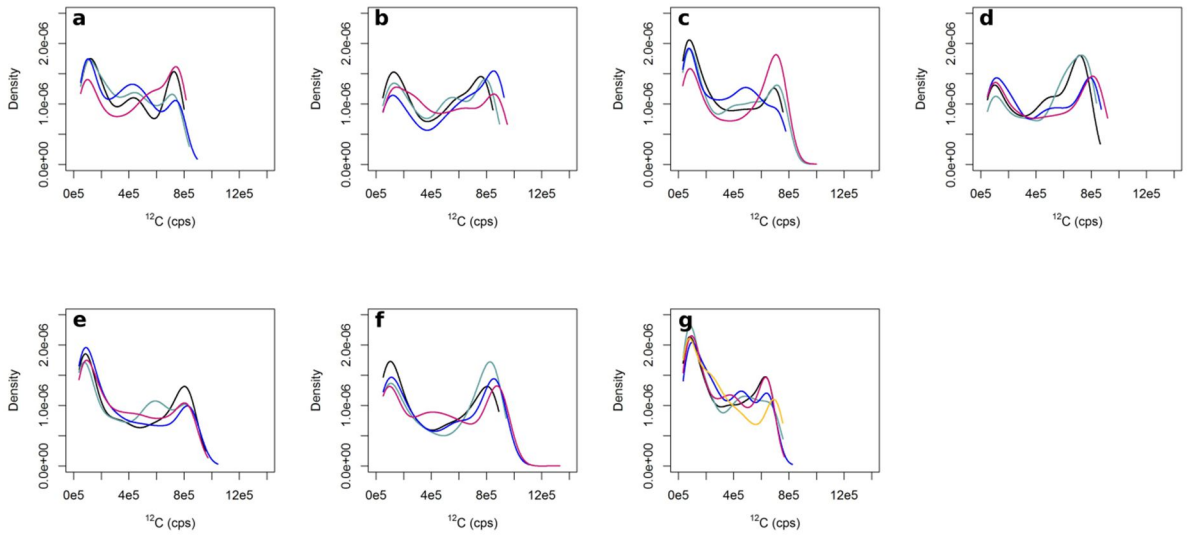

Fig. S9 Kernel density estimates of LA-ICP-MS intensity (cps) data for ^{12}C (using the density function in R3.3.2 with default smoothing settings). Pixels with intensities below the LOQ were removed. **a** control; **b** exposure from 95.5 to 96 hpf; **c** exposure from 95 to 96 hpf; **d** exposure from 94 to 96 hpf; **e** exposure from 92 to 96 hpf; **f** exposure from 86 to 96 hpf; **g** exposure from 72 to 96 hpf

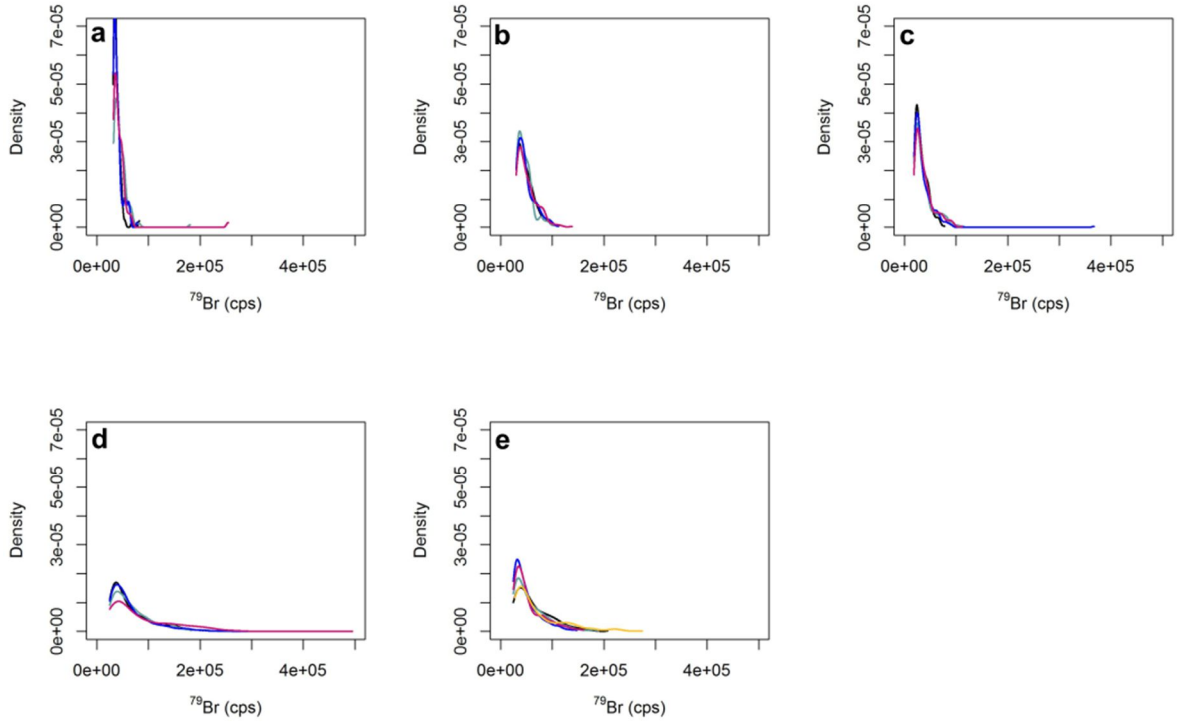

Fig. S10 Kernel density estimates of LA-ICP-MS intensity (cps) data for ^{79}Br (using the density function in R3.3.2 with default smoothing settings). Pixels with intensities below the LOQ were removed. **a** Exposure from 95 to 96 hpf; **b** exposure from 94 to 96 hpf; **c** exposure from 92 to 96 hpf; **d** exposure from 86 to 96 hpf; **e** exposure from 72 to 96 hpf

Table S3 Mean and relative standard deviation of the densities for the maxima in Fig. S9 and Fig. S10

Exposure duration	^{12}C		^{12}C		^{79}Br	
	Mean density maximum 1	%rsd	Mean density maximum 2	%rsd	Mean density maximum 1	%rsd
Control	1.66E-06	10.2	1.35E-06	20.4		
95.5 to 96 hpf	1.33E-06	12.0	1.40E-06	12.7		
95 to 96 hpf	1.87E-06	10.8	1.42E-06	18.9	6.60E-05	30.1
94 to 96 hpf	1.31E-06	9.92	1.63E-06	12.7	3.06E-05	7.86
92 to 96 hpf	1.82E-06	6.02	1.10E-06	13.7	3.84E-05	9.40
86 to 96 hpf	1.47E-06	12.5	1.45E-06	13.1	1.44E-05	20.5
72 to 96 hpf	2.15E-06	4.69	1.28E-06	13.8	1.93E-05	22.3

References

1. Berthold MR, Cebron N, Dill F, Gabriel TR, Kötter T, Meinl T, Ohl P, Sieb C, Thiel K, Wiswedel B (2008) KNIME: The Konstanz Information Miner. In: Preisach C, Burkhardt H, Schmidt-Thieme L, Decker R (eds) Data Analysis, Machine Learning and Applications: Proceedings of the 31st Annual Conference of the Gesellschaft für Klassifikation e.V., Albert-Ludwigs-Universität Freiburg, March 7–9, 2007. Springer Berlin Heidelberg, Berlin, Heidelberg, pp 319–326

2. Petrus JA, Chew DM, Leybourne MI, Kamber BS (2017) A new approach to laser-ablation inductively-coupled-plasma mass-spectrometry (LA-ICP-MS) using the flexible map interrogation tool 'Monocle.' Chem Geol 463:76–93 . doi: 10.1016/j.chemgeo.2017.04.027

Chapter 3 Effective processing and evaluation of chemical imaging data with respect to morphological features of the zebrafish embryo

Halbach, K., Holbrook, T., Reemtsma, T., Wagner, S. *Anal. Bioanal. Chem.* **2021**, *413* (6), 1675–1687.

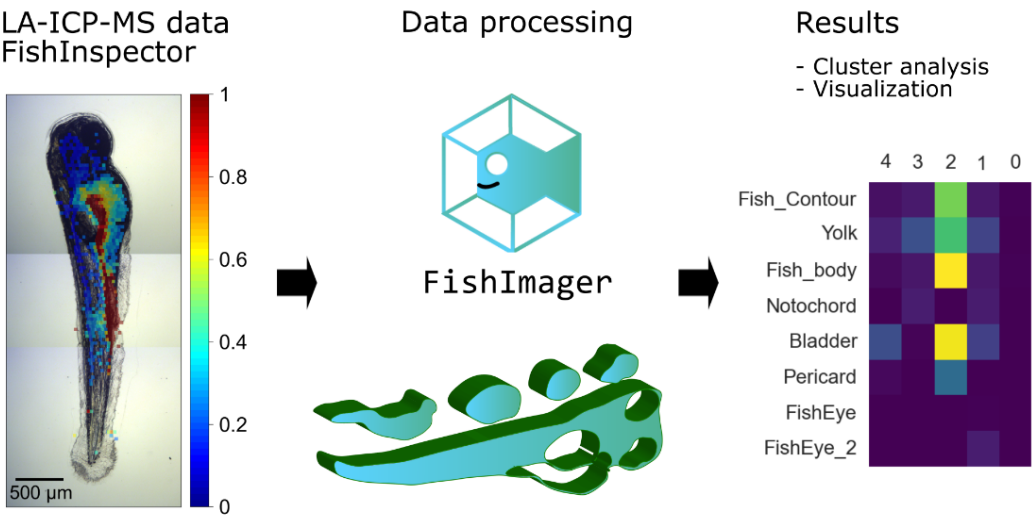

Link to the publication:

https://doi.org/10.1007/s00216-020-03131-4

Author's contribution:

T. Holbrook and I are the first authors of this publication. The study was conceptualized by S. Wagner and me. I carried out the exposure experiments of the zebrafish embryos and the LA-ICP-MS analyses. I designed the software FishImager together with T. Holbrook and had ideas for the visualizations. T. Holbrook coded the software. The discussion and structure of the manuscript were developed together with the co-authors. I wrote the manuscript.

Analytical and Bioanalytical Chemistry (2021) 413:1675–1687
https://doi.org/10.1007/s00216-020-03131-4

RESEARCH PAPER

Effective processing and evaluation of chemical imaging data with respect to morphological features of the zebrafish embryo

Katharina Halbach[1] · Timothy Holbrook[1] · Thorsten Reemtsma[1,2] · Stephan Wagner[1,3]

Received: 22 October 2020 / Revised: 1 December 2020 / Accepted: 15 December 2020 / Published online: 1 February 2021

Abstract

A workflow was developed and implemented in a software tool for the automated combination of spatially resolved laser ablation-inductively coupled plasma-mass spectrometry (LA-ICP-MS) data and data on the morphology of the biological tissue. Making use of a recently published biological annotation software, FishImager automatically assigns the biological feature as regions of interest (ROIs) and overlays them with the quantitative LA-ICP-MS data. Furthermore, statistical tools including cluster algorithms can be applied to the elemental intensity data and directly compared with the ROIs. This is effectively visualized in heatmaps. This allows gaining statistical significance on distribution and co-localization patterns. Finally, the biological functions of the assigned ROIs can then be easily linked with elemental distributions. We demonstrate the versatility of FishImager with quantitative LA-ICP-MS data of the zebrafish embryo tissue. The distribution of natural elements and xenobiotics is analyzed and discussed. With the help of FishImager, it was possible to identify compartments affected by toxicity effects or biological mechanisms to eliminate the xenobiotic. The presented workflow can be used for clinical and ecotoxicological testing, for example. Ultimately, it is a tool to simplify and reproduce interpretations of imaging LA-ICP-MS data in many applications.

Keywords MS imaging · Toxicokinetics · Biological samples · Cluster analysis · ICP-ToF-MS · Organ

Introduction

The zebrafish embryo (ZFE, *Danio rerio*) is an important model organism and used in various research fields such as developmental biology, biomedical research, and (eco)toxicology [1]. Imaging of biological or toxicological processes within the ZFE is increasingly reported [2–6]. One versatile quantitative elemental imaging technique for biological tissues is laser ablation-inductively coupled plasma-mass spectrometry (LA-ICP-MS). It is applied in various applications, such as determining the distribution of anti-cancer compounds in tumor tissue and nanoparticles in organisms, or the (immune) response on environmental contaminants, as well as localization of X-ray contrast agents [3, 7–11]. Spatial resolution and sensitivity have been strongly improved, acquisition time has been decreased, and new quantification strategies have been developed over the past years [12–14]. Although there are numerous software tools to combine and visualize the spatial laser ablation coordinates with the ICP-MS data [15–17], data post-processing is still in its infancy. The interpretation of imaging data is often solely based on the visual comparison of a color-coded picture representing the intensity or quantified amount. This interpretation relies on the expert knowledge of the analyst [18]. Furthermore, the combination of LA-ICP-MS results with biological information (e.g., at the sub-organ level) is achieved with manual overlays of different images using several software products [10]. Yet, the LA-ICP-MS data set may allow more objective information to be discovered. According to available studies, image analysis software for LA-ICP-MS data shall be extended with:

(i) Quality controls like measurement uncertainty and validation parameters such as limit of detection and quantification, linearity of the calibration range, precision, and accuracy.

✉ Stephan Wagner
stephan.wagner@ufz.de; stephan.wagner@hof-university.de

[1] Department of Analytical Chemistry, Helmholtz Centre for Environmental Research - UFZ, 04318 Leipzig, Germany

[2] Institute of Analytical Chemistry, University of Leipzig, 04103 Leipzig, Germany

[3] Present address: Institute for Water and Energy Management, University of Applied Sciences Hof, 95028 Hof, Germany

(ii) Tools for statistical analyses such as cluster analysis and principal component analysis. These have been recently included in the software HDIP (Hierarchical Data Format version 5-image processing) [19].
(iii) Algorithms to correlate spatial data from LA-ICP-MS and other imaging techniques.

Biological studies often require definitions of regions of interest (ROIs) to investigate research questions such as (co-)localization of chemicals/elements and toxicokinetic processes in certain tissue compartments. ROIs are often manually assigned in the data processing software to the LA-ICP-MS results and then compared [20, 21]. This, however, comes together with subjective identifications depending on the quality of the images and the expertise of the analyst and may be time-consuming. Automated identification of ROIs based on sample features (e.g., organs, body compartments) can be performed in application-specific software, but these results cannot be easily combined with the LA-ICP-MS data [17, 22]. The assignment might even be based on a different image other than that of the camera delivered with the laser ablation system, e.g., taken with a high-resolution microscope. The combination of spatially resolved information from different sources is still rarely reported due to the complexity of data transformation and missing software tools. However, the establishment of quantitative LA-ICP-MS image analysis for diagnostics in medicine, pharmacology studies, and (eco)toxicological studies requires an increased effort to generate reproducible data, to link them with data from other analyses, and with morphology and function, for example.

Here, we demonstrate the data post-processing software FishImager for the combination of results from an assessment of morphological features (biological ROIs) with chemical imaging data including statistical tools such as different cluster analysis algorithms. The automatically assigned biological ROIs can be linked with the quantitative LA-ICP-MS data (incl. LA-ICP-ToF-MS data) and be individually evaluated and compared with each other. For instance, quantified amounts or mean elemental intensities may be calculated for each ROI. The software allows applying different cluster algorithms, depending on the LA-ICP-MS data set structure, the biological tissue, and the research question. The assigned clusters can then be compared with the biological ROIs, e.g., overlapping areas and elemental content. The commercially available software Iolite and HDIP offer some statistical analyses and manual ROI drawings and investigations; however, importing and combining other biological information such as the morphological features is to our knowledge not supported [16, 19, 23]. The cluster algorithm k-means on LA-ICP-MS data was recently used to identify sub-organ regions [24]. While FishImager is not meant to replace these software, we wish to enhance the application of LA-ICP-MS data to biological and environmental research questions. FishImager is freely available and its innovation is to quantitatively compare the output of LA-ICP-MS data investigations to the result of an objective annotation of morphological features.

The features of FishImager will be demonstrated on the important alternative test system to animal testing, the ZFE. The recently published FishInspector software allows the automatic identification of morphological features [25]. Using this output, FishImager combines it with LA-ICP-MS results. In this study, we explore the distribution of natural elements and two xenobiotics in the ZFE. These examples point out how ablation reproducibility and toxicokinetics of xenobiotics in the ZFE can be assessed with the software. This is a step towards a more objective and reliable data analysis of LA-ICP-MS results.

Materials and methods

Culture of zebrafish, collection of eggs, and culture of embryos

We used the UFZ-OBI strain (*Danio rerio*, generation F13–14), obtained originally from a local breeder and kept for several generations at the UFZ. Fish were cultured and used according to German and European animal protection standards and approved by the Government of Saxony, Landesdirektion Leipzig, Germany (Aktenzeichen 75-9185.64) [26].

Exposure experiments

Details on the example data sets, i.e., the exposures of the ZFE and the LA-ICP-MS experiments, are partly given in Halbach et al. (for the ZFE discussed in R&D section a) and the exposure to naled) [27]. In addition, ZFEs were exposed starting from 3 h post-fertilization (hpf) for 48 and 96 h to 10.3 μM 4-iodophenol (Sigma-Aldrich, CAS no. 540-38-5) dissolved in ISO-water [28]. Nine ZFEs were exposed in 18 mL of exposure medium in three replicates. pH and oxygen content of the water were measured at the beginning and end of exposure to ensure the test requirements [29]. At the end of the exposure, ZFEs were dechorionated when necessary, and five ZFEs were placed in Eppendorf tubes. Excess water was removed, and ZFEs were washed twice with 1 mL Milli-Q water. The ZFEs were carefully placed on glass slides and dried at room temperature for at least three days. Microscopic images were taken (Leica, M205 FA).

Instrumental equipment, parameters, and data processing

Briefly, LA-ICP-MS measurements were performed with a G2 Analyte Laser (Teledyne CETAC Technologies Inc., Bozeman, MT, USA) connected to a double-focusing sector field ICP-MS based on a Mattauch-Herzog geometry (Spectro MS, Spectro,

Ametek, Kleve, Germany) [30]. Daily performance and fine-tuning of the ICP-MS were performed with a NIST610 glass reference material (SRM-610, LGC Ltd., Middlesex, UK). ^{12}C, ^{31}P, ^{39}K, ^{79}Br, and ^{127}I were the measured isotopes. Measurement parameters are given in Table 1. Calibration of the ^{127}I signal was performed using agarose gels spiked in different concentrations with an iodide solution (Sigma-Aldrich) (see Supplementary Information (ESM) Fig. S1) [27, 31]. Merging of the transient ICP-MS signal with the position data of the laser, baseline correction, and quantification was achieved with Iolite 3.6 in Igor Pro 7.04. A table with the elemental intensities, quantified elements, and *x*,*y*-coordinates was exported as a text-file. This file (in our case around 200 KB) was imported into FishImager (termed as LA-ICP-MS data).

Phenotypic features (biological ROIs) were detected with the FishInspector tool (version 1.03, Scientific Software Solutions, and Helmholtz Centre for Environmental Research) based on a microscopic image (Leica, M205 FA, denoted "reference image") [25]. The compartment fish body (area represented by the fish contour minus the yolk) was manually added to the phenotypic features from the FishInspector software.

Software layout

The workflow of FishImager (Fig. 1) starts with importing the LA-ICP-MS files (camera photo, coordinate file, and LA-ICP-MS data file) and the annotated image with morphological features. The workflow also offers the option to visualize the imported data. Download information and an installation guide are available at https://git.ufz.de/holbrook/fishi-LAICPMS-Imaging-Tool. Imaging data following the structure element1, element2,…, *X* coordinate, *Y* coordinate, or the structure of an ICP-ToF-MS data file (h5-file from Tofwerk, Switzerland) can be processed. A more detailed description of the workflow is given in ESM 1. Briefly, the coordinate systems of the camera photo from the laser device and the image from FishInspector are then transformed to create an overlay of the morphological features with the LA-ICP-MS data. The morphological features assigned by the FishInspector software are automatically defined as ROIs (Fig. S2). For each ROI, quantitative information on the sum, mean, standard deviation, median, variance, minimum, and maximum can be calculated. Different cluster algorithms (k-means, mean shift, affinity propagation, spectral clustering, density-based spatial clustering of applications with noise (DBSCAN), and hierarchical dbscan (HDBSCAN), ESM Table S1) can be applied to the LA-ICP-MS data, and this cluster data can be correlated with the ROIs. The k-means clustering has been previously applied for automatic segmentation of brain sections based on elemental intensities or classification of groups of ions measured in mammalian cells using the secondary ion mass spectrometry [32, 33]. Endocrine peptides were identified in mouse pancreatic tissue using spectral clustering of matrix-assisted laser desorption/ionization-MS imaging data [34]. Details on the algorithms can be found in the description of the sklearn.cluster module for Python [35] and ESM Table S1. The information about the imaging data in the ROIs and the clustering is visualized in heatmaps. We created a graphical user interface (Fig. 1) so that the application of FishImager is not dependent on the user's programming expertise. The input format for the assigned biological features (here the FishInspector) in FishImager may be easily edited to combine other tissue matrices with LA-ICP-MS data to develop further application areas. Extensive instruction to reproduce the data in the "Results and discussion" section is included in the ESM 2. A download link to the presented data set is also given in the git repository.

Results and discussion

LA-ICP-MS results were explored using FishImager with respect to (a) the distribution of natural elements in the ZFE and the reproducibility between ablations of different individuals, (b) the sites of accumulation of two different xenobiotics, and (c) how uptake and distribution of one xenobiotic changes with exposure time and developmental stage. Plotted intensities of the discussed data with the scale of the ablated tissues can be found in Figs. S3, S4, and S6. Biological ROIs (fish contour, bladder, notochord, eyes, pericard, yolk) were imported from the FishInspector software (ESM Fig. S2). The ROI fish body was assigned as the difference between the ROIs fish contour and yolk. It includes the bladder, notochord, eyes, and pericard.

(a) Distribution of natural elements in zebrafish embryos and reproducibility between ablations of different individuals

Table 1 Operational parameters of laser ablation and ICP-MS instrumentation

ICP-MS		
RF power	[W]	1250
Cooling gas flow rate, argon	[L/min]	13.50
Auxiliary gas flow rate, argon	[L/min]	2.6
Carrier gas flow rate, helium	[L/min]	0.8
Integration time	[s]	1
Base interval	[ms]	100
Laser ablation system		
Wavelength of ArF laser	[μm]	193
Laser beam diameter	[μm]	35
Laser scan speed	[μm/s]	35
Repetition frequency	[Hz]	125
Laser fluence	[J/cm^2]	1.77

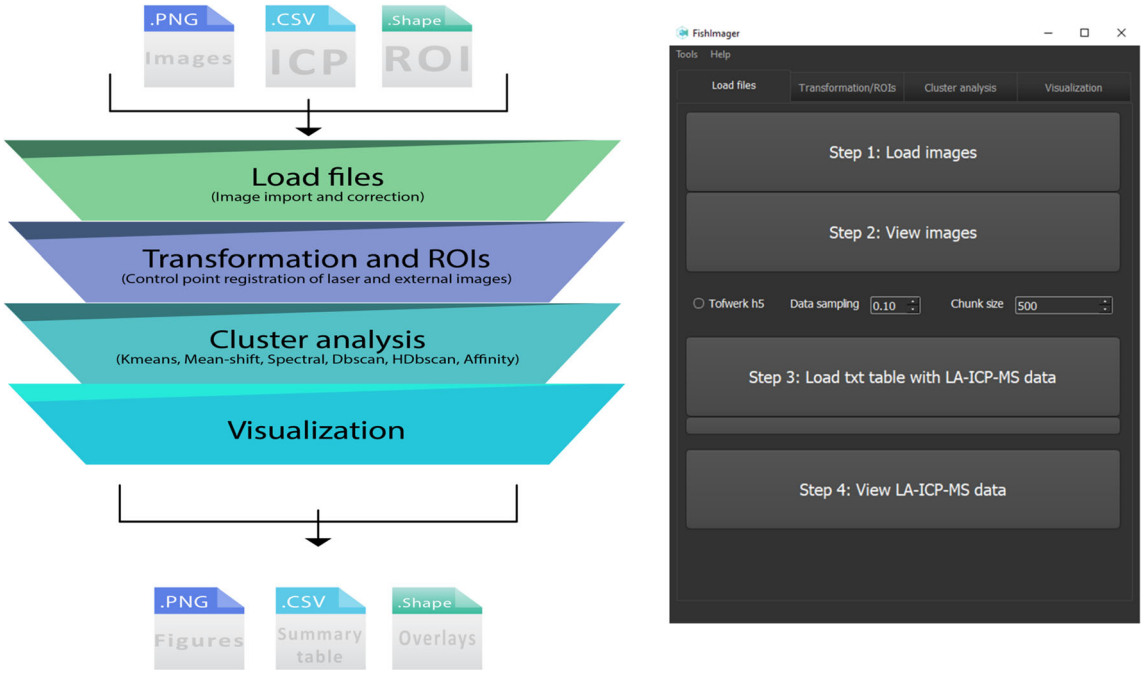

Fig. 1 Data analysis workflow of the software FishImager (left) and exemplary layout (right)

We applied FishImager to investigate the distribution of the essential elements carbon, phosphorus, and potassium in the different body compartments in ZFEs 96 hpf. These were chosen as they are accessible via ICP-MS and not present in the underlying support material. The ^{12}C signal has been shown before to correlate with the height profile of the sample [27]. The clustering of the ^{12}C signal between three different individual ZFEs was initially compared to gain information about the reproducibility, i.e., a combination of biological variability and measurement precision, of the three ablations (Fig. 2). The k-means algorithm was applied with the predefined numbers of clusters set to four (chosen with the elbow method [36]). Heatmaps in Fig. 2 depict the percentage of the overlapping area of the clusters and the ROIs, respectively (% counts), as well as the mean intensity in these overlapping areas (mean intensity per element). The visualization of the assigned clusters and ROIs as heatmaps is an important feature of the software, allowing easy and quick comparison between ablations and is to our knowledge not included in other available LA-ICP-MS software.

The size of cluster 3 in the ZFEs varied from 16 to 23% of the ablation area between the individuals (Table 2, Fig. 2). This cluster always contained the highest mean ^{12}C intensity (heatmaps of cluster 3 for the mean intensity ^{12}C in Fig. 2). The highest mean ^{12}C intensity overlapped with the ROIs fish eyes and the yolk. The precision of the carbon distribution among the three replicates can be assessed, e.g., by performing correlation analysis among the heatmaps of the replicates. These contain the information on the clustering and the ROI assignment. The three heatmaps of the mean ^{12}C intensity showed a significant correlation (Spearman's correlation coefficients between the individuals 0.71, 0.77, 0.91, $p < 0.001$ for all coefficients); e.g., the mean ^{12}C intensities in cluster 3 and the ROI fish body were 4.47 ± 0.94, 4.61 ± 0.73, and $4.74 \pm 0.98 \times 10^5$ cps. Therefore, we conclude that the percentage of the overlap of the clusters and the ROIs, thus the spatial distribution of the ^{12}C signal, showed a good agreement between the different replicates. The highest difference between the three individuals was observed for ^{12}C in cluster 2 and the ROI yolk in individual 1. This can be explained by the different number of pixels associated with cluster 2 and the ROI yolk (Fig. 2, middle column). Cluster 2 of individual 1 does not overlap with the ROI yolk. In contrast, very few LA-ICP-MS pixels are classified as cluster 2 and ROI yolk for individuals 2 and 3 resulting in the difference between individuals.

By using k-means clustering, the elements ^{31}P and ^{39}K were also assigned to four clusters, respectively (Fig. 3). The element ^{39}K partitioned into clusters 0 to 3; three of them (0 to 2) were evenly distributed over the ablation area and consisted of 18 to 32% of the total ablation area (Table 2). The fourth cluster (cluster 3, 26% of the ablation area) contained the highest mean intensity of the element per cluster (Table 2). The highest mean intensity of ^{39}K overlapped with the ROI fish eyes (Fig. 3a). A comparison of the ^{12}C and ^{39}K distribution showed a significant correlation (Spearman's correlation coefficients 0.77, $p < 0.001$) in various ROIs except for the ROI yolk. While the ROI yolk is mainly represented by cluster 3 for ^{12}C with the highest mean intensity, it is represented by cluster 1 for ^{39}K with a comparable low mean

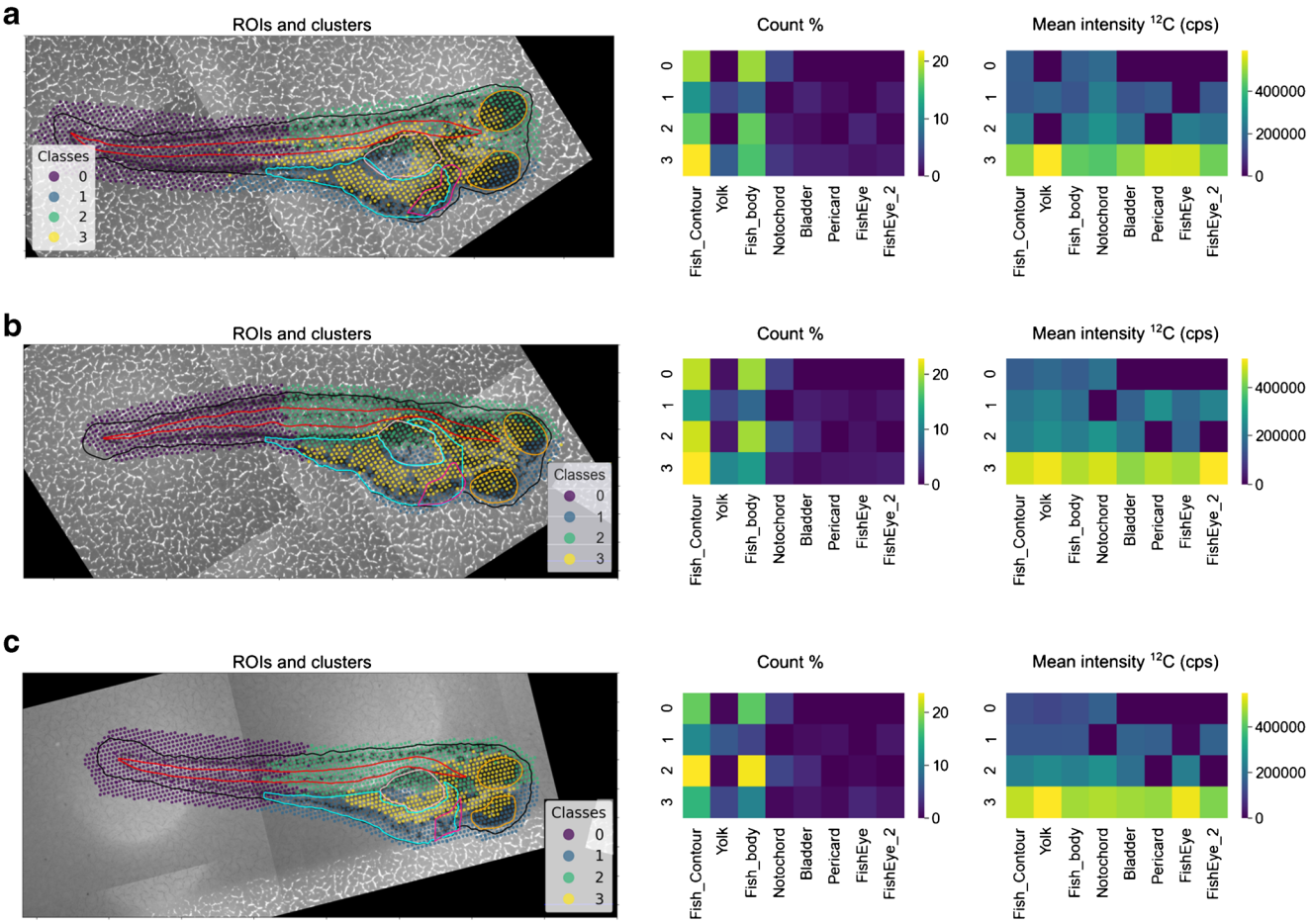

Fig. 2 **a**–**c** K-means clustering of the ^{12}C LA-ICP-MS signal intensity and the *x*- and *y*-coordinates in three zebrafish embryos. The heatmaps display the percentage of ablation area represented by the cluster and the body part (count %) and the mean intensity of the elements per cluster and per ROI (mean intensity ^{12}C)

intensity (Figs. 2a and 3a). This confirms that the ^{12}C signal may be used to reflect best the varying tissue densities of the ablated material as the yolk is a lipid- and protein-rich body compartment [27, 37]. The potassium channels are expressed mainly in the brain and trunk, which could be why the different distribution patterns of ^{39}K and ^{12}C were observed [38]. The element ^{31}P was partitioned into four clusters of nearly equal size, which were evenly distributed over the ZFE (Table 2, Fig. 3b). The ^{31}P signal intensity did not distribute in a specific body compartment. This is illustrated

Table 2 Cluster sizes as a percentage of total ablation area and mean signal intensities (cps) for the elements ^{12}C, ^{39}K, and ^{31}P for three single embryos ($n = 1$, individual 1 to 3)

Cluster	Individual 1						Individual 2		Individual 3	
	^{12}C		^{39}K		^{31}P		^{12}C		^{12}C	
	Percentage of ablation area (%)	Mean signal intensity (cps)	Percentage of ablation area (%)	Mean signal intensity (cps)	Percentage of ablation area (%)	Mean signal intensity (cps)	Percentage of ablation area (%)	Mean signal intensity (cps)	Percentage of ablation area (%)	Mean signal intensity (cps)
0	36.8	1.31×10^5	32.2	6.17×10^5	23.9	1.26×10^5	31.5	1.33×10^5	37.2	1.03×10^5
1	18.3	1.36×10^5	24.0	2.73×10^6	26.7	1.37×10^5	16.6	1.88×10^5	20.0	1.23×10^5
2	22.9	1.96×10^5	18.2	3.36×10^5	23.2	1.32×10^4	29.4	1.84×10^5	27.3	2.18×10^5
3	22.0	4.88×10^5	25.6	1.37×10^6	26.2	5.47×10^4	22.5	4.81×10^5	15.5	4.99×10^5

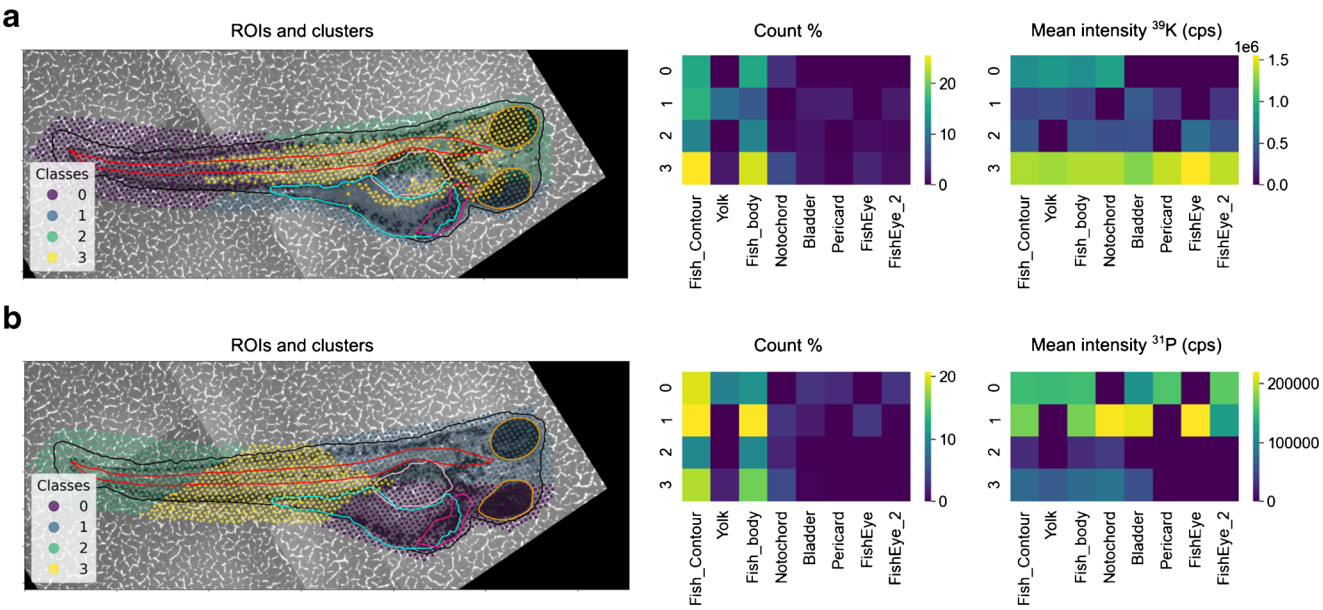

Fig. 3 Assignment of four clusters by the k-means algorithm of the *x*- and *y*-coordinates and the LA-ICP-MS intensity data for (**a**) ^{39}K and (**b**) ^{31}P, respectively, for a 96 hpf zebrafish embryo. The LA-ICP-MS data are color-coded into the four clusters (first column). Outlines of the biological ROIs are displayed. The heatmaps display the percentage of the ablation area represented by the cluster and the biological ROIs (count %) and the mean intensity of the elements per cluster and per ROI (mean intensity ^{39}K/^{31}P)

by the heatmap showing that no cluster overlaps with all the body compartments as for ^{39}K and ^{12}C; e.g., the ROI fish eyes are not represented by the same cluster as before for ^{12}C and ^{39}K.

The examples of the spatial distribution of the natural elements in the ZFE impressively illustrated the possibility of FishImager to calculate and visualize the means of the elemental distribution in several individual ZFEs. This forms the basis for routinely applying metrology principles (such as reproducibility) and performing statistical tests, e.g., to test for the significance of differences between different groups, for example, exposed and non-exposed organisms, compared to the difference between individuals within one group.

(b) Distribution of xenobiotics in the zebrafish embryo

FishImager allows analyzing correlations in the spatial distribution of different elements in one organism. Identifying positive or negative correlations of elements may be used to link exogeneous with endogenous elements, e.g., platinum-based anti-cancer compounds or tattoo ink [7, 39]. For demonstration, the distribution pattern and accumulation of two xenobiotics in the ZFE are explored. The two compounds contain characteristic elements suited for their determination by LA-ICP-MS: the bromine-containing compound naled and 4-iodophenol. Naled was shown to be an acetylcholinesterase inhibitor, and 4-iodophenol is presumably a baseline toxic compound that accumulates in the yolk of the ZFE [27, 40]. By applying the k-means algorithm, the baseline-corrected bromine or iodine intensities together with the carbon signal (as a thickness measure since whole ZFEs are ablated [27]) and the spatial information were partitioned into 5 clusters for

Table 3 Cluster sizes as a percentage of total ablation area for the naled and the 4-iodophenol exposure of zebrafish embryos (k-means clustering). The mean LA-ICP-MS intensities of ^{79}Br, ^{127}I, and ^{12}C in the clusters and the quantified bromine and iodine amounts are displayed

Cluster			Naled exposure			4-Iodophenol exposure		
	Percentage of ablation area (%)	Mean intensity ^{79}Br (cps)	Mean intensity ^{12}C (cps)	Total Br (ng)	Percentage of ablation area (%)	Mean intensity ^{127}I (cps)	Mean intensity ^{12}C (cps)	Total I (ng)
0	17.7	6.30×10^{4}	5.09×10^{5}	18.2	21.4	2.39×10^{3}	4.29×10^{3}	0.48
1	29.8	1.37×10^{3}	6.33×10^{4}	0.88	25.8	3.56×10^{4}	3.80×10^{5}	8.51
2	25.3	7.22×10^{3}	1.99×10^{5}	2.90	11.3	4.86×10^{5}	5.60×10^{5}	53.1
3	12.1	2.73×10^{3}	1.12×10^{5}	0.70	23.7	4.00×10^{4}	1.06×10^{5}	8.78
4	15.1	2.07×10^{4}	5.82×10^{5}	5.60	17.8	2.25×10^{4}	5.70×10^{4}	3.74

both exposures, respectively (selected based on the elbow method).

In the naled exposure, clusters 1 and 3 had the lowest mean bromine intensity (1.37×10^3 cps and 2.73×10^3 cps, Fig. 4) and together summed up to 42% of the area (Table 3). The tissue density was also lowest in these two clusters and represented the tail of the ZFE and partly one eye. Cluster 2 with medium bromine and carbon intensity overlapped with the ROI fish body and partly included the notochord. Interestingly, cluster 4 (15% of the ablation area) with the highest tissue density (mean intensity ^{12}C: 5.82×10^5 cps) overlapped mainly with the ROI yolk (ESM Fig. S5a) but did not contain the highest mean bromine intensity. The highest mean bromine intensity was assigned to cluster 0 (6.30×10^4 cps) and represented the ROI head of the ZFE body, including the ROIs notochord and fish eyes.

Provided that the LA-ICP-MS system is adequately calibrated [27, 31], the amount of an analyte in the respective ROI can be quantified (Table 3 and Fig. 4). The bromine amount in the ROI fish body is mainly accumulated in the notochord and the fish eyes. It was assumed that this accumulation originates from the neuroactive toxicity of naled [27]. By applying FishImager, the previously published [27] manual ROI assignment could now be automatically achieved, and single body parts were linked to the bromine accumulation. Previous results are confirmed and could be specified here with the localization of the bromine in the notochord and fish eyes.

For the ZFEs exposed to 4-iodophenol, the iodine intensity distribution and the LA coordinates partitioned into 5 clusters: clusters 0, 1, 3, and 4 represented each between 18 and 26% of the total pixels; cluster 2 only 11% (Table 3). The latter cluster contained the highest mean iodine intensity (4.86×10^5 cps), which was one magnitude higher than in the other clusters. This cluster is situated between the ROIs yolk and body. Seventy percent of the total iodine amount accumulated in cluster 2. It is suggested that the gastrointestinal (GI) tract develops in this region. A localization of iodine in the GI tract may be linked to biotransformation of 4-iodophenol to other iodine-containing transformation products or the elimination via the GI tract.

Localizing the site of enrichment of a toxicant (or its metabolites) within an organism and quantifying its amount in different organs is needed for toxicokinetic and toxicodynamic studies. The incorporation of morphological ROIs is an advantage of FishImager compared to available software. It may improve the understanding of toxicity mechanisms (e.g., by enrichment of a neurotoxic compound in the brain and notochord) and outline that a toxicant is metabolized (e.g., by enrichment in the liver) or eliminated via the GI tract.

In these two examples, the k-means algorithm was applied for the cluster analysis; it was previously used, e.g., to reveal different elemental fingerprints in brain tissue [32]. For statistical analysis, three partitioning (k-means, affinity propagation, spectral clustering) and three cluster (mean shift, DBSCAN, HDBSCAN) algorithms are provided by the software. These algorithms have different data knowledge requirements as well as different capabilities in coping with noisy data. An overview of their features is given in ESM Table S1. Furthermore, specific cluster parameters depending on the algorithms can be controlled. When applying cluster algorithms other than k-means, such as the HDBSCAN, to the data from the two examples above, the resulted segmentation differed (Fig. 5). In the case of the naled exposure, three clusters were obtained by the HDBSCAN. The cluster − 1 with a mean bromine intensity of 3.82×10^4 cps contained 12% of the pixel and may represent one fish eye and possibly measurement outliers (Fig. 5a; ESM Fig. S5 and Table S2). The ROIs eyes, notochord, pericard, and partly the yolk overlapped with cluster 0 of a similar mean bromine intensity (4.76×10^4 cps, 26% of the ablation area) in contrast to cluster 1 representing the rest of the ROI yolk and tail of the ZFE with a mean bromine intensity of 0 cps.

For the ZFE exposed to 4-iodophenol, the iodine and carbon intensity and the coordinates were assigned to four clusters based on HDBSCAN. Cluster − 1 displayed the GI tract with the highest mean iodine intensities of 4.20×10^5 cps (in total 37 ng, 9% of the ablation area, ESM Table S2). Cluster 0 had the second-highest mean iodine intensity (1.08×10^5 cps, 35.2 ng, 34% of the ablation area, ESM Table S2) representing the ROIs yolk and partly the fish body. Cluster 1 only included 2% of the ablation area and embodied the ROI bladder (mean iodine intensity 1.46×10^4 cps). Cluster 2 represented the rest of the ZFE with a low iodine intensity (mean 4.33×10^3 cps).

The HDBSCAN algorithm resulted in better differentiation between the body compartments of the ZFE with high iodine or bromine intensities and those compartments containing very low or no signal intensity than the k-means clustering. This conclusion can be made as knowledge on the anatomy of the biological tissue existed. FishImager offers the flexibility to test different cluster algorithms, and it may be useful to test these on the same data to gain more robustness of the clustering result.

(c) Identification of changes over time in the distribution of a xenobiotic in the zebrafish embryo

In addition to the identification of accumulation patterns and correlation of elements, toxicokinetics, i.e., determination of time-resolved changes in internal amounts and distribution, can be supported by FishImager. The distribution of the bromine-containing compound naled from section (b) for the 24 h exposure is compared to a shorter exposure time (4 h, Fig. 6a). The k-means clustering resulted in four clusters (Fig. 6a). Cluster 0

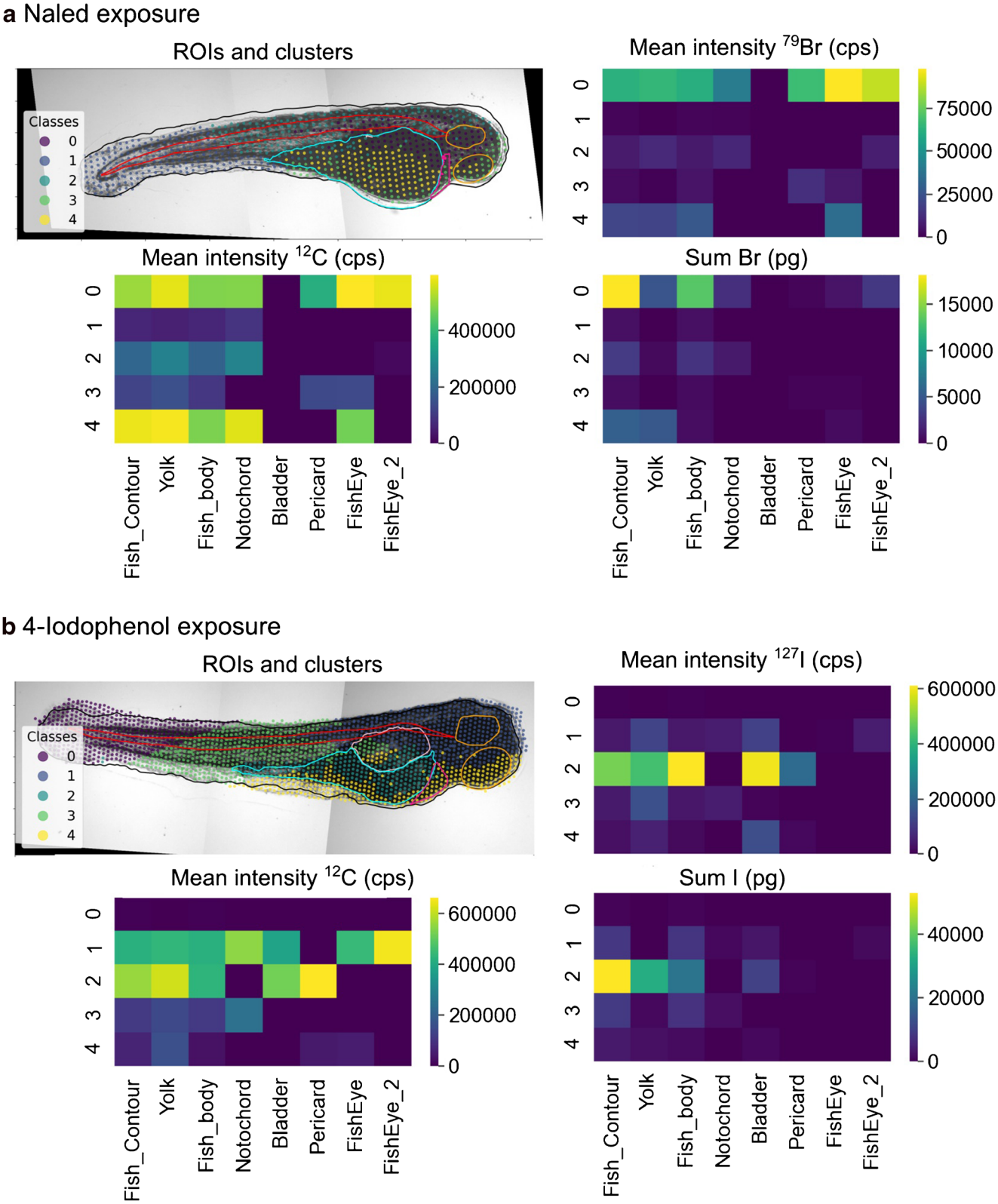

Fig. 4 K-means clustering of (**a**) the bromine and carbon intensities and the *x*,*y*-coordinates for the 24 h exposures with the bromine-containing naled (72 to 96 hpf) and (**b**) the iodine and carbon intensities and the *x*,*y*-coordinates for the 96-h exposure (0–96 hpf) with 4-iodophenol. The heatmaps display the mean intensity of each elements per cluster and per ROI (mean intensity $^{79}Br/^{12}C/^{127}I$) and the quantified bromine and iodine amount per cluster and ROI (sum Br, I)

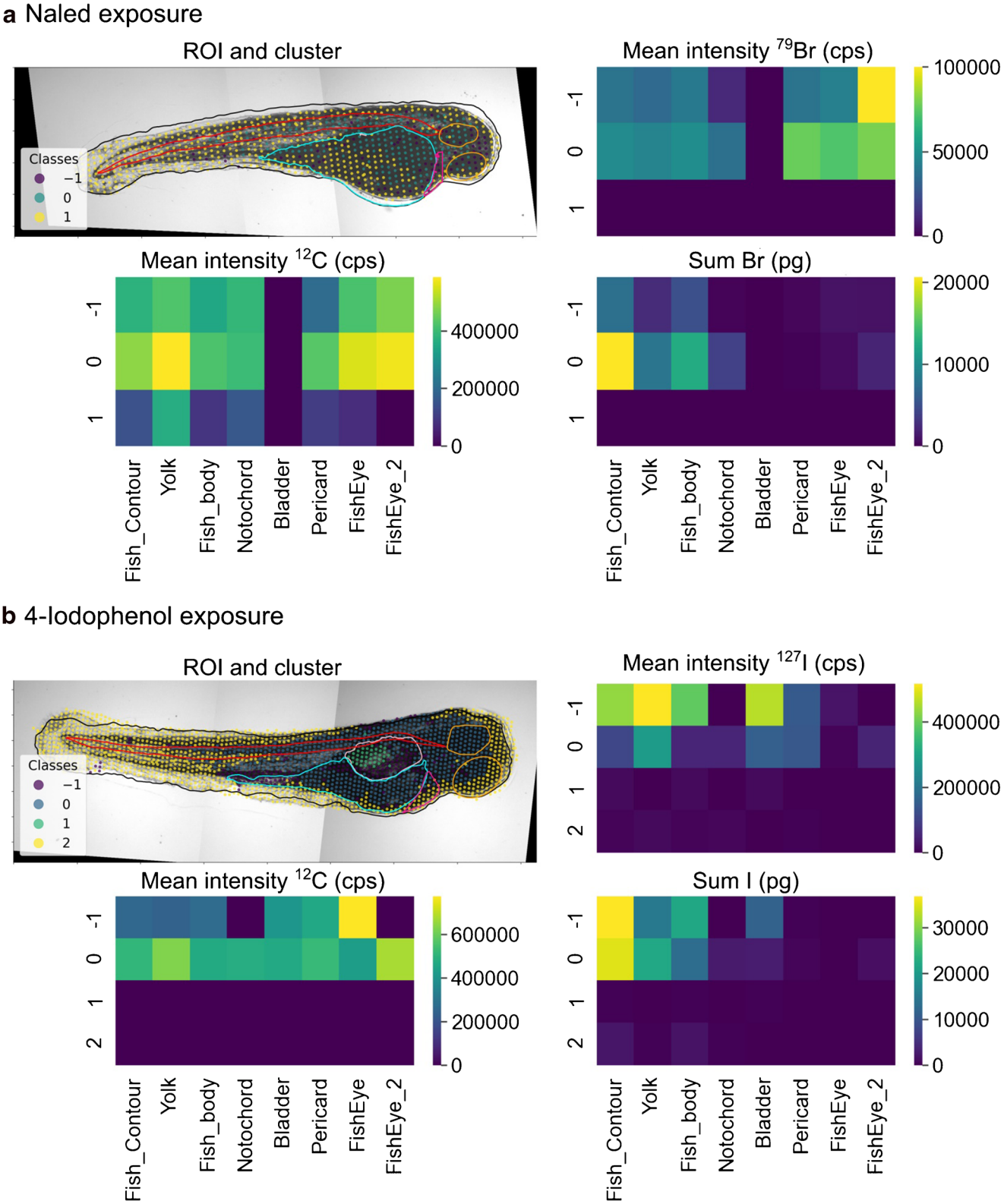

Fig. 5 HDBSCAN clustering of (**a**) the bromine and carbon intensities and the *x*,*y*-coordinates for the 96 h exposure to the bromine-containing naled (minimum cluster size set to 7) and (**b**) the iodine and carbon intensities and the *x*,*y*-coordinates for the 96 h exposure to 4-iodophenol (minimum cluster size set to 22). The heatmaps display the mean intensity of each element per cluster and per ROI (mean intensity ^{79}Br,^{12}C,^{127}I) and the total amount in the segments (sum)

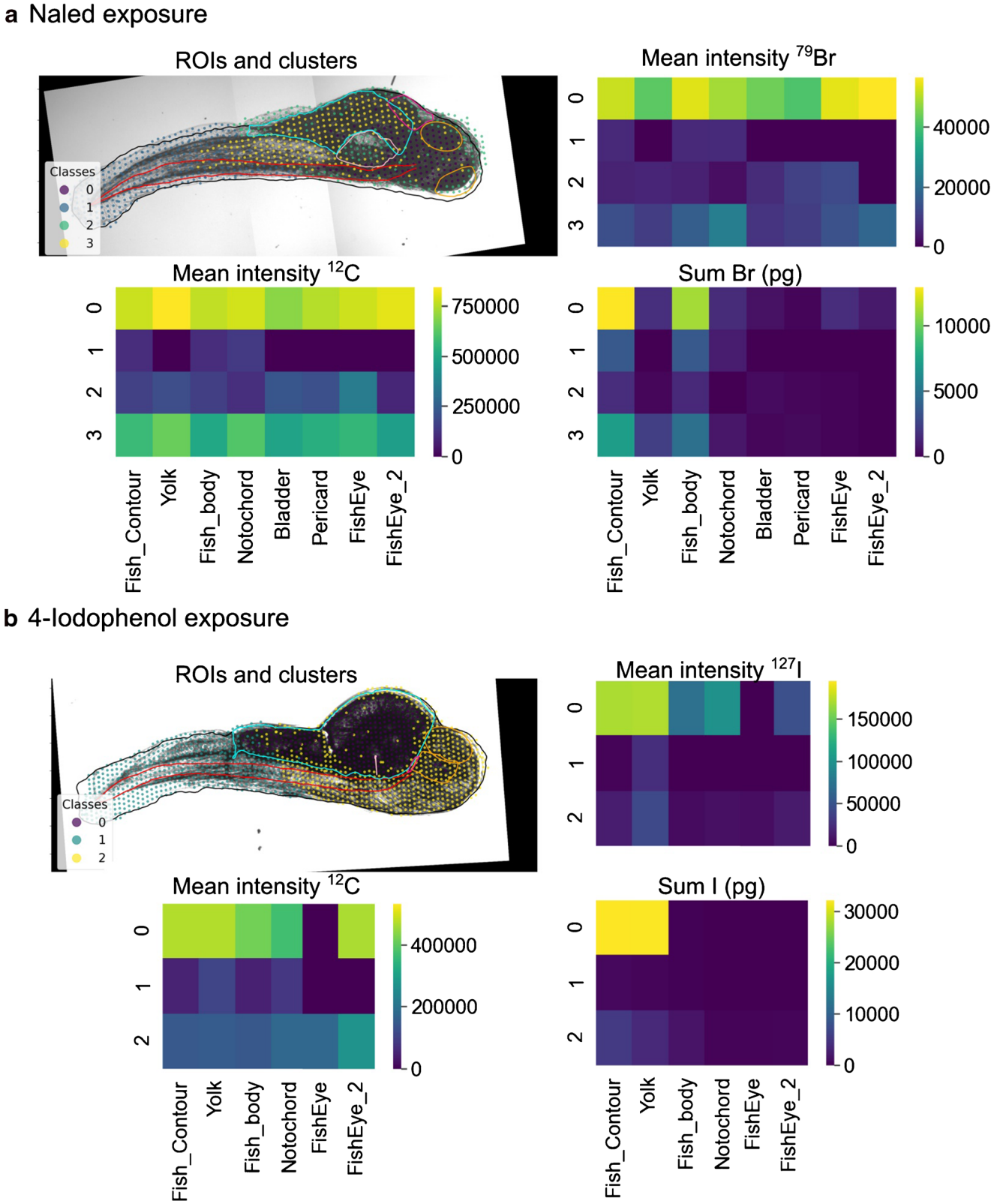

Fig. 6 K-means clustering of the (**a**) bromine and carbon intensities and the *x*,*y*-coordinates for a 4 h exposure (92 to 96 hpf) to naled (cluster number set to 4) and (**b**) iodine and carbon intensities and the *x*,*y*-coordinates for the 48 h exposure (0 to 48 hpf) to 4-iodophenol (cluster number set to 3). The bladder and pericard are not displayed for (**b**) because for this developmental stage, it is not meaningful. The heatmaps display the mean intensity of the elements per cluster and per ROI (mean intensity ^{79}Br, ^{127}I, ^{12}C) and the quantified amount per cluster and ROI (sum Br, I)

represented the highest mean bromine and carbon intensity (5.34×10^4 cps and 7.79×10^5 cps, ESM Table S3) and overlapped strongest with the ROIs fish eyes and notochord in the fish body (ESM Fig. S7). The total quantified bromine in cluster 0 was 13 ng after 4 h (ESM Table S3) and increased only slightly to 18 ng in the same body compartments after 24 h of exposure (Table 3, cluster 0). Thus, neither the site of the accumulation nor the target site of the toxicity appears to change with exposure duration.

The k-means clustering was also applied with three chosen clusters (confirmed with the elbow method) for a shorter exposure period of 4-iodophenol in a younger ZFE (48 h, 48 hpf, Fig. 6b). Cluster 1 and cluster 2 mainly represented the ROI fish body of the ZFE with the ROIs notochord and eyes (ESM Fig. S7). The ROI yolk was primarily represented by cluster 0. The mean iodine and carbon intensity are also highest in this cluster (ESM Table S3). At shorter exposure times, 32 ng iodine accumulated in the ROI yolk (cluster 0) increasing to 53 and 4 ng in the GI tract and ROI yolk at longer exposure times (see Table 3 and ESM Table S2). Contrary to the bromine case, the 4-iodophenol showed a more dynamic behavior: With continuing exposure and ZFE development, the iodine is transferred from the yolk to the GI tract. This may be explained by an increased metabolizing capacity of older ZFEs [42, 43] as well as the development of the elimination pathways via the liver and kidney [44]. It has recently been shown that the distribution of toxicants between the yolk and the ZFE body of developing ZFEs can be highly dynamic [40]. Imaging mass spectrometry in combination with FishImager allows direct access to the amount of the toxicant in the yolk.

Conclusions

The developed workflow with its implementation in the software FishImager combines quantitative LA-ICP-MS imaging data with annotated biological features. This was demonstrated here for the distribution of natural elements as well as for two xenobiotics in the model organism ZFE with its morphological features obtained by the FishInspector software. Namely, (i) the reproducibility and biological variation of LA-ICP-MS results were assessed by calculating localized mean intensities of the elements and performing a correlation analysis among replicates; (ii) different cluster algorithms were applied on the LA-ICP-MS data and visualized; (iii) biological ROIs were imported, automatically allocated to the LA-ICP-MS data and combined with the cluster results. This combination makes it possible to move from visual observations and interpretations towards validation and statistical proof and an automatic, more reliable ROI definition. Results can be compared in heatmaps. Finally, the data evaluation time can be significantly reduced using FishImager.

The built-in tool for importing and processing LA-ICP-ToF-MS data increases the application possibilities of these simultaneous multielement detection techniques. The developed tool can be applied in the future to other solid or soft matrix samples and data from different imaging methods. For example, brain sections [45] annotated with morphological features may be combined with MS imaging data in this freely available software. Moreover, the approach may also be applied to other important test organisms such as *Daphnia magna* or *Xenopus* which are used for instance in toxicokinetic studies and risk assessment of chemicals [41, 46] but also for quality control in material development where the distribution of elements is crucial, for instance in composite materials. Ultimately, the developed workflow allows a combination of different imaging data and its systematic and reproducible interpretation.

Supplementary Information The online version contains supplementary material available at https://doi.org/10.1007/s00216-020-03131-4 .

Acknowledgments This work is part of the Integrated Project "Exposome" of the topic "Chemicals in the Environment" of the Helmholtz Centre for Environmental Research, UFZ. We thank the department of Bioanalytical Ecotoxicology with Stefan Scholz at the UFZ for providing the zebrafish embryos and the FishInspector software.

Availability and requirements

- Project name: FishImager
- Project homepage: https://git.ufz.de/holbrook/fishi-LAICPMS-Imaging-Tool
- Operating system: Windows
- Programming language: Python 3.7
- Other requirements: no
- License: GNU GPL
- Any restrictions to use by non-academics: no

Authors' contributions Katharina Halbach and Timothy Holbrook contributed equally to the manuscript. Katharina Halbach performed the exposure experiments with the zebrafish embryos and LA-ICP-MS measurements. Katharina Halbach, Timothy Holbrook, Stephan Wagner, and Thorsten Reemtsma conceptualized FishImager. Timothy Holbrook coded FishImager and analyzed the zebrafish embryo with the LA-ICP-ToF-MS. Katharina Halbach wrote the manuscript with input from Timothy Holbrook, Stephan Wagner, and Thorsten Reemtsma. Stephan Wagner supervised the project. All authors have approved the final version of the manuscript.

Funding Open Access funding enabled and organized by Projekt DEAL. This project was funded by the Helmholtz Association as part of the research unit Chemicals in the Environment at the UFZ.

Data availability The data sets supporting the conclusions of this article are included within the additional files of this article or linked to the project homepage.

Compliance with ethical standards

Conflict of interest The authors declare that they have no conflict of interest.

References

1. Strähle U, Scholz S, Geisler R, Greiner P, Hollert H, Rastegar S, et al. Zebrafish embryos as an alternative to animal experiments-a commentary on the definition of the onset of protected life stages in animal welfare regulations. Reprod Toxicol. 2012;33:128–32. https://doi.org/10.1016/j.reprotox.2011.06.121 .
2. Kirla KT, Groh KJ, Poetzsch M, Banote RK, Stadnicka-Michalak J, Eggen RIL, et al. Importance of toxicokinetics to assess the utility of zebrafish larvae as model for psychoactive drug screening using meta-chlorophenylpiperazine (mCPP) as example. Front Pharmacol. 2018;9:414. https://doi.org/10.3389/fphar.2018.00414 .
3. Böhme S, Stärk H-J, Kühnel D, Reemtsma T. Exploring LA-ICP-MS as a quantitative imaging technique to study nanoparticle uptake in Daphnia magna and zebrafish (Danio rerio) embryos. Anal Bioanal Chem. 2015;407:5477–85.
4. Dolgova NV, Hackett MJ, MacDonald TC, Nehzati S, James AK, Krone PH, et al. Distribution of selenium in zebrafish larvae after exposure to organic and inorganic selenium forms. Metallomics. 2016;8:305–12. https://doi.org/10.1039/c5mt00279f .
5. Ackerman CM, Weber PK, Xiao T, Thai B, Kuo TJ, Zhang E, et al. Multimodal LA-ICP-MS and nanoSIMS imaging enables copper mapping within photoreceptor megamitochondria in a zebrafish model of Menkes disease. Metallomics. 2018;10:474–85. https://doi.org/10.1039/c7mt00349h .
6. Pirro V, Guffey SC, Sepúlveda MS, Mahapatra CT, Ferreira CR, Jarmusch AK, et al. Lipid dynamics in zebrafish embryonic development observed by DESI-MS imaging and nanoelectrospray-MS. Mol BioSyst. 2016;12:2069–79. https://doi.org/10.1039/C6MB00168H .
7. Theiner S, Van Malderen SJM, Van Acker T, Legin AA, Keppler BK, Vanhaecke F, et al. Fast high-resolution LA-ICP-MS imaging of the distribution of platinum-based anti-cancer compounds in multicellular tumor spheroids. Anal Chem. 2017;89:12641–5. https://doi.org/10.1021/acs.analchem.7b02681 .
8. Barst BD, Gevertz AK, Chumchal MM, Smith JD, Rainwater TR, Drevnick PE, et al. Laser ablation ICP-MS co-localization of mercury and immune response in fish. Environ Sci Technol. 2011;45:8982–8. https://doi.org/10.1021/es201641x .
9. Lingott J, Lindner U, Telgmann L, Esteban-Fernández D, Jakubowski N, Panne U. Gadolinium-uptake by aquatic and terrestrial organisms-distribution determined by laser ablation inductively coupled plasma mass spectrometry. Environ Sci Process Impacts. 2016;18:200–7. https://doi.org/10.1039/c5em00533g .
10. Köppen C, Reifschneider O, Castanheira I, Sperling M, Karst U, Ciarimboli G. Quantitative imaging of platinum based on laser ablation-inductively coupled plasma-mass spectrometry to investigate toxic side effects of cisplatin. Metallomics. 2015;7:1595–603. https://doi.org/10.1039/C5MT00226E .
11. Pugh JAT, Cox AG, McLeod CW, Bunch J, Writer MJ, Hart SL, et al. Elemental imaging of MRI contrast agents: benchmarking of LA-ICP-MS to MRI. Anal Bioanal Chem. 2012;403:1641–9. https://doi.org/10.1007/s00216-012-5973-z .
12. Westerhausen MT, Bishop DP, Dowd A, Wanagat J, Cole N, Doble PA. Super-resolution reconstruction for two-and three-dimensional LA-ICP-MS bioimaging. Anal Chem. 2019;91:14879–86. https://doi.org/10.1021/acs.analchem.9b02380 .
13. Bauer OB, Köppen C, Sperling M, Schurek HJ, Ciarimboli G, Karst U. Quantitative bioimaging of platinum via online isotope dilution-laser ablation-inductively coupled plasma mass spectrometry. Anal Chem. 2018;90:7033–9. https://doi.org/10.1021/acs.analchem.8b01429 .
14. Barbosa LD, Sussulini A. Recent advances in LA-ICP-MS for biomedical applications. Biomed Spectrosc Imaging. 2020;8:47–54. https://doi.org/10.3233/bsi-200193 .
15. López-Fernández H, De S, Pessôa G, Arruda MAZ, Capelo-Martínez JL, Fdez-Riverola F, et al. LA-iMageS: a software for elemental distribution bioimaging using LA-ICP-MS data. J Cheminform. 2016;8:1–10. https://doi.org/10.1186/s13321-016-0178-7 .
16. Paton C, Hellstrom J, Paul B, Woodhead J, Hergt J. Iolite: freeware for the visualisation and processing of mass spectrometric data. J Anal At Spectrom. 2011;26:2508–18. https://doi.org/10.1039/c1ja10172b .
17. Weiskirchen R, Weiskirchen S, Kim P, Winkler R. Software solutions for evaluation and visualization of laser ablation inductively coupled plasma mass spectrometry imaging (LA-ICP-MSI) data: a short overview. J Cheminform. 2019;11:16.
18. Lingott J. Untersuchungen zur Aufnahme und Verteilung von gadoliniumbasierten Kontrastmitteln in biologischen Proben mittels Laserablation mit induktiv gekoppelter Plasma-Massenspektrometrie. 2016.
19. HDIP LA-ICP-MS imaging software. http://www.teledynecetac.com/products/laser-ablation/hdip-imaging-software. Accessed 11 Sep 2020.
20. Portbury SD, Hare DJ, Bishop DP, Finkelstein DI, Doble PA, Adlard PA. Trehalose elevates brain zinc levels following controlled cortical impact in a mouse model of traumatic brain injury. Metallomics. 2018;10:846–53. https://doi.org/10.1039/c8mt00068a .
21. Hare DJ, Raven EP, Roberts BR, Bogeski M, Portbury SD, McLean CA, et al. Laser ablation-inductively coupled plasma-mass spectrometry imaging of white and gray matter iron distribution in Alzheimer's disease frontal cortex. Neuroimage. 2016;137:124–31. https://doi.org/10.1016/j.neuroimage.2016.05.057 .
22. Software download : SHIMADZU (Shimadzu Corporation). https://www.shimadzu.com/form/ana/lifescience/imaging/imagereveal.html. Accessed 3 Apr 2020.
23. Petrus JA, Chew DM, Leybourne MI, Kamber BS. A new approach to laser-ablation inductively-coupled-plasma mass-spectrometry (LA-ICP-MS) using the flexible map interrogation tool 'Monocle.'. Chem Geol. 2017;463:76–93. https://doi.org/10.1016/j.chemgeo.2017.04.027 .
24. Castellanos-García LJ, Gokhan Elci S, Vachet RW. Reconstruction, analysis, and segmentation of LA-ICP-MS imaging data using Python for the identification of sub-organ regions in tissues. Analyst. 2020;145:3705–12. https://doi.org/10.1039/c9an02472g .
25. Teixidó E, Kießling TR, Krupp E, Quevedo C, Muriana A, Scholz S. Automated morphological feature assessment for zebrafish embryo developmental toxicity screens. Toxicol Sci. 2019;167:438–49. https://doi.org/10.1093/toxsci/kfy250 .
26. Fetter E, Smetanová S, Baldauf L, Lidzba A, Altenburger R, Schüttler A, et al. Identification and characterization of androgen-

responsive genes in zebrafish embryos. Environ Sci Technol. 2015;49:11789–98. https://doi.org/10.1021/acs.est.5b01034 .
27. Halbach K, Wagner S, Scholz S, Luckenbach T, Reemtsma T. Elemental imaging (LA-ICP-MS) of zebrafish embryos to study the toxicokinetics of the acetylcholinesterase inhibitor naled. Anal Bioanal Chem. 2019;411:617–27. https://doi.org/10.1007/s00216-018-1471-2 .
28. ISO. Water quality - determination of the acute lethal toxicity of substances to a freshwater fish. ISO. 1996:7346–1.
29. OECD guidelines for the testing of chemicals - fish embryo acute toxicity (FET) test. OECD 236. 2013.
30. Ardelt D, Polatajko A, Primm O, Reijnen M. Isotope ratio measurements with a fully simultaneous Mattauch-Herzog ICP-MS. Anal Bioanal Chem. 2013;405:2987–94. https://doi.org/10.1007/s00216-012-6543-0 .
31. Stärk H-J, Wennrich R. A new approach for calibration of laser ablation inductively coupled plasma mass spectrometry using thin layers of spiked agarose gels as references. Anal Bioanal Chem. 2011;399:2211–7. https://doi.org/10.1007/s00216-010-4413-1 .
32. Oros-Peusquens AM, Matusch A, Becker JS, Shah NJ. Automatic segmentation of tissue sections using the multielement information provided by LA-ICP-MS imaging and k-means cluster analysis. Int J Mass Spectrom. 2011;307:245–52. https://doi.org/10.1016/j.ijms.2011.03.014 .
33. Szakal C, Narayan K, Fu J, Lefman J, Subramaniam S. Compositional mapping of the surface and interior of mammalian cells at submicrometer resolution. Anal Chem. 2011;83:1207–13. https://doi.org/10.1021/ac1030607 .
34. Minerva L, Ceulemans A, Baggerman G, Arckens L. MALDI MS imaging as a tool for biomarker discovery: methodological challenges in a clinical setting. Proteomics Clin Appl. 2012;6:581–95. https://doi.org/10.1002/prca.201200033 .
35. Comparing Python clustering algorithms — hdbscan 0.8.1 documentation. https://hdbscan.readthedocs.io/en/latest/comparing_clustering_algorithms.html. Accessed 21 Apr 2020.
36. Kodinariya TM, Makwana PR. Review on determining of cluster in K-means clustering review on determining number of cluster in K-means clustering. Int J Adv Res Comput Sci Manag Stud. 2013;1:90–5.
37. Miyares RL, de Rezende VB, Farber SA. Zebrafish yolk lipid processing: a tractable tool for the study of vertebrate lipid transport and metabolism. Dis Model Mech. 2014;7:915–27. https://doi.org/10.1242/dmm.015800 .
38. Stengel R, Rivera-Milla E, Sahoo N, Ebert C, Bollig F, Heinemann SH, et al. Kcnh1 voltage-gated potassium channels are essential for early zebrafish development. J Biol Chem. 2012;287:35565–75. https://doi.org/10.1074/jbc.M112.363978 .
39. van der Bent SAS, Berg T, Karst U, Sperling M, Rustemeyer T. Allergic reaction to a green tattoo with nickel as a possible allergen. Contact Dermatitis. 2019;81:64–6. https://doi.org/10.1111/cod.13226 .
40. Halbach K, Ulrich N, Goss K-U, Seiwert B, Wagner S, Scholz S, et al. Yolk sac of zebrafish embryos as backpack for chemicals? Environ Sci Technol. 2020;54:10159–69. https://doi.org/10.1021/acs.est.0c02068 .
41. Wang M, Dubiak K, Zhang Z, Huber PW, Chen DDY, Dovichi NJ. MALDI-imaging of early stage Xenopus laevis embryos. Talanta. 2019;204:138–44. https://doi.org/10.1016/j.talanta.2019.05.060 .
42. Saad M, Cavanaugh K, Verbueken E, Pype C, Casteleyn C, Van Ginneken C, et al. Xenobiotic metabolism in the zebrafish: a review of the spatiotemporal distribution, modulation and activity of cytochrome P450 families 1 to 3. J Toxicol Sci. 2016;41:1–11. https://doi.org/10.2131/jts.41.1 .
43. Brox S, Seiwert B, Haase N, Küster E, Reemtsma T. Metabolism of clofibric acid in zebrafish embryos (Danio rerio) as determined by liquid chromatography-high resolution-mass spectrometry. Comp Biochem Physiol Part - C Toxicol Pharmacol. 2016;185–186:20–8. https://doi.org/10.1016/j.cbpc.2016.02.007 .
44. van Wijk RC, Krekels EHJ, Kantae V, Harms AC, Hankemeier T, van der Graaf PH, et al. Impact of post-hatching maturation on the pharmacokinetics of paracetamol in zebrafish larvae. Sci Rep. 2019;9:2149. https://doi.org/10.1038/s41598-019-38530-w .
45. Brain map - brain-map.org. https://portal.brain-map.org/. Accessed 21 Apr 2020.
46. Brun NR, Fields PD, Horsfield S, Mirbahai L, Ebert D, Colbourne JK, et al. Mixtures of aluminum and indium induce more than additive phenotypic and toxicogenomic responses in Daphnia magna. Environ Sci Technol. 2019;53:1639–49. https://doi.org/10.1021/acs.est.8b05457 .

Supplementary information

Effective processing and evaluation of chemical imaging data with respect to morphological features of the zebrafish embryo

Halbach, K., Holbrook, T., Reemtsma, T., Wagner, S.

Department of Analytical Chemistry, Helmholtz Centre for Environmental Research - UFZ, 04318 Leipzig, Germany

Institute of Analytical Chemistry, University of Leipzig, 04103 Leipzig, Germany

*Corresponding author: Stephan Wagner

E-mail address: Stephan.wagner@ufz.de

Calibration of LA-ICP-MS data

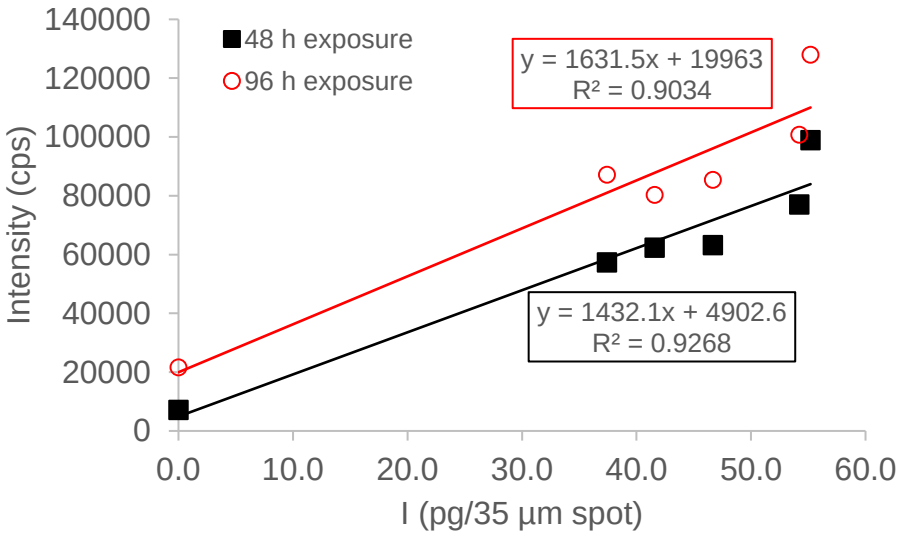

Fig. S1 Calibration curves with a spotsize of 35 µm conducted on the day of the ablations of the embryos exposed from 2-50 hpf (black square) and 2-98 hpf (red dot). The unit of the x-axis refers to the iodine content of the agarose standards and the corresponding intensity is displayed on the y-axis. Limit of detection = 14.2 x 10^3 cps (black) and 29.8 x 10^3 cps (red); limit of quantification = 30.5 x 10^3 (red) and 48.92 x 10^3 (black)

Implementation in FishImager

Load files

The image taken by the camera of the LA-system (Analyte G2, Teledyne CETAC Technologies) (termed “laser camera image”) and the corresponding file with the coordinates and image size are imported (*Step 1: Load images*). The two files have the format produced by Chromium 2.4 (Teledyne Photon Machines). Additionally, the image used to create the morphological features (termed “reference image”) is imported. Both imported images can be viewed in *Step 2: View images*. The transient ICP-MS with the laser coordinates are imported as a tab-delimited text file in *Step3: Load txt table with LA-ICP-MS data*. The text file is structured with columns (element1, element2, …, X coordinate, Y coordinate) and rows containing the measured data (see link to cloud with example files in https://git.ufz.de/holbrook/fishi-LAICPMS-Imaging-Tool/-/tree/master/test_data). Currently, the file format of Tofwerk (.h5) is also supported. For other file formats, either these need to be transformed into the same structure or programming adjustments in FishImager are needed.

We have also included the option to load ICP-ToF-MS data as an H5-file. This is the output file of TOFpilot (version 2.5.4.1) and TofDaq (Tofwerk, Switzerland) with all selected m/z values from the measurement. As the large file size requires a high computing time, data sampling is implemented as a float value to downsample the buff/write coordinates. Due to the limitation of the large list iterations, chunk size allows the user to select a size of data chunk for increased iterations performance. The file size tested had a dimension of 1144 x 50 x 1 x 315; larger dimensions were not tested. An exemplary workflow for one h5-file is shown in ESI 2.

The imported LA-ICP-MS data can then be checked with *Step 4: View LA-ICP-MS data*. The channel which is displayed can be selected in the drop-down menu. To view another channel, close the figure and select the new one in the drop-down menu, and press *Step 4* again.

Transformation and ROI

The aim of this tab is first to transform coordinates of the LA-ICP-MS data to fit the reference image (or another image of the same sample) from which the ROIs are determined. This allows combining two independent analyses of the biological specimen (here LA-ICP-MS and the FishInspector tool). Secondly, the LA-ICP-MS data are combined with the data of the morphological features.

The registration of the two images is performed by choosing first a point in the laser camera image, then the corresponding one in the reference image, and then repeating this for a minimum of 3 points (*Step 1: Choose control points*). The algorithm produces an affine transformation matrix of the two images for registration of the laser camera image (source, src) to the reference image (destination, dst). Different registration methods are available by changing the parameter in the code from affine to the desired algorithm (https://scikit-image.org/docs/dev/api/skimage.transform.html#skimage.transform.estimate_transform). The overlay is visible in *Step 2: Image registration*. The same transformation is performed with the coordinates of the ablation pattern in the text file with the LA-ICP-MS data.

The data of morphological features (here the SHAPES.JSON file from the FishInspector) are imported in *Step 3: Load JSON file and create ROIs*. This file format is the _Shapes.JSON from the FishInspector software and contains the outline coordinates of the different assigned body parts.[1] This module of the FishImager software may be adjusted to different referencing methods for other applications.[2] The imported ROIs are plotted over the ablated area of the LA-ICP-MS data in *Step 4: Display LA-ICP-MS data together with ROIs*.

Cluster analysis

After these steps, the data are ready for further exploration. From the imported LA-ICP-MS data table, you can select the elements for clustering, which are then normalized using a min_max_Scaler. You may also include the x- and y-coordinates as variables. This is an advantage of FishImager as not only the identification of similar elements distribution but also homogenous areas of single elements is possible.

Six different cluster algorithms have been implemented: k-means, mean shift, affinity propagation, spectral clustering, DBSCAN, and HDBSCAN can be chosen depending on the purpose and preknowledge of the data (Table S1). The cluster parameters can be chosen and varied in FishImager, e.g., number of clusters for k-means, spectral clustering, and HDBSCAN, epsilon for DBSCAN. For the k-means clustering, we have also implemented a plot showing the sum of squared errors to determine the optimal number of clusters (elbow method[3]).

Table S1 Overview of the available cluster algorithms in FishImager and adjustable parameters.

Cluster algorithm	Description	Parameters to be known	Application
K-means	Algorithm that partitions your data in a predefined number of groups with equal variance (within-cluster sum-of-squares), all data points are grouped incl. noise	number of clusters	General purpose, also for large data sets applicable, even cluster size
Mean shift	Centroid based method, returns clusters and not partitions/groups, does not cluster every point, slow algorithm	bandwidth	Many clusters with uneven cluster size
Affinity propagation	Data votes for their preferred exemplar, graph distance, problematic for noisy data (similar to k-means), slow algorithm, so not recommended for large datasets	damping, sample preference	Many clusters, uneven cluster size, non-flat geometry
Spectral clustering	Graph clustering based on graph distance (e.g., nearest-neighbor graph), partitioning algorithm, includes noise	number of clusters	Small number of clusters, even cluster size
DBSCAN	Density based algorithm, extracts dense clusters and excludes background data as noise, problems with clusters of varying density.	Epsilon as a distance value	Large data sets, uneven cluster size
HDBSCAN	Allows varying density clusters, other similar to DBSCAN, high stability	Minimum cluster size	Large data sets, uneven cluster size

Visualization

The obtained clusters and the assigned ROIs are visually overlaid in one figure (*Step 1: Visualization of the clusters and the ROIs*). Next, a table (*Step 2: Calculate table with descriptive statistics*) with the descriptive statistics of a chosen elemental channel for the different clusters is compiled: sum, mean, standard deviation, median, variance, minimum and maximum. The total pixel number and percentage of the ablation area in the clusters are shown in a table using the *Cluster counts* function.

Heatmaps then visually merge the cluster and ROI data. The heatmap *Total ion count (sum)* may be used to look at the sum of the selected elemental channel per cluster and ROI. This heatmap contains absolute values; the percentage can be viewed in *%Total ion count per cluster*. Important information may not only be the sum of the selected channel but also the mean. The heatmaps *Total ion count (mean)* and *Total ion count (std)* show the color-coded mean and standard deviation of the elemental channel per cluster and per ROI, respectively. Another information shown is the number of counts of the LA-ICP-MS data per cluster normalized to the shape of the data matrix as a percentage (*Count %*). The underlying data for the heatmaps can be exported by using the *Export CSV* function. Additionally, a table with the percentage areas of the ROIs can be compiled (*ROI areas*).

Annotation of morphological features of the zebrafish embryo

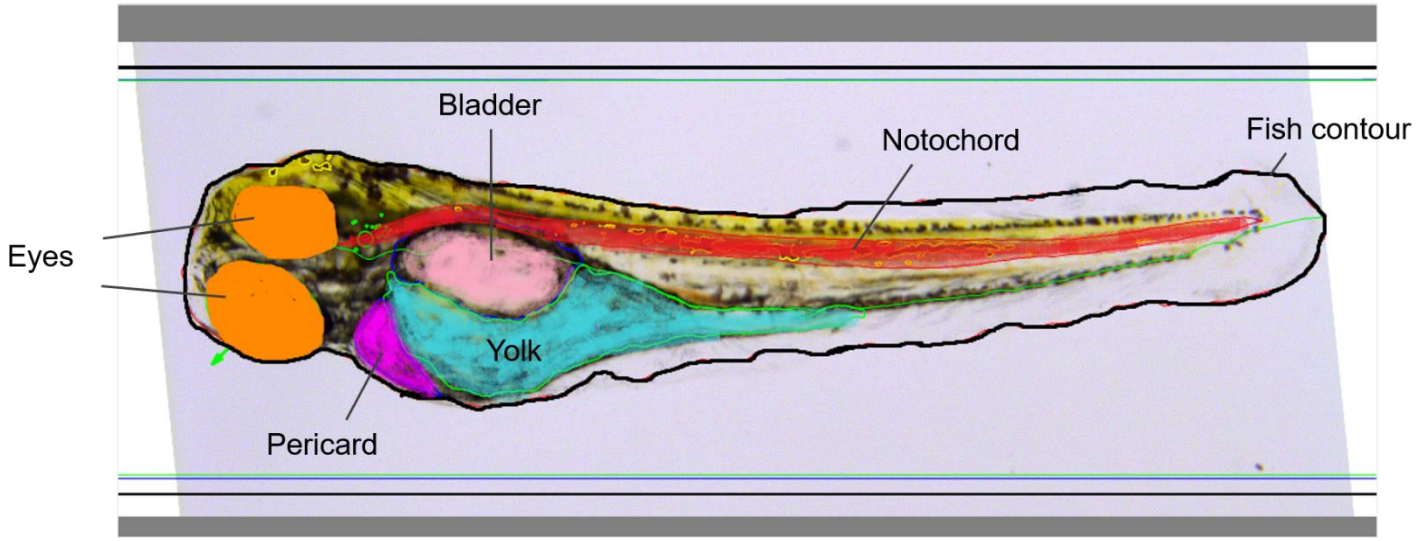

Fig. S2 Annotated zebrafish embryo by the FishInspector software. The embryo displayed is 96 hours post fertilization. In the manuscript, the term “fish body” refers to the area inside the fish contour minus the yolk.

Distribution of natural elements in zebrafish embryos and reproducibility between ablations of different individuals

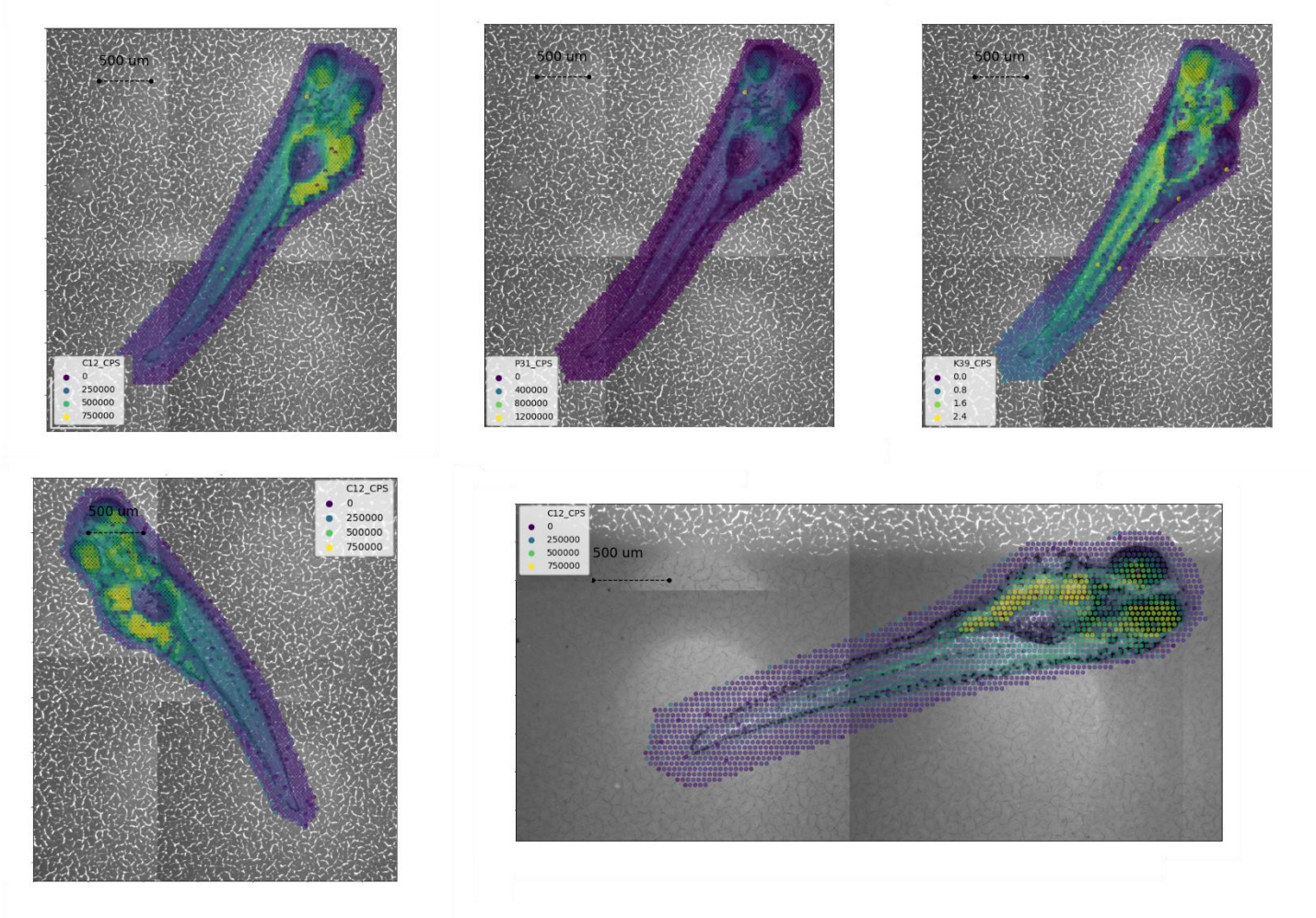

Fig. S3 Intensities of the baseline-corrected carbon (^{12}C), phosphorus (^{31}P), and potassium (^{39}K) LA-ICP-MS signals for zebrafish embryo individuum 1 (first row). Intensities of the baseline-corrected carbon (^{12}C) for zebrafish embryo individuum 2 (second row left) and 3 (second row right). Scale bars indicate 500 µm.

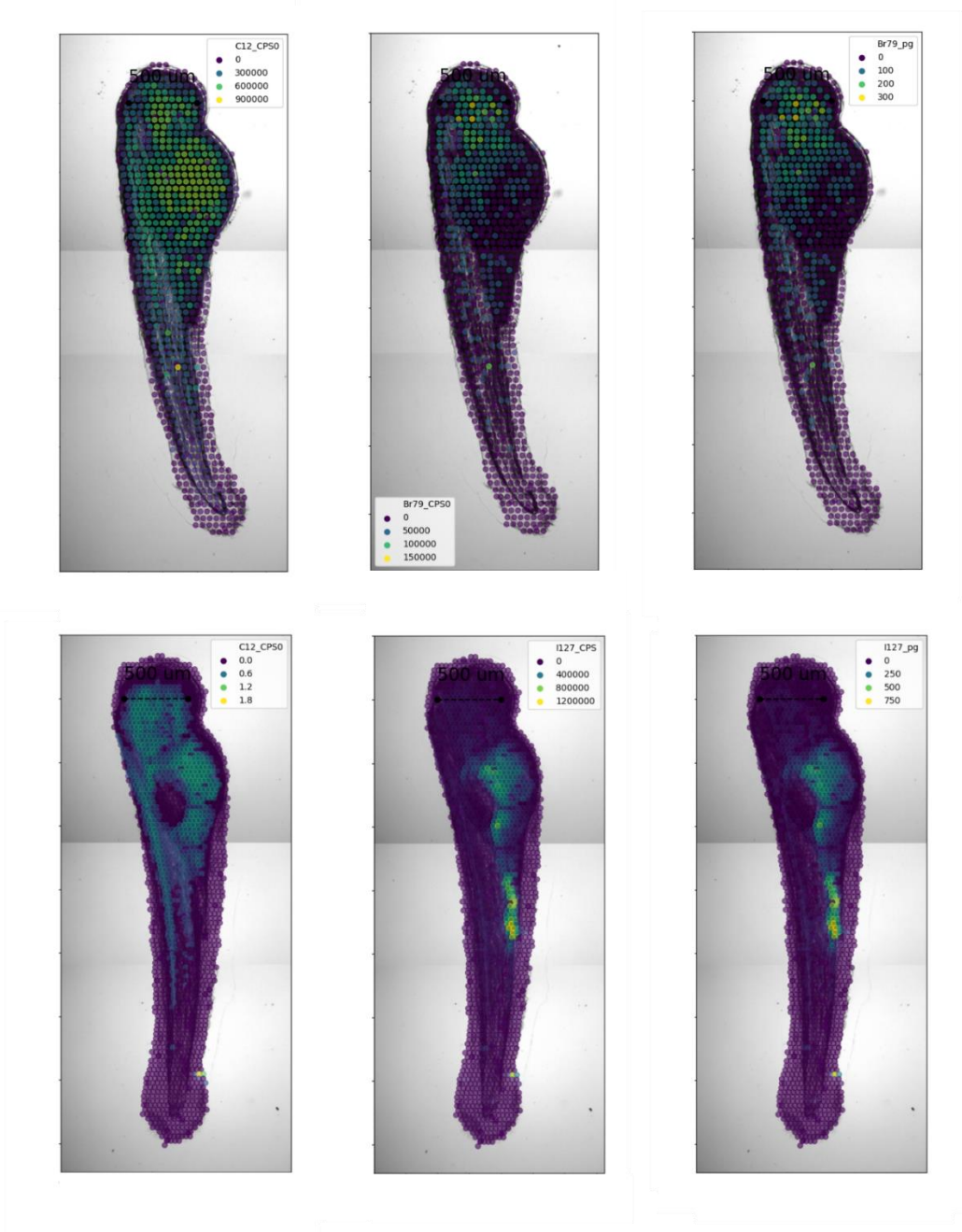

Fig. S4 Intensities of the baseline-corrected carbon (^{12}C), bromine (^{79}Br), and quantified bromine (in pg) LA-ICP-MS signals for the 24 of the zebrafish embryo (first row). Intensities of the baseline-corrected carbon (^{12}C), iodine (^{127}I), and quantified iodine (in pg) LA-ICP-MS signals for the 96 of the zebrafish embryo (first row). Scale bars indicate 500 µm.

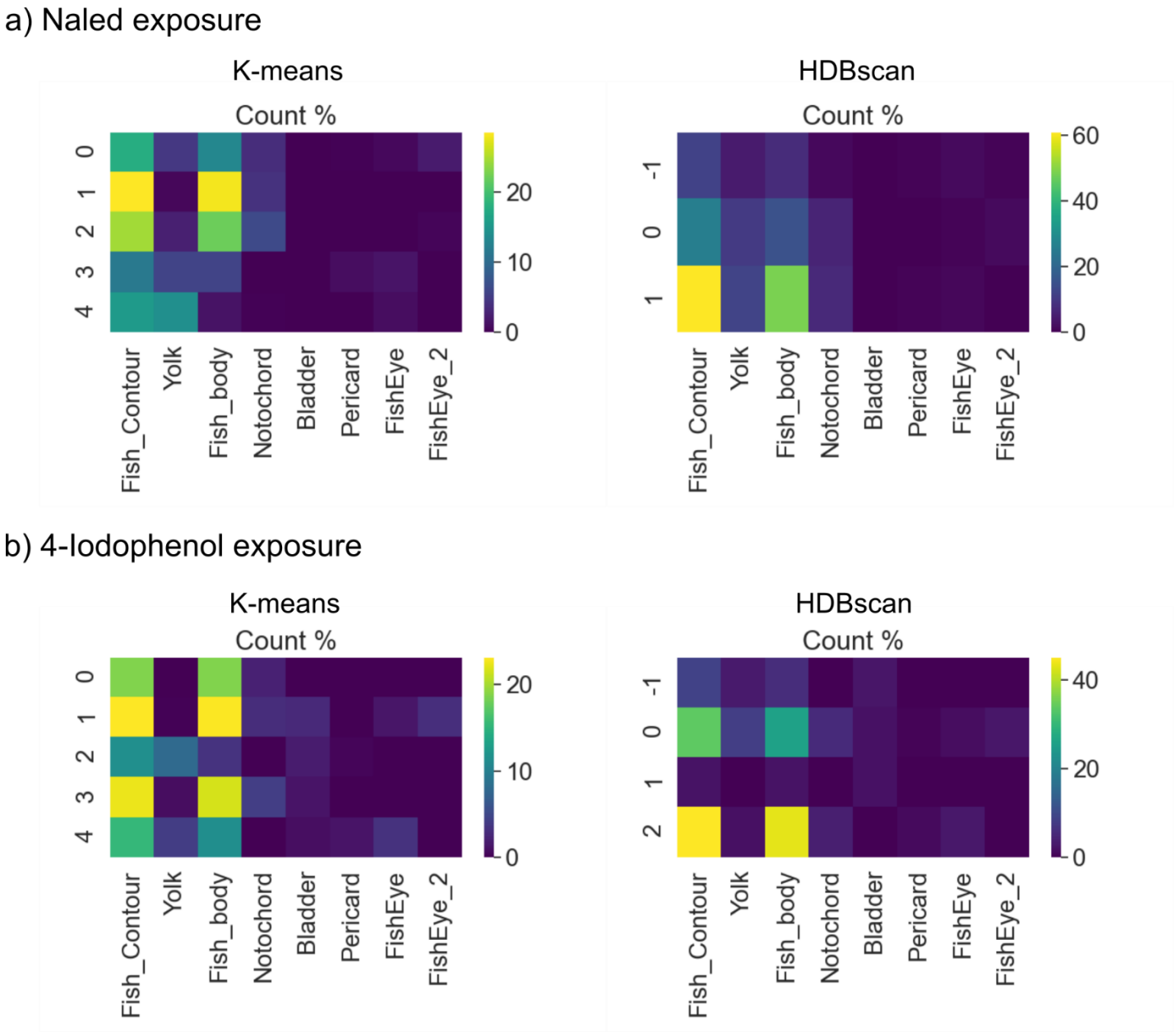

Fig. S5K-means (numbers of clusters set to 5) and HDBscan (minimum cluster size set to 8 for the naled exposure and 22 for the 4-iodophenol exposure) clustering of ^{12}C and the x- and y-coordinate in embryos exposed a) for 24 h to naled and b) for 96 h to 4-iodophenol. The heatmaps display the percentage of ablation area represented by the cluster and the body part (Count %).

Table S2 Cluster sizes as percentage of total ablation area for the naled exposure and the 4-iodophenol exposure of zebrafish embryos (HDBscan clustering, minimum cluster size set to 8 for the naled exposure and 22 for the 4-iodophenol exposure). The mean intensities of ^{79}Br, ^{127}I, ^{12}C in the clusters, and the quantified bromine and iodine amounts are displayed.

Cluster	Naled exposure				4-Iodophenol exposure			
	Percentage of ablation area (%)	mean intensity ^{79}Br (cps)	mean intensity ^{12}C (cps)	Total Br (ng)	Percentage of ablation area (%)	mean intensity ^{127}I (cps)	mean intensity ^{12}C (cps)	Total I (ng)
-1	12.0	3.82×10^4	3.77×10^5	7.58	9.1	4.20×10^5	2.51×10^5	37.0
0	25.7	4.76×10^4	4.88×10^5	20.7	34.4	1.08×10^5	5.08×10^5	35.2
1	62.3	0	1.44×10^5	0	2.2	1.33×10^4	0	0.27
2	-				54.3	4.33×10^3	0	2.15

Identification of changes over time in the distribution of a xenobiotic in the zebrafish embryo

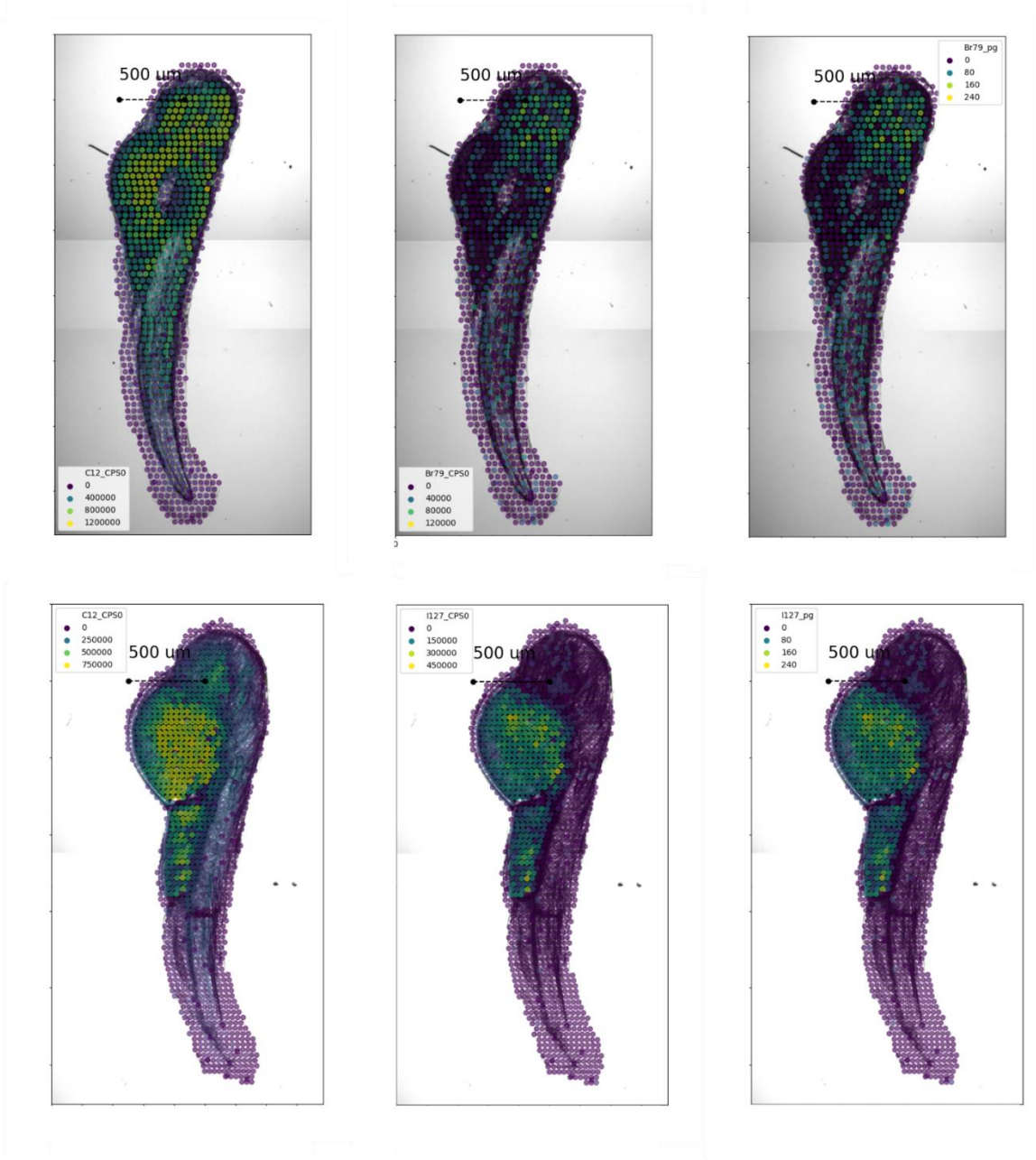

Fig. S6 Intensities of the baseline-corrected carbon (^{12}C), bromine (^{79}Br), and quantified bromine (in pg) LA-ICP-MS signals for the 4 of the zebrafish embryo (first row). Intensities of the baseline-corrected carbon (^{12}C), iodine (^{127}I), and quantified iodine (in pg) LA-ICP-MS signals for the 48 of the zebrafish embryo (first row). Scale bars indicate 500 µm.

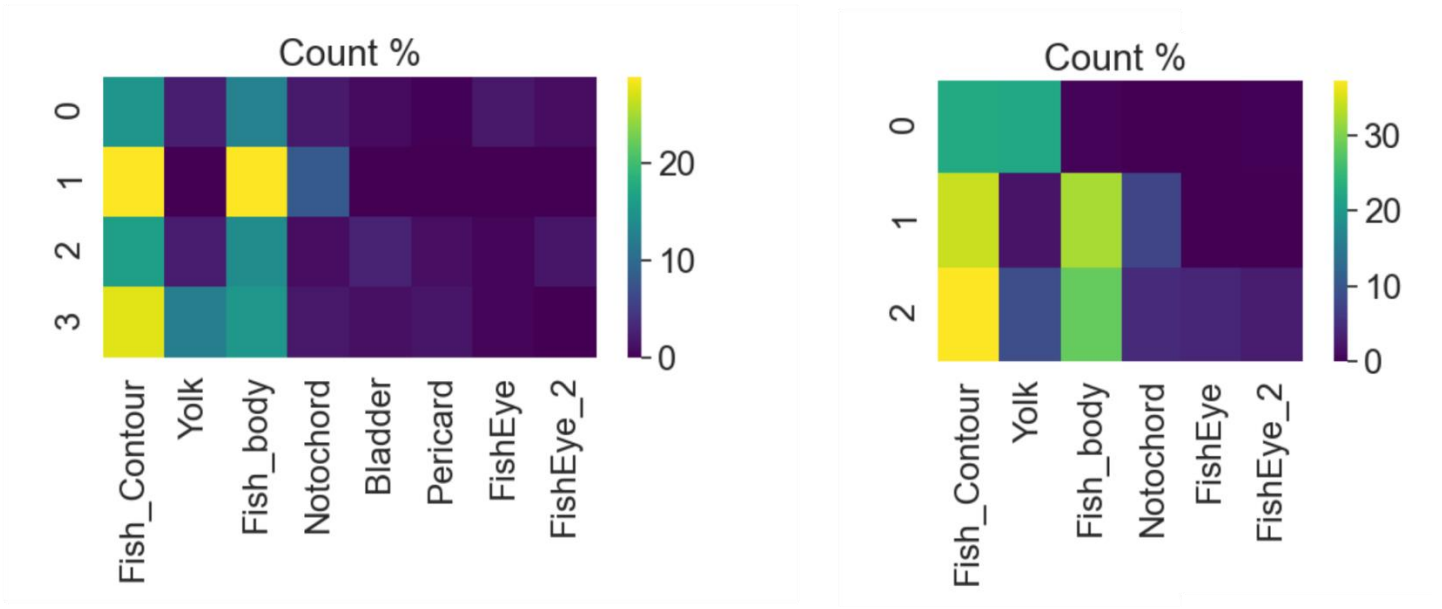

Fig. S7K-means (numbers of clusters set to 4 for the naled exposure and 3 for the 4-iodophenol exposure) clustering of the elemental intensities of ^{12}C, ^{127}I, and the x- and y-coordinate in embryos exposed a) for 4 h to naled and b) for 48 h to 4-iodophenol. The heatmaps display the percentage of ablation area represented by the cluster and the body part (Count %).

Table S3 Cluster sizes as percentage of total ablation area for the naled exposure and the 4-iodophenol exposure of zebrafish embryos (k-means clustering). The mean intensities of ^{79}Br, ^{127}I, ^{12}C in the clusters and the quantified bromine and iodine amounts are displayed.

Cluster	Naled exposure				4-Iodophenol exposure			
	Percentage of ablation area (%)	mean intensity ^{79}Br (cps)	mean intensity ^{12}C (cps)	Total Br (ng)	Percentage of ablation area (%)	mean intensity ^{127}I (cps)	mean intensity ^{12}C (cps)	Total I (ng)
0	15.1	5.34×10^4	7.79×10^5	12.7	22.7	1.71×10^5	4.70×10^5	32.2
1	33.6	6.14×10^3	9.59×10^4	3.93	36.6	1.95×10^3	4.94×10^4	0.71
2	23.8	4.08×10^3	1.33×10^5	1.92	40.7	1.39×10^4	1.37×10^5	5.56
3	27.5	1.41×10^4	5.76×10^5	7.47				

References

1. Teixidó E, Kießling TR, Krupp E, Quevedo C, Muriana A, Scholz S (2019) Automated Morphological Feature Assessment for Zebrafish Embryo Developmental Toxicity Screens. Toxicol Sci 167:438–449 . https://doi.org/10.1093/toxsci/kfy250

2. Brain Map - brain-map.org. https://portal.brain-map.org/. Accessed 21 Apr 2020

3. Kodinariya TM, Makwana PR (2013) Review on Determining of Cluster in K-means Clustering Review on determining number of Cluster in K-Means Clustering. Int J Adv Res Comput Sci Manag Stud 1:90–95

Instructions to reproduce the examples with the software

Slide 4- 20	a) Distribution of natural elements in zebrafish embryos and reproducibility between ablations of different individuals – first example
Slide 21	a) Distribution of natural elements in zebrafish embryos and reproducibility between ablations of different individuals – second example
Slide 22	a) Distribution of natural elements in zebrafish embryos and reproducibility between ablations of different individuals – third example
Slide 23	b) Distribution of xenobiotics in the zebrafish embryo – naled exposure
Slide 24	b) Distribution of xenobiotics in the zebrafish embryo – 4-iodophenol exposure
Slide 25	c) Identification of changes over time in the distribution of a xenobiotic in the zebrafish embryo – naled exposure
Slide 26	c) Identification of changes over time in the distribution of a xenobiotic in the zebrafish embryo - 4-iodophenol exposure
Slide 27	d) LA-ICP-tof-MS dataset

1

Load files | Transformation and ROIs | Cluster analysis | Visualization

General

See for an installation guide in https://git.ufz.de/holbrook/fishi-LAICPMS-Imaging-Tool/-/tree/master/test_data

To analyze the data, the software is structured into four tabs which build upon each other:

- Load files
- Transformation and ROIs
- Cluster analysis
- Visualization

The software can be closed by clicking the X in the right upper corner. To load more data tables or images for comparison the *Tools: Table Viewer* or *Tools: Image Viewer* can be used any time during the data analysis. The *Help* menu allows viewing the documentation of the software (*Documentation*), information on the license (*About*), and the version and github (*Read me*). Each created figure may be exported (*Save the figure*) to different image formats (e.g. png, tiff, jpeg). Tables can be easily copied to other files.

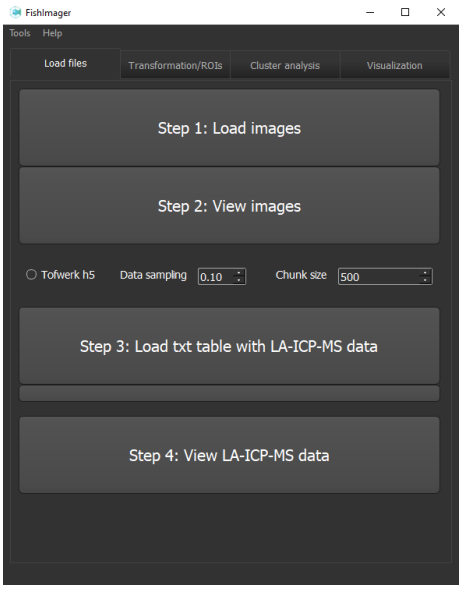

2

Load files | Transformation and ROIs | Cluster analysis | Visualization

General

The arrow bar at the top of each slide shows at which tab the current instructions belong

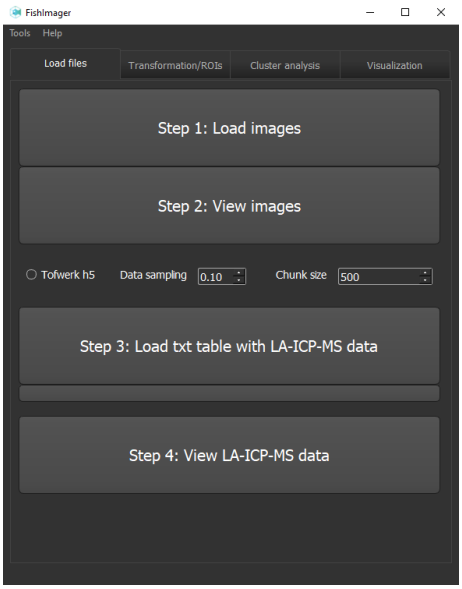

3

Load files | Transformation and ROIs | Cluster analysis | Visualization

a) Distribution of natural elements in zebrafish embryos and reproducibility between ablations of different individuals – first example

1. Go to the Load files tab.
2. Click *Step 1: Load images*
   - Open in the cloud the folder “Data sets“ -> “R&D a).
   - First choose the laser image (Z18NCs_b_1_Img06_Mapped.png).
   - Select cropped Fish inspector image (Z18NCsb1_cropped.png).
   - Select the corresponding coord-file for the laser image (Z18NCs_b_1_Img06.xml).
3. Click *Step 2: View images*
   - Close Figure 1 again.

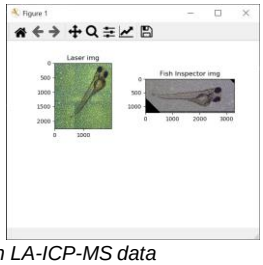

4. Click *Step 3: Load txt table with LA-ICP-MS data*
   - Select the txt file (NC_b_1_tableexport.txt).

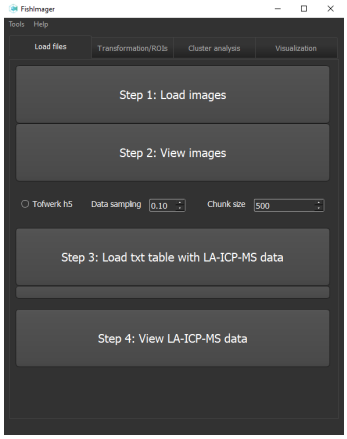

4

a) Distribution of natural elements in zebrafish embryos and reproducibility between ablations of different individuals – first example

5. You can use the drop-down menu to choose the channel which is displayed for Step 4
   - Select *C12_CPS*

6. Click *Step 4: View LA-ICP-MS data*
   - The imported LA-ICP-MS data are displayed in Figure 1 for the channel selected under 4.
   - You can close Figure 1 again and may select another channel in the drop-down menu from 4, repeat 5.

The figure can also be exported to a png, jpeg, tiff,…

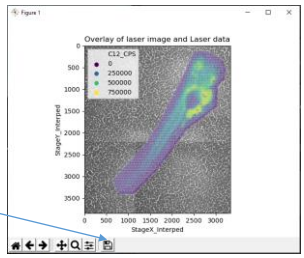

a) Distribution of natural elements in zebrafish embryos and reproducibility between ablations of different individuals – first example

7. Change to the *Transformation and ROIs* tab. Click *Step 1: Choose control points* in order to create an overlay of the laser image and the microscopic image
   - A window appears to inform to close the figure before proceeding with *Step 2*. Click *Okay*.
   - Figure 1 appears showing both images.
   - Choose first one feature on the left image (*Laser img*) and then the corresponding position of this feature with another click on the right image.
   - Perform this for at least 3 control points (here four pints were chosen).
   - The chosen coordinates from the *Laser img* and the corresponding wrapped ones appear in red.
   - **Close Figure 1.**

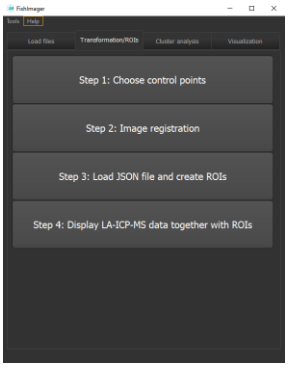

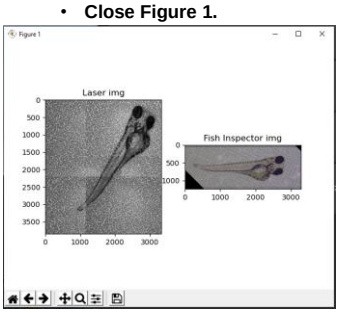

Choose control points

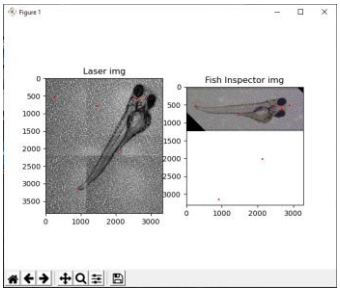

a) Distribution of natural elements in zebrafish embryos and reproducibility between ablations of different individuals – first example

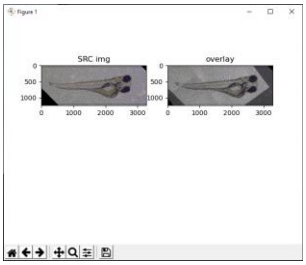

8. Click *Step 2: Image registration* to see the overlay in the appearing window "Figure 1"
   - A window appears to inform to close the figure before proceeding with *Step 3*. Click *Okay*.
   - **Close Figure 1.**
   - A window appears to inform whether the transformation was successful. Click *Okay*.

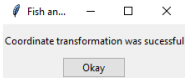

9. The file with the shapes of the biological body compartments from the FishInspector software is loaded with *Step 3: Load JSON file and create ROIs* (Z18NCsb1_cropped__SHAPES.json)
   - The window "Figure 1" opens and displays the outlines of the biological compartment on the transformed laser image ("Laser img wrapped") and the microscopic image ("Fish Inspector img").
   - Close Figure 1.

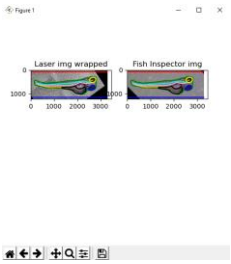

a) Distribution of natural elements in zebrafish embryos and reproducibility between ablations of different individuals – first example

10. Click *Step 4: Display LA-ICP-MS data together with ROIs*
    - The window "Figure 1" opens and displays LA-ICP-MS data on the transformed laser image with the biological compartments.
    - The notochord consists out of two lines in the FishInspector software. Here the area is calculated between the two lines and all coutns belonging to this area are colored white.
    - Close Figure 1.

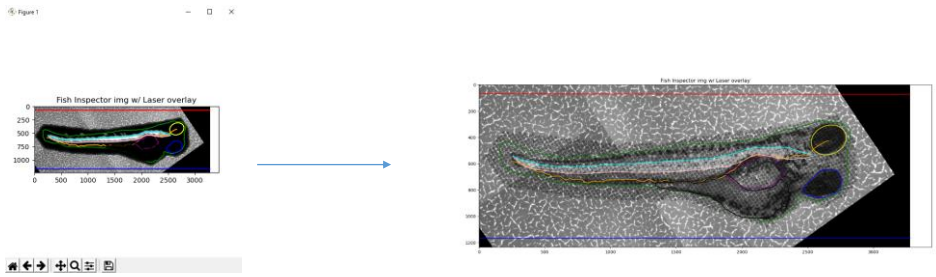

a) Distribution of natural elements in zebrafish embryos and reproducibility between ablations of different individuals – first example

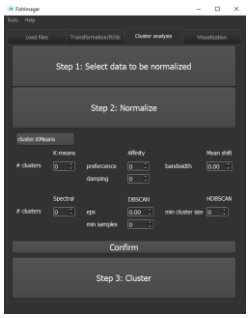

11. Change to the *Cluster analysis* tab. Click *Step 1: Select data to be normalized.*
    - Open the LA-ICP-MS data table (NC_b_1_tableexport.txt).
    - This opens the table with the measured elements and the coordinates.
    - Delete the columns which should **not** be included in the cluster analysis by right click on the respective column head.
    - The remaining columns should be “C12_CPS, StageX_Interped, StageY_Interped“.
    - Close the table app.
12. Click *Step 2: Normalize*.
    - In order to change the selection, go back to 4. Repeat 11. and 12.

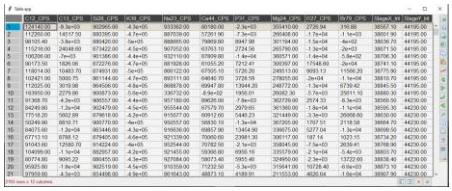

a) Distribution of natural elements in zebrafish embryos and reproducibility between ablations of different individuals – first example

13. The cluster algorithm can be chosen at this point.
    - Choose *cluster.Kmeans* and set the number of clusters *(# cluster)* to 4.

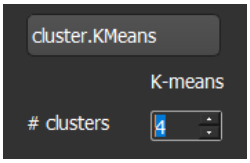

14. Click *Confirm*. In the case of the Kmeans clustering, a graphic with the elbow method to choose the optimal k for k=1-9 appears
    - Instruction number 12 may be repeated if the numbers of cluster should be changed.
    - Close Figure 1.

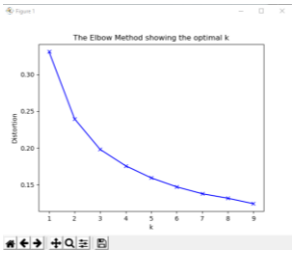

Load files | Transformation and ROIs | Cluster analysis | Visualization

a) Distribution of natural elements in zebrafish embryos and reproducibility between ablations of different individuals – first example

15. Click *Step 3: Cluster*.
    - The clustered LA-ICP-MS data appear in Figure 1.
    - Close Figure 1.

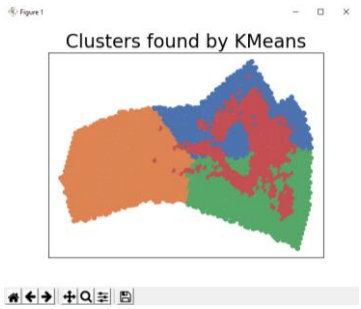

11

Load files | Transformation and ROIs | Cluster analysis | Visualization

a) Distribution of natural elements in zebrafish embryos and reproducibility between ablations of different individuals – first example

16. Change to the *Visualization* tab. Click *Step 1: Visualization*.
    - The Figure 1 (*ROI Cluster Image overlay*) shows the color-coded, clustered LA-ICP-MS data with the ROIs.
    - Close Figure 1.

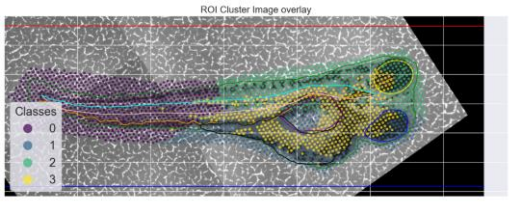

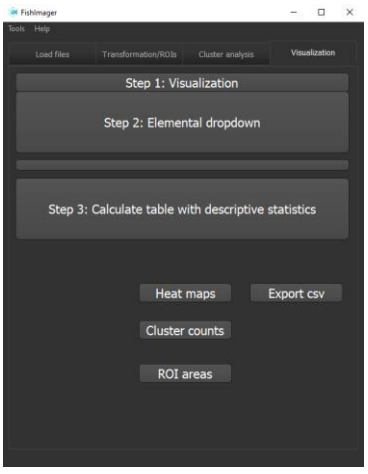

12

a) Distribution of natural elements in zebrafish embryos and reproducibility between ablations of different individuals – first example

17. Click *Step 2: Elemental dropdown*.
    - A warning message advises to choose an elemental channel in the following drop-down menu. Click *OK* to remove the message.

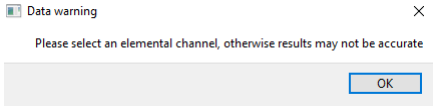

18. Choose an elemental channel in the drop-down menu which had been included for the cluster analysis (C12_CPS) to investigate.

a) Distribution of natural elements in zebrafish embryos and reproducibility between ablations of different individuals – first example

19. Click *Step 3: Calculate table with descriptive statistics*.
    - A table opens with the descriptive statistics of the chosen elemental channel for each cluster.
    - The sum, mean, standard deviation, median, variance, minimum and maximum is displayed for the channel (P31_CPS) for each cluster.
    - Close the *Table app*.

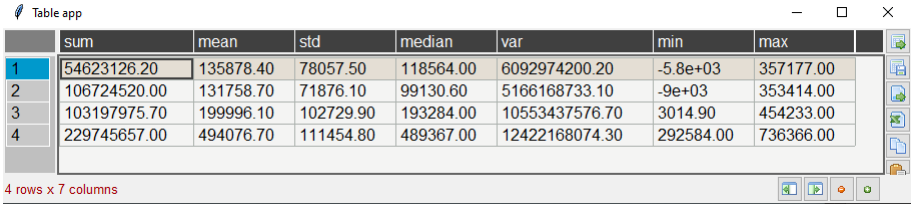

	sum	mean	std	median	var	min	max
1	54623126.20	135878.40	78057.50	118564.00	6092974200.20	-5.8e+03	357177.00
2	106724520.00	131758.70	71876.10	99130.60	5166168733.10	-9e+03	353414.00
3	103197975.70	199996.10	102729.90	193284.00	10553437576.70	3014.90	454233.00
4	229745657.00	494076.70	111454.80	489367.00	12422168074.30	292584.00	736366.00

a) Distribution of natural elements in zebrafish embryos and reproducibility between ablations of different individuals – first example

20. Click *Heatmaps*.
    - Five heatmaps appear relating to the elemental channel selected under 18.
    - In case the margins of the heatmaps need to be adjusted, use the *Configure subplots* button (see arrow).
    - The calculation of the different heatmaps are explained on the following slides.
    - The data for the calculation of the heatmaps can be exported as csv-file (*Export csv*).

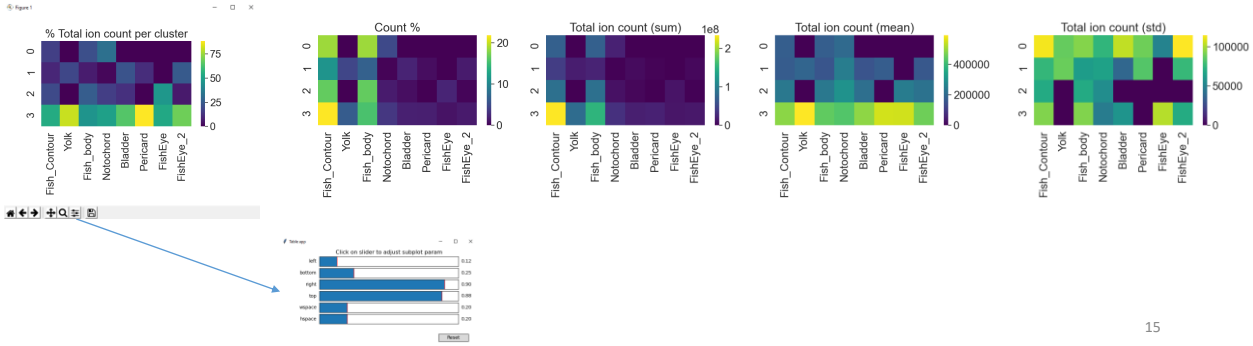

Load files | Transformation and ROIs | Cluster analysis | Visualization

a) Distribution of natural elements in zebrafish embryos and reproducibility between ablations of different individuals – first example

Total ion count (sum) – Figure 3

- This heatmap displays the sum of the elemental channel (selected under 18.) per cluster and body part.
- E.g. the total intensity in the bladder is partly represented by cluster 2 and 3: both have a total intensity of around 0.25e8.
- E.g. the total intensity of the area overlapping of cluster 3 and the yolk is circa 1e8, of cluster 0 and the yolk 0.25e8.

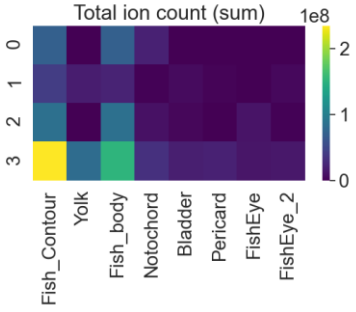

a) Distribution of natural elements in zebrafish embryos and reproducibility between ablations of different individuals – first example

% Total ion count per cluster – Figure 1

- This heatmap displays the sum of the elemental channel (selected under 18.) per cluster normalized to each body part as percentage.
- I.e. the sum of the elemental channel in each cluster per body part sums up to 100%, respectively.
- The heatmap represents the same information as *Total ion count (sum)* but in percentage per each body compartment.
- E.g. the total intensity in the bladder is around 60% represented by cluster 3 and between 15 and 25% by cluster 1 and 2.
- E.g. circa 70% of the total intensity in the yolk is represented by cluster 3, 30% by cluster 0.

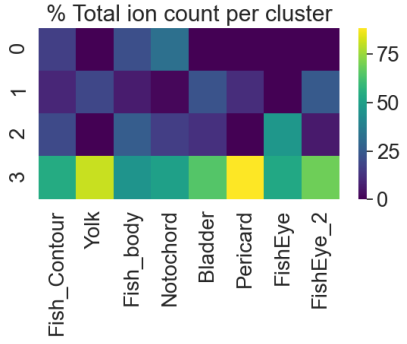

17

a) Distribution of natural elements in zebrafish embryos and reproducibility between ablations of different individuals – first example

Total ion count (mean) – Figure 4

- This heatmap displays the mean of the elemental channel (selected under 18.) per cluster and per body compartment, respectively.
- E.g. the mean intensity of C12_CPS in the area shared by the bladder and cluster 3 is circa 4.5e6, the mean intensity in the area shared by the bladder and cluster 2 is circa 2.5e6, by the bladder and cluster 0 1.5e6.
- E.g. The mean intensity in the ROI yolk represented by cluster 3 is circa 6e6, by cluster 0 1.5e6.
- The corresponding standard deviation (std) is also visualized in a heatmeap (*Total ion count (std)*).

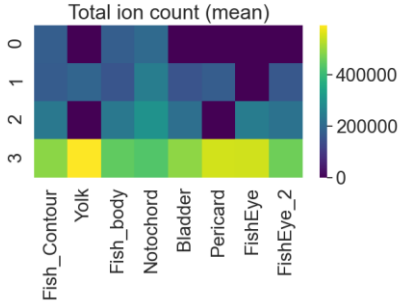

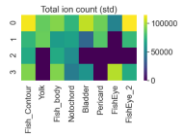

18

a) Distribution of natural elements in zebrafish embryos and reproducibility between ablations of different individuals – first example

Count %

- This heatmap displays the number of counts (pixels) of the LA-ICP-MS data per cluster normalized to the shape of the data matrix as percentage.
- E.g. around 4% of the counts in cluster 2 are represented by the body compartment bladder, 10% of cluster 2 is represented by the body compartment yolk.

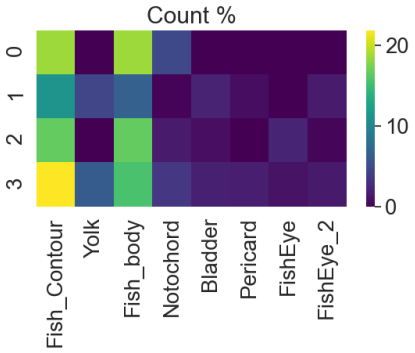

a) Distribution of natural elements in zebrafish embryos and reproducibility between ablations of different individuals – first example

21. Click *Cluster counts*.
    - The table show the total counts in each cluster and the percentage of the total measured counts.
    - Close the Table app.
22. Click *ROI areas*.
    - The table displays the percentage of each body compartment on the whole Fish Contour.

cluster_labels	Total counts	percent total
0	806	36.75331
1	402	18.33105
2	503	22.93662
3	482	21.97902

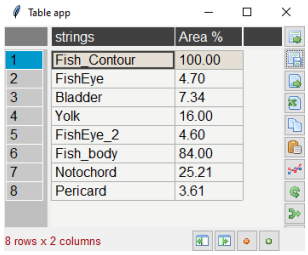

Load files | Transformation and ROIs | Cluster analysis | Visualization

a) Distribution of natural elements in zebrafish embryos and reproducibility between ablations of different individuals – second example

- First choose the laser image (Z18NCs_b_2_Img05_Mapped.png).
- Select cropped Fish inspector image (Z18NCsb2__cropped.png).
- Select the corresponding coord-file for the laser image (Z18NCs_b_Img05.xml).
- NCs_b_2_tableexport.txt
- Z18NCsb2_cropped__SHAPES.json
- Cluster 12C_CPS, X_Stage_Interped, Y_Interped

21

Load files | Transformation and ROIs | Cluster analysis | Visualization

a) Distribution of natural elements in zebrafish embryos and reproducibility between ablations of different individuals – third example

- First choose the laser image (Z18NCs_b_Img04_Mapped.png).
- Select cropped Fish inspector image (Z18NCsb3_cropped.png).
- Select the corresponding coord-file for the laser image (Z18NCs_b_Img04.xml).
- NCs_b_3_tableexport.txt
- Z18NCsb3_cropped__SHAPES.json
- Cluster 12C_CPS, X_Stage_Interped, Y_Interped

22

b) Distribution of xenobiotics in the zebrafish embryo – naled exposure

- First choose the laser image (Z18A12u3A21u2_Img06_Mapped.png).
- Select cropped Fish inspector image (Z18A2_1_cropped.png).
- Select the corresponding coord-file for the laser image (Z18A12u3A21u2_Img06.xml).
- Z18A2_1_table_iolite_output.txt
- Z18A2_1_cropped__SHAPES.json
- Cluster 12C_CPS0, 79Br_CPS0, X_Stage_Interped, Y_Interped

23

b) Distribution of xenobiotics in the zebrafish embryo – 4-iodophenol exposure

- First choose the laser image (Z19D1_4_Img06_Mapped.png).
- Select cropped Fish inspector image (Z19D1_4_cropped.png).
- Select the corresponding coord-file for the laser image (Z19D1_4_Img06.xml).
- Z19D1_4_TableExport.txt
- Z19D1_4_cropped__SHAPES.json
- Cluster 12C_CPS0, 127I_CPS0, X_Stage_Interped, Y_Interped

24

c) Identification of changes over time in the distribution of a xenobiotic in the zebrafish embryo – naled exposure

- First choose the laser image (Z18C11u2C23Img05_Mapped.png).
- Select cropped Fish inspector image (Z18C2_4_cropped.png).
- Select the corresponding coord-file for the laser image (Z18C11u2C23Img05.xml).
- Z18C2_4_iolite_output.txt
- Z18C2_4_cropped__SHAPES.json
- Cluster 12C_CPS0, 127Ir_CPS0, X_Stage_Interped, Y_Interped

25

d) Identification of changes over time in the distribution of a xenobiotic in the zebrafish embryo – 4-iodophenol exposure

- First choose the laser image (Z19B1_2_Img09_Mapped.png).
- Select cropped Fish inspector image (Z19B1_2_cropped.png).
- Select the corresponding coord-file for the laser image (Z19B1_2_Img09.xml).
- Z19B1_2_TableExport.xml
- Z19B1_2_cropped__SHAPES.json
- Cluster 12C_CPS0, 127Ir_CPS0, X_Stage_Interped, Y_Interped

26

d) LA-ICP-tof-MS dataset

- First choose the laser image (Z34D3_3_Img01_Mapped.png).
- Select cropped Fish inspector image (Z34D3_3_cropped.png).
- Select the corresponding coord-file for the laser image (Z34D3_3_Img01.xml).

d) LA-ICP-tof-MS dataset

- Go to the Load files tab.
- Check the Tofwerk h5 button.
- Choose 0.5 for data sampling and 500 for chunk size.
- Click *Step 3.*
- The following message appears, Click *OK.*

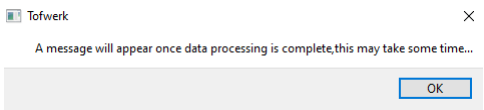

- Select the following file Laser_2020.05.18.13h45m30s_Z34D3_4_50x50_50umsec_50hz_2J.h5
- After a short time, FishI shows that the data processing is complete.

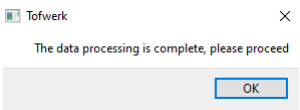

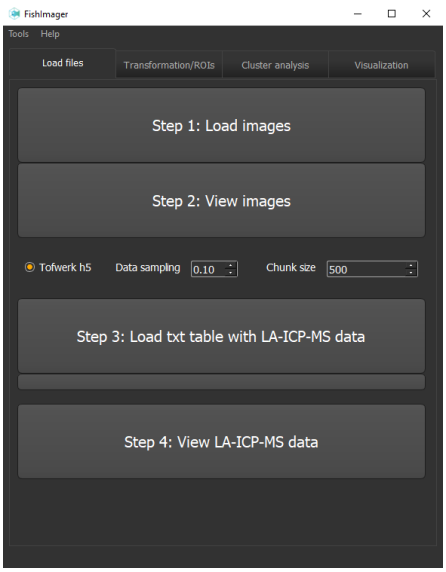

d) LA-ICP-tof-MS dataset

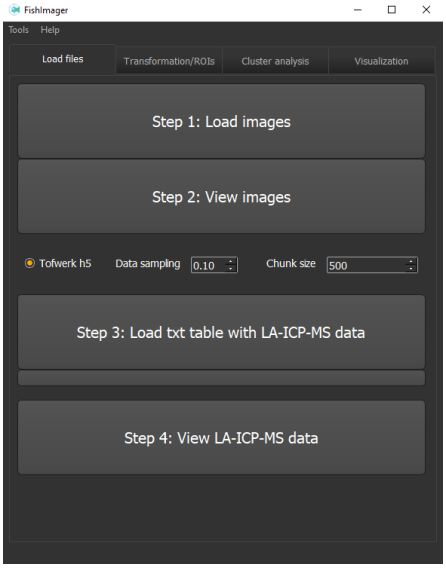

- You can proceed now as with the other examples.
- Corresponding FishInspector file
  - Z34D3_3_cropped__SHAPES.json
- For tof-data visualization, please disregard the plot appearing in *Cluster analysis*, *Step 3: Cluster*

  -> the data which are displayed are not in the correct coordinate system
- For normalization in the *Cluster analysis* tab choose, e.g. 12C, 13C, 14N, 15N, 23Na, 31P, 15N, 32S, 33S, 34S, 35Cl, 36S, 37Cl, 39K, 40Ar, 40Ca, 41K, 42Ca, 43Ca, 44Ca, 46Ca, 48Ca, 37Cl, 127I

Chapter 4 Yolk Sac of Zebrafish Embryos as Backpack for Chemicals?

Halbach, K.; Ulrich, N.; Goss, K.-U.; Seiwert, B.; Wagner, S.; Scholz, S.; Luckenbach, T.; Bauer, C.; Schweiger, N.; Reemtsma, T. *Environ. Sci. Technol.* **2020**, *54* (16), 10159–10169.

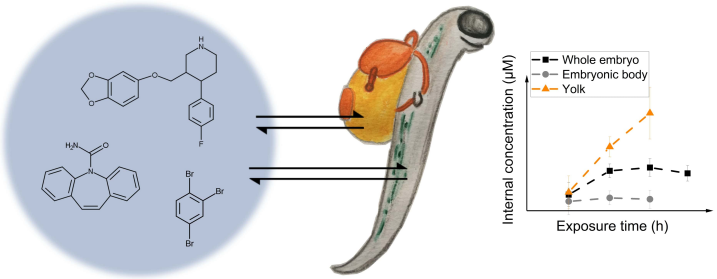

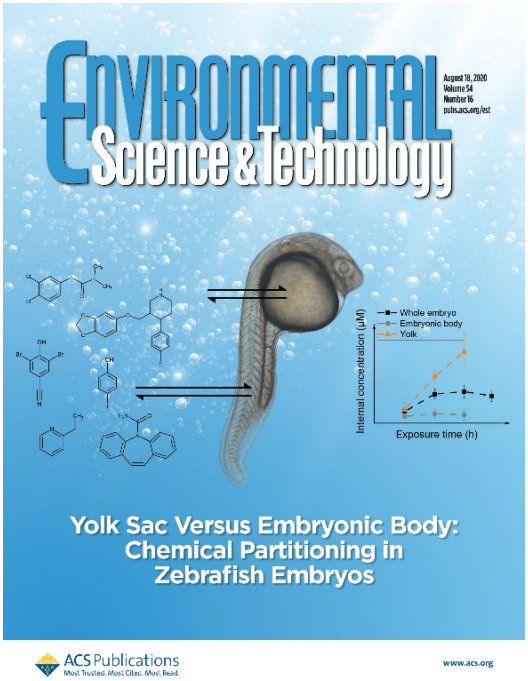

Link to the publication:

https://pubs.acs.org/doi/10.1021/acs.est.0c02068

Author's contribution:

I am the first author of this publication. The study was conceptualized by me, S. Wagner, and K.-U. Goss. I designed the experiments, carried out the exposures, sample preparation, and GC-MS analysis. N. Schweiger carried out fish embryo toxicity tests for defining a dose-response curve. C. Bauer and B. Seiwert carried out the SCF- and LC-MS measurements. N. Ulrich performed the dialysis experiments. I conducted the data analysis for the internal concentrations. K.-U. Goss provided the kinetic model and assisted with the adaptation and interpretation. The discussion and structure of the manuscript were developed together with the co-authors. I wrote the manuscript.

Environmental Science & Technology

pubs.acs.org/est

Article

Yolk Sac of Zebrafish Embryos as Backpack for Chemicals?

Katharina Halbach, Nadin Ulrich, Kai-Uwe Goss, Bettina Seiwert, Stephan Wagner, Stefan Scholz, Till Luckenbach, Coretta Bauer, Nicole Schweiger, and Thorsten Reemtsma*

Cite This: *Environ. Sci. Technol.* 2020, 54, 10159–10169

Read Online

ACCESS | Metrics & More | Article Recommendations | Supporting Information

ABSTRACT: The zebrafish embryo (*Danio rerio*) has developed into one of the most important nonsentient animal models for the hazard assessments of chemicals, but the processes governing its toxicokinetics (TK) are poorly understood. This study compares the uptake of seven test compounds into the embryonic body and the yolk sac of the zebrafish embryo using TK experiments, a dialysis approach, thermodynamic calculations, and kinetic modeling. Experimental data show that between 95% (4-iodophenol) and 67% (carbamazepine) of the total internal amount in 26 h post fertilization (hpf) embryos and between 80 and 49% in 74 hpf embryos were found in the yolk. Thus, internal concentrations determined for the whole embryo overestimate the internal concentration in the embryonic body: for the compounds of this study, up to a factor of 5. Partition coefficients for the embryonic body and a one-compartment model with diffusive exchange were calculated for the neutral test compounds and agreed reasonably with the experimental data. For prevalently ionic test compounds at exposure pH (bromoxynil, paroxetine), however, the extent and the speed of uptake were low and could not be modeled adequately. A better understanding of the TK of ionizable test compounds is essential to allow assessment of the validity of this organismic test system for ionic test compounds.

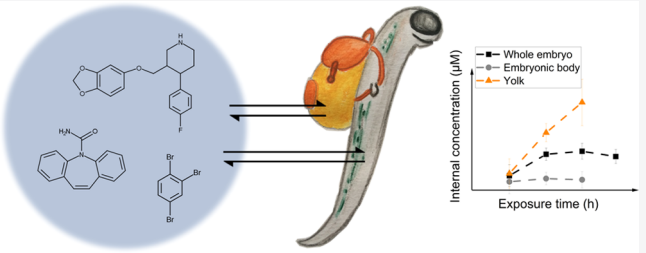

INTRODUCTION

The zebrafish embryo (*Danio rerio*) is an important nonsentient animal model and an alternative to animal testing in the hazard and risk assessments of chemicals.[1] It was initially used to assess acute fish toxicity and is nowadays also increasingly used to study mammalian toxicity because essential biological pathways are preserved in all vertebrates.[2,3] An understanding of the internal concentration and distribution of chemicals in fish embryos is crucial for the interpretation of the effects of those chemicals. Information on the internal chemical concentrations is, for instance, important to discriminate between baseline and specific or reactive modes of toxic action. Furthermore, internal concentrations are important when extrapolating toxicological data across test systems or species. Toxicokinetic (TK) experiments, e.g., time-resolved internal concentrations, can elucidate the processes determining the uptake kinetics. While some studies assumed a steady state and only determined the internal concentration at the end of the exposure,[4] other studies point toward slow uptake kinetics for some compounds. The reason for this, e.g., ionizable/ionic chemicals,[5] metabolism,[5,6] active transport,[7] and the presence of the chorion,[8] has yet to be investigated.

At present, internal chemical concentrations in fish embryos are determined from whole-body homogenates,[6,9] while the distribution of chemicals within the zebrafish embryo and its influence on the TK are rarely considered.[10] However, the yolk sac represents a compartment that is unique to the fish embryo. Differences in the composition of the yolk compared to that of the embryonic body, e.g., its higher phospholipoprotein content, may result in different sorption properties. Moreover, the compositions of the yolk and the embryonic body change during development and thus may also the sorption properties.[11,12] In the early stages of development, the yolk of the zebrafish embryo makes up a large proportion of the mass of the whole embryo, but quantitative data are not available. Thus, a large fraction of a test chemical determined in a whole embryo homogenate may be located in the yolk compartment rather than in the embryonic body.

Astonishingly, it has not been systematically studied how the sorption properties and TK of the yolk differ from those of the embryonic body. It is not clear yet which parameters, e.g., developmental stage and physicochemical properties of the test substances, influence the distribution of a substance between the exposure medium, the yolk, and the embryonic body and how this may change during the rapid development of the embryo.[4,13,14] Furthermore, a model that describes the uptake kinetics and distribution of chemicals in the embryonic body and the yolk would be highly useful to transfer the data of

Received: April 2, 2020
Revised: July 2, 2020
Accepted: July 8, 2020
Published: July 8, 2020

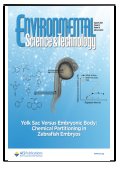

https://dx.doi.org/10.1021/acs.est.0c02068
Environ. Sci. Technol. 2020, 54, 10159–10169

tested chemicals to nontested ones and, thus, to reduce the need for experiments.

Moreover, a distinction between the internal concentration of the embryo and its freely dissolved fraction would be desirable because the latter is expected to be most relevant for biological effects, either in the embryonic body or in the yolk.[14] Recently, a multicompartment model for the zebrafish embryo has been proposed.[15] In the publication, an instantaneous partitioning was assumed. Here, we applied a one-compartment model to explore also the kinetic limitations for the test chemicals, such as membrane permeability and an aqueous boundary layer (ABL).

This study aims to improve the understanding of how chemicals partition between the exposure medium and the compartments, yolk and embryonic body (defined as the whole embryo without the yolk sac), and how the partitioning of the chemicals is related to their physicochemical properties. Experimental data were obtained for a diverse set of test substances ($\log K_{OW}$ range from 1.28 to 4.62; neutral and ionizable) comprising the pharmaceuticals carbamazepine and paroxetine, the pesticides bromoxynil and diuron, and the chemicals 4-iodophenol, 1,2,4-tribromobenzene, and 2-ethylpyridine.

The approaches employed here were (i) quantification of the test compounds over time in whole zebrafish embryos and the embryonic body (TK experiment); (ii) determination of the yolk−water partitioning of the test compounds using zebrafish embryo yolk in a dialysis approach and calculation of partition coefficients; and (iii) modeling of chemical uptake by the zebrafish embryos with a diffusive first-order kinetic model.

MATERIALS AND METHODS

Chemicals. Details on the used chemicals and standards can be found in the Supporting Information (SI).

Culture of Zebrafish, Collection of Eggs, and Culture of Embryos. We used the UFZ-OBI strain (generation F14−15) obtained originally from a local breeder and kept for several generations at the UFZ. Fish were cultured and used according to the German and European animal protection standards and approved by the Government of Saxony, Landesdirektion Leipzig, Germany (Aktenzeichen 75-9185.64).[16]

Exposure (TK) Experiments. Seven chemicals were selected for the TK experiments based on their range of physicochemical properties, their ionic character, and their environmental relevance (Table S1); specific toxic effects are not addressed in this study. The concentrations in the exposure solutions were below the EC_{50} of morphological differences to controls, except for 4-iodophenol that caused depigmentation in the embryos at the applied concentration. For chemicals for which no effect concentrations were available, fish embryo acute toxicity tests were performed according to OECD 236.[17] All chemicals were directly dissolved in ISO-water,[18] except for 1,2,4-tribromobenzene, for which a stock solution was prepared in dimethyl sulfoxide (DMSO), resulting in a final DMSO concentration of 0.05% in the exposure water.

Zebrafish embryos were exposed from 2 h post fertilization (hpf) on for 24, 48, 72, and 96 h (±1 h) to each chemical under static conditions. Exposures to paroxetine lasted up to 120 h. The chorion was not removed prior to the exposure. As the neutral chemicals have a low molecular weight (<330 g/mol; Table S1), an influence of the chorion on the uptake kinetics is not expected.[19] The influence of the chorion on the uptake of the mainly ionic compounds was demonstrated by comparing the internal concentration time courses with manually dechorionated embryos (Figure S8).

For exposures, nine zebrafish embryos at 2 hpf in 90 μL water were transferred together into glass vials containing 18 mL of exposure solution or pure ISO-water or ISO-water with 0.05% DMSO. For each substance, the uptake and distribution in the zebrafish embryo were determined with embryos from one egg batch. Per substance and exposure duration, six replicates were set up; i.e., for four exposure times, 216 embryos were exposed. Vials were closed with a metal lid and placed in an incubator at 26 ± 1 °C and a light/dark cycle of 14:10 h. Vials were horizontally agitated at 75 rpm. At the beginning and the end of the exposures, aliquots of the exposure solutions (data in Table S1) and the blind controls (data in Table S2) were taken to determine the concentration C_{extern} in the exposure solutions and to monitor the stability of the chemical concentration over the exposure time. Control solutions with pure ISO-Water and ISO-water with 0.05% DMSO (control for 1,2,4-tribromobenzene) were sampled as well. The samples were stored at −20 °C.

The pH and oxygen contents were measured at the beginning and the end of the exposures to ensure that the pH change (set to 7.4 at the beginning) was less than 1.5 units and the oxygen saturation above 80% in the exposure solutions.[17] No buffer was used to stabilize the pH in the exposure solutions to avoid effects by additional chemicals in the exposure solution. A pH change was noted in the range of about 0.5 pH units over 96 h of exposure. Chemical concentrations in the blind controls remained constant over the exposure time (Table S2). Experiments were included in the analyses only when no contamination of control media and embryos was found and the mortality of embryos did not exceed 20% in the controls (see Table S10).

Yolk Removal and Sample Preparation for Internal Concentration Analysis. After 24, 48, and 72 h of exposure, the yolk was removed from three embryos per replicate with a glass capillary fabricated with a micropipette puller. Removal of the yolk was achieved by partially sucking the yolk into the capillary and by additional mechanical removal of the yolk sac with the capillary (Figure S1) similar to Fraher et al.[11] In certain cases, fragments of the yolk sac could not be removed completely from the body. However, the subsequent washing step was assumed to wash away the remaining test substance. If the chorion was still present, it was carefully removed with forceps prior to the washing step. Three pooled whole embryos or pooled embryonic bodies were transferred together with 50 μL water/exposure solution into 1.5 mL Eppendorf tubes. The analysis of 4-iodophenol was performed in single embryos/embryonic bodies as the analytical sensitivity was sufficiently high. The water/exposure solution was removed, and the three pooled embryos (except single embryos for 4-iodophenol) were rinsed twice with 1 mL Milli-Q water. Subsequently, the embryos were transferred to FastPrep tubes containing 0.75 mm glass beads, the water was removed, 1 mL Milli-Q water was added for a further rinse, and the access liquid was then removed. The FastPrep tubes were closed, shock-frozen in liquid nitrogen, and stored at −20 °C until extraction.

For the chemicals 4-iodophenol, diuron, carbamazepine, bromoxynil, paroxetine, 2-ethylpyridine and 1,2,4-tribromobenzene the following internal standards were used: 4-

https://dx.doi.org/10.1021/acs.est.0c02068
Environ. Sci. Technol. 2020, 54, 10159−10169

bromophenol, diuron-d_6, carbamazepine-d_{10}, bromoxynil-d_2, paroxetine-d_6 maleate, 3-ethylpyridine and hexachlorobenzene.

Embryos and embryonic bodies were extracted with 200 μL solvent (methanol, acetonitrile, or toluene depending on the chemical) containing the internal standard. The embryos were homogenized in a FastPrep-homogenizer (MP Biomedicals) for 20 s at 6.5 m/s, placed in an ultrasonic bath for 15 min, and then centrifuged for 15 min at 13 000 rpm. The supernatant was transferred to a glass vial and stored at −20 °C until analysis. Extracts were diluted in 50/50 methanol/water (v/v) for UPLC-MS, in acetonitrile for SFC-MS and in toluene for GC-MS measurements to a concentration in the linear calibration range.

4-Iodophenol, diuron, carbamazepine, bromoxynil, and paroxetine were analyzed with ultraperformance liquid chromatography quadrupole-time-of-flight mass spectrometry (UPLC-QToF-MS), 2-ethylpyridine with supercritical fluid chromatography-QToF-MS (SFC-QToF-MS), and 1,2,4-tribromobenzene with gas chromatography-MS (GC-MS). Details on the instrumental parameters are given in the Supporting Information. For 1,2,4-tribromobenzene, a few embryos were additionally extracted with methanol analyzed by UPLC-QTOF-MS to check for biotransformation products, which are presumably more polar than 1,2,4-tribromobenzene and, thus, detectable with UPLC-QTOF-MS.

In the case of carbamazepine, an influence of the solvent type or solvent amount on the extraction of carbamazepine was ruled out (additional experiments with acetonitrile and acetone and with extraction volumes of 2 and 15 mL methanol; Tables S8 and S9). For the determination of the concentration in the exposure solution of 1,2,4-tribromobenzene, liquid−liquid extraction was performed of 950 μL exposure water with 300 μL hexachlorobenzene in toluene (1 μg/mL) in a 1.5 mL glass vial. The vial was horizontally shaken overnight at 150 rpm. The supernatant was then taken and analyzed on the same day.

Yolk/Water Partition Experiments (Dialysis Approach). Yolk/water partition coefficients were determined in dialysis experiments. For the dialysis experiments, 2−3 hpf zebrafish eggs (fertilized and nonfertilized) were washed with tank water and test medium and then transferred to polypropylene tubes. Zebrafish eggs (2−3 hpf) mainly consist of yolk components.[20] After water removal, the eggs were homogenized with an ultra turrax (speed 6.0, 2 × 2 min, T10 basic, IKA) and centrifuged (5 min at 13 000 rpm and 4 °C). The supernatant was taken and used in the consecutive dialysis experiments (for further details, refer to Henneberger et al.[21] and Allendorf et al.[22]). Dialysis experiments were performed with triplicates with different amounts of yolk (0.1−5 mL). For the setup with 5 mL yolk in each cell, 17 mL was used in total (including the determination of the dry weight), which corresponds to ∼50 000 eggs (for further details, see Ulrich et al.[23]). The amount of yolk used in the experiments was adopted for each chemical to ensure a fraction of the chemical bound to the yolk components between 20 and 80%. Three replicates were determined at 48 and 72 h.

Dry Weight and Volume. Dry weights of five pooled dechorionated zebrafish embryos or embryonic bodies were determined according to Hachicho et al.[24] at different developmental stages of embryos from two egg batches. The dry weight of the yolk was calculated by subtracting the dry weight of the embryonic body from the dry weight of the whole embryo. The volumes were estimated from microscopic images by using an automated imaging system and a KNIME workflow (for further details, refer to Halbach et al.[25] and the Supporting Information).

Data Treatment and Analysis. Six replicates with three pooled whole embryos or with three pooled embryonic bodies (except 4-iodophenol, for which 18 single whole embryos or embryonic bodies were analyzed instead of pools of three embryos) per exposure duration were determined. Individual embryo uptake was calculated from the measured concentrations divided by the number of pooled embryos. Internal chemical amounts in the yolk were calculated by subtracting the value for the chemical amount in the embryonic body from the one for the whole embryo. Data analysis was performed in OriginPro 2018.

Since dry weights or volumes can be used as a reference for the developmental stage of the embryo and both parameters differently evolve over the observed age of the embryo (Figure 1), steady-state partition ratios based on the volume (PR_{vol}) and on the dry weight (PR_{dry}) were calculated. PR_{vol} was calculated from the analytically determined internal concentration per volume in the zebrafish embryo and the measured concentration (C_{extern}) in the exposure solution. PR_{dry} was calculated with the internal concentration per dry weight and the measured concentration (C_{extern}) in the exposure solution.

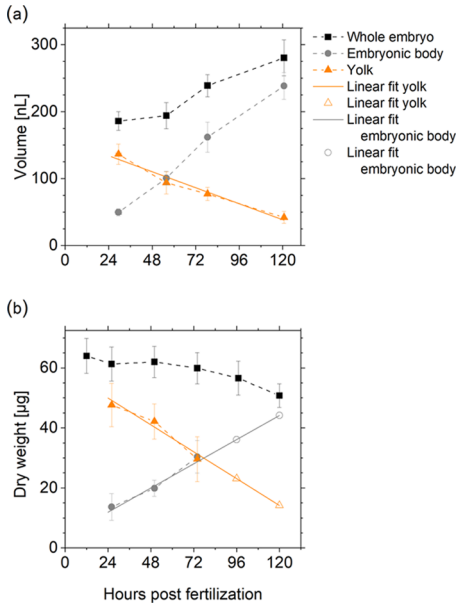

Figure 1. (a) Volumes of whole embryos, embryonic bodies, and yolk (linear regression: $y = 0.996x + 158$; $R^2 = 0.85$) of zebrafish embryos. (b) Dry weights of whole embryos, embryonic bodies (linear regression: $y = 0.336 + 3.83$; $R^2 = 0.92$), and yolk (linear regression: $y = -0.373 + 58.9$; $R^2 = 0.94$) of zebrafish embryos during 120 h post fertilization; data from two independent experiments with six whole embryos and six embryonic bodies were analyzed at each developmental stage.

Calculation of Equilibrium Partition Coefficient for the Embryonic Body. Equilibrium partition coefficients for the embryonic body were calculated using values in the LSER database for the neutral compounds for two different zebrafish life stages: (a) the whole embryo at 96 hpf and (b) adult female zebrafish (see the Supporting Information for details).

Toxicokinetic Modeling of the Uptake of the Test Compounds into Zebrafish Embryos. To model a first-order chemical uptake into the zebrafish embryo, we started by

https://dx.doi.org/10.1021/acs.est.0c02068
Environ. Sci. Technol. 2020, 54, 10159−10169

Table 1. Steady-State Partition Ratios (PR_{vol}) in the Whole Embryo, Embryonic Body and Yolk (n = 6, Respectively) for the Exposure Times of 24, 48, and 72 h with Standard Deviation (sd)[b]

substance	exposure time (h)[a]	PR_{vol} in the whole embryo [$L_{water}/L_{whole\ embryo}$] (sd)	PR_{vol} in the embryonic body [$L_{water}/L_{embryonic\ body}$] (sd)	PR_{vol} in the yolk [L_{water}/L_{yolk}] (sd)
2-ethylpyridine	24	0.52 (0.18)	0.19 (0.05)	0.64 (0.21)
	48	0.66 (0.26)	0.19 (0.05)	1.1 (0.5)
	72	0.51 (0.14)	0.28 (0.07)	0.92 (0.35)
carbamazepine	24	2.7 (0.9)	3.6 (1.5)	2.4 (1.1)
	48	2.9 (0.6)	2.2 (0.3)	3.4 (0.8)
	72	2.3 (0.5)	1.9 (0.2)	3.0 (1.0)
diuron	24	28 (9.0)	14 (8.4)	32 (10)
	48	26 (6.8)	9.5 (3.8)	40 (11)
	72	22 (3.2)	11 (3.8)	43 (8.0)
4-iodophenol	24	43 (23)	8.7 (8.6)	55 (29)
	48	40 (12)	16 (5.9)	63 (18)
	72	41 (12)	14 (4.5)	88 (27)
1,2,4-tribromobenzene	24	1300 (980)	730 (1100)	1500 (1300)
	48	3200 (580)	1000 (560)	5100 (860)
	72	3500 (730)	900 (730)	7800 (2100)

[a]Start of exposure at 2 hpf. [b]Data from one egg batch per substance with six replicates (with three pooled whole embryos or three embryonic bodies) per exposure duration are presented. (Mainly) ionic compounds are not displayed as they did not reach a steady state within the exposure time (for data, see Table S7).

considering diffusion through a 400 μm aqueous boundary layer (ABL) and a single cell layer with two membranes.[26] The interior of the embryo was assumed to be well mixed. The total permeability was calculated after Bittermann and Goss[27] with the UFZ-LSER-database and was then used in the compartment model for diffusive exchange.[28,29] The model was adapted for the two compartments "water" and "embryo" (see the excel file in the Supporting Information). The model included the assumption that the water compartment is large enough so that the uptake by the zebrafish embryo would not change the exposure concentration in the water.

The embryo was modeled with the body parameters of an embryo at 96 hpf: a spherical compartment with a surface area of 0.019 cm^2 (calculated from a volume of 253 nL) and a dry weight of 57 μg. The calculated partition coefficients of the substances $\log K_{body/water}$ were used (Table 2, column 5) to calculate the uptake kinetics. To also explore the possibility of a not-well-mixed embryo in additional model calculations, we assumed that membrane-bound yolk granules with a diameter of 50 μm can be distributed along the radius (0.035 cm at the beginning of the development).[20] This corresponds to a maximum of 6 yolk granules, and thus 12 cell layers as the maximal diffusive transport resistance are conceivable (adapted in the model by dividing the calculated permeability by 12). A two-compartment model (yolk and embryonic body) showed only minor changes in the predicted uptake kinetics (see the Supporting Information on how to adapt the excel sheet for two compartments).

For the mainly ionic substances bromoxynil and paroxetine, pH = 7.4 for the exposure solution was used to calculate the ionic speciation required for estimating the total permeability. The following calculated partition coefficients $\log K_{body/water}$ were used: 2.6 $L_{water}/kg_{dry\ weight}$ (bromoxynil) and 1.8 $L_{water}/kg_{dry\ weight}$ (paroxetine). The parameters used, e.g., calculated permeabilities, can be found in the excel sheet of the model in the Supporting Information.

RESULTS AND DISCUSSION

Dry Weight and Volume of the Zebrafish Embryo and the Two Compartments, Embryonic Body and Yolk. Values for volumes and dry weights of the yolk and body compartments of zebrafish embryos at different developmental stages were determined (Figure 1). Dry weights of the whole embryo continuously decreased from 64 μg at 12 hpf to 50 μg at 120 hpf (Figure 1a), whereas the volume increased from 170 nL at 24 hpf to 280 nL at 120 hpf (Figure 1b). While the whole embryo dry weights determined here are in the same range as previously reported, the volumes of whole embryos derived by image analysis were 30−40% lower than previous estimates.[5,24,30] In this study, an automated positioning system was used to measure dimensions in the lateral and dorsoventral positions of dechorionated embryos, resulting in potentially more accurate volume estimations. Furthermore, strain differences cannot be completely excluded.

Until 120 hpf, the zebrafish embryo is not actively feeding but consumes its yolk for growth and differentiation. Correspondingly, the yolk decreases in weight and volume, while the embryonic body increases in size with development (Figure 1a,b). At an early developmental stage (26 hpf), the yolk comprises approx. 80% (48 μg/individual) of the dry weight of the whole embryo, while at 74 hpf, the yolk makes up about 50% (30 μg/individual). Assuming a linear decrease of the yolk's mass during embryonic development, the yolk's mass makes up approx. 40% of the whole embryo at the end of the exposure period (96 hpf) (Figure 1b) and is completely consumed at about 160 hpf. Previous observations agree with this pace of yolk consumption in the fish embryo.[31]

Steady-State Partition Ratios for the Whole Embryo. The seven test chemicals comprise neutral and ionizable compounds (five are (mainly) nonionic, one cationic, and one anionic at the exposure pH) with the molecular weights ranging from 107 to 329 g/mol and the octanol−water coefficients ($\log K_{OW}$) ranging from 1.28 to 4.62 ($\log D$ 0.83−4.28 at pH 7.4) (Table S1).

The amounts of the test chemicals in dechorionated whole embryos and embryos without yolk were determined at various

https://dx.doi.org/10.1021/acs.est.0c02068
Environ. Sci. Technol. 2020, 54, 10159−10169

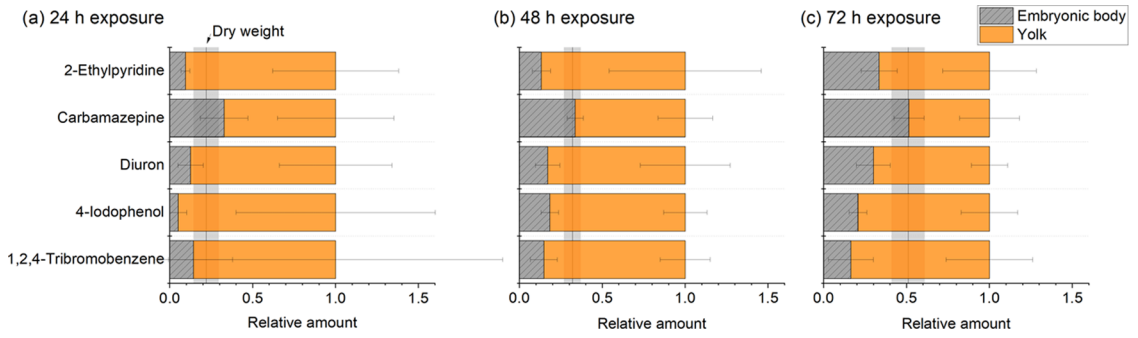

Figure 2. Relative proportion of the total internal amount of the five (mainly) neutral test compounds between the embryonic body and yolk after (a) 24, (b) 48, and (c) 72 h of exposure (start of exposure at 2 hpf; each value error represents the mean with the standard deviation, $n = 6$). For the total quantity, see Figure S5. The vertical line represents the relative proportion of the dry weight of the embryonic body at the respective age of the embryo. Data from one egg batch per substance with six replicates ($n = 6$) with three pooled whole embryos or three embryonic bodies per exposure time are presented.

sampling time points until 96 h of exposure. In addition, the concentrations of test compounds in the exposure solutions were determined. Based on these data and the volume estimates (Figure 1b), PR_{vol} was calculated (Table 1). For the five neutral compounds, a steady state, i.e., a stable internal concentration within the standard deviation margins, was reached within 72 h of exposure (Figure S5 and Table S6). At 96 h of exposure, a decrease of the internal concentration is observed for diuron and 4-iodophenol (likely also 2-ethylpyridine), presumably due to increased biotransformation.[5,32] The PR_{vol} for the whole embryo ranged from 0.5 for 2-ethylpyridine to 3500 for 1,2,4-tribromobenzene. For the five substances, the order of the PR_{vol} generally followed their log K_{OW} values (Tables 1 and S1).

PR_{vol} for the polar compounds 2-ethylpyridine and carbamazepine have not been reported before, but the values found here are in the range of values reported for other chemicals with a similar log K_{OW}.[5,33] PR_{vol} ranging around 3500 were previously also observed for compounds with a similar log K_{OW} as 1,2,4-tribromobenzene.[6,34] The presented PR_{vol} for carbamazepine and 1,2,4-tribromobenzene are within a factor of 2 of bioconcentration factors of the adult fish per wet weight.[35,36]

Distribution of Chemicals between Exposure Medium, the Embryonic Body, and the Yolk Sac. Generally, the PR_{vol} values were lower for the embryonic body than for the yolk for all five neutral compounds (Table 1 and Figure S2). Thus, the usual determination of partition coefficients from whole-body homogenates, comprising the embryo's body and its yolk, overestimates the internal concentration of the embryonic body.

Strongest differences were found for 1,2,4-tribromobenzene, the least polar test compound, for which the PR_{vol} for the yolk was about 9 times higher than for the body after 72 h of exposure (Figure S2). For carbamazepine, the difference was weakest, with a 2-times higher PR_{vol} for the yolk compared to that for the body after 72 h of exposure. The other three compounds, 2-ethylpyridine, 4-iodophenol, and diuron, showed PR_{vol} differences between these two extremes (Figure S2). These differences indicate that partitioning of neutral compounds from the exposure media into the yolk sac is stronger than into the embryonic body; this may be explained by the comparatively high phospholipoprotein content of the yolk.[11,37,38]

The importance of the yolk for compound uptake into the whole body (embryonic body and yolk) becomes even more obvious if one also considers its higher contribution to the total mass in the early stages of development (Figure 1). The total quantities of the chemicals in the whole embryo and the two compartments are displayed in Figure S5, and the relative proportion of the total quantity is shown in Figure 2. For example, for 4-iodophenol after 24 h of exposure, more than 90% of the total amount found in the whole body is located in the yolk, rather than in the embryonic body (Figure 2a). With ongoing embryo development and decreasing mass percentage of the yolk, this imbalance becomes less pronounced. However, even after 74 h of exposure (76 hpf), 85% of 1,2,4-tribromobenzene and 80% of 4-iodophenol are in the yolk (Figure 2c), while only 15−20% is located in the embryonic body. For carbamazepine still, only 50% is in the body upon 74 h of exposure. The relative amount of chemical in the embryonic body is expected to further increase in the later developmental stages (>74 hpf) until it reaches 100% after full consumption of the yolk at approximately 160 hpf.

If internal amounts in the embryonic body and the yolk are normalized to the respective dry weight rather than to the volumes, the differences between the embryonic body and yolk are less pronounced, as the volume changes more drastically than the dry weight (Table S3 and Figure S3).

The sorption of a test chemical to the body and the yolk of fish embryos was determined before only in a study with the nonionic compound estradiol.[13] Upon exposure of the embryos to radiolabeled estradiol, this compound was quantified in the yolk and the embryonic body separately. Comparable to the results for the compounds examined here, the proportion of estradiol found in the embryonic body was lower than in the yolk after 1 h of exposure (36%) but increased to 63% at 24 h of exposure. The authors attributed this to the lipid-rich composition of the yolk and its decrease in mass over time, as compared to that of the embryonic body. The data for the five neutral chemicals in this study support and extend this previous finding. Therefore, the developmental stage, reflected by the changes in dry weight and volume of the two-body compartments, and the sorption properties of the different body constituents are important factors controlling the distribution of the absolute amounts of a chemical in zebrafish embryos. This includes the freely dissolved concentration. While it has been previously shown that the chorion and the perivitelline space have to be removed from

https://dx.doi.org/10.1021/acs.est.0c02068
Environ. Sci. Technol. 2020, 54, 10159−10169

Table 2. Measured Partition Coefficients for the Yolk and Embryonic Body in the TK Experiments ($\log K_{yolk/water}$, $\log K_{embryonic\ body/water}$; $n = 6$), Measured Equilibrium Partition Coefficients ($\log K_{yolk/water}$) from the Dialysis Experiment ($n = 3$), Calculated Equilibrium Partition Coefficients of the Zebrafish Body and the Water ($\log K_{body/water}$) from the LSER Database with the Composition of the Zebrafish Embryo at 96 hpf and that of the Female Adult Zebrafish[c]

	$\log(K_{yolk/water}/[L_{water}/kg_{dry\ weight}])$ (sd)[a]		$\log(K_{embryonic\ body/water}/[L_{water}/kg_{dry\ weight}])$ (sd)[a]		
	TK experiment		TK experiment		
	24 h exposure[a]		24 h exposure[a]	$\log(K_{body/water}/[L_{water}/kg_{dry\ weight}])$	$\log(K_{body/water}/[L_{water}/kg_{dry\ weight}])$
	48 h exposure[a]	$\log(K_{yolk/water}/[L_{water}/kg_{dry\ weight}])$ (sd)	48 h exposure[a]	calculated	calculated
substance	72 h exposure[a]	dialysis approach	72 h exposure[a]	96 hpf zebrafish embryo	adult female zebrafish
2-ethylpyridine	0.24 (0.16)	1.14 (0.23)	0.20 (0.15)	0.09	0.25
	0.44 (0.19)		−0.05 (0.12)		
	0.42 (0.20)		0.11 (0.14)		
carbamazepine	0.82 (0.21)	1.83 (0.04)	1.05 (0.21)	0.90	1.07
	0.95 (0.11)		0.99 (0.07)		
	0.94 (0.18)		0.95 (0.09)		
diuron	1.95 (0.15)	1.79 (0.02)	1.65 (0.28)	1.42	1.67
	2.01 (0.13)		1.65 (0.18)		
	2.09 (0.13)		1.71 (0.17)		
4-iodophenol	2.18 (0.24)	2.51 (0.16)	1.45 (0.44)	1.33	1.69
	2.20 (0.13)		1.88 (0.17)		
	2.40 (0.17)		1.81 (0.16)		
1,2,4-tribromobenzene	3.61 (0.40)[b]	2.85 (0.15)	3.37 (0.65)[b]	3.09	3.15
	4.12 (0.09)		3.68 (0.24)		
	4.35 (0.16)		3.63 (0.36)		

[a]Start of exposure at 2 hpf. [b]No steady state. [c](Mainly) ionic compounds are not displayed as they did not reach a steady state within the exposure time (for data, see Table S7). sd, standard deviation.

https://dx.doi.org/10.1021/acs.est.0c02068
Environ. Sci. Technol. 2020, 54, 10159−10169

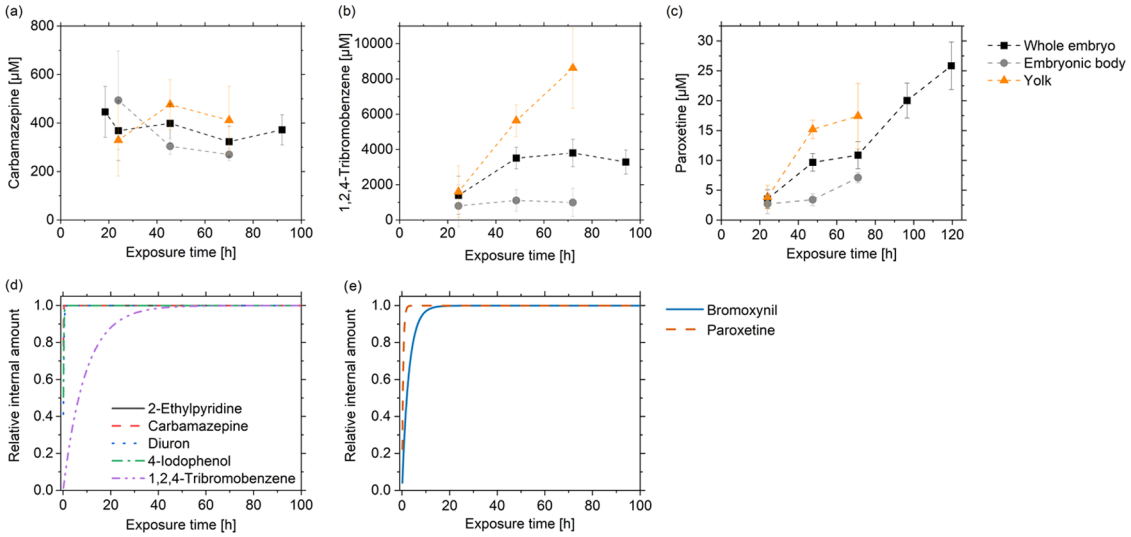

Figure 3. Internal concentrations for the whole embryo, embryonic body and yolk of zebrafish embryos exposed to (a) carbamazepine, (b) 1,2,4-tribromobenzene, and (c) paroxetine (mean with standard deviation, $n = 6$). The start of exposure was at 2 hpf. Data from one egg batch per substance with six replicates with three pooled whole embryos or three embryonic bodies per exposure time are presented. Concentrations in the yolk were calculated from the measured values in the whole embryo and embryonic body (see the text for details). Modeled relative internal amount to the equilibrium concentration in the embryonic body versus time of exposure assuming first-order uptake kinetics (d) for the (mainly) neutral test compounds and (e) for the (mainly) ionic chemicals bromoxynil and paroxetine.

the embryo to avoid an overestimation of the internal concentration in the early stages of development,[39] this study outlines that the same is true for the yolk.

Internal effect concentrations were calculated with respect to lipid concentrations and to estimate whether compounds could be classified as baseline toxic compounds by comparison to the reference value of 226 mmol/kg lipid[40] (Tables S11 and S12). In contrast to an approach based on toxic ratios (calculated baseline toxicity LC50/observed LC50), all compounds were classified as baseline toxic. However, whether the whole embryo or the embryonic body was used as reference had no impact on the classification. Internal concentrations of 1,2,4-tribromobenzene were exceeding 226 mmol/kg lipid largely without causing mortality. This may represent an extrapolation error, given that internal concentrations were measured below the LC50 to avoid the confounding effects of toxicity on internal concentrations and were linearly extrapolated to the LC50.

Partition Experiment with Yolk/Water (Dialysis Approach) and Prediction of the Equilibrium Concentration in the Embryonic Body. Since the distribution between the exposure medium and yolk and the exposure medium and the embryonic body was shown to differ for the investigated nonionic chemicals, a comparison with a dialysis experiment and a modeling approach to predict the equilibrium concentration of test chemicals in yolk and embryonic body was expected to be useful.

Therefore, yolk harvested from nonexposed zebrafish embryos at around 2 hpf was employed in partitioning experiments (dialysis approach) to determine the equilibrium partition coefficients ($\log K_{\text{yolk/water}}$). These values were in good agreement with the partition coefficients determined in the TK experiments for two of the compounds, 4-iodophenol and diuron, with 0.33 and 0.16 log unit deviations (Table 2). For two compounds, carbamazepine and 2-ethylpyridine, the data from the dialysis approach were about one log unit higher than the TK results, while for the fifth compound, 1,2,4-tribromobenzene, the dialysis approach results were 0.8 log units lower (Table 2).

This limited agreement of both approaches may result from experimental differences: yolk from embryos after 2 hpf was used for the dialysis approach, while the first TK data were obtained after 26 hpf (Table 2). At this age, yolk consumption and metabolic transformation of lipids had started.[11] Moreover, the yolk in the dialysis approach was observed to age and decompose over the experimental time, which could affect the sorption properties. Minor changes of the sorption properties were reported for nitrogen- containing compounds during the decomposition of the yolk in the dialysis approach.[23] Furthermore, the internal concentrations in zebrafish embryos may not follow a simple partitioning between the exposure solution and the organism but are affected by metabolic biotransformation and, possibly, active transport.[5,32,41,42] Accordingly, several biotransformation products were detected in these experiments: two metabolites (0.10 ± 0.015 pmol/embryo acridine and 0.14 ± 0.033 pmol/embryo 3-OH-carbamazepine) were detected for carbamazepine in the extracts of whole embryos, and for 2-ethylpyridine as well, after 96 h of exposure (Table S6).

Additionally, equilibrium concentrations for the embryonic body were predicted for the five (mainly) nonionic compounds, with the composition of the embryo and with the composition of an adult fish body. For both predictions, similar sorption properties of yolk and muscle proteins were assumed.[4,5,29] The equilibrium concentrations predicted for the embryonic body ($\log K_{\text{body/water}}$) with the estimated composition of a female adult zebrafish are in good agreement with the TK data after 72 h of exposure, with a deviation between 0.1 and 0.5 log units (Table 2). The agreement between predicted concentrations and the TK data was slightly weaker for diuron and 4-iodophenol when the composition of a zebrafish larvae at 96 hpf from literature was used for the calculation. Recently, a polyparameter linear free-energy relationship was developed with the dialysis approach; thus,

https://dx.doi.org/10.1021/acs.est.0c02068
Environ. Sci. Technol. 2020, 54, 10159−10169

the prediction of the sorption properties of the zebrafish embryo should become more accurate in the future.[23]

Prediction of the Uptake Kinetics. Experimental data for 4-iodophenol, diuron, carbamazepine, and 2-ethylpyridine showed a steady-state situation in the embryo within 24 h of exposure and for 1,2,4-tribromobenzene between 48 and 72 h of exposure (Figures 3 and S5). The uptake of the chemicals into the two compartments, the embryonic body and the yolk, followed similar kinetics as into the whole embryo. It appears that the biotransformation of 2-ethylpyridine, diuron, or 4-iodophenol did not lower the steady-state concentration substantially in the first 72 h of exposure, while this became visible later on (see Figure S5).

Uptake kinetics into the embryo was modeled assuming first-order kinetics. Equilibrium for the neutral compounds was predicted to be reached within 24 h of exposure for 4-iodophenol, diuron, carbamazepine, and 2-ethylpyridine and within 60 h of exposure for 1,2,4-tribromobenzene (Figure 3d). This is in agreement with the measured uptake curves for these compounds (Figure 3a−c and S5). According to the model, the ABL is the dominant barrier for the test chemicals rather than the intrinsic membrane permeability. This would also hold if one assumes that the embryo's interior was not well mixed and that only diffusion would have transported the chemicals through the approximately 12 cell layers from the outside to the center of the embryo. Generally, the establishment of the steady state takes longer for neutral compounds with a higher partition coefficient, e.g., 1,2,4-tribromobenzene, because a larger amount of chemical needs to diffuse into the body to reach the equilibrium concentration.

The model predicts that for compounds even more hydrophobic than 1,2,4-tribromobenzene, e.g., permethrin and PCB 126, the equilibration time would exceed the maximum exposure time of 120 h in the zebrafish embryo test (see Figure S7). This is in agreement with experimental data.[43,44] Therefore, we suggest to include kinetic limitations, such as the membrane permeability and diffusion, in PBPK models.[15]

As the investigated compounds can permeate membranes, there is the potential of the embryonic body to absorb chemicals directly from the yolk. The TK experiments did not provide evidence along which way the test compounds are transported into the yolk and body to establish the respective steady states. In the case of an established steady state, the same number of molecules diffusing from the yolk into the embryonic body are expected to also diffuse back to the exposure medium. During the development of the zebrafish embryo, the sorption capacity decreases for the yolk and increases in the embryonic body (Figure 2). The diffusion should also follow this gradient to re-establish the steady state. Our modeling suggests that this re-establishment might be rather slow for hydrophobic substances (e.g., 1,2,4-tribromobenzene) and an internal concentration in the yolk higher than the steady state might be shortly possible (Figure 3b).

Uptake and Distribution of the (Mainly) Ionic Compounds Bromoxynil and Paroxetine. During the 96 h of exposure, no steady state was reached for the two ionizable test substances, bromoxynil and paroxetine, for the latter not even within 120 h of exposure (Figures 3c and S6). Bromoxynil was taken up in similar concentrations into the yolk and embryonic body, and paroxetine showed higher concentrations in the yolk. The observed uptake of paroxetine (Table S7) is by a factor of 1.6 higher than previously reported.[45]

A slow uptake and long equilibration times of 72 h and above were previously reported for other ionic compounds into whole zebrafish embryos, and it was assumed that this was due to the hindered diffusion of the ionic species,[5] developmental stage,[46] or the presence of the chorion.[8]

In contrast to these experimental observations, the diffusive uptake model used here predicted a steady state for bromoxynil and paroxetine within 24 h of exposure (Figure 3e). For ionic compounds, the intrinsic membrane permeability is lower because only the neutral fraction permeates the membrane.[47] However, also for the two ionic compounds, the ABL is the predicted main barrier, and the diffusion across the ABL is not dependent on the ionic state.[48] The calculated total permeability only deviates by a factor of 2 among the seven compounds because the aqueous diffusion coefficients are very similar.[49] Thus, the neutral fraction of 0.6 and 0.02% for paroxetine and bromoxynil, respectively, is sufficient so that the intrinsic membrane permeability is still faster than the diffusion across the ABL. In the following, we explore the reasons for the deviation of the predicted and measured uptake kinetics.

Our model results for the uptake kinetics were dominated by the ABL resistance and were therefore not very sensitive to errors in the estimated intrinsic membrane permeabilities (see the SI for further discussion). To confirm the comparability of the modeled membrane permeability with the zebrafish embryo membrane, repeated samplings within the first hours of exposure would be useful in the future. By this, a more precise comparison of the modeled data and the TK data can be achieved as the TK data start with a 24 h exposure and the model predicted equilibrium within less than 24 h for most test compounds.

Based on further experiments with dechorionated embryos, it can also be ruled out that the net negative charge of the chorion has affected the uptake kinetics for the nonhatched embryos, either by repelling the negatively charged bromoxynil, as suggested for perfluorinated alkyl acids, or by a preferred accumulation of positively charged paroxetine at the chorion (Figure S8).[8,50] Furthermore, an ion-trapping effect was rejected for either compound by additional calculations (see the Supporting Information). The partition shown by the dialysis approach, the calculated partition coefficient body/water, and the TK experiment were compared: the uptake of bromoxynil in the TK experiment is lower than predicted, while for paroxetine it is similar or higher (Table S7). Data on active transport of the two compounds by cellular transporter proteins are not yet reported but cannot be ruled out.

Moreover, the thickness and the net charge of the mucus hydrogel at the epidermis could reduce the uptake kinetics and should be investigated in the future more closely.[51,52] Another factor to consider might be the growth dilution by increase in the body size that can be important for ionic compounds.[15] More research is needed to understand and correctly predict the uptake kinetics of ionic compounds into zebrafish embryos.

Implications for TK Studies of Chemicals in Zebrafish Embryos. The combination of TK experiments and a dialysis approach with thermodynamic calculations and kinetic modeling provided insight into the uptake of test compounds, separately, into the body and the yolk of zebrafish embryos and its dependence on the physicochemical properties of the test compounds. The outcome has some implications of practical relevance for future TK and effect studies.

https://dx.doi.org/10.1021/acs.est.0c02068
Environ. Sci. Technol. 2020, 54, 10159−10169

The (mainly) nonionic compounds ($\log K_{OW}$ of 1.3−4.6) sorbed stronger to the yolk than to the embryonic body, and this difference in sorption property increased with increasing hydrophobicity of the test compounds. Consequently, the total internal concentration, which is usually determined in TK studies, increasingly overestimates the internal concentration in the embryonic body up to a factor of 5 at 72 h of exposure. The same trend may be seen for the freely dissolved concentration in the embryo: with increasing affinity of a test compound to constituents such as those in the yolk, it is also expected to be proportionally lower than the total internal concentration. Moreover, imaging data have recently shown that even within the embryonic body of the zebrafish, reactive toxicants may not be evenly distributed.[10,25,39]

The first-order one-compartment model with diffusive exchange adequately describes the uptake kinetics of nonionic compounds. It shows that in the case of very hydrophobic compounds ($\log K_{OW} > 4.6$) the uptake can be too slow to reach the equilibrium between the external and the internal concentrations in the time frame of the fish embryo toxicity test of 96 h. Modeling also shows that for compounds having a higher partition coefficient to the yolk than to the embryonic body and having uptake kinetics slower than the dry weight loss of the yolk, as for 1,2,4-tribromobenzene, increased exposure of the embryonic body by yolk consumption might occur.

In agreement with earlier studies, the uptake of (mainly) ionic compounds such as bromoxynil and paroxetine turned out to be slow, so that no equilibrium was reached during the test duration. This may limit the validity of the test results for ionizable compounds. The uptake was also much slower than predicted by the presented uptake model. Equally challenging is to better understand the effect of biotransformation in the zebrafish embryo. Metabolic competence is an important advantage of an organism employed in toxicity testing because certain test compounds may require metabolic activation before exerting their toxic potential. Particularly for compounds taken up slowly and at longer exposure times, biotransformation or active transport can keep the internal concentration below the expected equilibrium.

The partitioning of neutral chemicals between the exposure medium and yolk and embryonic body and hence the internal concentrations over the time of exposure can be explained by the physicochemical properties and predicted by models; however, the behavior of ionizable compounds is still not well understood.

■ ASSOCIATED CONTENT

Supporting Information

The Supporting Information is available free of charge at https://pubs.acs.org/doi/10.1021/acs.est.0c02068.

Details of analytical methods and of exposure experiments, properties of the test compounds, and additional experimental and modeling results and information on transformation products (PDF)

Diffusion through four consecutive compartments (XLSX)

■ AUTHOR INFORMATION

Corresponding Author

Thorsten Reemtsma − *Department of Analytical Chemistry, Helmholtz Centre for Environmental Research—UFZ, 04318 Leipzig, Germany; Institute of Analytical Chemistry, University of Leipzig, 04103 Leipzig, Germany;* orcid.org/0000-0003-1606-0764; Phone: +49 341 235 1261; Email: thorsten.reemtsma@ufz.de

Authors

Katharina Halbach − *Department of Analytical Chemistry, Helmholtz Centre for Environmental Research—UFZ, 04318 Leipzig, Germany*

Nadin Ulrich − *Department of Environmental Analytical Chemistry, Helmholtz Centre for Environmental Research—UFZ, 04318 Leipzig, Germany*

Kai-Uwe Goss − *Department of Environmental Analytical Chemistry, Helmholtz Centre for Environmental Research—UFZ, 04318 Leipzig, Germany; Institute of Chemistry, University of Halle-Wittenberg, 06120 Halle, Germany;* orcid.org/0000-0002-9707-5505

Bettina Seiwert − *Department of Analytical Chemistry, Helmholtz Centre for Environmental Research—UFZ, 04318 Leipzig, Germany*

Stephan Wagner − *Department of Analytical Chemistry, Helmholtz Centre for Environmental Research—UFZ, 04318 Leipzig, Germany;* orcid.org/0000-0002-3184-2599

Stefan Scholz − *Department of Bioanalytical Ecotoxicology, Helmholtz Centre for Environmental Research—UFZ, 04318 Leipzig, Germany*

Till Luckenbach − *Department of Bioanalytical Ecotoxicology, Helmholtz Centre for Environmental Research—UFZ, 04318 Leipzig, Germany*

Coretta Bauer − *Department of Analytical Chemistry, Helmholtz Centre for Environmental Research—UFZ, 04318 Leipzig, Germany*

Nicole Schweiger − *Department of Bioanalytical Ecotoxicology, Helmholtz Centre for Environmental Research—UFZ, 04318 Leipzig, Germany*

Complete contact information is available at: https://pubs.acs.org/10.1021/acs.est.0c02068

Notes

The authors declare no competing financial interest.

■ ACKNOWLEDGMENTS

This work is part of the Integrated Project "Exposome" of the topic "Chemicals in the Environment" of the Helmholtz Centre for Environmental Research, UFZ. The authors acknowledge the support of Teresa Split by generating zebrafish images and calculating the volumes of embryos and embryo body parts.

■ REFERENCES

(1) Strähle, U.; Scholz, S.; Geisler, R.; Greiner, P.; Hollert, H.; Rastegar, S.; Schumacher, A.; Selderslaghs, I.; Weiss, C.; Witters, H.; Braunbeck, T. Zebrafish Embryos as an Alternative to Animal Experiments-A Commentary on the Definition of the Onset of Protected Life Stages in Animal Welfare Regulations. *Reprod. Toxicol.* **2012**, *33*, 128−132.

(2) Belanger, S. E.; Rawlings, J. M.; Carr, G. J. Use of Fish Embryo Toxicity Tests for the Prediction of Acute Fish Toxicity to Chemicals. *Environ. Toxicol. Chem.* **2013**, *32*, 1768−1783.

(3) Weigt, S.; Huebler, N.; Strecker, R.; Braunbeck, T.; Broschard, T. H. Zebrafish (*Danio rerio*) Embryos as a Model for Testing Proteratogens. *Toxicology* **2011**, *281*, 25−36.

(4) Bittner, L.; Klüver, N.; Henneberger, L.; Mühlenbrink, M.; Zarfl, C.; Escher, B. I. Combined Ion-Trapping and Mass Balance Models

To Describe the PH-Dependent Uptake and Toxicity of Acidic and Basic Pharmaceuticals in Zebrafish Embryos (*Danio rerio*). *Environ. Sci. Technol.* **2019**, 7877.
(5) Brox, S.; Seiwert, B.; Küster, E.; Reemtsma, T. Toxicokinetics of Polar Chemicals in Zebrafish Embryo (*Danio rerio*): Influence of Physicochemical Properties and of Biological Processes. *Environ. Sci. Technol.* **2016**, *50*, 10264−10272.
(6) Kühnert, A.; Vogs, C.; Altenburger, R.; Küster, E. The Internal Concentration of Organic Substances in Fish Embryos-A Toxicokinetic Approach. *Environ. Toxicol. Chem.* **2013**, *32*, 1819−1827.
(7) Popovic, M.; Zaja, R.; Fent, K.; Smital, T. Interaction of Environmental Contaminants with Zebrafish Organic Anion Transporting Polypeptide, Oatp1d1 (Slco1d1). *Toxicol. Appl. Pharmacol.* **2014**, *280*, 149−158.
(8) Vogs, C.; Johanson, G.; Näslund, M.; Wulff, S.; Sjödin, M.; Hellstrandh, M.; Lindberg, J.; Wincent, E. Toxicokinetics of Perfluorinated Alkyl Acids Influences Their Toxic Potency in the Zebrafish Embryo (*Danio rerio*). *Environ. Sci. Technol.* **2019**, *53*, 3898−3907.
(9) Brox, S.; Ritter, A. P.; Küster, E.; Reemtsma, T. A Quantitative HPLC-MS/MS Method for Studying Internal Concentrations and Toxicokinetics of 34 Polar Analytes in Zebrafish (*Danio rerio*) Embryos. *Anal. Bioanal. Chem.* **2014**, *406*, 4831−4840.
(10) Kirla, K. T.; Groh, K. J.; Poetzsch, M.; Banote, R. K.; Stadnicka-Michalak, J.; Eggen, R. I. L.; Schirmer, K.; Kraemer, T. Importance of Toxicokinetics to Assess the Utility of Zebrafish Larvae as Model for Psychoactive Drug Screening Using Meta-Chlorophenylpiperazine (MCPP) as Example. *Front. Pharmacol.* **2018**, *9*, No. 414.
(11) Fraher, D.; Sanigorski, A.; Mellett, N. A.; Meikle, P. J.; Sinclair, A. J.; Gibert, Y. Zebrafish Embryonic Lipidomic Analysis Reveals That the Yolk Cell Is Metabolically Active in Processing Lipid. *Cell Rep.* **2016**, *14*, 1317−1329.
(12) Miyares, R. L.; de Rezende, V. B.; Farber, S. A. Zebrafish Yolk Lipid Processing: A Tractable Tool for the Study of Vertebrate Lipid Transport and Metabolism. *Dis. Models Mech.* **2014**, *7*, 915−927.
(13) Souder, J. P.; Gorelick, D. A. Quantification of Estradiol Uptake in Zebrafish Embryos and Larvae. *Toxicol. Sci.* **2017**, *158*, 465−474.
(14) Sant, K. E.; Timme-Laragy, A. R. Zebrafish as a Model for Toxicological Perturbation of Yolk and Nutrition in the Early Embryo. *Curr. Environ. Health Rep.* **2018**, *5*, 125−133.
(15) Siméon, S.; Brotzmann, K.; Fisher, C.; Gardner, I.; Silvester, S.; Maclennan, R.; Walker, P.; Braunbeck, T.; Bois, F. Y. Development of a Generic Zebrafish Embryo PBPK Model and Application to the Developmental Toxicity Assessment of Valproic Acid Analogs. *Reprod. Toxicol.* **2020**, *93*, 219−229.
(16) Fetter, E.; Smetanová, S.; Baldauf, L.; Lidzba, A.; Altenburger, R.; Schüttler, A.; Scholz, S. Identification and Characterization of Androgen-Responsive Genes in Zebrafish Embryos. *Environ. Sci. Technol.* **2015**, *49*, 11789−11798.
(17) OECD. *OECD Guidelines for the Testing of Chemicals—Fish Embryo Acute Toxicity (FET) Test*, No. 236; OECD, 2013.
(18) ISO. Water Quality—Determination of the Acute Toxicity of Waste Water to Zebrafish Eggs (Danio rerio), ISO 15088:2007, 2007.
(19) Scholz, S.; Fischer, S.; Gündel, U.; Küster, E.; Luckenbach, T.; Voelker, D. The Zebrafish Embryo Model in Environmental Risk Assessment - Applications beyond Acute Toxicity Testing. *Environ. Sci. Pollut. Res.* **2008**, *15*, 394−404.
(20) Kimmel, C. B.; Ballard, W. W.; Kimmel, S. R.; Ullmann, B.; Schilling, T. F. Stages of Embryonic Development of the Zebrafish. *Dev. Dyn.* **1995**, *203*, 253−310.
(21) Henneberger, L.; Goss, K. U.; Endo, S. Equilibrium Sorption of Structurally Diverse Organic Ions to Bovine Serum Albumin. *Environ. Sci. Technol.* **2016**, *50*, 5119−5126.
(22) Allendorf, F.; Berger, U.; Goss, K. U.; Ulrich, N. Partition Coefficients of Four Perfluoroalkyl Acid Alternatives between Bovine Serum Albumin (BSA) and Water in Comparison to Ten Classical Perfluoroalkyl Acids. *Environ. Sci.: Processes Impacts* **2019**, *21*, 1852−1863.
(23) Ulrich, N.; Schweiger, N.; Pfennigsdorff, A.; Scholz, S.; Goss, K. Yolk/Water Partitioning of Neutral Organic Compounds in the Model Organism *Danio rerio*. *Environ. Toxicol. Chem.* **2020**, 1−11.
(24) Hachicho, N.; Reithel, S.; Miltner, A.; Heipieper, H. J.; Küster, E.; Luckenbach, T. Body Mass Parameters, Lipid Profiles and Protein Contents of Zebrafish Embryos and Effects of 2,4-Dinitrophenol Exposure. *PLoS One* **2015**, *10*, No. e0134755.
(25) Halbach, K.; Wagner, S.; Scholz, S.; Luckenbach, T.; Reemtsma, T. Elemental Imaging (LA-ICP-MS) of Zebrafish Embryos to Study the Toxicokinetics of the Acetylcholinesterase Inhibitor Naled. *Anal. Bioanal. Chem.* **2019**, *411*, 617−627.
(26) Karlsson, J.; Artursson, P. A Method for the Determination of Cellular Permeability Coefficients and Aqueous Boundary Layer Thickness in Monolayers of Intestinal Epithelial (Caco-2) Cells Grown in Permeable Filter Chambers. *Int. J. Pharm.* **1991**, 55.
(27) Bittermann, K.; Goss, K. U. Predicting Apparent Passive Permeability of Caco-2 and MDCK Cell-Monolayers: A Mechanistic Model. *PLoS One* **2017**, *12*, No. e0190319.
(28) Larisch, W.; Goss, K. U. Calculating the First-Order Kinetics of Three Coupled, Reversible Processes. *SAR QSAR Environ. Res.* **2017**, *28*, 651−659.
(29) Ulrich, N.; Endo, S.; Brown, T. N.; Watanabe, N.; Bronner, G.; Abraham, M. H.; Goss, K.-U. *UFZ-LSER Database*, version 3.2.1 [Internet]; Helmholtz Centre for Environmental Research-UFZ: Leipzig, Germany, 2019. http://www.ufz.de/lserd (accessed Aug 10, 2019).
(30) Massei, R.; Vogs, C.; Renner, P.; Altenburger, R.; Scholz, S. Differential Sensitivity in Embryonic Stages of the Zebrafish (*Danio rerio*): The Role of Toxicokinetics for Stage-Specific Susceptibility for Azinphos-Methyl Lethal Effects. *Aquat. Toxicol.* **2015**, *166*, 36−41.
(31) Wilson, C. Aspects of Larval Rearing Carole. *ILAR J.* **2012**, *53*, 169−178.
(32) Brox, S.; Seiwert, B.; Haase, N.; Küster, E.; Reemtsma, T. Metabolism of Clofibric Acid in Zebrafish Embryos (*Danio rerio*) as Determined by Liquid Chromatography-High Resolution-Mass Spectrometry. *Comp. Biochem. Physiol., Part C: Toxicol. Pharmacol.* **2016**, *185*−*186*, 20−28.
(33) van Wijk, R. C.; Krekels, E. H. J.; Kantae, V.; Harms, A. C.; Hankemeier, T.; van der Graaf, P. H.; Spaink, H. P. Impact of Post-Hatching Maturation on the Pharmacokinetics of Paracetamol in Zebrafish Larvae. *Sci. Rep.* **2019**, *9*, No. 2149.
(34) El-Amrani, S.; Pena-Abaurrea, M.; Sanz-Landaluze, J.; Ramos, L.; Guinea, J.; Cámara, C. Bioconcentration of Pesticides in Zebrafish Eleutheroembryos (*Danio rerio*). *Sci. Total Environ.* **2012**, *425*, 184−190.
(35) Garcia, S. N.; Foster, M.; Constantine, L. A.; Huggett, D. B. Field and Laboratory Fish Tissue Accumulation of the Anti-Convulsant Drug Carbamazepine. *Ecotoxicol. Environ. Saf.* **2012**, *84*, 207−211.
(36) Lu, X.; Tao, S.; Hu, H.; Dawson, R. W. Estimation of Bioconcentration Factors of Nonionic Organic Compounds in Fish by Molecular Connectivity Indices and Polarity Correction Factors. *Chemosphere* **2000**, *41*, 1675−1688.
(37) Pirro, V.; Guffey, S. C.; Sepúlveda, M. S.; Mahapatra, C. T.; Ferreira, C. R.; Jarmusch, A. K.; Cooks, R. G. Lipid Dynamics in Zebrafish Embryonic Development Observed by DESI-MS Imaging and Nanoelectrospray-MS. *Mol. BioSyst.* **2016**, *12*, 2069−2079.
(38) Link, V.; Shevchenko, A.; Heisenberg, C. P. Proteomics of Early Zebrafish Embryos. *BMC Dev. Biol.* **2006**, *6*, No. 1.
(39) Brox, S.; Ritter, A. P.; Küster, E.; Reemtsma, T. Influence of the Perivitelline Space on the Quantification of Internal Concentrations of Chemicals in Eggs of Zebrafish Embryos (*Danio rerio*). *Aquat. Toxicol.* **2014**, DOI: 10.1016/j.aquatox.2014.10.008.
(40) Bittner, L.; Teixido, E.; Seiwert, B.; Escher, B. I.; Klüver, N. Influence of PH on the Uptake and Toxicity of B-Blockers in Embryos of Zebrafish, Danio Rerio. *Aquat. Toxicol.* **2018**, *201*, 129−137.
(41) Vogs, C.; Kühnert, A.; Hug, C.; Küster, E.; Altenburger, R. A Toxicokinetic Study of Specifically Acting and Reactive Organic

Chemicals for the Prediction of Internal Effect Concentrations in Scenedesmus Vacuolatus. *Environ. Toxicol. Chem.* **2015**, *34*, 100−111.
(42) Gordon, W. E.; Espinoza, J. A.; Leerberg, D. M.; Yelon, D.; Hamdoun, A. Uptake and Efflux of Xenobiotic Transporter Substrates in Zebrafish Embryo Ionocytes. *Aquat. Toxicol.* **2019**, 88−97.
(43) Di Paolo, C.; Groh, K. J.; Zennegg, M.; Vermeirssen, E. L. M.; Murk, A. J.; Eggen, R. I. L.; Hollert, H.; Werner, I.; Schirmer, K. Early Life Exposure to PCB126 Results in Delayed Mortality and Growth Impairment in the Zebrafish Larvae. *Aquat. Toxicol.* **2015**, *169*, 168−178.
(44) Tu, W.; Lu, B.; Niu, L.; Xu, C.; Lin, C.; Liu, W. Dynamics of Uptake and Elimination of Pyrethroid Insecticides in Zebrafish (*Danio rerio*) Eleutheroembryos. *Ecotoxicol. Environ. Saf.* **2014**, *107*, 186−191.
(45) Nowakowska, K.; Giebułtowicz, J.; Kamaszewski, M.; Adamski, A.; Szudrowicz, H.; Ostaszewska, T.; Solarska-Dzięciołowska, U.; Nałęcz-Jawecki, G.; Wroczyński, P.; Drobniewska, A. Acute Exposure of Zebrafish (*Danio rerio*) Larvae to Environmental Concentrations of Selected Antidepressants: Bioaccumulation, Physiological and Histological Changes. *Comp. Biochem. Physiol., Part C: Toxicol. Pharmacol.* **2020**, *229*, No. 108670.
(46) Kristofco, L. A.; Haddad, S. P.; Chambliss, C. K.; Brooks, B. W. Differential Uptake of and Sensitivity to Diphenhydramine in Embryonic and Larval Zebrafish. *Environ. Toxicol. Chem.* **2018**, *37*, 1175−1181.
(47) Flewelling, R. F.; Hubbell, W. L. The Membrane Dipole Potential in a Total Membrane Potential Model. Applications to Hydrophobic Ion Interactions with Membranes. *Biophys. J.* **1986**, *49*, 541−552.
(48) Avdeef, A. *Absorption and Drug Development: Solubility, Permeability, and Charge State*; John Wiley and Sons, 2012.
(49) Hills, E. E.; Abraham, M. H.; Hersey, A.; Bevan, C. D. Diffusion Coefficients in Ethanol and in Water at 298K: Linear Free Energy Relationships. *Fluid Phase Equilib.* **2011**, *303*, 45−55.
(50) Bodewein, L.; Schmelter, F.; Di Fiore, S.; Hollert, H.; Fischer, R.; Fenske, M. Differences in Toxicity of Anionic and Cationic PAMAM and PPI Dendrimers in Zebrafish Embryos and Cancer Cell Lines. *Toxicol. Appl. Pharmacol.* **2016**, *305*, 83−92.
(51) Armitage, J. M.; Erickson, R. J.; Luckenbach, T.; Ng, C. A.; Prosser, R. S.; Arnot, J. A.; Schirmer, K.; Nichols, J. W. Assessing the Bioaccumulation Potential of Ionizable Organic Compounds: Current Knowledge and Research Priorities. *Environ. Toxicol. Chem.* **2017**, 882−897.
(52) Shaw, L. R.; Irwin, W. J.; Grattan, T. J.; Conway, B. R. The Influence of Excipients on the Diffusion of Ibuprofen and Paracetamol in Gastric Mucus. *Int. J. Pharm.* **2005**, *290*, 145−154.

https://dx.doi.org/10.1021/acs.est.0c02068
Environ. Sci. Technol. 2020, 54, 10159−10169

Supporting information

The yolk sac of zebrafish embryos as backpack for chemicals?

Katharina Halbach[1], Nadin Ulrich[2], Kai-Uwe Goss[2], Bettina Seiwert[1], Stephan Wagner[1], Stefan Scholz[3], Till Luckenbach[3], Coretta Bauer[1], Nicole Schweiger[2], Thorsten Reemtsma [1,5]

1) Department of Analytical Chemistry, Helmholtz Centre for Environmental Research - UFZ, 04318 Leipzig, Germany
2) Department of Environmental Analytical Chemistry, Helmholtz Centre for Environmental Research - UFZ, 04318 Leipzig, Germany
3) Department of Bioanalytical Ecotoxicology, Helmholtz Centre for Environmental Research - UFZ, 04318 Leipzig, Germany
4) Institute of Chemistry, University of Halle-Wittenberg, 06120 Halle, Germany
5) Institute of Analytical Chemistry, University of Leipzig, 04103 Leipzig, Germany

*Corresponding author: Thorsten Reemtsma

E-mail address: thorsten.reemtsma@ufz.de

Phone: +49 341 235 1261

41 Pages, 12 Tables, 8 Figures

Table of Contents

Chemicals

Chemicals were purchased from the following vendors with highest available purity: 4-iodophenol (CAS 540-38-5, Sigma-Aldrich), 2-bromophenol (CAS 95-56-7, Supelco), diuron (CAS 330-54-1, Sigma-Aldrich), diuron-d6 (CAS 1007536-67-5, Toronto Research Chemicals), carbamazepine (CAS 298-46-4, ICN Biomedicals), carbamazepine-d10 (CAS 132183-78-9, Sigma-Aldrich), 1,2,4-tribromobenzene (CAS 615-54-3, abcr GmbH), hexachlorobenzene (CAS 118-74-1, Serva), 2-ethylpyridine (CAS 100-71-0, Alfa Aesar), 3-ethylpyridine (CAS 536-75-4, Sigma-Aldrich), bromoxynil (CAS 1689-84-5, Sigma-Aldrich), bromoxynil-d2 (CAS 1219798-95-4, neochema), paroxetine (CAS 110429-35-1, Sigma-Aldrich), paroxetine-d6 (CAS 1435728-64-5, Sigma-Aldrich), and the transformation products of diuron didemethyldiuron (DCPU, CAS 2327-02-8, Toronto Research Chemicals) and N-demethoxy linuron (DCPMU, CAS 3567-62-2, Toronto Research Chemicals). The purchaising information for the transformation products of carbamazepine (acridine-9-carboxylic acid, acridine, 10,11-dihydro-10-hydroxycarbamazepine, carbamazepine 10-11-epoxide, rac trans-10,11-dihydro-10,11-dihydroxy carbamazepine, 3-hydroxycarbamazepine, 9(10H) acridone, 2-hydroxycarbamazepine) can be found in Riemenschneider et al.[1]

Table S1. Selected compounds with molecular weight (M_W), log K_{OW}, log D, pKa, measured exposure concentration, LC_{50}, EC_{50} values and indication of whether transformation products were detected.

Substance	**M_w (g/mol)**	**Calculated log (K_{OW}/ [$L_{water}/L_{solvent}$]) [a]**	**Calculated log D at pH=7.4 [b]**	**pKa**	**%ionisation at pH=7.4**	**Concentration exposure solution [µM]**	**LC50, EC50, EC20 t96 hpf [µM]**	**Transformation products detected in the embryo**
(Mainly) neutral								
2-ethylpyridine	107.16	1.28	1.58	5.64[2]	1.71% cationic	844 ± 92	>9300	Yes
carbamazepine	236.27	2.3	2.77	13.9[3]	0.00% anionic	139 ± 7.8	>511, 277	Yes
diuron	233.09	2.89	2.53	13.18[2]	0.00% anionic	17.2 ± 1.5	27.1, 18.7, 13.0 (EC10)[4]	Yes
4-iodophenol	220.01	2.66	2.59	9.10[2]	1.96% anionic	12.9 ± 3.2[c]	>22.7, 1.6, 0.7	Yes
1,2,4-tribromobenzene	314.80	4.62	4.28		Not ionizable	1.10 ± 0.056	>31.8	No

(Mainly) ionic							
bromoxynil	276.92	1.19	3.75[5]	99.98% anionic	10.5 ± 0.48	27.1, 19.6, 3.5	Yes
paroxetine	329.37	0.83	9.6[6]	99.4% cationic	0.281 ± 0.0262	30.4[7]	(Yes[7])

[a]Calculated with[8]; [b]calculated with[2];[c]less pigmentation was observed

Yolk removal

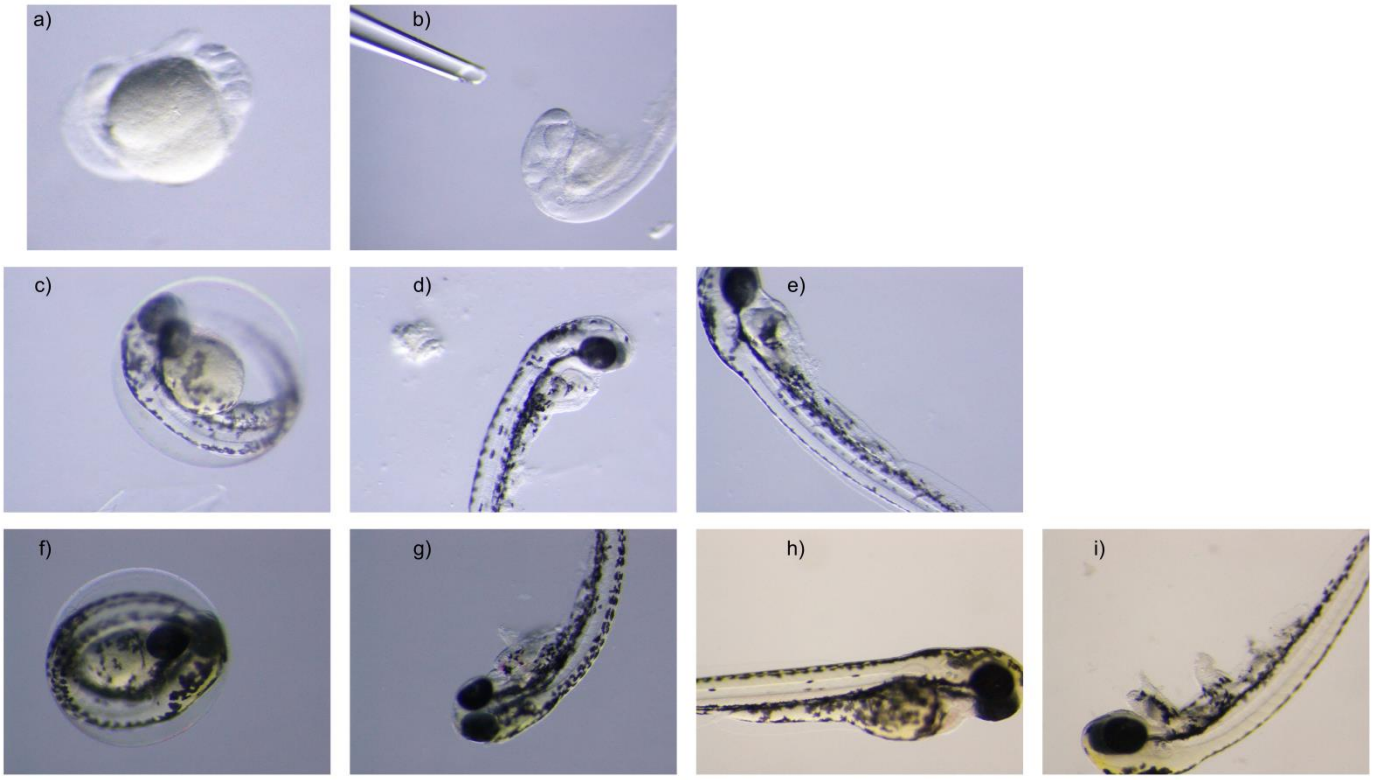

Figure S1. Examples for mechanical yolk removal: a) and b) 26±1 hpf embryos, c) to e) 48±1 hpf embryos, f) to i) 74±1 hpf.

Instrumentation

UPLC-QToF-MS measurements

The analysis was performed with an ACQUITY UPLC system coupled to a XEVO XS with electrospray ionization (Waters, Eschborn). Injection volumes were 10 or 100 µL. Separation was achieved with an ACQUITY UPLC HSS T3 column (Waters, 100 x 2.1 mm, 1.7 µm), the flow rate was set to 0.45 µL/min at 45°C. The mobile phase was water with 0.1% formic acid (A) and methanol with 0.1% formic acid (B). The gradient was: 0–0.25 min, 2% B; 12.25–15 min, 99% B; 15.1–17 min, 98% B. During ionization a capillary voltage of 0.7 kV (pos), -1.3 kV (neg), source temperature of 140°C and desolvation temperature of 550°C, a sampling cone voltage of 20 V and a source offset of 50 V was applied. Nitrogen and argon were used as cone and collision gas. Desolvation flow rate was 950 L/h and a mass range of m/z 50 to 1200 was scanned with a scan time of 0.15 s in negative and positive mode. Leucine enkephalin was used as lock spray reference. To obtain information about the MS fragmentation, a MS^E experiment was conducted: two collision energies were applied: 15 and 35 eV.

The following precursor ions were used: 4-iodophenol (m/z 218.93, retention time (rt)=8.43 min) and 2-bromophenol (m/z 170.94, rt=7.43 min); diuron (m/z 233.02, rt=8.82 min) and d6-diuron (m/z 239.06 rt=8.81 min), carbamazepine (m/z 237.10 rt=8.36 min) and d10-carbamazepine (m/z 247.17 rt=8.28 min); paroxetine (m/z 330.15 rt=7.85 min) and d6-paroxetine (m/z 336.19 rt=7.85 min); bromoxynil (m/z 275.85 rt=8.31 min) and d2-bromoxynil (m/z 277.85 rt=8.31 min). For carbamazepine and diuron available transformation products (see chemicals section) were also quantified[1]. Peak integration executed with TargetLynx (MassLynx V4.1, Waters). Untargeted metabolite screening was performed as described in Brox et al.[9] and results can be found in Table S6.

SFC-QToF-MS

2-Ethylpyridine was analyzed using SFC-HRMS analysis. The analyses were carried out with a Waters ACQUITY UPC^2 coupled to an SYNAPT G2-S Mass Spectrometer (Waters) with electrospray ionization. Separation was achieved with a CSH Fluoro-Phenyl (Waters, 3 mm x 100 mm, 1.7 µm) column. The injection volume was 5 µL. The flow rate was set to 1.5 µL/min. The eluents were: CO_2 in supercritical state (solvent

A) and a methanol/water mixture (95/5; v:v) with 0.2% formic acid (solvent B). The gradient was as follows: 0-3.5 min 1% B, 3.5-4 min 20% B, 4-6.5 min 40% B, 6.5-9 min 1% B. A mass range from m/z 50 to 1200, a scan time of 0.08 s and a cone voltage of 20 V was applied. The lock mass was 556.2771 (leucine encephalin). The capillary voltage was set to 0.7 kV, the source temperature to 140°C, the sampling cone to 20 V, the source offset to 40 V, the desolvation temperature to 550°C, the cone gas flow to 100 L/h, the desolvation gas flow to 950 L/h and the nebulizer gas flow to 7 bar. Peak integration was performed with TargetLynx (MassLynx V4.1, Waters) for 2-ethylpyridine (m/z 108.081, retention time 2.0 min) and 3-ethylpyridine (m/z 108.081, retention time 2.2 min). Untargeted metabolite screening was also performed (see for procedure Brox et al.[9]).

GC-MS

GC-MS analysis for 1,2,4-tribromobenzene was performed with an Agilent 6890 with a 5973N mass selective detector with an electron ionization source. Selected ion monitoring was used for quantification. The gas chromatograph was equipped with an HP-5ms column (Agilent, 30 m×0.25 mm×0.25 µm). Helium was used as carrier gas with a constant flow of 1.1 mL/min. The injection volume was 1 µL. The following oven program was run: 2 minutes at 80°C followed by a gradient until 280°C at a rate of 20°C/min. The total run time was 14 min. Peak integration was performed with MSD Chemstation Software (Agilent Technologies). Parameters used for 1,2,4-tribromobenzene were: m/z 314, retention time 7.9 min; hexachlorobenzene; m/z 284, retention time 9.4 min.

Volume of the zebrafish embryo and the two compartments yolk sac and embryonic body

The procedure for estimating the volume of embryos had been described previously in detail (Halbach et al.[10]). Briefly, an automated imaging system (VAST BioImager, Pardo-Martin et al.[11]) had been used to obtain lateral images. Using a KNIME workflow for image processing, the areas covered by the embryonic body and the yolk were manually labeled.[12] Subsequently, each embryo was separated into 10 µm virtual slices. Each slice was considered as an elliptic cylinder and the diameters from lateral and dorsoventral images were used to calculate the volume of each slice. The sum of the slice volumes was used to calculate whole embryo and yolk volumes.

Calculation of equilibrium partition coefficient for the embryonic body

Equilibrium partition coefficients in the embryonic body were calculated using values in the LSER database for the neutral compounds for two different zebrafish life stages: a) the whole embryo at 96 hpf with a volume of 253 nL (2 µg (1.46 v/v%) membrane lipids/embryo and 20.83 µg (8.23 v/v%) muscle proteins) and b) that corresponding to an adult female zebrafish (1.03 g, 0.97 mL) in v/v%: 3.13% storage lipids, 1.35% phospholipids, 0.23% serum albumin, 5.88% collagen and muscle protein, 89.42% water.[8,13–22] Adult female zebrafish were included because quantitative data on the different sorption components are available while exact data for the zebrafish embryo are missing. Estimating lipid and protein contents for the embryonic body from data for whole embryos would involve assumptions for the partitioning between the exposure medium and yolk and embryonic body which are not available from literature yet. The partition coefficients were calculated in the units $L_{water}/L_{organism}$ and transferred to $L_{water}/kg_{dry\ weight}$ with the following densities: 1.4 kg/L for serum albumin, 0.93 kg/L for storage lipids, 1 kg/L for membrane lipids and muscle proteins.[23]

The body/water partition coefficients of the ions bromoxynil and paroxetine were estimated by the use of the structure protein/water, storage lipid/water, membrane lipid/water, and serum albumin/water partition coefficients of the neutral form. The log $K_{serum\ albumin/water}$ value for bromoxynil was adopted according to the experimentally determined partition coefficient (log $K_{serum\ albumin/water}$ 5.18), as well as the log $K_{membrane\ lipid/water}$ (1.87 – calculated value for the ion). The pKa values and corresponding dissociation at the exposure pH can be found in Table S1.

Measured concentration in the exposure solution in the blind control

Table S2. Measured concentration (C_{extern}) in the blind control (exposure medium without embryos) at the start of the exposure (t0) and end (t96 h), mean with standard deviation (sd, n=3). nd: extraction of the samples was not successful (internal standard was not detected)

Substance	C_{extern} t0 [µM] (sd)	C_{extern} t96 h [µM] (sd)
2-Ethylpyridine	890 (183)	827 (33)
Carbamazepine	132 (12)	138 (8)
Diuron	17.4 (0.8)	18.4 (0.6)
4-Iodophenol	12.0 (0.7)	12.6 (0.5)
1,2,4-Tribromobenzene	1.10 (0.06)	nd
Bromoxynil	9.9 (0.2)	9.4 (0.0)
Paroxetine	0.28 (0.04)	0.26 (0.02)

Steady-state partition ratios (PR_{vol}) for neutral compounds

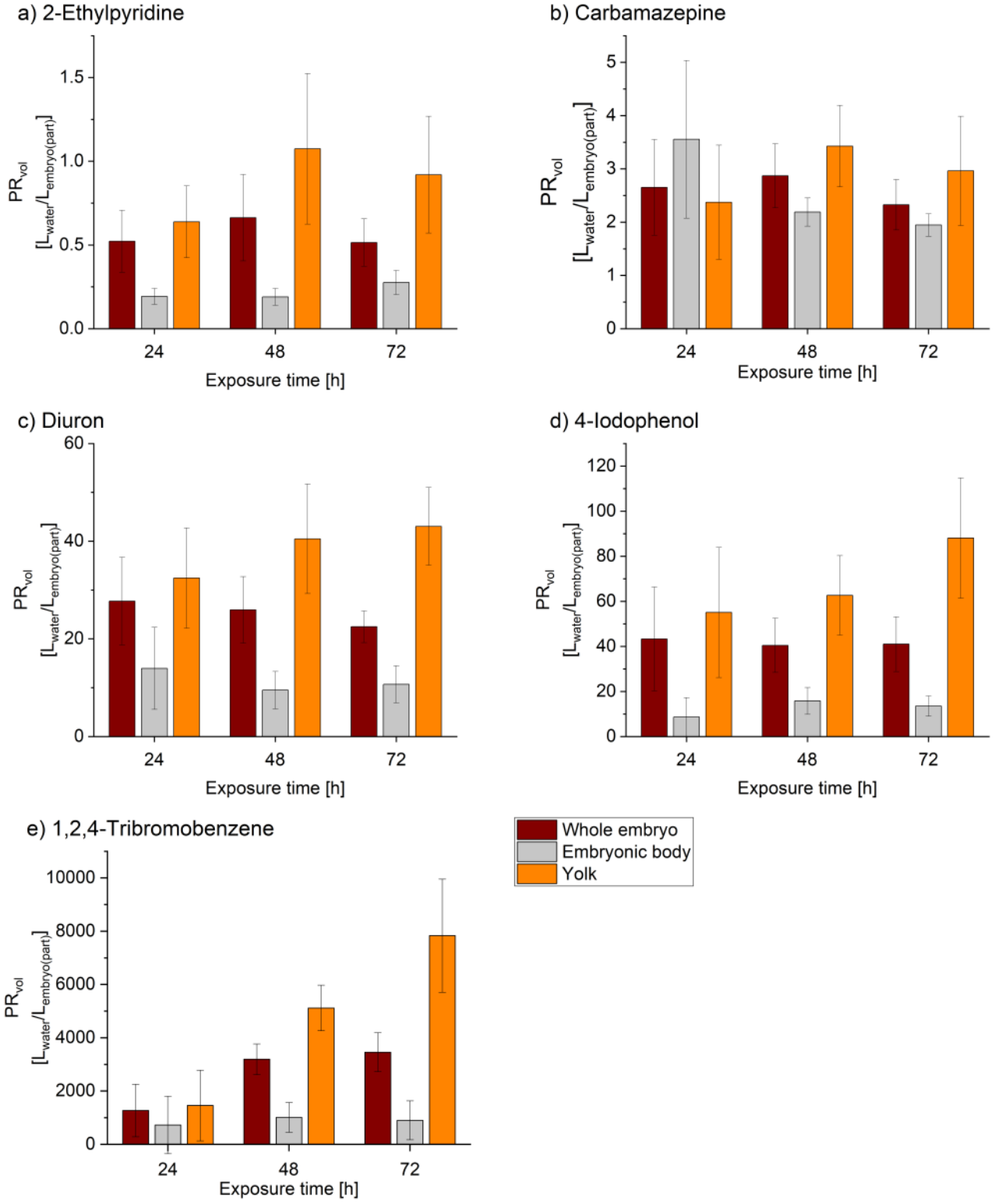

Figure S2. Steady-state partition ratios based on the volume (PR_{vol}) of a) 2-ethylpyridine, b) diuron and c) 4-iodophenol for the whole embryo, the embryonic body and the yolk for three of the five non-ionic test chemicals at 24, 48, 72 hours of exposure (start of the exposure at 2 hpf; mean with standard deviations). Data

from one egg batch per substance with 6 replicates (n=6 per column) with three pooled whole embryos and three embryonic bodies per exposure duration are presented.

Steady-state partition ratios (PR_{dry}) for neutral compounds

Table S3. Steady-state partition ratio (PR_{dry}) calculated out of internal concentrations per dry weight of the whole embryo and the measured concentration in the exposure solution (n=6, respectively) for the exposure times of 24, 48 and 72 h with standard deviation (sd).

Substance	Exposure time [h][a]	PR_{dry} in the whole embryo [$L_{water}/kg_{dry\ weight}$] (sd)	PR_{dry} in the embryonic body [$L_{water}/kg_{dry\ weight}$] (sd)	PR_{dry} in the yolk [$L_{water}/kg_{dry\ weight}$] (sd)
2-ethylpyridine	24	1.5 (0.5)	0.63 (0.22)	1.8 (0.6)
	48	2.2 (0.8)	0.89 (0.25)	2.8 (1.2)
	72	2.0 (0.5)	1.3 (0.4)	2.6 (1.2)
carbamazepine	24	7.6 (2.3)	11.2 (5.3)	6.6 (3.1)
	48	9.2 (1.6)	9.7 (1.5)	9.0 (2.3)
	72	8.8 (1.7)	8.9 (1.8)	8.6 (3.7)
diuron	24	80 (22)	45 (29)	90 (31)
	48	85 (20)	45 (19)	103 (31)
	72	86 (11)	51 (20)	122 (38)
4-iodophenol	24	124 (63)	28 (28)	151 (82)
	48	132 (36)	76 (30)	159 (49)

	72	156 (45)	64 (24)	251 (98)
	24	3700 (2900)	2300 (3500)	4000 (3700)
1,2,4-tribromobenzene	48	10400 (1400)	4800 (2700)	13100 (2700)
	72	13200 (2600)	4300 (3500)	22300 (8200)

Data from one egg batch per substance with six replicates with three pooled whole embryos and three embryonic bodies per exposure duration, respectively, are presented. (Mainly) Ionic compounds are not displayed as they did not reach a steady-state within the exposure time. [a]Start of exposure 2 hpf.

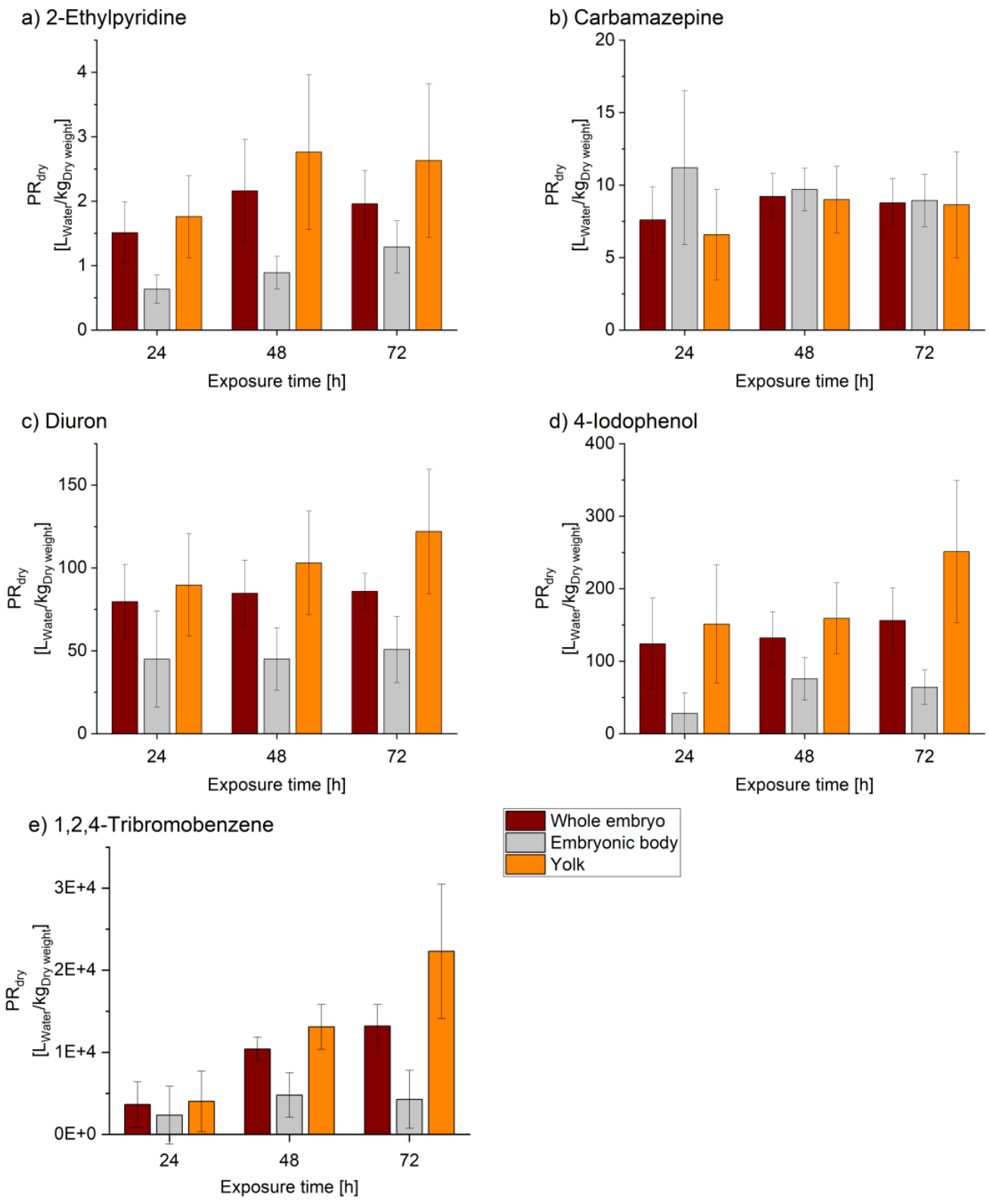

Figure S3. Steady-state partition ratios based on the dry weight (PR_{dry}) calculated out of the measured internal concentration per dry weight and the free concentration in the exposure solution. PRs are displayed for the whole embryo and the two body compartments embryonic body and yolk for exposures with 2-ethylpyridine (a), carbamazepine (b), diuron (c), 4-iodophenol (d) and 1,2,4-tribromobenzene (e) for 24, 48, 72 h (start of

exposure 2 hpf; mean with standard deviation). Data from one egg batch per substance with six replicates (n=6 per column) with three pooled whole embryos and three embryonic bodies per exposure time are presented.

Relative distribution of the chemicals between yolk and embryonic body

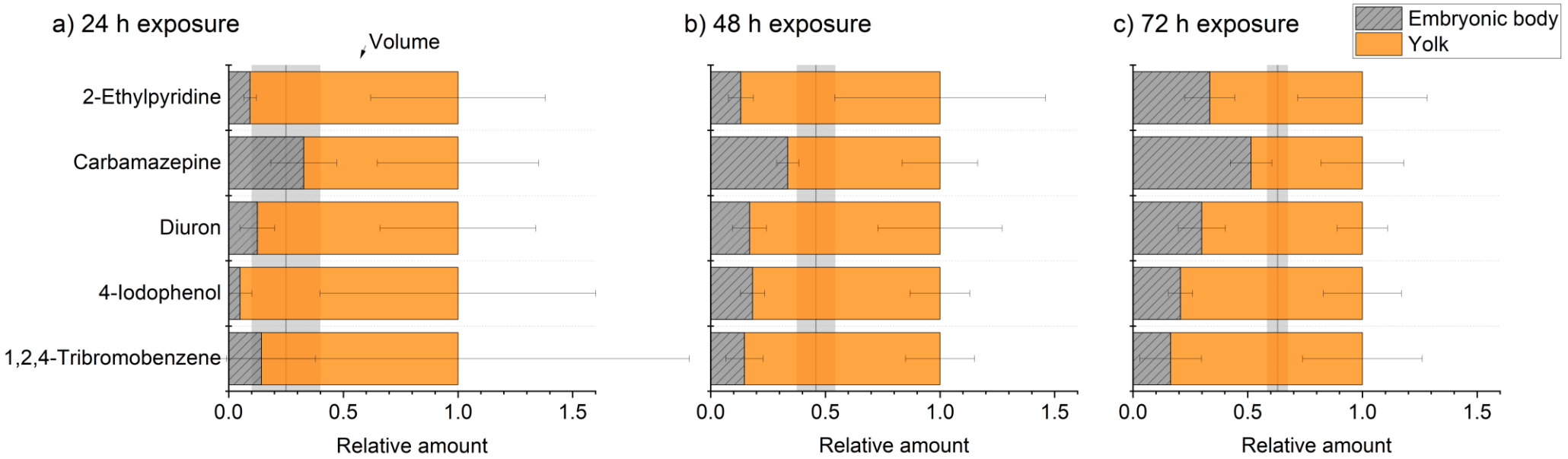

Figure S4. Relative distribution of the total internal amount of the compounds between embryonic body and yolk after a) 24, b) 48 and c) 72 hours of exposure (start of exposure 2 hpf). (Vertical line represents the relative proportion of the volume of the embryonic body at the respective age of the embryo). Data from one egg batch per substance with six replicates (n=6) with three pooled whole embryos or three embryonic bodies per exposure time are presented.

Internal concentration kinetics

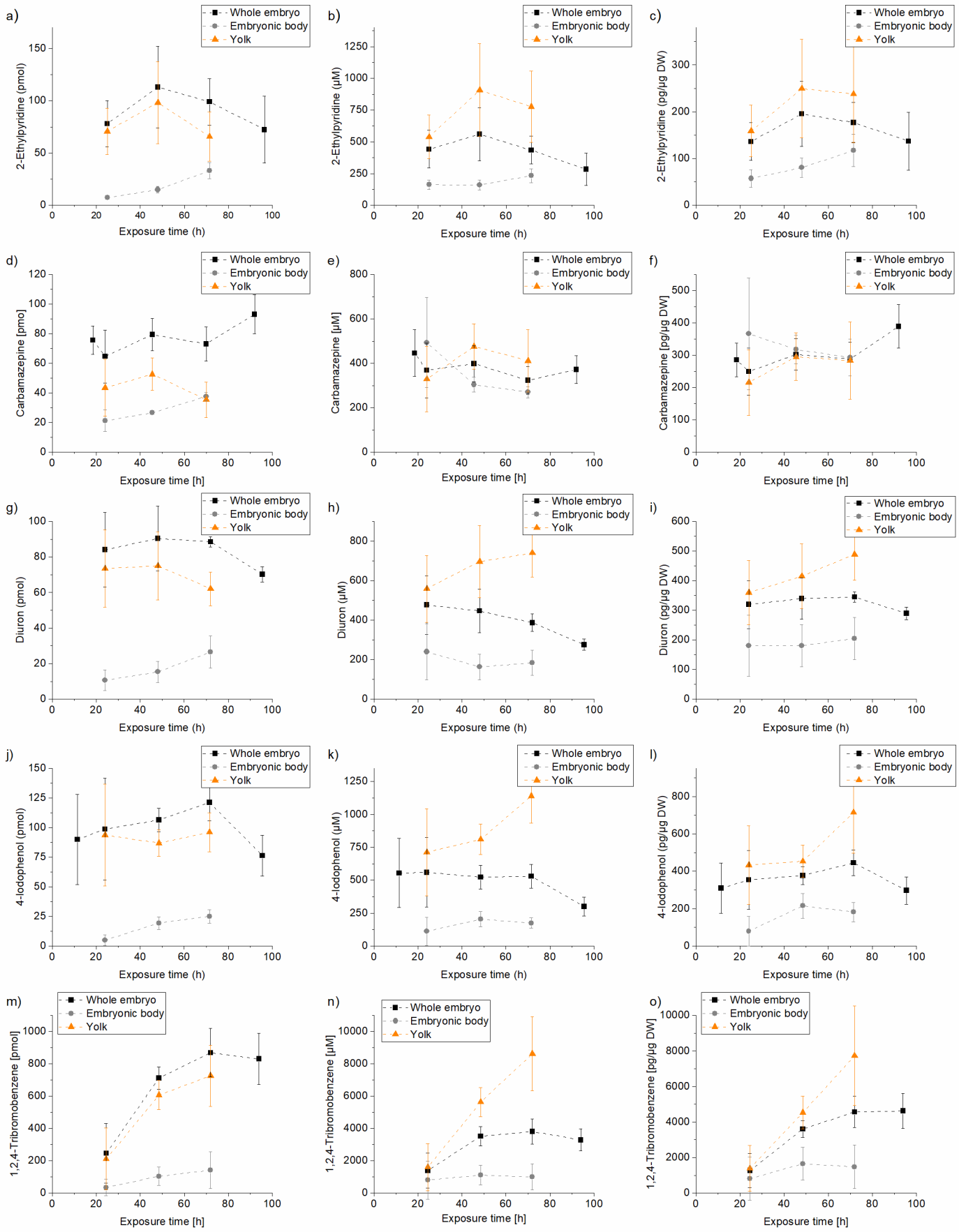

Figure S5. Absolut internal amount (pmol/embryoa, d, g, j m), internal concentration per volume (middle, e, h, k, n) or dry weight (c, f, I, l, o) for the whole embryo and embryonic body (each value represents the mean with the standard deviation, n=6). By subtracting the internal amount in the embryonic body from the one in the whole embryo the internal amount in the yolk was calculated and related to the dry weight or volume of the yolk. Displayed are the non-ionic compounds: 2-ethylpyridine (a to c), carbamazepine (d to f), diuron (g to i), 4-iodophenol (j to l) and 1,2,4-tribromobenzene (m to o). Start of exposure was 2 hpf. Data from one egg batch per substance with 6 replicates of three pooled whole embryos or three embryonic bodies per exposure time are presented. See for the (mainly) ionic compounds Figure S6.

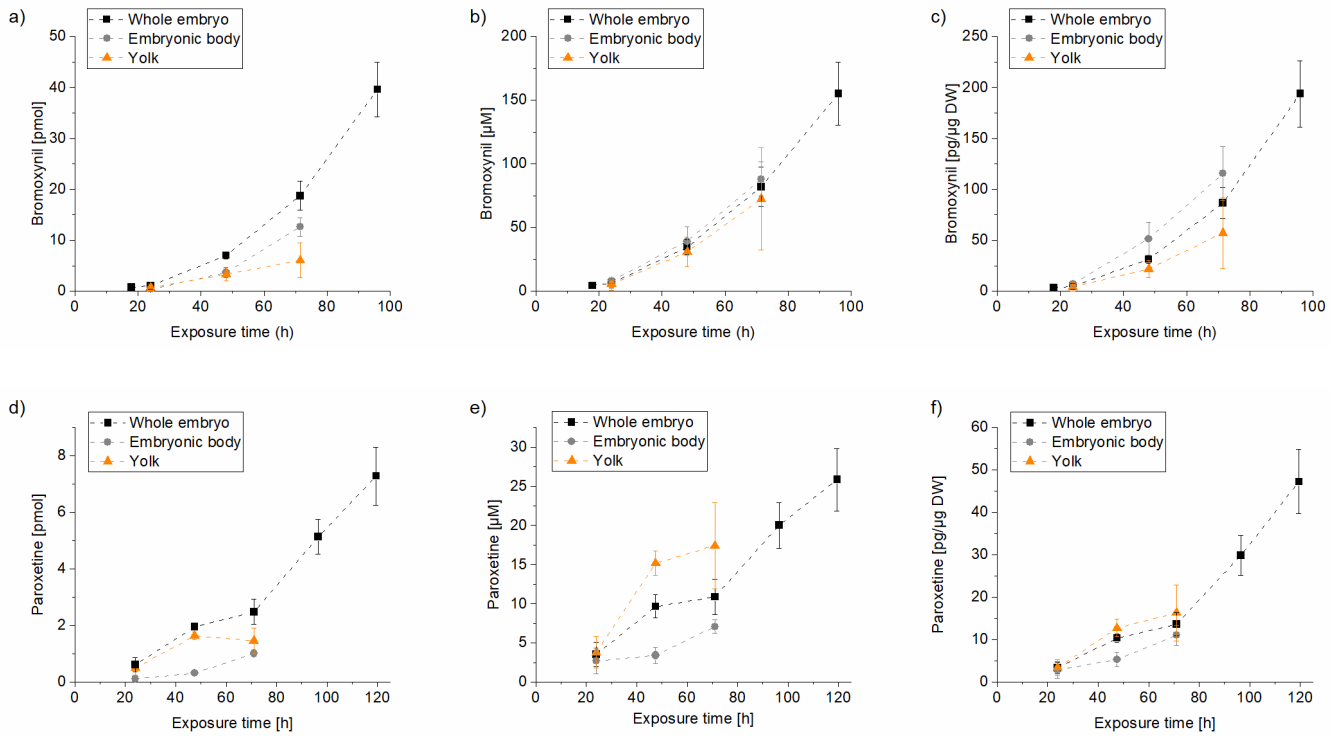

Figure S6. Internal amount (pmol/embryo), internal concentration per volume or dry weight for the whole embryo and embryonic body exposed to bromoxynil (a to c) and paroxetine (d to f) (each value error represents the mean with the standard deviation, n=6). By subtracting the internal amount in the embryonic body from the one in the whole embryo the internal amount in the yolk was calculated and related to the dry weight or volume of the yolk. Start of exposure was 2 hpf. Data from one egg batch per substance with six replicates of three pooled whole embryos or three embryonic bodies per exposure time are presented.

Partition coefficients

Table S4. Comparison of calculated octanol – water partition coefficients with the calculated ones for a zebrafish embryo at 96 hpf and a female adult zebrafish; calculated with[8]

Substance	log (K_{OW}/ [L_{water}/$L_{solvent}$]) calculated	log ($K_{body/water}$/ [L_{water}/$L_{organism}$]) calculated, 96 hpf embryo	log ($K_{body/water}$/ [L_{water}/$L_{organism}$]) calculated, female adult zebrafish
2-ethylpyridine	1.28	0.69	0.20
carbamazepine	2.3	1.24	0.88
diuron	2.89	1.59	1.41
4-iodophenol	2.66	2.19	1.34
1,2,4-tribromobenzene	4.62	3.26	3.67

Table S5. Measured partition coefficients of the whole embryo after 72 h of exposure (74 hpf) and 96 h of exposure (98 hpf) with standard deviations (sd).

Substance	Exposure time [h][a]	log ($K_{whole\ embryo/water}$/ [L_{water}/$kg_{dry\ weight}$]) (sd)
2-Ethylpyridine	72	0.29 (0.12)
	96	0.18 (0.20)
Carbamazepine	72	0.94 (0.08)
	96	1.07 (0.08)
Diuron	72	1.93 (0.06)
	96	1.86 (0.06)

4-Iodophenol	72	2.19	(0.13)
	96	2.02	(0.15)
1,2,4-Tribromobenzene	72	4.12	(0.09)
	96	4.12	(0.10)

Data from one egg batch per substance with 6 replicates (n=6) à three pooled whole embryos or three embryonic bodies per exposure time, are presented. [a]Start of exposure 2 hpf.

First-order kinetic uptake model with diffusive exchange

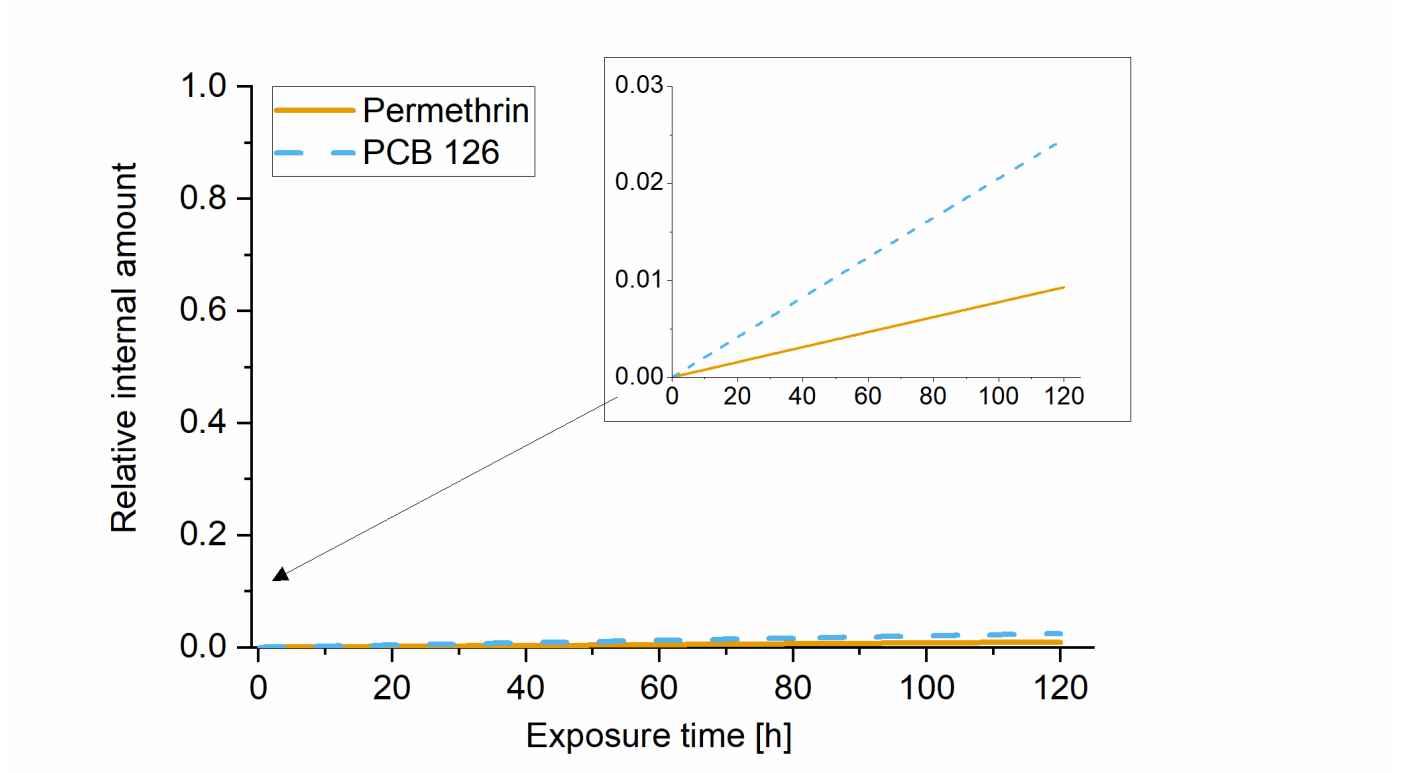

Figure S7. Modeled first-order uptake kinetics into the embryo for permethrin and PCB 126. Displayed is the relative internal amount to the equilibrium concentration at the y-axis.

Calculation with ion trapping for paroxetine

A possible acidic compartment might be the lysosome-like, membrane-bound yolk granules[24,25] which contain the proteins in the yolk. An ion-trap factor of circa 100 would result out of the pKa, an internal pH of 5.6[26] in the granules and a pH of 7.55[27] in the embryo. With an estimated volume of 1% of the granules to the yolk, the ion-trap factor translates into a very small changing partition coefficient of 1.82 instead of 1.80. This still results in a steady-state within 24 h. A possible basic compartment might be the mitochondria. An ion-trap factor of circa 5 would result out of the pKa, an internal pH of 8[28] in the granules and a pH of 7.55[27] in the embryo. With an estimated volume of 0.1% of the embryo[29], the ion-trap factor does not translate into changing partition coefficient (still 2.6).

Intrinsic membrane permeabilities

A plausibility control of our permeability values is helpful: The modeled membrane permeability was shown to be comparable to the permeability of Caco-2 cells[30]. Whether this membrane permeability is comparable to the permeability of the zebrafish embryo membrane, can be assessed with neutral, very

hydrophilic substances such as triamcinolone or theophylline. For these compounds, the main barrier is the permeability of the membrane and not the aqueous boundary layer. Triamcinolone showed an internal concentration after 5 min of exposure that was similar to that after 96 h of exposure. The model predicted a steady-state within circa 15 min. In addition, triamcinolone showed some metabolism which may have lowered the steady-state concentration and increased the establishment of the steady-state.[31] Data for theophylline are inconclusive.[9]

2-compartment model

The attached excel file with the model allows also to calculate the uptake kinetics for 2-compartments. In order to modify this, compartment 1 is adjusted to represent the yolk and compartment 3 the embryonic body. the following adjustments are needed for a 96 hpf embryo:

- Exposure time (sheet *Systems*, cell *G7*) can be varied
- Dry weight embryonic body (sheet *Systems*, cell *S11*): 0.036 mg
- $K_{body/water}$ (sheet *Systems*, cell *S14*): depending on the selected chemical choose the log $K_{body/water}$ from cells *AC41* to *AC54*
- Dry weight yolk (sheet *Systems*, cell *C11*): 0.023 mg
- $K_{yolk/water}$ (sheet *Systems*, cell *C14*): depending on the selected chemical choose the log $K_{yolk/water}$ from cells *AD41* to *AD54*
- Permeability through barrier (sheet *Systems*, cell *G12* and *O12*): Choose depending on the selected chemical from cells *Z41* to *Z54*
- Interfacial area between yolk and water (sheet *Systems*, cell *G14*): estimating that ¾ of the surface area of the yolk (62 nL, 0.0076 cm^2) is in direct contact with the water = 0.0057 cm^2
- Interfacial area between body and water (sheet *Systems*, cell *O14*): estimating that ¾ of the surface area of the body (189 nL, 0.016 cm^2) is in direct contact with the water = 0.012 cm^2
- Initial concentration in the yolk (sheet *Systems*, cell *C20*): 0

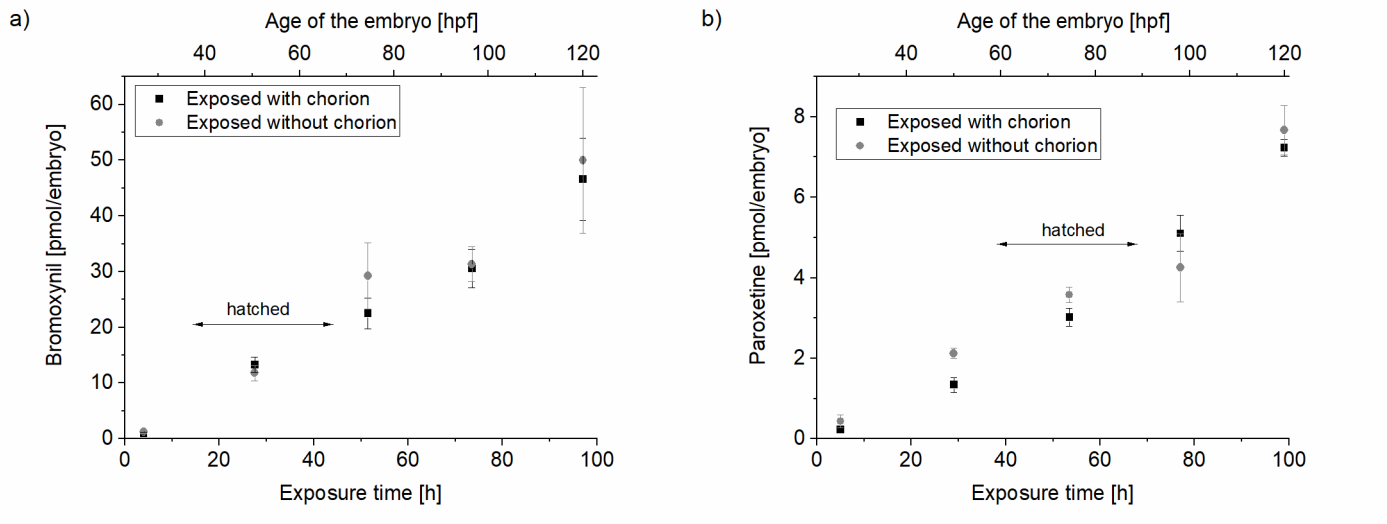

Figure S8. Internal amount of a) bromoxynil and b) paroxetine for embryos that were dechorionated prior to exposure start (n=6 per exposure duration) compared to embryos that were not dechorionated prior to exposure start (n=6 per exposure duration). All embryos were dechorionated at the end of the exposure if necessary. Exposure concentrations: a) 17±3 µM b) 0.41±0.06 µM. Data from one egg batch are presented, respectively. Start of exposure was 2 hpf

Transformation products

Table S6. Information on detected transformation products in zebrafish embryos and on their mass spectrometric data. w: whole embryo, eb: embryonic body

Transformation product	**Exposure time [h][a]**	**Ionization mode**	**detection confidence**	**Retention time [min]**	**Molecular ion [m/z] (Δppm)**	**Assigned elemental composition**	**Fragment ions [m/z] (proposed elemental composition)**
Exposure with 2-ethylpyridine							
ethanalpyridine	96 (w)	pos		0.87	122.061 (3.3)	C_7H_8NO	
hydroxyethylpyridine	96 (w)	pos		3.44	124.076 (1.6)	$C_7H_{10}NO$	
Expsoure with carbamazepine							
3-hydroxy-carbamazepine	96 (w)	pos	comparision with standard	8.32	275.079 (2.2)	$C_{15}H_{12}N_2O_2Na$	
acridine	96 (w)	pos	comparision with standard	5.96	180.081 (1.7)	$C_{13}H_{10}N$	
Exposure with diuron							
N-didemethyldiuron (DCPU)	72 (w, eb) 96 (w)	pos	comparision with standard	8.13	201.9470 (3.5 ppm)	$C_7H_2NO_2Cl_2$	161.9859 ($C_6H_4NCl_2$) 127.0814 (C_6H_6NCl)

N-dimethyldiuron (DCPMU)	24 (w, eb) 48 (w, eb) 72 (w, eb) 96 (w)	pos	comparision with standard	8.59	219.0090 (0.9)	$C_8H_9N_2OCl_2$	161.9859 ($C_6H_4NCl_2$) 127.0814 (C_6H_6NCl)
hydroxy-DCPMU glucuronide	96 (w)	pos		7.63	443.190 (3.2 ppm)	$C_{14}H_{16}N_2O_8NaCl_2$	256.9856 ($C_8H_8N_2O_2NaCl_2$)
hydroxy diuron glucuronide	96 (w)	pos		7.56	447.033 (1.8 ppm)	$C_{15}H_{18}N_2O_8NaCl_2$	271.002 ($C_9H_{10}N_2O_2NaCl_2$) 173.988 ($C_7H_6NCl_2$)
di-hydroxydiuron	48 (w) 72 (w, eb) 96 (w)	pos		7.95	286.9960 (2.1 ppm)	$C_9H_{10}N_2O_3NaCl_2$	-
hydroxy-DCPMU	72 (w, eb) 96 (w, eb)	pos		8.12	256.9856 (1.9)	$C_8H_8N_2O_2NaCl_2$	204.9937 ($C_7H_7N_2OCl_2$)
hydroxydiuron	24 (eb) 48 (w)	pos		8.75	271.002 (1.1)	$C_9H_{10}N_2O_2NaCl_2$	-

	72 (w, eb)						
	96 (w)						
Exposure with 4-iodophenol							
glucuronide	12 (w)	neg	6.69	394.963	(0.5 ppm)	$C_{12}H_{12}O_7I$	218.936 (C_6H_4OI), 126.904 (I)
	24 (w, eb)						
	48 (w, eb)						
	72 (w, eb)						
	96 (w)						
sulfate	12 (w)	neg	6.91	298.888	(1.7 ppm)	$C_6H_4O_4SI$	126.904 (I)
	24 (w, eb)						
	48 (w, eb)						
	72 (w, eb)						
	96 (w)						
dimer sulfate	12 (w)	neg	10.14	390.914	(0.8 ppm)	$C_{12}H_8O_5SI$	310.957 ($C_{12}H_8O_2I$)
	24 (w, eb)						126.904 (I)
	48 (w, eb)						
	72 (w, eb)						

	96 (w)						
hydroxy methyl sulfate	12 (w) 24 (w, eb) 48 (w, eb) 72 (w, eb) 96 (w)	neg	5.97	344.893 ppm)	(0	$C_7H_6O_6SI$	264.936 ($C_7H_6O_3I$); 249.912 ($C_6H_3O_3I$); 126.904 (I)
glucuronide sulfate	12 (w) 24 (w, eb) 48 (w, eb) 72 (w, eb) 96 (w)	neg	5.39	476.936 ppm)	(1.7	$C_{12}H_{14}O_{10}SI$	314.882 ($C_6H_4O_5SI$); 234.926 ($C_6H_4O_2I$), 126.904 (I)
hydroxy sulfate	12 (w) 24 (w, eb) 48 (w, eb) 72 (w, eb) 96 (w)	neg	6.44+6.52	314.883 ppm)	(1.9	$C_6H_4O_5SI$	126.904 (I)

dimer hydroxyl sulfate	12 (w) 24 (w, eb) 48 (w, eb) 72 (w, eb) 96 (w)	neg	9.95	406.909 ppm)	(1	$C_{12}H_8O_6SI$	326.951 ($C_{12}H_8O_3I$); 126.904 (I)
hydroxy cysteine glucuronide	12 (w) 24 (w, eb) 48 (w, eb) 72 (w, eb) 96 (w)	neg	6.74	585.989		$C_{18}H_{21}NO_{11}SI$	409.956 ($C_{12}H_{13}NO_5SI$), 280.913 ($C_7H_6O_2SI$), 126.904 (I)
Exposure with bromoxynil							
sulfate	72 (w, eb) 96 (w)	neg	5.62	371.817 ppm)	(1.9	$C_7H_2NO_5SBr_2$	289.846 ($C_7H_2NO_2Br_2$)
sulfate	72 (w, eb) 96 (w)	neg	6.12	371.817 ppm)	(1.9	$C_7H_2NO_5SBr_2$	289.846 ($C_7H_2NO_2Br_2$)
hydrolyzed bromoxynil	18 (w) 24 (w)	neg	6.45	273.8504 ppm)	(0.4	$C_7O_2NH_5Br_2$	-

	48 (w)					
	72 (w, eb)					
	96 (w)					
hydrolyzed	48 (w)	neg	6.05	273.8504 (0.4	$C_7O_2NH_5Br_2$	
bromoxynil	72 (w, eb)			ppm)		
	96 (w)					
N-acetylcysteine	72 (w)	neg	5.29	505.8215 (2.8	$C_{11}H_{10}NO_8S_2Br_2$	296.8226
sulfate	96 (w)			ppm)		($C_6H_3O_2SBr_2$)
N-acetylcysteine	72 (w)	neg	4.92	427.9109 (2.1	$C_{11}H_{11}NO_8S_2Br$	
sulfate, debrominated	96 (w)			ppm)r		

[a]Start of exposure 2 hpf.

Partition ratios and coefficients, sorption experiment to yolk (dialysis approach) and prediction of the equilibrium concentration in the embryonic body for ionic compounds

Table S7. Measured partition ratios for the whole embryo (PR_{vol} and PR_{dry}) and coefficients for the whole embryo, yolk and embryonic body from the TK experiments (log $K_{whole\ embryo/water}$, log $K_{yolk/water}$, log $K_{embryonic\ body/water}$; n=6), measured equilibrium partition coefficients (log $K_{yolk/water}$) from the dialysis approach (n=3), calculated equilibrium partition coefficients of the zebrafish body and the water (log $K_{body/water}$) with the LSER database with the composition of the zebrafish embryo at 96 hpf and the female adult zebrafish.

Substance	PR_{vol} in the whole embryo [$L_{water}/L_{whole\ embryo}$] (sd)	PR_{dry} in the whole embryo [$L_{water}/kg_{dry\ weight}$] (sd)	log ($K_{Whole\ embryo/water}$/ [$L_{water}/kg_{dry\ weight}$]) (sd)	log ($K_{yolk/water}$/ [$L_{water}/kg_{dry\ weight}$]) (sd)	log ($K_{yolk/water}$/ [$L_{water}/kg_{dry\ weight}$]) (sd)	log ($K_{embryonic\ body/water}$/ [$L_{water}/kg_{dry\ weight}$]) (sd)	log ($K_{body/water}$/ [$L_{water}/kg_{dry\ weight}$])
	TK experiment	TK experiment	TK experiment	TK experiment	dialysis approach	TK experiment	calculated
	24 h exposure[a], 48 h exposure[a], 72 h exposure[a], 96 h exposure[a], 120 h exposure[a]	24 h exposure[a], 48 h exposure[a], 72 h exposure[a], 96 h exposure[a], 120 h exposure[a]	24 h exposure[a], 48 h exposure[a], 72 h exposure[a], 96 h exposure[a], 120 h exposure[a]	24 h exposure[a], 48 h exposure[a], 72 h exposure[a]		24 h exposure[a], 48 h exposure[a], 72 h exposure[a]	96 hpf zebrafish embryo and adult female zebrafish
bromoxynil	0.60 (0.37)[b] 3.3 (0.6)[b] 7.8 (1.5)[b] 15 (2)[b]	1.71 (1.02)[b] 11 (1)[b] 30 (5)[b] 67 (12)[b]	0.23 (0.23)[b] 1.03 (0.06)[b] 1.47 (0.08)[b] 1.82 (0.08)[b]	0.17 (0.38)[b] 0.88 (0.17)[b] 1.29 (0.26)[b]	2.34 (0.11)	0.40 (0.14)[b] 1.25 (0.14)[b] 1.60 (0.10)[b]	2.6
paroxetine	13 (6)[b] 34 (6)[b] 39 (9)[b] 71 (12)[b] 92 (17)[b]	36 (15)[b] 113 (15)[b] 148 (32)[b] 323 (59)[b] 511 (95)[b]	1.56 (0.18)[b] 2.05 (0.06)[b] 2.17 (0.09)[b] 2.51 (0.08)[b] 2.71 (0.08)[b]	1.58 (0.23)[b] 2.14 (0.08)[b] 2.25 (0.18)[b]	2.26 (0.12)	1.50 (0.29)[b] 1.76 (0.14)[b] 2.08 (0.10)[b]	1.8

sd: standard deviation; [a]Start of exposure 2 hpf; [b]No steady-state.

Influence of solvent type and extraction amount for the extraction of carbamzepine

Table S8. Extraction 3 embryos exposed for 96 h (start 1 hpf) to 24.0 mg/L carbamazepine with 1 mL solvent, n=4.

Extraction solvent	Carbamazepine ng/embryo (sd)
MeOH	23.5 (3.5)
ACN	21.9 (2.5)
Acetone	18.1 (3.3)

Table S9. Extraction with methanol of 3 embryos exposed for 48 h (start 1 hpf) to 26.6 mg/L carbamazepine with different solvent amounts, n=3.

Methanol amount (mL)	Carbamazepine ng/embryo (sd)
0.2	13.2 (1.2)
2	15.1 (5.6)
15	17.2 (1.9)

Mortality in the TK experiments

Table S10. Observed mortality in the TK experiments.

Substance	%mortality exposed embryos	%mortality control
4-iodophenol	3	2
diuron	13	17
carbamazepine	3	4
bromoxynil	6	0
paroxetine	4	4
1,2,4-tribromobenzen	1	0
2-ethylpyridine	3	3

Mode of action classification

The toxic ratios (baseline toxicity LC50/observed LC50) are often used as an indicator for a reactive, uncoupling, or specific mode of action. Compounds with a TR < 10 are considered as baseline toxic. A more precise estimation of baseline toxicity would relate the internal membrane concentration to the baseline internal membrane concentration of 226 mmol/kg lipid (e.g. Bittner et al.[32]). Therefore, measured internal concentrations are ideally required. If whole embryonic body concentrations are used, potential accumulation in the yolk may lead to an overestimation of internal concentration. Therefore, the baseline toxicity was calculated using the toxic ratio as well as the internal concentrations per kg lipid (extrapolated from the concentration where it was measured to the LC50, Table S11). No difference in classification was observed for neutral compounds except for Diuron. Only when using the internal concentration per lipid, diuron was classified as baseline toxic. However, the differences were moderate (TR of 12 versus 3.5). For ionic compounds using the regression equation for neutral compounds for the calculation of baseline toxicity resulted in high TRs (>100). However, when using the internal concentrations in the embryonic body, these compounds were shown indeed to rather represent baseline toxic compounds. Due to the moderate difference between the whole embryo and embryonic body concentrations, similar results and classifications were obtained regardless of whether whole embryo or embryonic body concentrations were used as reference (Table S12). Internal concentrations from 72 hpf were used as reference given that at this stage measurements of the embryonic body versus the whole embryo were possible. For neutral compounds, the internal concentration appears to be already in equilibrium at this state. For ionic compounds, the internal concentrations for comparison to baseline toxicity may be underestimated given that no equilibrium has been reached.

Table S11. Mode of action classification based on toxic ratios (TR) or internal concentrations. The baseline toxicity LC50 was estimated using the logD and the equation given in Klüver et al.[33] 2016. The internal concentration in relation to the lipid content was calculated as described in Bittner et al.[32] A compound was classified as baseline toxic in case of a TR<10 or if the internal concentration at the LC50 was within 10fold of 226 mmol/kg lipid. Internal concentrations were obtained from 72 h of exposure (74 hpf) given that at this stage data for both the embryonic body and the whole embryo were available (see corresponding Table S12 for estimations based on the whole embryo). *Calculation may not be valid given that the baseline toxicity regression has been established for neutral compounds and no steady-state was observed for the (mainly) ionic compounds.

Compound	Baseline toxicity LC50 [µM]	LC50 [µM]	Toxic ratio (Baseline toxicity/ LC50)	Classification as baseline toxic based on TR	Measured concentration in exposure solution for internal concentration analysis [µM]	Corresponding internal concentration Embryonic body [µM]	Extrapolated internal concentration at LC50 [µM]	LC50 [internal mmol/ kg Lipid]	Ratio 226 mmol/kg to internal concentration	Classification as baseline toxic based on internal concentration estimation
2-Ethylpyridine	2856	9300	0.31	x	844	233	2567	566	0.40	x
Carbamazepine	190	>511	<0.37	x	139	270	993	>219	<1.03	x
Diuron	328	27.1	12.1		17.2	184	290	63.9	3.53	x
4-Iodophenol	286	>22.7	<12.6	(x)	12.9	175	308	>67.8	<3.33	x
1,2,4-Tribromobenzene	6.06	>31.8	<0.19	x	1.1	994	28736	>6329	<0.04	x
Bromoxynil	6949*	27.1	256*		10.5	88.1	227	50.1	4.54	x
Paroxetine	15787*	30.4	519*		0.281	7.1	768	169	1.35	x

Table S12. Mode of action classification based on toxic ratios (TR) or internal concentrations. The table corresponds to Table S11, except that the whole embryo (embryonic body plus yolk) was used as the reference compartment for internal concentration determination.

Compound	Baseline toxicity LC50 [µM]	LC50 [µM]	Toxic ratio (Baseline toxicity/ LC50)	Classifi-cation as baseline toxic based on TR	Measured concentration in exposure solution for internal concentration analysis [µM]	Corresponding internal concentration Whole embryo [µM]	Extrapolated internal concentration at LC50 [µM]	LC50 [internal mmol/ kg Lipid]	Ratio 226 mmol/kg to internal concentra-tion	Classification as baseline toxic based on internal concentration estimation
2-Ethylpyridine	2856	9300	0.307	x	844	434	4782	1053	0.22	x
Carbamazepine	190	>511	<0.37	x	139	323	>1187	>262	<0.86	x
Diuron	328	27.1	12.1		17.2	71.2	112	24.7	9.2	x
4-Iodophenol	286	>22.7	<12.6	(x)	12.9	530	>933	>205	<1.1	x
1,2,4-Tribromobenzene	6.06	>31.8	<0.19	x	1.1	3800	>109854	>24197	<0.0093	x
Bromoxynil	6949*	27.1	256*		10.5	82.1	212	46.7	4.8	x
Paroxetine	15787*	30.4	519*		0.281	10.9	11.8	258	0.87	x

References

(1) Riemenschneider, C.; Seiwert, B.; Moeder, M.; Schwarz, D.; Reemtsma, T. Extensive Transformation of the Pharmaceutical Carbamazepine Following Uptake into Intact Tomato Plants. **2017**. https://doi.org/10.1021/acs.est.6b06485.

(2) Chemicalize - Instant Cheminformatics Solutions https://chemicalize.com/#/calculation (accessed Jul 12, 2019).

(3) Jones, O. A. H.; Voulvoulis, N.; Lester, J. N. Aquatic Environmental Assessment of the Top 25 English Prescription Pharmaceuticals. *Water Res.* **2002**, *36* (20), 5013–5022. https://doi.org/10.1016/S0043-1354(02)00227-0.

(4) Velki, M.; Di Paolo, C.; Nelles, J.; Seiler, T.-B.; Hollert, H. Diuron and Diazinon Alter the Behavior of Zebrafish Embryos and Larvae in the Absence of Acute Toxicity. *Chemosphere* **2017**, *180*, 65–76. https://doi.org/10.1016/j.chemosphere.2017.04.017.

(5) Machado, F.; Collin, L.; Boule, P. Photolysis of Bromoxynil (3,5-dibromo-4-hydroxybenzonitrile) in Aqueous Solution. *Pesticide Science*. 1995, pp 107–110. https://doi.org/10.1002/ps.2780450203.

(6) Cunningham, V. L.; Constable, D. J. C.; Hannah, R. E. Environmental Risk Assessment of Paroxetine. *Environ. Sci. Technol.* **2004**, *38* (12), 3351–3359. https://doi.org/10.1021/es035119x.

(7) Dürkop, K. Einflussfaktoren Auf Die Biotransformation von Metoprolol Im Zebrabärblingsembryo – Untersucht Mittels LC-MS, University Leipzig, 2016.

(8) Ulrich, N.; Endo, S.; Brown, T. N.; Watanabe, N.; Bronner, G.; Abraham, M. H.; Goss, K.-U. UFZ-LSER database v 3.2.1 [Internet], Leipzig, Germany, Helmholtz Centre for Environmental Research-UFZ http://www.ufz.de/lserd (accessed Aug 10, 2019).

(9) Brox, S.; Seiwert, B.; Haase, N.; Küster, E.; Reemtsma, T. Metabolism of Clofibric Acid in Zebrafish Embryos (Danio Rerio) as Determined by Liquid Chromatography-High Resolution-Mass Spectrometry. *Comp. Biochem. Physiol. Part - C Toxicol. Pharmacol.* **2016**, *185–186*, 20–28.

https://doi.org/10.1016/j.cbpc.2016.02.007.

(10) Halbach, K.; Wagner, S.; Scholz, S.; Luckenbach, T.; Reemtsma, T. Elemental Imaging (LA-ICP-MS) of Zebrafish Embryos to Study the Toxicokinetics of the Acetylcholinesterase Inhibitor Naled. *Anal. Bioanal. Chem.* **2019**, *411* (3), 617–627. https://doi.org/10.1007/s00216-018-1471-2.

(11) Pardo-Martin, C.; Chang, T. Y.; Koo, B. K.; Gilleland, C. L.; Wasserman, S. C.; Yanik, M. F. High-Throughput in Vivo Vertebrate Screening. *Nat. Methods* **2010**, *7* (8), 634–636. https://doi.org/10.1038/nmeth.1481.

(12) Berthold, M. R.; Cebron, N.; Dill, F.; Gabriel, T. R.; Kötter, T.; Meinl, T.; Ohl, P.; Sieb, C.; Thiel, K.; Wiswedel, B. KNIME: The Konstanz Information Miner. In *Data Analysis, Machine Learning and Applications: Proceedings of the 31st Annual Conference of the Gesellschaft für Klassifikation e.V., Albert-Ludwigs-Universität Freiburg, March 7–9, 2007*; Preisach, C., Burkhardt, H., Schmidt-Thieme, L., Decker, R., Eds.; Springer Berlin Heidelberg: Berlin, Heidelberg, 2008; pp 319–326.

(13) Bittner, L.; Klüver, N.; Henneberger, L.; Mühlenbrink, M.; Zarfl, C.; Escher, B. I. Combined Ion-Trapping and Mass Balance Models To Describe the PH-Dependent Uptake and Toxicity of Acidic and Basic Pharmaceuticals in Zebrafish Embryos (Danio Rerio). *Environ. Sci. Technol.* **2019**, acs.est.9b02563. https://doi.org/10.1021/acs.est.9b02563.

(14) Lee, R. F.; Phleger, C. F.; Horn, M. H. Composition of Oil in Fish Bones: Possible Function in Neutral Buoyancy. *Comp. Biochem. Physiol. -- Part B Biochem.* **1975**, *50* (1), 13–16. https://doi.org/10.1016/0305-0491(75)90291-6.

(15) Nichols, J. W.; Schultz, I. R.; Fitzsimmons, P. N. In Vitro-in Vivo Extrapolation of Quantitative Hepatic Biotransformation Data for Fish. I. A Review of Methods, and Strategies for Incorporating Intrinsic Clearance Estimates into Chemical Kinetic Models. *Aquatic Toxicology*. June 10, 2006, pp 74–90. https://doi.org/10.1016/j.aquatox.2006.01.017.

(16) Péry, A. R. R.; Devillers, J.; Brochot, C.; Mombelli, E.; Palluel, O.; Piccini, B.; Brion, F.; Beaudouin,

R. A Physiologically Based Toxicokinetic Model for the Zebrafish Danio Rerio. *Environ. Sci. Technol.* **2014**, *48* (1), 781–790. https://doi.org/10.1021/es404301q.

(17) Petersen, G. I.; Kristensen, P. Bioaccumulation of Lipophilic Substances in Fish Early Life Stages. *Environ. Toxicol. Chem.* **1998**, *17* (7), 1385–1395. https://doi.org/10.1002/etc.5620170724.

(18) Chizinski, C. J.; Sharma, B.; Pope, K. L.; Patiño, R. A Bioenergetic Model for Zebrafish Danio Rerio (Hamilton). *J. Fish Biol.* **2008**, *73* (1), 35–43. https://doi.org/10.1111/j.1095-8649.2008.01900.x.

(19) Vutukuru, S. S.; Basani, K. Acute Effects of Mercuric Chloride on Glycogen and Protein Content of Zebra Fish, Daniorerio. *J. Environ. Biol.* **2013**, *34* (2), 277–281.

(20) Sancho, E.; Villarroel, M. J.; Fernández, C.; Andreu, E.; Ferrando, M. D. Short-Term Exposure to Sublethal Tebuconazole Induces Physiological Impairment in Male Zebrafish (Danio Rerio). *Ecotoxicol. Environ. Saf.* **2010**, *73* (3), 370–376. https://doi.org/10.1016/j.ecoenv.2009.09.020.

(21) Siccardi, A. J.; Padgett-Vasquez, S.; Garris, H. W.; Nagy, T. R.; D'Abramo, L. R.; Watts, S. A. Dietary Strontium Increases Bone Mineral Density in Intact Zebrafish (Danio Rerio): A Potential Model System for Bone Research. *Zebrafish* **2010**, *7* (3), 267–273. https://doi.org/10.1089/zeb.2010.0654.

(22) James Henderson, R.; Tocher, D. R. The Lipid Composition and Biochemistry of Freshwater Fish. *Progress in Lipid Research*. 1987, pp 281–347. https://doi.org/10.1016/0163-7827(87)90002-6.

(23) Endo, S.; Brown, T. N.; Goss, K.-U. General Model for Estimating Partition Coefficients to Organisms and Their Tissues Using the Biological Compositions and Polyparameter Linear Free Energy Relationships. *Environ. Sci. Technol.* **2013**, *47* (12), 6630–6639. https://doi.org/10.1021/es401772m.

(24) Kimmel, C. B.; Ballard, W. W.; Kimmel, S. R.; Ullmann, B.; Schilling, T. F. Stages of Embryonic Development of the Zebrafish. *Dev. Dyn.* **1995**, *203*, 253–310.

(25) Miyares, R. L.; de Rezende, V. B.; Farber, S. A. Zebrafish Yolk Lipid Processing: A Tractable Tool for the Study of Vertebrate Lipid Transport and Metabolism. *Dis. Model. Mech.* **2014**, *7* (7), 915–927. https://doi.org/10.1242/dmm.015800.

(26) Fagotto, F. Regulation of Yolk Degradation, or How to Make Sleepy Lysosomes. *J. Cell Sci.* **1995**, *108*, 3645–3647.

(27) Mölich, A.; Heisler, N. Determination of PH by Microfluorometry: Intracellular and Interstitial PH Regulation in Developing Early-Stage Fish Embryos (Danio Rerio). *J. Exp. Biol.* **2005**, *208* (21), 4137–4149. https://doi.org/10.1242/jeb.01878.

(28) Siméon, S.; Brotzmann, K.; Fisher, C.; Gardner, I.; Silvester, S.; Maclennan, R.; Walker, P.; Braunbeck, T.; Bois, F. Y. SI: Development of a Generic Zebrafish Embryo PBPK Model and Application to the Developmental Toxicity Assessment of Valproic Acid Analogs. *Reprod. Toxicol.* **2020**, *93*, 219–229. https://doi.org/10.1016/j.reprotox.2020.02.010.

(29) Siméon, S.; Brotzmann, K.; Fisher, C.; Gardner, I.; Silvester, S.; Maclennan, R.; Walker, P.; Braunbeck, T.; Bois, F. Y. Development of a Generic Zebrafish Embryo PBPK Model and Application to the Developmental Toxicity Assessment of Valproic Acid Analogs. *Reprod. Toxicol.* **2020**, *93* (February), 219–229. https://doi.org/10.1016/j.reprotox.2020.02.010.

(30) Bittermann, K.; Goss, K. U. Predicting Apparent Passive Permeability of Caco-2 and MDCK Cell-Monolayers: A Mechanistic Model. *PLoS One* **2017**, *12* (12). https://doi.org/10.1371/journal.pone.0190319.

(31) Maas, H. Wovon Ist Die Aufnahme in Den Zebrabärblingsembryo Abhängig - Untersuchung Zu Neutralen Substanzen Analysiert Mittels LC-MS, 2016.

(32) Bittner, L.; Teixido, E.; Seiwert, B.; Escher, B. I.; Klüver, N. Influence of PH on the Uptake and Toxicity of B-Blockers in Embryos of Zebrafish, Danio Rerio. *Aquat. Toxicol.* **2018**, *201*, 129–137. https://doi.org/10.1016/j.aquatox.2018.05.020.

(33) Klüver, N.; Vogs, C.; Altenburger, R.; Escher, B. I.; Scholz, S. Development of a General Baseline Toxicity QSAR Model for the Fish Embryo Acute Toxicity Test. *Chemosphere* **2016**, *164*, 164–173. https://doi.org/10.1016/j.chemosphere.2016.08.079.

Chapter 5 Zebrafish Oatp1d1 acts as cellular efflux transporter of bromoxynil

Katharina Halbach, Silke Aulhorn, Oliver Lechtenfeld, Marion Lecluse, Sophia Leippe, Bettina Seiwert, Stephan Wagner, Thorsten Reemtsma, Jörg König, Till Luckenbach

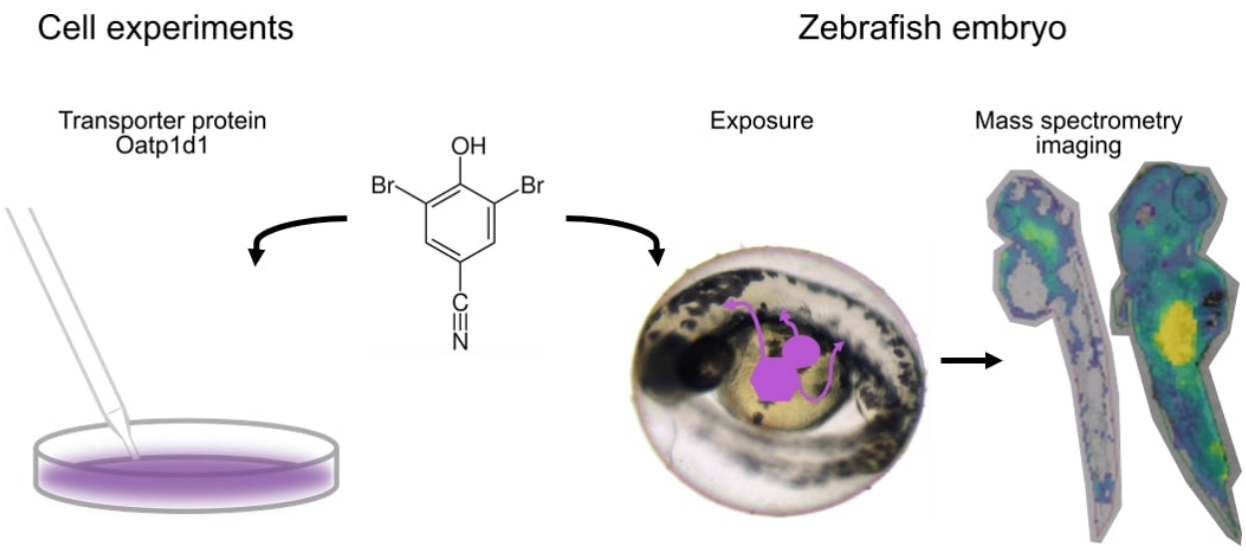

In preparation

Author's contribution:

The idea and the concept to study the spatial distribution of bromoxynil was developed by me. The hypothesis of the involvement of the organic anion transporter was developed by T. Luckenbach and me. The choice for Oatp1d1 was made together with T. Luckenbach and J. König. The cell experiments were carried out by J. König. The sample preparation and measurements of the cell samples were conducted by B. Seiwert and me. The exposure experiments were carried out by me, M. Lecluse, and S. Aulhorn. LA-ICP-MS measurements were performed by M. Lecluse with my assistance and of S. Wagner. S. Leippe conducted the MALDI-MS imaging experiments with the help of O. Lechtenfeld and myself. Data analysis was carried out by me, M. Lecluse, and S. Leippe. As the first author, I wrote the manuscript. The structure and discussion were finalized with the help of T. Luckenbach and J. König at the current status.

Abstract

We previously discovered that the accumulation of the anionic herbicide bromoxynil in the embryonic body of zebrafish embryos was high in comparison to the yolk compartment. This was in contrast to other tested compounds that showed higher accumulation in the yolk. Furthermore, there were indications that beyond passive diffusion, other processes are involved in the uptake kinetics of bromoxynil. Using mass spectrometry imaging, we here measured comparatively high bromoxynil levels in the gastrointestinal tract and found its presence also in the head region of zebrafish embryos. In these tissues, uptake and efflux of chemicals are driven by several cellular transporter types, such as the cellular uptake transporter Oatp1d1, known to be expressed in zebrafish embryos and to transport environmentally relevant chemicals. In zebrafish Oatp1d1 transfected HEK293 cells, the transition of bromoxynil and diclofenac, a known Oatp1d1 substrate, across the cellular membrane was enhanced compared to mock-transfected control cells; however, strikingly, not cellular uptake but efflux were increased. For carbamazepine, previously shown to only weakly interact with zebrafish Oatp1d1, no difference between Oatp1d1-transfected and control cells was found. In zebrafish embryo exposure experiments, accumulation of the test compounds in the tissue was enhanced when the Oatp1d1-inhibitor bromosulfophthalein (BSP) was also present, indicating inhibition of efflux activity by BSP. In more advanced developmental stages, accumulation of bromoxynil and diclofenac was enhanced, which may be related to increased functionality of transporter proteins or development-specific sorption property changes. The action of Oatp1d1 as efflux transporter of environmental compounds in zebrafish embryos is novel and should be considered in analyses of absorption, distribution, metabolism, and elimination (ADME) processes.

Keywords: Organic anion transporting polypeptide, zebrafish embryo, MALDI-MS imaging, LA-ICP-MS, toxicokinetics

Introduction

The zebrafish embryo is widely used as an alternative model for chemical testing in toxicology and pharmacology[1,2]. The toxicities of chemicals to zebrafish embryos and adult fish generally correlate to a high degree[3]. Zebrafish embryos are therefore suggested as a replacement for adult fish in toxicity testing. However, there are also considerable discrepancies in toxicities of chemicals with certain modes of action in zebrafish embryos and adult fish, such as for neuroactive compounds[4]. Fish embryo and adult stages differ to a large extent regarding morphology and cell differentiation, and physiology, which may affect toxicokinetics. We recently showed for various chemicals that they accumulated to a large extent - up to 95% depending on the compound and the embryo stage - in the yolk of zebrafish embryos[5]. This predominant presence of the accumulated chemicals in the yolk, a compartment absent in adult fish, indicates differences in the distribution of chemicals and suggests that the chemical levels at target sites may differ in embryo and adult stages. Potentially, this could be a reason for differing toxicities in the different stages.

In contrast to the other studied chemicals that accumulated to a higher degree in the yolk, the levels of the anionic bromoxynil were similar in the embryonic body and the yolk of the embryos upon 48 h of exposure; after 72 h, 67% of bromoxynil accumulated in the embryonic body.[5]

For neutral compounds, the predictions of the uptake kinetics in zebrafish embryos, taking into account passive diffusion and an aqueous boundary layer, corresponded to the measured data.[5] In contrast, measured and predicted uptake kinetics of the ionic compounds bromoxynil and paroxetine considerably differed. This indicates that the uptake kinetics of these compounds are majorly influenced by other processes than the ones considered in the prediction model. These could be biological processes, such as activities of cellular transporter proteins, biotransformation processes, and developmental differentiation resulting in a morphological reorganization, such as the opening of the gastrointestinal (GI) tract.

It was previously observed that the uptake of several ions by zebrafish embryos proceeds at a particularly slow pace.[5–8] The slow uptake kinetics of perfluorinated alkyl acids that were modeled with a two-compartment model were explained by the presence of an uptake barrier. It was suggested that such a barrier might be formed by the chorion enclosing the embryo.[6] The chorion as an uptake barrier could, however, be excluded for bromoxynil and paroxetine.[5]

In this study, we investigated the distribution of bromoxynil in the embryonic body intending to determine potential tissue-specific affinities. Such information may provide insights that could explain why measured and predicted uptake kinetics of bromoxynil in zebrafish embryos differ.

For certain compounds, uptake is not only driven by passive diffusion but can also be dominated by active cellular uptake or expulsion processes. This was, e.g., shown for certain fluorescent dyes that in zebrafish embryos were effluxed by the ATP-binding cassette (ABC) transporter Abcb4[9]. Also, the accumulation of cocaine and meta-chlorophenylpiperazine, positively charged psychoactive substances, in zebrafish embryos were hypothesized to be mediated by cellular uptake transporter proteins[10]. Indeed, a range of environmental compounds was shown to interact with uptake transporters Oatp1d1[11] and Oat2a-e[12] from zebrafish, organic anion transporters from the SLC (Solute carriers) superfamily, in cellular tests.

We investigated here whether the activity of the uptake transporter Oatp1d1 explains the uptake kinetics and distribution of the anionic environmental contaminant bromoxynil in zebrafish embryos. This transporter was considered potentially relevant. It was found that environmental contaminants act as Oatp1d1 substrates and that Oatp1d1 is expressed in zebrafish embryos from 24 hours post fertilization (hpf) on[13].

Using mass spectrometry (MS) imaging, we investigated the spatial distribution of accumulated bromoxynil in zebrafish embryos and the interaction of the compound with zebrafish Oatp1d1. These examinations were performed with cellular assays using Oatp1d1 overexpressing cells and with zebrafish embryos, using Oatp1d1 inhibiting compounds. For comparison, we included diclofenac and carbamazepine in the Oatp1d1 experiments. Diclofenac, a substrate of Oatp1d1[11], has a similar pKa (pKa=3.99[14]) as bromoxynil (pKa=3.75[15]), and more than 99.9% are anionic at pH=7.4 of the zebrafish embryo exposure medium. The uptake kinetics of diclofenac were also shown to be slow/continuous.[16] Carbamazepine was included as a neutral compound having no or minor interactions with Oatp1d1.[11]

Materials and methods

Chemicals

For experiments with cells and zebrafish embryos, the following chemicals were used for the exposure and incubation experiments: bromoxynil (CAS 1689-84-5, Seelze, Sigma-Aldrich), bromosulfophthalein (BSP, CAS 71-67-0, Cayman chemical), [^{3}H]-BSP (Hartmann Analytic, Braunschweig, Germany), carbamazepine (CAS 298-46-4, ICN Biomedicals), cyclosporin A (CsA, CAS 59865-13-3), diclofenac sodium salt (CAS 15307-79-6, Sigma-Aldrich). Chemicals were directly dissolved in ISO-water[17] for the exposure experiments of the zebrafish embryos.

For uptake quantification with ultraperformance liquid chromatography quadrupole-time-of-flight MS (UPLC-QToF-MS) and MS-imaging measurements with zebrafish embryos additionally, the following chemicals were used: bromoxynil-d2 (CAS 1219798-95-4, NEOCHEMA), diclofenac-d4 (CAS 153466-65-0, HPC standards), carbamazepine-d10 (CAS 132183-78-9, Sigma-Aldrich), 9-aminoacridine (9-AA, CAS 90-45-9, Sigma-Aldrich), Neg50 (Thermo Scientific).

Culture of zebrafish, collection of eggs, and culture of embryos

We used the UFZ-OBI/WIK zebrafish strain (generation F3-4), obtained originally from a local breeder and kept for several generations at the UFZ. Adult zebrafish were maintained and bred according to standard protocols[18]. Collection of eggs and culturing of the embryos were performed as described[19]. Fish were cultured and used according to German and European animal protection standards and approved by the Government of Saxony, Landesdirektion Leipzig, Germany (Aktenzeichen 75-9185.64).[20]

Uptake kinetics experiments with zebrafish embryos

Zebrafish embryos at minimum 4-cell stage (circa 1 hpf) were selected after spawning and transferred with 50 µL ISO-water (100 µL in case of 72 hpf embryos) into the exposure solution. At the end of each exposure, effects were recorded according to OECD 236[21] (see Table 1, S4, S5, and S6). Three pooled embryos were transferred together in one Fast-Prep tube filled with glass beads, were quickly washed twice with 1 mL Milli-Q water, excess water was removed, and tubes were snap-frozen in liquid N_2. Three replicates were taken per treatment. At the start and end of each exposure, aliquots from the exposure solutions were taken and frozen until analysis. Results of the measured exposure concentrations can be found in Table S2.

Nominal exposure concentrations corresponding to EC5 and EC25 values were 6.76 and 11.1 µM for bromoxynil, 4.63 and 5.24 µM for diclofenac[22], and 231 and 259 µM[23] for carbamazepine. Fish

embryo toxicity (FET) test dose-response curves for BSP and bromoxynil are depicted in Figure S1. BSP concentrations were set to 50 and 100 µM corresponding to 20 and 40-times the Km-value from cell experiments (Figure S3). These BSP concentrations were in the sublethal range of BSP when singly applied (refer to the FET test dose-response curve for BSP in Figure S1) and caused a reduced hatching rate.

Each exposure experiment was conducted in two independent exposures with embryos from separate egg batches. In experiment 1, embryos at 1±1 hpf were exposed for 96 h; in experiment 2, embryos at 1±1 hpf and 72±1 hpf, respectively, were exposed for 24 h; in experiment 3, embryos at 1±1 hpf were exposed for 96 h and embryos at 1±1 hpf and 72±1 hpf, respectively, for 24 h. In the following, the 24 h exposure scenarios are termed either 24 h – 1 hpf or 24 h – 72 hpf. For an overview of exposure experiments and applied concentrations, refer to Table S1. Embryos without any or minor effects on the phenotype were used for internal concentrations. In order to ensure this, more replicates than three (Table S1) were conducted per experiment. In addition, one experiment of mixed exposure to diclofenac and bromoxynil over 96 h (start at 1±1 hpf) was performed with five replicates à three embryos for the EC5 and 7 replicates à three embryos for the EC25 experiment. For each treatment, blind controls (exposure solution without embryos) were run in parallel, and aliquots were sampled to monitor the compound's stability. The stability of BSP was monitored via ultraviolet-visible spectroscopy (UVIKON 923, Bio-Tek Kontron Instruments, results in Figure S2).

MS imaging experiments with zebrafish embryos

LA-ICP-MS imaging sample preparation and measurements

Zebrafish embryos at 1 hpf were exposed for 96 h to bromoxynil at 6.8 µM (≙EC5), and they were washed twice with 1 mL Milli-Q water after the exposure. The embryos were then mounted on glass slides with NEG-50 and dried at room temperature in a desiccator. LA-ICP-MS imaging measurements were carried out with a laser (193 nm ArF laser, Analyte G2, Teledyne CETAC Technologies, USA) coupled to a double-focusing sector field ICP-MS (Spectro, Ametek, Germany) with a Mattauch-Herzog geometry[24]. 50 µM spot size was chosen. The following ICP-MS settings were used: 1000 W radiofrequency power, 12 L/min plasma gas (argon), 2.3 L/min auxiliary gas (argon), 1 s integration time with a base interval of 100 ms. The following laser parameters were applied: 100 Hz laser frequency, 50 µm/s scan speed, 1.65 J/cm^2 fluence. ^{13}C, ^{12}C, ^{79}Br, and ^{81}Br were measured. Results for ^{13}C and ^{79}Br are reported. Background intensities of ^{79}Br in a zebrafish embryo exposed for 96 h to ISO-water are shown in Figure S11.

LA-ICP-MS imaging data were analyzed with Iolite 3.6 in Igor Pro 7.04. Exported data were overlaid with the optical microscopic image in MATLAB R2015b.

MALDI-FT-ICR-MS imaging sample preparation and measurements

The spatial distribution of bromoxynil in the zebrafish embryo was imaged using matrix-assisted laser desorption/ionization coupled to a Fourier transform ion cyclotron resonance mass spectrometer (MALDI-FT-ICR-MS) and laser ablation inductively coupled plasma MS (LA-ICP-MS). For preparation, zebrafish embryos at 1 hpf were exposed to bromoxynil at 6.8 µM (≙EC5) for 72 h and were washed twice with 1 mL Milli-Q water after the exposure. Using a plastic pipette, the embryos were first carefully placed in NEG50 and moved through it to completely cover the embryo with it, remove excess water, and then transferred to a cryomold containing NEG50. The cryomolds with the embryos were immediately placed on dry ice and frozen, wrapped in aluminum foil, and stored until sectioning at -80 °C. 24 h prior to sectioning, the cryomolds were placed in a microtome (Cryo-Star HM 560, Microm International, Walldorf, Germany) at -17 °C. Twelve µM sections were cut and transferred to an ITO-coated glass slide (Bruker, Bremen, Germany). The sections were attached to the slide by carefully warming the glass slide with the hand. Glass slides were dried and stored for a maximum of 5 days in a desiccator at 200-300 mbar. Prior to analysis, marks were drawn onto the glass slides with a white pen, and the slides were weighed and scanned (OpticLab H580, Plustek, Ahrensfelde, Germany). The organic matrix molecule 9-AA was applied with a sublimation device. A sand bath to heat the sublimation device was heated for 1 h at 150 °C, and then 300 mg of 9-AA were filled into the sublimation device, and the slide was mounted with a double-sided adhesive tape. Ice was filled in the top chamber. A vacuum was applied, and a pressure of 2-5 mbar was measured. After 30 min the sublimation was stopped. Slides were weighed again (results were 91 and 117 µg/cm^2 9-AA).

MALDI-MS imaging measurements were carried out with a MALDI ion source (1kHz Laser of 335 nm, Smartbeam II, Bruker Daltonics, Bremen, Germany) coupled to an FT-ICR-MS (solarix XR 12T, Bruker Daltonics, Bremen, Germany). Parameter setting and measurement were conducted with ftms Control Software (Bruker Daltonics, Bremen, Germany) and teaching of the position with Flex Imaging Software (Bruker Daltonics, Bremen, Germany). Bromoxynil was measured in negative mode with 15% laser power, 500 shots, 1000 Hz, minimum laser focus, 25 µM raster width, and applied isolation windows (m/z 283 ± 20, 308 ± 30, 335 ± 20, 365 ± 36, 392 ± 13, 414 ± 26, 436 ± 14, 458 ± 26, 484 ± 22, 505 ± 16, 540 ± 50, 592 ± 50, 618 ± 2). The isolation windows were chosen in order to detect bromoxynil and previously reported[5] transformation products. Bromoxynil was detected as $[M-H]^-$ (275.84671 m/z ± 0.19313 mDa). Bromoxynil was

confirmed by the detection of the three most abundant isotope peaks (273.84877 m/z ± 0.30818 mDa, 275.84671 m/z ± 0.19313 mDa, 277.8447 m/z ± 0.27828 mDa, Figure S10).

Data were analyzed with SCiLs Lab 2017. Weak denoising, hotspot removal, and total ion count normalization were applied.

Cell experiments

Cloning of zebrafish Oatp1d1

The cDNA encoding zebrafish Oatp1d1 (*drSlco1d1*) was cloned by a reverse transcriptase polymerase chain reaction-based approach using the primer oOatp1d1-5'for (5´-gga cac cat gag tac gga gaa-3') and oOatp1d1-RT.rev (5´-gcc tgc agg act tca gat gg-3') and zebrafish liver total RNA as a template. The amplified fragment was cloned into the cloning vector pCR2.1.TOPO (Thermo Fisher Scientific) and finally subcloned into the expression vector pcDNA3.1(+) (Thermo Fisher Scientific), resulting in the plasmid pOatp1d1.31. The sequence was verified, and base pair exchanges (compared to the reference sequence NM_001348986.1[25]) resulting in amino acid exchanges after translation were corrected by site-directed mutagenesis. The final cDNA encodes for an Oatp1d1 protein 100% identical to the protein encoded by the reference sequence.

Cell culture and transfection

Human embryonic kidney (HEK293) cells were cultured in minimal essential medium containing 10% heat-inactivated fetal bovine serum, 100 U/mL penicillin, and 100 µg/mL streptomycin at 37 °C and 5% CO_2. The cells were routinely cultivated by trypsinization. HEK293 cells were transfected with the plasmid pOatp1d1.31 using Effectene transfection reagent (Qiagen GmbH). After geneticin (G418, 800 µg/mL) selection, single colonies were characterized for *drSlco1d1* expression by real-time PCR. The clone (HEK-drOatp1d1) with the highest *drSlco1d1* expression (related to the expression of the housekeeping gene *ß-actin*) was selected for further transport experiments.

Uptake and inhibition assays

Uptake and inhibition assays were conducted for two independent replicates (at least one day between experiments) with three replicates per treatment. For uptake and inhibition assays, 7 x 10^5 HEK-drOatp1d1 and the same amount of the respective control cells (HEK-Co; transfected with the empty vector pcDNA3.1(+) and selected under the same conditions) were seeded in poly-D-lysine coated 12-well plates (Sarstedt). The cells were cultured for 24 h and induced with 10 mM sodium butyrate for an additional 24 h.

Before the uptake experiments, the cells were washed with prewarmed (37 °C) uptake buffer (142 mM NaCl, 5 mM KCl, 1 mM K_2HPO_4, 1.2 mM $MgSO_4$, 1.5 mM $CaCl_2$, 5 mM glucose, and 12.5 mM HEPES pH 7.3). The test compounds bromoxynil, diclofenac, carbamazepine, and BSP as Oatp1d1 specific substrate were dissolved in uptake buffer at the desired concentrations, and the cells were incubated with this solution for 10 min as described previously[26]. Radioactively labeled [^{3}H]BSP served as a positive control for an Oatp1d1 substrate. Unlabeled BSP at 50 µM and 100 µM (20 and 40-times the Km-value in HEK-Oatp1d1 cells, Figure S3) was used as an inhibitor. Bromoxynil, diclofenac, and [^{3}H]BSP were also applied together with the Oatp1d1 inhibitor CsA at 5 µM. Additionally, a mixed incubation experiment with bromoxynil and diclofenac at 10 or 100 µM each was performed. Table S3 gives an overview of the different chemical concentrations applied in the different experiments. Upon exposure, the cells were washed three times with an ice-cold uptake buffer and lyzed with 80% methanol. The substrate's intracellular accumulation was measured by UPLC-QToF-MS measurements (see next section) or by liquid scintillation counting. The protein concentration in each extract was determined as a reference point by the bicinchoninic acid assay (BCA Protein Assay Kit).

The net transport of test chemicals in the cells was calculated as the difference of accumulation rate of the chemical in the Oatp1d1 cells and the vector control cells.

UPLC-QToF-MS sample preparation and measurement

Embryos were extracted with 500 µL methanol containing the deuterated internal standard. Extraction was performed by placing the samples in an ultrasonic bath at room temperature for 15 min, shaking the sample for 15 min, and then centrifuging for 15 min at 13 rpm. The supernatant was taken and diluted with Milli-Q to 50:50 Milli-Q/methanol (v/v). Samples were stored at -20 °C until measurement.

Lysed cells were centrifuged (15 min at 13 rpm) and diluted with Milli-Q water (with dissolved internal standards), yielding 50:50 (v/v) Milli-Q/methanol at the day of measurement.

Details of bromoxynil and carbamazepine measurements can be found in Halbach et al.[5] Diclofenac was measured with the same method parameters as bromoxynil and detected in negative mode (m/z 250.019 at 10.60 min, d4-diclofenac m/z 254.045 at 10.58 min).

Data analysis

Data were plotted with R 4.0.3. Permutation tests (Manly's, 5000 repetitions) were carried to test for statistical significance when two independent experiments were performed. The experiment and the treatment were taken as categorical variables.

Results

Spatial distribution of bromoxynil in zebrafish embryos

Imaging of tissue areas with bromoxynil was performed with MALDI-FT-ICR-MS and LA-ICP-MS with zebrafish embryos exposed to bromoxynil only. A bromine signal detected with LA-ICP-MS was comparatively strong in the region of the gastrointestinal (GI) tract (Figure 1); a low-intensity signal occurred in the head region. It was shown before that bromoxynil is metabolized in the embryo[5]; the bromine signal thus represents not only the parent compound but also all possible bromine-containing transformation products of bromoxynil. The accumulation of bromoxynil in the GI tract was confirmed by the MALDI-MS imaging results, which also indicated accumulation of the compound in the head region (Figure 2); the signal intensity of bromoxynil in the GI tract is about twice as high as the signal intensity in the head region.

Cellular uptake experiments

The zebrafish Oatp1d1-mediated uptake of test compounds was investigated in experiments with transfected HEK cells compared to vector-transfected cells as controls (HEK-Co). Radiolabeled BSP was used as a positive control in the uptake assays because it is a known substrate of Oatp1d1[27]. The uptake (in nmol/mg protein/min) of [^{3}H]BSP by the Oatp1d1-cells was significantly enhanced compared to the HEK-Co cells (Figure 3). The Oatp1d1 transporter in the transfected cells caused a net uptake of 43 pmol x mg protein^{-1} x min^{-1} at 1 µM incubation. In contrast, Oatp1d1 prevented the cellular uptake of bromoxynil and diclofenac; the uptake was significantly lower in Oatp1d1-cells compared to the HEK-Co cells (Figures 3). At a concentration of 10 µM in the medium, the Oatp1d1-mediated efflux rate of bromoxynil and diclofenac was -5 and -6 pmol x mg protein^{-1} x min^{-1}, respectively, and 4- to 5-fold higher at a higher incubation concentration (Figure S4). No difference was seen between Oatp1d1- and HEK-Co-cells for carbamazepine, indicating no Oatp1d1 mediated transport of this compound under the chosen test conditions (Figures 3 and S4).

The effect of the addition of unlabeled BSP on the cellular uptake of the test compounds was investigated. BSP being an Oatp1d1 substrate acts as a competitive inhibitor of Oatp1d1-mediated transport. In the treatments with unlabeled BSP at 50 or 100 µM applied together with 1 µM [^{3}H]BSP, the values for net-uptake of [^{3}H]BSP were significantly lower than in the 1 µM [^{3}H]BSP treatment without unlabeled BSP (Figure 4). The differences between treatments without unlabeled BSP and with 50 or 100 µM unlabeled BSP added were highly statistically significant, despite a large variation (~3-fold) among replicate experiments in the treatment without unlabeled BSP. The

net accumulation rate values in the treatments with 50 or 100 µM unlabeled BSP were close to zero because uptake of [^{3}H]BSP in the Oatp1d1- and HEK-Co-cells was almost equal.

The generally negative accumulation rates in the bromoxynil, diclofenac, and carbamazepine experiments show that accumulation of the test compounds was higher in the HEK-Co- than in the Oatp1d1-cells. Data of these compounds in the mixed incubation with BSP varied largely, indicated by both large standard deviations within replicate experiments and variations between replicate experiments. In the experiments with bromoxynil and diclofenac, the results are therefore ambiguous, and trends are not statistically significant (Figure 4 and S5). In the bromoxynil experiment, the replicates of the treatment without BSP differed by about three-fold, and the data for the bromoxynil-BSP combinations were within the range of the treatment with bromoxynil only. However, cellular accumulation rates for bromoxynil combined with 100 µM BSP were two- to three-times lower than when bromoxynil was combined with 50 µM BSP, which could point to an effect of BSP on the efflux of bromoxynil, resulting in enhanced accumulation of the compound in the cells. Similarly, in the diclofenac experiment, the treatment replicates without BSP considerably varied. In the carbamazepine experiment, however, the data for the treatment replicates varied to a smaller extent (Figure 4 and S5). Values for the treatments with BSP are lower than for the treatment without BSP; the difference is statistically significant for the treatment with 100 µM BSP (Figure S5). An export of up to -9 pmol x mg protein^{-1} x min^{-1} at 100 µM incubation was observed.

Additionally, experiments were performed in which CsA, an inhibitor of different cellular transporters including Oatp1d1, was applied in combination with [^{3}H]BSP, bromoxynil, and diclofenac, respectively. While the net cellular uptake of [^{3}H]BSP was significantly reduced in the presence of CsA, no CsA effect was observed on the cellular levels of bromoxynil and diclofenac (Figure S6).

The mixed incubation of the cells with bromoxynil and diclofenac showed a decreasing Oatp1d1-mediated export of the respective other compound (Figure S7).

Toxicokinetic experiments in the zebrafish embryo

Measurements of internal concentrations and toxicity of the substances bromoxynil, diclofenac, and carbamazepine were conducted by exposing embryos to the EC5 and EC25 values of the respective substance and adding two concentrations of the Oatp1d1-substrate BSP as an inhibitor. Toxicity and internal concentrations were examined in an exposure of 96 h. Additionally, the

influence of the developmental stage was investigated in a shorter exposure time of 24 h starting at 1 hpf and 72 hpf.

Toxicity

At single compound exposures, BSP and carbamazepine showed only the effect of delayed or no hatching within the exposure period of 96 h (Table 1). Bromoxynil and diclofenac showed other effects on the phenotype, such as missing heartbeat and edemas. Increased toxicity was observed for both added BSP concentration to the bromoxynil and diclofenac exposures (EC5 and EC25, Table 1). Observed effects were, e.g., missing heartbeats, coagulation, no blood circulation, and edemas (Figure S8). At the EC25 exposure of diclofenac and bromoxynil with the addition of 100 µM BSP, 100% of the embryos were adversely affected after 96 h in both experiments (for diclofenac also at the EC5 exposure with 100 µM BSP). The mixture of carbamazepine and BSP only showed an increased number of not hatched embryos (Table 1). The mixture of diclofenac and bromoxynil (both EC5 and EC25, Table S6) increased the number of affected embryos (about double), and similar sublethal/lethal effects were observed as single compound exposures.

Nearly no effects for shorter exposures were observed for the exposure to bromoxynil, diclofenac, and carbamazepine (Tables S2 and S3). Carbamazepine exposures decreased the movement of the embryos at shorter exposures of the older stage at single compound exposure and in the mixture with BSP.

Internal concentration

In addition to the observation of effects on the phenotype, internal concentrations were measured of bromoxynil, diclofenac, and carbamazepine (Figure 5). At the long exposure time (96 h), observed high mortality in the cases of bromoxynil and diclofenac in the mixture exposure with BSP led to a reduced number of samples for internal concentration measurements. Especially in the case of bromoxynil, interpretations are thus difficult. Because we observed increased toxicity specific for bromoxynil and not BSP, this suggests an increased internal concentration. Furthermore, our results showed a significantly increased internal concentration of diclofenac and carbamazepine with BSP addition. The internal concentrations of bromoxynil and diclofenac were also determined in mixed exposures with the respective other compound. Indications for an increased internal concentration of diclofenac and decreased internal concentrations of bromoxynil were obtained (Figure S9).

For the shorter exposure periods (24 h), an influence of the developmental stage on the uptake of bromoxynil and diclofenac was observed at single compound exposure (Figure 5). The uptake of

bromoxynil was about 6.4 (EC5) and 6.8 (EC25) times higher in the older developmental stage than the younger calculated, taking the volume change into account. The uptake was 2.5 (EC5) and 3 (EC25) times higher in the older developmental stage for diclofenac. For carbamazepine, no difference of the developmental stage in the amount taken up was noticeable.

Furthermore, the BSP addition significantly increased the internal concentrations (Figure 5) of bromoxynil and carbamazepine at shorter exposure times (24 h). The significance of this increase of the internal concentration was more pronounced at 24 h - 72 hpf compared to 24 h - 1 hpf exposure. For diclofenac, the effect of BSP was not significant at the two shorter exposure times (Figure 5).

Discussion

In this study, we aimed to examine the toxicokinetics of bromoxynil in zebrafish embryos in more detail, which in a previous study showed some peculiarities: The uptake of the compound by the embryos proceeded particularly slowly and, in contrast to other tested compounds, accumulated to a large extent in the embryonic body and to a lesser extent in the yolk[5].

Ion-trapping as a conceivable reason for bioaccumulation of bromoxynil in the GI tract of the embryos can be ruled out: The intestinal bulb was reported to have a pH of 5.0-5.4[28], and thus bromoxynil will not be more ionized (pKa = 3.75[15]).

Furthermore, the affinity of bromoxynil to certain biological molecules causing this bioaccumulation pattern, such as pigments in the eye binding psychoactive drugs[10], seems unlikely.

Since bromoxynil showed accumulation in the embryonic body to a comparatively large extent, we considered it conceivable that a cellular transporter may influence the accumulation pattern in the zebrafish embryo. As an uptake transporter, zebrafish Oatp1d1 seemed a likely candidate since it was shown to mediate the transport of environmentally relevant chemicals[11]. Furthermore, it was found to be expressed in various organs of adult zebrafish, particularly in liver and brain but also in intestine, gonads, and kidney.[27] Activity of this transporter was indicated by the finding that the fluorescent MC-LR-Texas red, found to act as a zebrafish Oatp1d1 substrate, was taken up by the cells of the glomerulus of the pronephros.[13]

As an SLC transporter, Oatp1d1 facilitates the transport of substrates across the cellular membrane along the concentration gradient, as seen for BSP used as a positive control compound: Compared to control cells, the uptake of [^{3}H]BSP was enhanced in Oatp1d1 overexpressing cells.

For bromoxynil and diclofenac, however, significantly lower accumulation in HEK-Oatp1d1 than in HEK-Co cells indicated that Oatp1d1 mediated cellular efflux; no effect on the intracellular concentration by Oatp1d1 was seen for carbamazepine (Figure 3).

Interaction of diclofenac and carbamazepine with zebrafish Oatp1d1 was investigated in a previous study, in which the fluorescent Oatp1d1-substrate lucifer yellow was used as a proxy for transporter activity[11]. The tests clearly indicated, in agreement with this study, the interaction of diclofenac but not of carbamazepine with Oatp1d1[11]. The indirect method with a fluorescent dye, however, in which an intracellular change in fluorescence by a modified cellular uptake of the dye is recorded, does not indicate whether a transporter-interacting compound is taken up or effluxed by the cell.

The results obtained here thus specified the mode of substrate interaction of test compounds with Oatp1d1, i.e., as taken up or effluxed substrate.

There is evidence that the transport mechanism of Oatps/OATPs is based on anion exchange: Cellular uptake of organic compounds was shown to be coupled with the efflux of bicarbonate, glutathione, and/or glutathione-S-conjugates[29–31]. Whether the mechanism of a chemical's cellular efflux is based on co-transport with cellular ions, such as the ones above, or on an exchange mechanism involving ions, e.g., contained in the medium, is not known and needs exploration.

The action of an OATP protein as efflux transporter has been observed before: The human renal transport protein OATP4C1 was found to mediate cellular efflux of the compounds digoxin, asymmetric dimethylarginine, L-arginine, L-homoarginine.[32] The results in this study were obtained by direct measurements of the intra- and extra-cellular levels of radio-labeled test compounds.[32]

There is no evidence for interaction of carbamazepine with zebrafish Oatp1d1 from the cellular tests with the fluorescent substrate dye Lucifer yellow[11] and when comparing the accumulation rates in HEK-Co and HEK-Oatp1d1 cells (Figure 3). However, accumulation of carbamazepine was reduced in the HEK-Oatp1d1 cells in dependence on the concentration of BSP that was present (Figure 4). It may be assumed that stimulation of cellular efflux of carbamazepine by Oatp1d1 is caused by an allosteric BSP effect. The effect by BSP was rather little: In the presence of BSP, the net export was low with -2 (10 µM carbamazepine) and -9 (100 µM carbamazepine) pmol x mg protein^{-1} x min^{-1} (average of the two experiments with 100 µM BSP added); yet the effect was significant. The chosen test conditions, such as incubation concentration or time, before could not have suited to show the Oatp1d1-mediated transport of carbamazepine. Considering that the proportion of carbamazepine crossing the membrane *via* passive diffusion can, in comparison to bromoxynil, be assumed to be high, as membrane permeability is two orders of magnitude higher for carbamazepine compared to bromoxynil (1.5 and 226 cm/sec[5]), an incubation time of 10 min could have been too long to be in the linear range.

The finding of the action of Oatp1d1 as an efflux transporter of bromoxynil in the cellular assays indicates that the activity of this transporter is not responsible for the comparatively high accumulation of this compound in the embryonic body. Rather, Oatp1d1 appears to constitute a mechanism keeping bromoxynil out of the body. This is supported by the finding that bromoxynil levels in the embryo tissue were higher when the compound was combined with BSP in the exposure (Figure 5), indicating that BSP blocks efflux - presumably by Oatp1d1 inhibition - of bromoxynil from the body. The action of Oatp1d1 as an efflux transporter of bromoxynil also

coincides with comparatively high bromoxynil levels in the GI tract (Figures 1, 2). Thus, the GI tract is a region of expression of Oatp1d1, and it may confer the active transport of the compound into the region of the lumen of the gut anlage.

It seems likely that other cellular transporters are involved in the toxicokinetics of bromoxynil in the zebrafish embryo. Thus, BSP[26,33] and Cyclosporin A[34] inhibit a range of transporters; it needs to be taken into account that their inhibiting action was not specific for Oatp1d1 when applied in the tests with zebrafish embryos that express a range of transporter proteins. These may include other uptake transporters from the SLC family that could cause the comparatively high accumulation of bromoxynil in the embryonic body. E.g., Oatp2b1 was shown to be also present in zebrafish embryos[13]. Diclofenac was found to be a substrate of zebrafish Oat2a, Oat2b, and Oat2d in cell experiments[12], potentially expressed in zebrafish embryos. Also, the interaction of test compounds with ABC efflux transporters, such as zebrafish Abcb4, is conceivable. Diclofenac, which in this study showed similar interaction with Oatp1d1 as bromoxynil, was previously examined for interaction with zebrafish Abcb4. The effect of diclofenac, lowering both the basal and verapamil-stimulated ATPase activity of recombinant Abcb4, indicated that this compound acts as an inhibitor of Abcb4 but not as a substrate transported by this protein[35]. This indicates that the toxicokinetics of diclofenac is not influenced by zebrafish Abcb4. Whether this is also the case for bromoxynil needs to be tested.

There is a more pronounced effect on the internal concentration of bromoxynil and diclofenac by BSP in the more advanced developmental stages. This may be seen as an indication of the involvement of cellular transporters in the uptake of bromoxynil by zebrafish embryos. Thus, it correlates with increased expression levels of *oatp1d1* transcripts, accompanied by a more pronounced transporter activity in more advanced stages.[13] Along these lines, bromoxynil and diclofenac were taken up by tissue of the more advanced developmental stages to a larger extent in the single compound exposures (i.e., without addition of BSP; Figure 5). This was most pronounced for bromoxynil, with an about 7 times higher uptake. When comparing 48 and 96 hpf stages, increased uptake in the more advanced developmental stage was also reported for paracetamol and diphenhydramine.[8,36] It is conceivable that the chorion may act as an uptake barrier in the earlier stages; however, for bromoxynil, paracetamol, and diphenhydramine, it was excluded that the chorion has an effect on the uptake.[5,8,36] As the expression of Oatp1d1 and other transporter proteins increases with the development of the zebrafish embryo; this may result in higher functionality. However, other explanations for stage-specific chemical uptake are conceivable. Thus, changes in the sorption capacity with the development of the GI tract have been suggested[36].

Conclusions

Our study shows that Oatp1d1 acts as both cellular uptake and efflux transporter. By acting bidirectionally, this transport protein[32] may have a dual protective role. Our results point to the need to apply direct measurements more commonly to determine the direction of translocation of compounds across cellular membranes. It was previously suggested that uptake kinetics of ionic substances in zebrafish embryos are, beyond passive diffusion, majorly influenced by cellular transporters.[5,10] Our results concur with this assumption and show that the approach of combining cellular test systems overexpressing proteins relevant for toxicokinetics with toxicokinetics studies with live zebrafish embryos and MALDI-MS imaging provides important insights. Thus, chemical interaction with relevant proteins and bioaccumulation patterns in the embryo can be correlated. Experiments with knockdown zebrafish embryos will be useful to obtain quantitative results on the roles of certain proteins in toxicokinetics. Beyond transporter and metabolic proteins, certain developmental stage-specific morphological features, such as the opening of the GI tract[36] and the mouth[37], and organ-specific parameters, such as the formation of the microbiome in the GI tract[38], could be relevant for toxicokinetics.

Acknowledgments

We thank Stefan Scholz for the discussion of the spatial distribution of bromoxynil and Nicole Schweiger for providing the zebrafish embryo eggs. We acknowledge Janet Krüger and Gianina Jakobs for performing fish embryo toxicity tests and calculating dose-response curves for diclofenac. We thank Mick Wu for statistical advice and Coretta Bauer for measurements with the UPLC-QToF-MS.

References

(1) Cassar, S.; Adatto, I.; Freeman, J. L.; Gamse, J. T.; Iturria, I.; Lawrence, C.; Muriana, A.; Peterson, R. T.; Van Cruchten, S.; Zon, L. I. Use of Zebrafish in Drug Discovery Toxicology. *Chem. Res. Toxicol.* **2020**, *33* (1), 95–118. https://doi.org/10.1021/acs.chemrestox.9b00335.

(2) Hill, A. J.; Teraoka, H.; Heideman, W.; Peterson, R. E. Zebrafish as a Model Vertebrate for Investigating Chemical Toxicity. https://doi.org/10.1093/toxsci/kfi110.

(3) Belanger, S. E.; Rawlings, J. M.; Carr, G. J. Use of Fish Embryo Toxicity Tests for the Prediction of Acute Fish Toxicity to Chemicals. *Environ. Toxicol. Chem.* **2013**, *32* (8), 1768–1783. https://doi.org/10.1002/etc.2244.

(4) Klüver, N.; König, M.; Ortmann, J.; Massei, R.; Paschke, A.; Kühne, R.; Scholz, S. Fish Embryo Toxicity Test: Identification of Compounds with Weak Toxicity and Analysis of Behavioral Effects to Improve Prediction of Acute Toxicity for Neurotoxic Compounds. *Environ. Sci. Technol.* **2015**, *49* (11), 7002–7011. https://doi.org/10.1021/acs.est.5b01910.

(5) Halbach, K.; Ulrich, N.; Goss, K.-U.; Seiwert, B.; Wagner, S.; Scholz, S.; Luckenbach, T.; Bauer, C.; Schweiger, N.; Reemtsma, T. Yolk Sac of Zebrafish Embryos as Backpack for Chemicals? *Environ. Sci. Technol.* **2020**, *54* (16), 10159–10169. https://doi.org/10.1021/acs.est.0c02068.

(6) Vogs, C.; Johanson, G.; Näslund, M.; Wulff, S.; Sjödin, M.; Hellstrandh, M.; Lindberg, J.; Wincent, E. Toxicokinetics of Perfluorinated Alkyl Acids Influences Their Toxic Potency in the Zebrafish Embryo (Danio Rerio). *Environ. Sci. Technol.* **2019**, *53* (7), 3898–3907. https://doi.org/10.1021/acs.est.8b07188.

(7) Brox, S.; Seiwert, B.; Küster, E.; Reemtsma, T. Toxicokinetics of Polar Chemicals in Zebrafish Embryo (Danio Rerio): Influence of Physicochemical Properties and of Biological Processes. *Environ. Sci. Technol.* **2016**, *50* (18), 10264–10272. https://doi.org/10.1021/acs.est.6b04325.

(8) Kristofco, L. A.; Haddad, S. P.; Chambliss, C. K.; Brooks, B. W. Differential Uptake of and Sensitivity to Diphenhydramine in Embryonic and Larval Zebrafish. *Environ. Toxicol. Chem.* **2018**, *37* (4), 1175–1181. https://doi.org/10.1002/etc.4068.

(9) Fischer, S.; Klüver, N.; Burkhardt-Medicke, K.; Pietsch, M.; Schmidt, A. M.; Wellner, P.; Schirmer, K.; Luckenbach, T. Abcb4 Acts as Multixenobiotic Transporter and Active Barrier against Chemical Uptake in Zebrafish (Danio Rerio) Embryos. *BMC Biol.* **2013**, *11* (69). https://doi.org/10.1186/1741-7007-11-69.

(10) Kirla, K. T.; Groh, K. J.; Poetzsch, M.; Banote, R. K.; Stadnicka-Michalak, J.; Eggen, R. I. L.; Schirmer, K.; Kraemer, T. Importance of Toxicokinetics to Assess the Utility of Zebrafish Larvae as Model for Psychoactive Drug Screening Using Meta-Chlorophenylpiperazine (MCPP) as Example. *Front. Pharmacol.* **2018**, *9*, 414. https://doi.org/10.3389/fphar.2018.00414.

(11) Popovic, M.; Zaja, R.; Fent, K.; Smital, T. Interaction of Environmental Contaminants with Zebrafish Organic Anion Transporting Polypeptide, Oatp1d1 (Slco1d1). *Toxicol. Appl. Pharmacol.* **2014**, *280* (1), 149–158. https://doi.org/10.1016/j.taap.2014.07.015.

(12) Dragojević, J.; Mihaljević, I.; Popović, M.; Zaja, R.; Smital, T. In Vitro Characterization of Zebrafish (Danio Rerio) Organic Anion Transporters Oat2a-E. *Toxicol. Vitr.* **2018**, *46*, 246–256. https://doi.org/10.1016/j.tiv.2017.09.026.

(13) Faltermann, S.; Grundler, V.; Gademann, K.; Pernthaler, J.; Fent, K. Comparative Effects of Nodularin and Microcystin-LR in Zebrafish: 2. Uptake and Molecular Effects in Eleuthero-Embryos and Adult Liver with Focus on Endoplasmic Reticulum Stress. *Aquat. Toxicol.* **2016**, *171*, 77–87. https://doi.org/10.1016/j.aquatox.2015.12.001.

(14) Klüver, N.; Bittermann, K.; Escher, B. I. QSAR for Baseline Toxicity and Classification of Specific Modes of Action of Ionizable Organic Chemicals in the Zebrafish Embryo Toxicity Test. *Aquat. Toxicol.* **2019**, *207* (December 2018), 110–119. https://doi.org/10.1016/j.aquatox.2018.12.003.

(15) Machado, F.; Collin, L.; Boule, P. Photolysis of Bromoxynil (3,5-dibromo-4-hydroxybenzonitrile) in Aqueous Solution. *Pesticide Science*. 1995, pp 107–110. https://doi.org/10.1002/ps.2780450203.

(16) Nawaji, T.; Yamashita, N.; Umeda, H.; Zhang, S. Cytochrome P450 Expression and Chemical Metabolic Activity before Full Liver Development in Zebrafish. **2020**, 1–17.

(17) ISO. Water Quality — Determination of the Acute Toxicity of Waste Water to Zebrafish Eggs (Danio Rerio). *ISO 150882007* **2007**.

(18) Westerfield, M. *The Zebrafish Book. A Guide for the Laboratory Use of Zebrafish (Danio Rerio).*, 4th ed.; University of Oregon Press: Eugene, 2000.

(19) Nagel, R. DarT: The Embryo Test with the Zebrafish Danio Rerio -a General Model in Ecotoxicology and Toxicology. *ALTEX* **2002**, *19*, 38–48.

(20) Fetter, E.; Smetanová, S.; Baldauf, L.; Lidzba, A.; Altenburger, R.; Schüttler, A.; Scholz, S. Identification and Characterization of Androgen-Responsive Genes in Zebrafish Embryos. *Environ. Sci. Technol.* **2015**, *49* (19), 11789–11798. https://doi.org/10.1021/acs.est.5b01034.

(21) OECD Guidelines for the Testing of Chemicals - Fish Embryo Acute Toxicity (FET) Test. *OECD 236* **2013**.

(22) Jakobs, G.; Krüger, J.; Schüttler, A.; Altenburger, R.; Busch, W. Mixture Toxicity Analysis in Zebrafish Embryo: A Time and Concentration Resolved Study on Mixture Effect Predictivity. *Environ. Sci. Eur.* **2020**, *32* (1), 143. https://doi.org/10.1186/s12302-020-00409-3.

(23) Schmidt, S. Bewertung Der Mischungstoxizität von Gentoxischen Substanzen Auf Embryonen Des Zebrabärblings (Danio Rerio) Unter Berücksichtigung Der Spezifischen Wirkweisen Und Reaktionen Auf, Masterarbeit, Martin-Luther-Universität Halle-Wittenberg, 2013.

(24) Ardelt, D.; Polatajko, A.; Primm, O.; Reijnen, M. Isotope Ratio Measurements with a Fully Simultaneous Mattauch-Herzog ICP-MS. *Anal. Bioanal. Chem.* **2013**, *405* (9), 2987–2994. https://doi.org/10.1007/s00216-012-6543-0.

(25) Danio rerio solute carrier organic anion transporter family, member 1D - Nucleotide - NCBI https://www.ncbi.nlm.nih.gov/nuccore/NM_001348086.1 (accessed Feb 3, 2021).

(26) Michalski, C.; Cui, Y.; Nies, A. T.; Nuessler, A. K.; Neuhaus, P.; Zanger, U. M.; Klein, K.; Eichelbaum, M.; Keppler, D.; König, J. A Naturally Occurring Mutation in the SLC21A6 Gene Causing Impaired Membrane Localization of the Hepatocyte Uptake Transporter. *J. Biol. Chem.* **2002**, *277* (45), 43058–43063. https://doi.org/10.1074/jbc.M207735200.

(27) Popovic, M.; Zaja, R.; Fent, K.; Smital, T. Molecular Characterization of Zebrafish Oatp1d1 (Slco1d1), a Novel Organic Anion-Transporting Polypeptide. *J. Biol. Chem.* **2013**, *288* (47), 33894–33911. https://doi.org/10.1074/jbc.M113.518506.

(28) Gurkov, A.; Sadovoy, A.; Shchapova, E.; Teh, C.; Meglinski, I.; Timofeyev, M. Microencapsulated Fluorescent PH Probe as Implantable Sensor for Monitoring the Physiological State of Fish Embryos. *PLoS One* **2017**, *12* (10), 1–12. https://doi.org/10.1371/journal.pone.0186548.

(29) Li, L.; Lee, T. K.; Meier, P. J.; Ballatori, N. Identification of Glutathione as a Driving Force and Leukotriene C4 as a Substrate for Oatp1, the Hepatic Sinusoidal Organic Solute Transporter. *J. Biol. Chem.* **1998**, *273* (26), 16184–16191. https://doi.org/10.1074/jbc.273.26.16184.

(30) Li, L.; Lee, T. K.; Meier, P. J.; Ballatori, N. Identification of Glutathione as a Driving Force and Leukotriene C4 as a Substrate for Oatp1, the Hepatic Sinusoidal Organic Solute Transporter. *J. Biol. Chem.* **1998**, *273* (26), 16184–16191. https://doi.org/10.1074/jbc.273.26.16184.

(31) Satlin, L. M.; Amin, V.; Wolkoff, A. W. Organic Anion Transporting Polypeptide Mediates Organic Anion/HCO3/- Exchange. *J. Biol. Chem.* **1997**, *272* (42), 26340–26345. https://doi.org/10.1074/jbc.272.42.26340.

(32) Taghikhani, E.; Maas, R.; Fromm, M. F.; König, J. The Renal Transport Protein OATP4C1 Mediates Uptake of the Uremic Toxin Asymmetric Dimethylarginine (ADMA) and Efflux of Cardioprotective L-Homoarginine. *PLoS One* **2019**, *14* (3), e0213747. https://doi.org/10.1371/journal.pone.0213747.

(33) Kindla, J.; Müller, F.; Mieth, M.; Fromm, M. F.; König, J. Influence of Non-Steroidal Anti-Inflammatory Drugs on Organic Anion Transporting Polypeptide (OATP) 1B1- and OATP1B3-Mediated Drug Transport. *Drug Metab. Dispos.* **2011**, *39* (6), 1047–1053. https://doi.org/10.1124/dmd.110.037622.

(34) Qadir, M.; O'Loughlin, K. L.; Fricke, S. M.; Williamson, N. A.; Greco, W. R.; Minderman, H.; Baer, M. R. Cyclosporin A Is a Broad-Spectrum Multidrug Resistance Modulator. *Clin. Cancer Res.* **2005**, *11* (6), 2320–2326. https://doi.org/10.1158/1078-0432.CCR-04-1725.

(35) Cunha, V.; Burkhardt-Medicke, K.; Wellner, P.; Santos, M. M.; Moradas-Ferreira, P.; Luckenbach, T.; Ferreira, M. Effects of Pharmaceuticals and Personal Care Products (PPCPs) on Multixenobiotic Resistance (MXR) Related Efflux Transporter Activity in Zebrafish (Danio Rerio) Embryos. *Ecotoxicol. Environ. Saf.* **2017**, *136* (October 2016), 14–23. https://doi.org/10.1016/j.ecoenv.2016.10.022.

(36) van Wijk, R. C.; Krekels, E. H. J.; Kantae, V.; Harms, A. C.; Hankemeier, T.; van der Graaf, P. H.; Spaink, H. P. Impact of Post-Hatching Maturation on the Pharmacokinetics of Paracetamol in Zebrafish Larvae. *Sci. Rep.* **2019**, *9* (1), 2149. https://doi.org/10.1038/s41598-019-38530-w.

(37) Verbueken, E.; Bars, C.; Ball, J. S.; Periz-Stanacev, J.; Marei, W. F. A.; Tochwin, A.; Gabriëls, I. J.; Michiels, E. D. G.; Stinckens, E.; Vergauwen, L.; et al. From MRNA Expression of Drug Disposition Genes to in Vivo Assessment of CYP-Mediated Biotransformation during Zebrafish Embryonic and Larval Development. *Int. J. Mol. Sci.* **2018**, *19* (12), 1–30. https://doi.org/10.3390/ijms19123976.

(38) Catron, T. R.; Gaballah, S.; Tal, T. Using Zebrafish to Investigate Interactions Between Xenobiotics and Microbiota. *Curr. Pharmacol. Reports* **2019**, *5*, 468–480. https://doi.org/10.1007/s40495-019-00203-7.

Tables

Table 1. Observed toxicity on the phenotype in the exposure of 96 h. See for measured concentrations of EC5 and EC25 values Table S2. Pictures of observed effects can be found in Figure S8. k: coagulation; mtail: tail deformation; nohb: no heartbeat; nobc: no blood circulation; EdP: edema pericard; (beh: observed less movement)

Substance A (exposure concentration)	**Substance B (exposure concentration)**	**Total effects [%] Experiment 1**	**Total effects [%] Experiment 3**	**Effects**
Control		0	8	k
BSP (50 µM)		60	0	no hatching
BSP (100 µM)		39	0	no hatching
Bromoxynil (EC5)		0	7	mtail
Bromoxynil (EC5)	BSP (50 µM)	41	27	no hatching, nohb
Bromoxynil (EC5)	BSP (100 µM)	88	47	nohb, nobc
Bromoxynil (EC25)		10	29	nohb, nobc
Bromoxynil (EC25)	BSP (50 µM)	100	86	nohb, k
Bromoxynil (EC25)	BSP (100 µM)	100	100	nohb, k, no hatching
Diclofenac (EC5)		27	13	EdP, no hatching
Diclofenac (EC5)	BSP (50 µM)	93	93	nobc, EdP, no hatching, (beh)
Diclofenac (EC5)	BSP (100 µM)	100	100	nobc, EdP, hf, no hatching, (beh)
Diclofenac (EC25)		43	5	EdP
Diclofenac (EC25)	BSP (50 µM)	100	67	EdP, hf, nohb, no hatching
Diclofenac (EC25)	BSP (100 µM)	100	100	EdP, nohb, no hatching
Carbamazepine (EC5)		73	22	no hatching
Carbamazepine (EC5)	BSP (50 µM)	100	22	no hatching
Carbamazepine (EC5)	BSP (100 µM)	100	89	no hatching
Carbamazepine (EC25)		81	33	no hatching
Carbamazepine (EC25)	BSP (50 µM)	100	89	no hatching
Carbamazepine (EC25)	BSP (100 µM)	100	89	no hatching

Figures

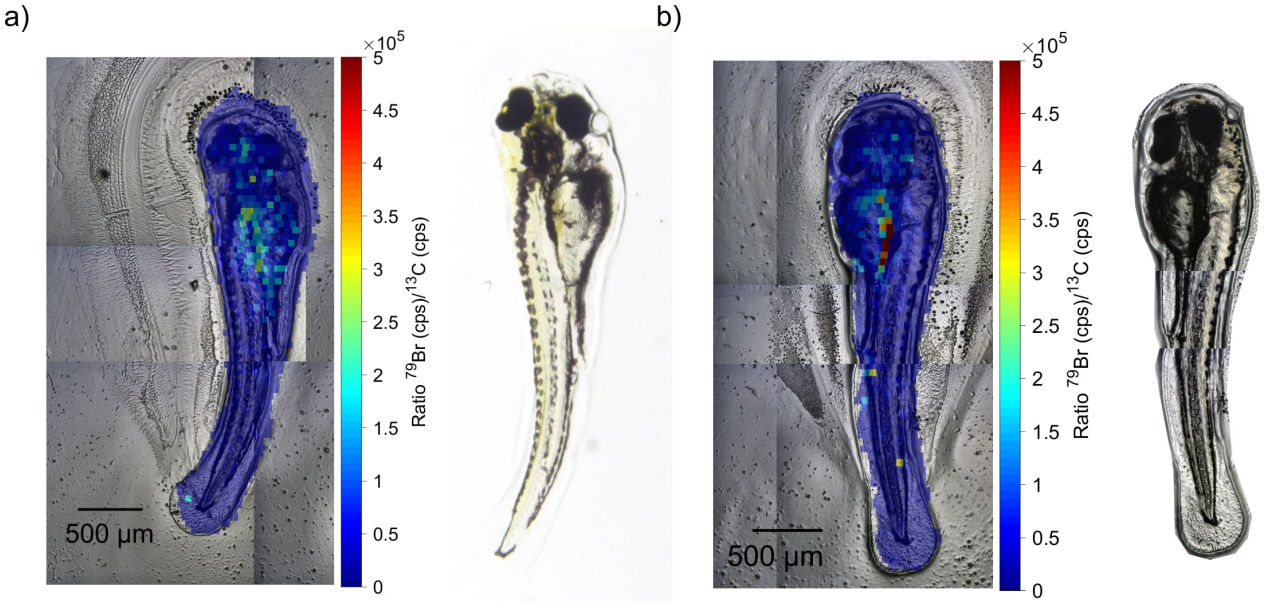

Figure 1. Tissue distribution of bromoxynil in two zebrafish embryos at approximately 97 hpf; two individuals are shown. The images show the regions of the embryos with the tissue of 79Br (normalized to tissue density represented by 13C) colorimetrically indicated. The bright-field images (right column) show the embryos before the ablation.

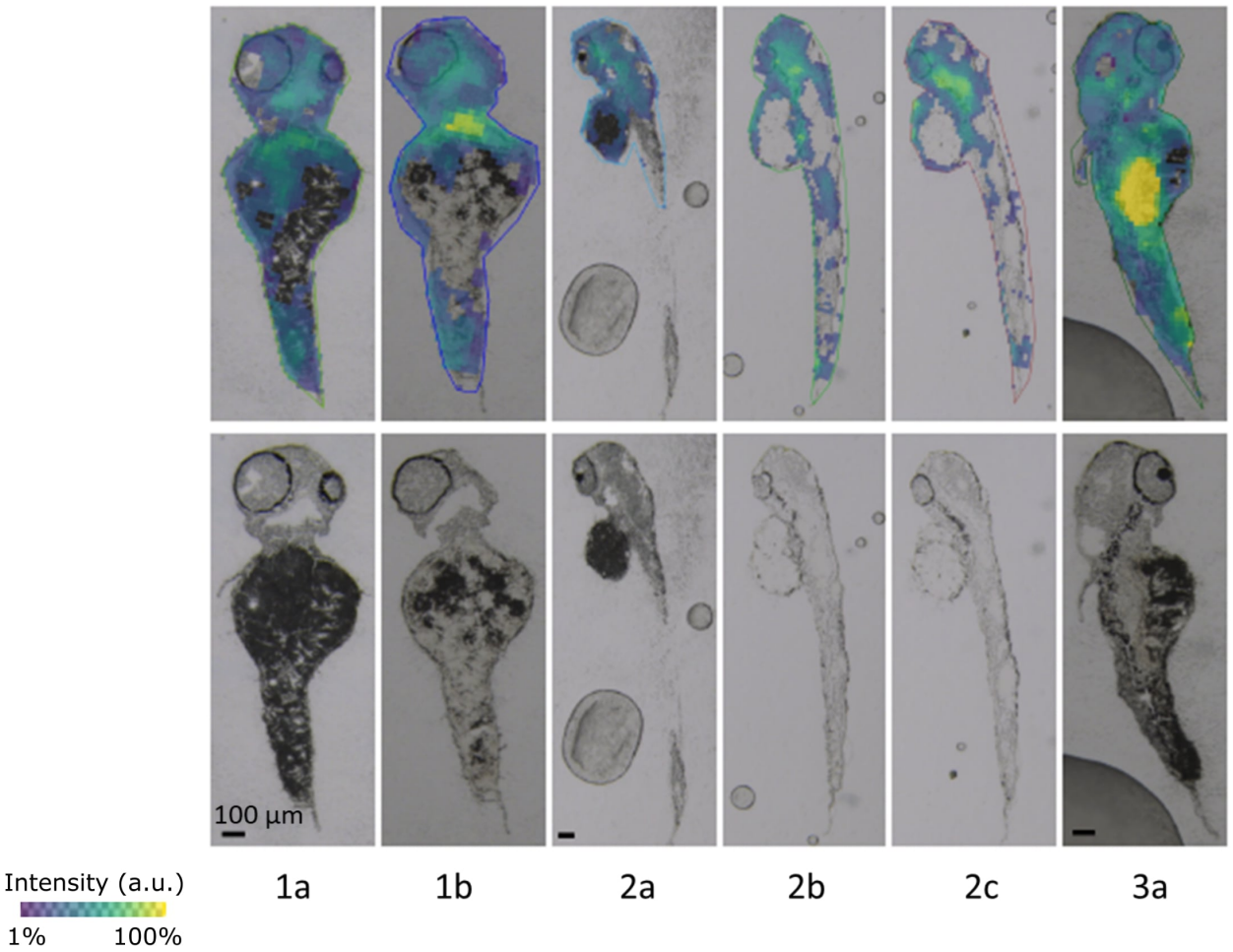

Figure 2. Distribution of bromoxynil (upper row, 275.84671 m/z ± 0.19313 mDa) in three exposed zebrafish embryos (1-3) with different cross-sections a-c and corresponding pictures (lower row). The colored line (upper row) shows the measured area. The exposure duration of all zebrafish embryos was 72 h. The scale bar is 100 µm. The color bar shows the range from low (purple) to high bromoxynil intensity (yellow).

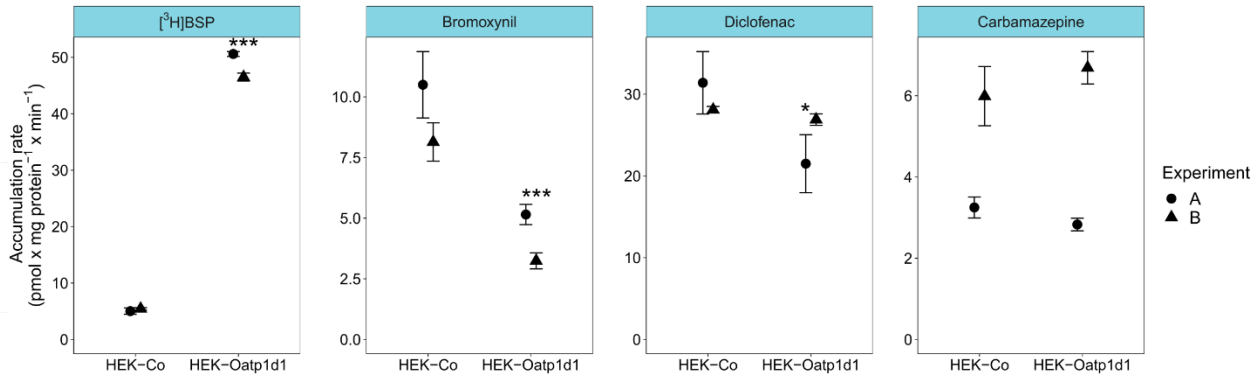

Figure 3. Accumulation rates for [3H]BSP (1 µM incubation) and bromoxynil, diclofenac, carbamazepine (10 µM incubation) in HEK-Co and HEK-Oatp1d1 cells. The incubation period was 10 minutes. The data of two independent experiments (A and B) are separately depicted; means ± SD of three replicates per concentration are shown. Net transport values: 46 and 41 pmol x mg protein^{-1} x min^{-1} ([3H]BSP), -5.3 and -4.9 (bromoxynil), -9.9 and -9.1 (diclofenac), -0.4 and 0.7 (carbamazepine). * indicates statistical significance (Manly's permutation test, * $p < 0.05$, *** $p < 0.001$). For cellular accumulation data upon incubation to test compounds at 100 µM, refer to Figure S4.

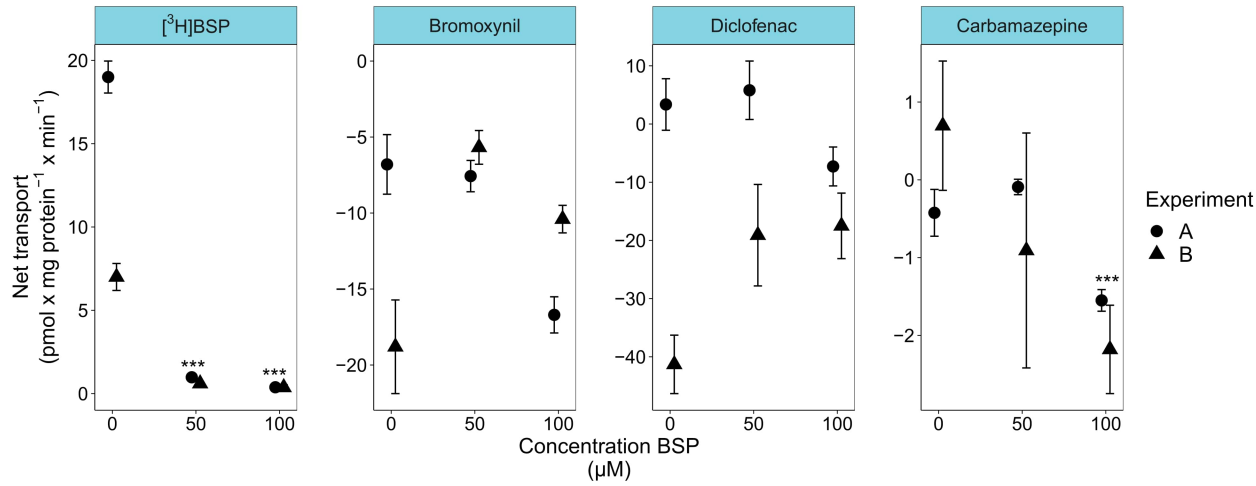

Figure 4. Oatp1d1-mediated transport of test compounds without or with 50 or 100 µM unlabeled BSP added. Test compounds were [3H]BSP (1 µM incubation), bromoxynil (10 µM incubation), diclofenac (10 µM incubation), and carbamazepine (10 µM incubation). The incubation period was 10 min. Net transport was calculated by subtracting the transport into HEK-Co cells from that into HEK-Oatp1d1 cells. The data of two independent experiments (A and B) are separately depicted; means ± SD of three replicates per concentration are shown. * indicates statistical significance (Manly's permutation test, *** $p < 0.001$). For net transport data upon incubation to test compounds at 100 µM, refer to Figure S5.

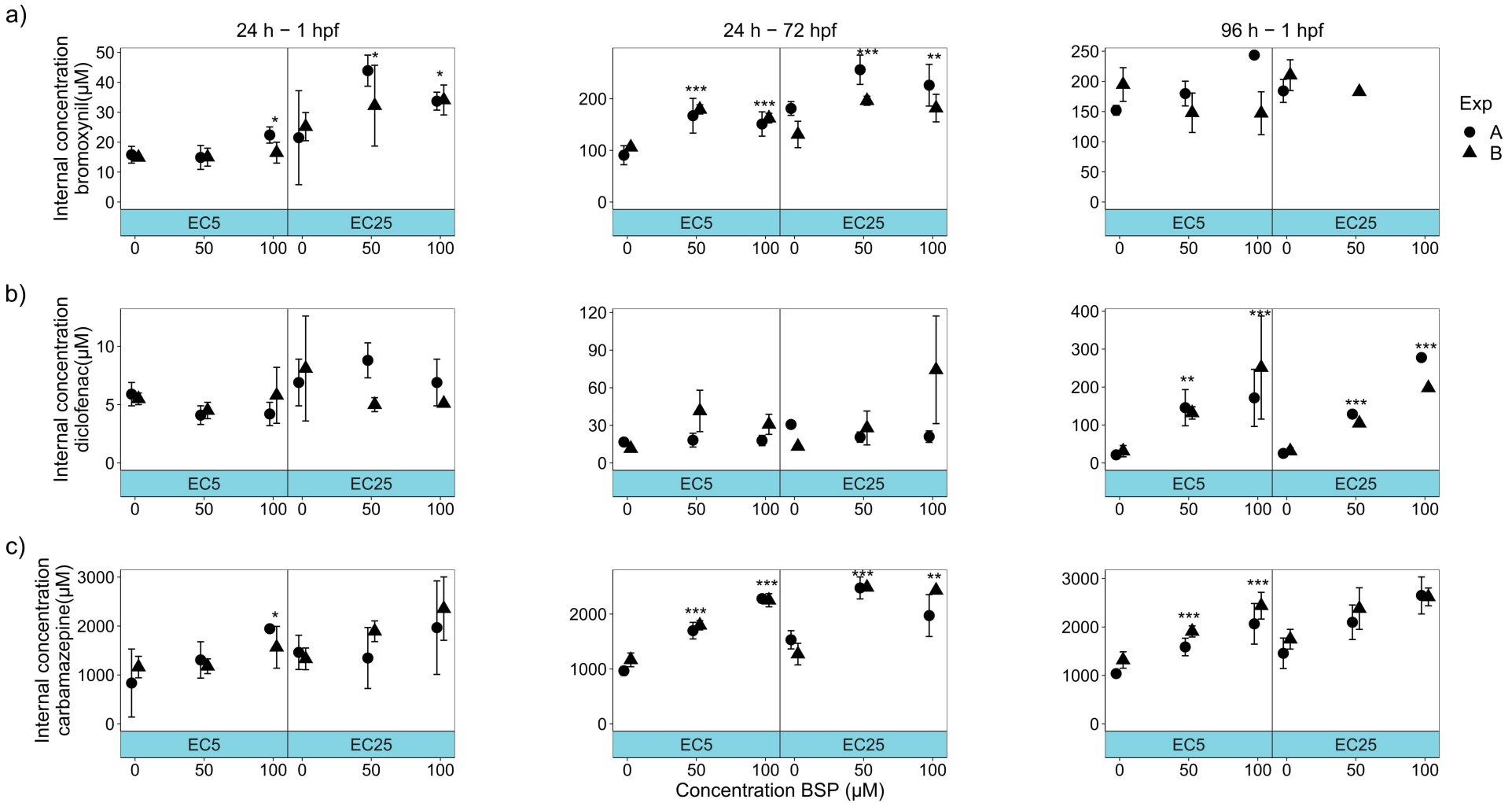

Figure 5. Internal bromoxynil (a), diclofenac (b), and carbamazepine (c) concentrations in zebrafish embryos. The embryos were exposed to the compounds at EC5 or EC25 alone or in combination with 50 or 100 µM BSP for 24 h and 96 h. Exposures were performed twice in independent experiments (Exp) with embryos from different egg batches; data from the two experiments are separately shown (experiment A - circle, experiment B - triangle). Data are shown as means (symbols) and standard deviations (bars) from three replicates; each replicate consists of data from three pooled embryos. Significant differences between the data for treatments with 50 µM or 100 µM BSP and the respective treatments without BSP are indicated by asterisks (Manly's permutation test, * $p < 0.05$, ** $p < 0.01$, *** $p < 0.001$).

Electronic Supporting information

Zebrafish Oatp1d1 acts as cellular efflux transporter of bromoxynil

Katharina Halbach, Silke Aulhorn, Oliver Lechtenfeld, Marion Lecluse, Sophia Leippe, Thorsten Reemtsma, Bettina Seiwert, Stephan Wagner, Jörg König, Till Luckenbach

Dose-response curve bromosulfophthalein and bromoxynil

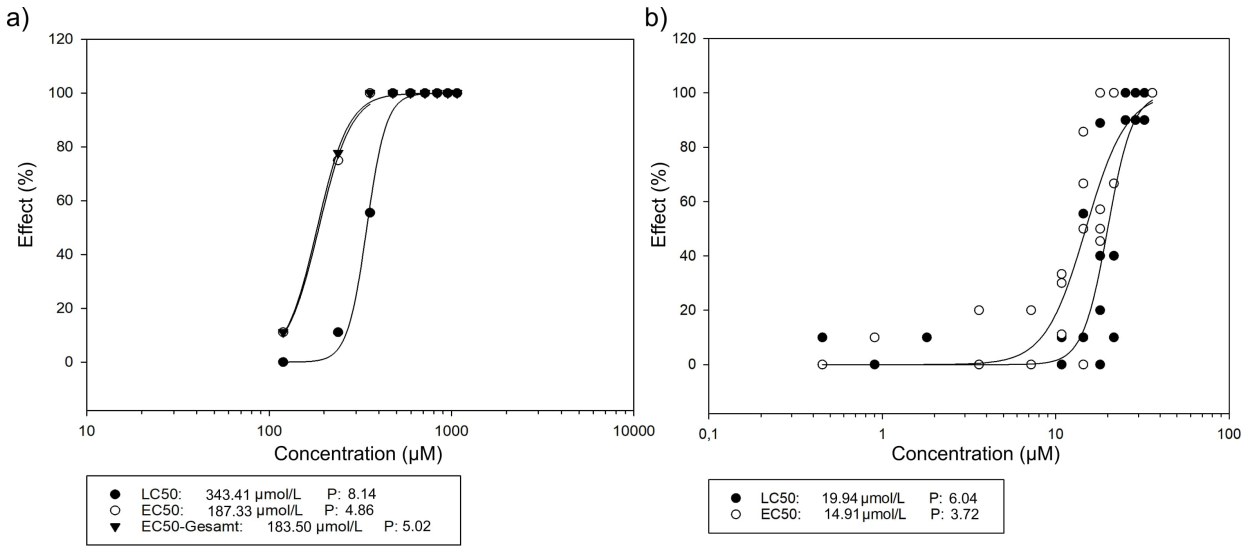

Figure S1. Effects of a) bromosulfophthalein and b) bromoxynil on zebrafish embryos in a 96 h toxicity test. Recorded were mortality and sublethal effects. N = 9 for each data point. The regression was modeled with the 4-parameter HILL equation: (f=y0+a*xb/(cb+xb).

Overview zebrafish embryo exposure

Table S1. Overview of all exposure experiments and with the nominal concentrations of the test compounds. For measured concentrations, see Table S2. Two independent experiments were conducted for each treatment.

Substance	Diclofenac	Bromoxynil	Carbamazepine	BSP	Replicates with 3 embryos	
	(µM)	(µM)	(µM)	(µM)	96 h exposure	24 h exposures
Control	/	/	/	/	5	4
BSP Control	/	/	/	50	5	4
BSP Control	/	/	/	100 (EC5)	7	4
Bromoxynil	/	6.76 (EC5)	/	/	5	4
Bromoxynil	/	6.76 (EC5)	/	50	5	4
Bromoxynil	/	6.76 (EC5)	/	100 (EC5)	5	4
Bromoxynil	/	11.1 (EC25)	/	/	7	4
Bromoxynil	/	11.1 (EC25)	/	50	7	4
Bromoxynil	/	11.1 (EC25)	/	100 (EC5)	7	4
Diclofenac	4.63 (EC5)	/	/	/	5	4
Diclofenac	4.63 (EC5)	/	/	50	5	4
Diclofenac	4.63 (EC5)	/	/	100 (EC5)	5	4
Diclofenac	5.24 (EC25)	/	/	/	7	4
Diclofenac	5.24 (EC25)	/	/	50	7	4
Diclofenac	5.24 (EC25)	/	/	100 (EC5)	7	4
Diclofenac[a]	4.63 (EC5)	6.76 (EC5)				
Diclofenac[a]	4.63 (EC5)	6.76 (EC5)				
Carbamazepine	/	/	231 (EC5)	/	5	4
Carbamazepine	/	/	231 (EC5)	50	5	4
Carbamazepine	/	/	231 (EC5)	100 (EC5)	5	4
Carbamazepine	/	/	259 (EC25)	/	7	4
Carbamazepine	/	/	259 (EC25)	50	7	4
Carbamazepine	/	/	259 (EC25)	100 (EC5)	7	4

[a]Only one independent experiment was conducted.

Table S2. Measured concentrations in the exposure solutions

Substance	Experiment number	EC5 (µM)	EC 25 (µM)
Bromoxynil	1	9.63±2.26	14.9±3.3
	2	11.9±1.5	21.3±2.9
	3	10.6±2.4	18.9±1.5
Diclofenac	1	5.91±1.08	6.31±0.93
	2	2.67±0.43	3.55±1.05
	3	2.48±0.33	3.07±0.49
Carbamazepine	1	217±14	244±13
	2	213±17	214±20
	3	235±48	233±77

Overview cell experiments

Table S3. Overview of the cell experiments. Experiments were performed using HEK-VC and HEK-Oatp1d1 cells, respectively. Two independent experiments with three replicates were conducted.

Substrate	Concentration substrate (µM)	Inhibitor	Concentration inhibitor (µM)
Experiment: Oatp1d1-mediated transport			
[^{3}H]BSP	1	/	
Bromoxynil	10, 100	/	
Diclofenac	10, 100	/	
Carbamazepine	10, 100	/	
Experiment: Addition of BSP			
[^{3}H]BSP	1	BSP	0, 10, 100
Bromoxynil	10, 100	BSP	0, 10, 100
Diclofenac	10, 100	BSP	0, 10, 100
Carbamazepine	10, 100	BSP	0, 10, 100
Experiment: Addition of CsA			
[^{3}H]BSP	1	CsA	0, 5
Bromoxynil	10, 100	CsA	0, 5
Diclofenac	10, 100	CsA	0, 5
Carbamazepine	10, 100	CsA	0, 5
Experiment: Mixed exposure to bromoxynil and diclofenac			
Bromoxynil[a]	10, 100	Diclofenac	10, 100
Diclofenac[a]	10, 100	Bromoxynil	10, 100

[a]Only performed in one independent experiment.

UV/vis absorbance BSP

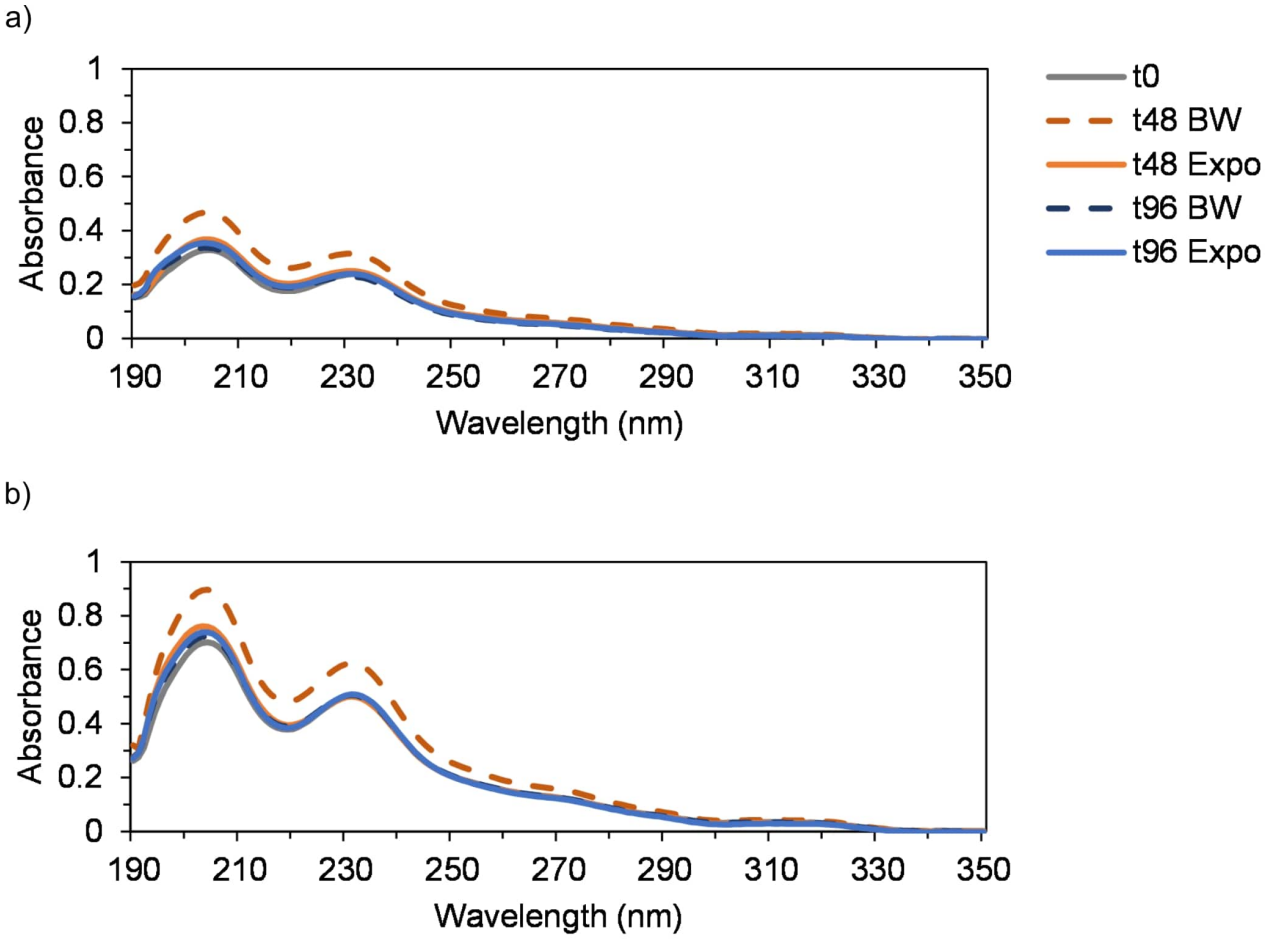

Figure S2. Absorbance measured for the BSP solution at a concentration of a) 50 µM and b) 100 µM. It was measured at the beginning of exposure (grey) and after 48 h and 96 h in the blind control without embryos (BW) and in the exposure solution (Expo).

Results cell experiments

BSP uptake

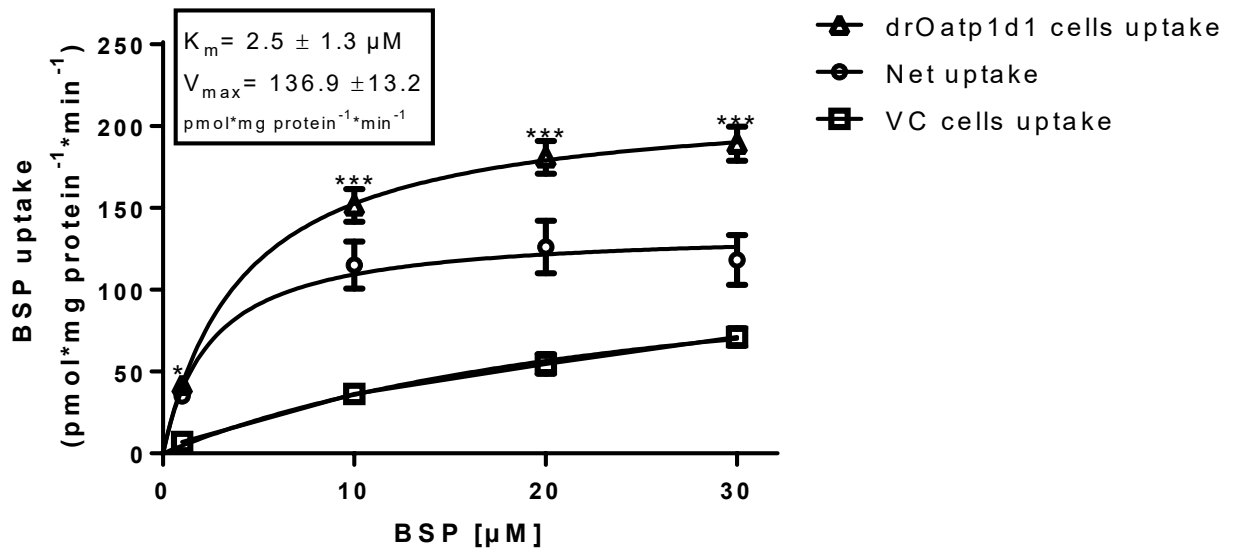

Figure S3. Uptake of [^{3}H]BSP in HEK-Oatp1d1 cells (drOatp1d1), vector control cells (VC cells uptake), and calculated net uptake.

Comparison 100 µM incubation HEK-Co and HEK-Oatp1d1

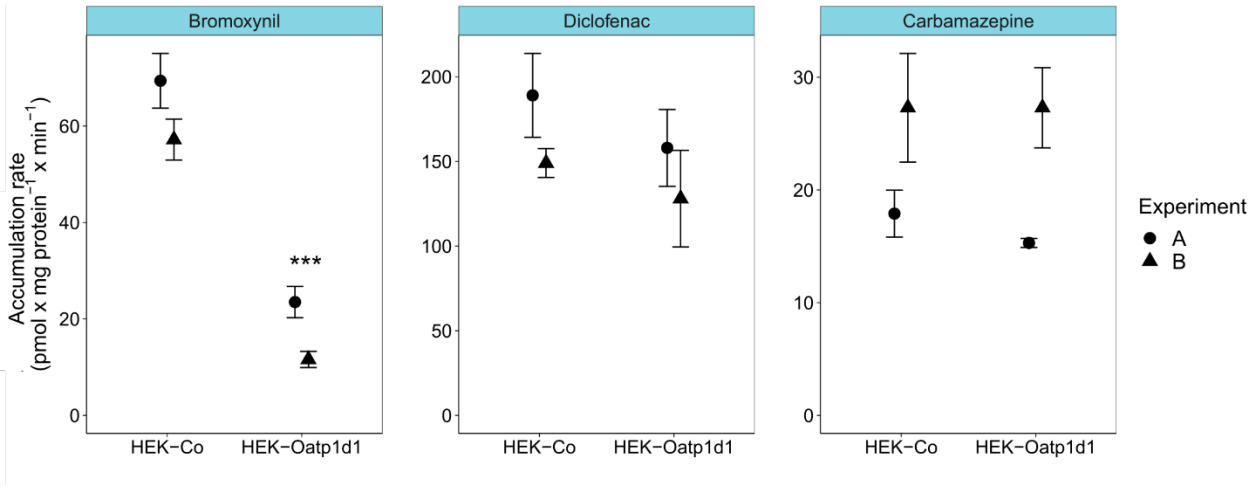

Figure S4. Accumulation rates for bromoxynil, diclofenac, carbamazepine (100 µM incubation) in HEK-Co and HEK-Oatp1d1 cells. The incubation period was 10 minutes. The data of two independent experiments (A and B) are separately depicted; means ± SD of three replicates per concentration are shown.
Net transport values: -45.9 and -45.6 pmol x mg protein^{-1} x min^{-1} (bromoxynil), -30.6 and -21.1 (diclofenac), -2.6 and 0.1 (carbamazepine). * indicates statistical significance (indicates statistical significance (Manly's permutation test, *** $p < 0.001$)). For cellular accumulation data upon incubation to test compounds at 10 µM, refer to Figure 3.

BSP effects on uptake of bromoxynil, diclofenac and carbamazepine at 100 µM

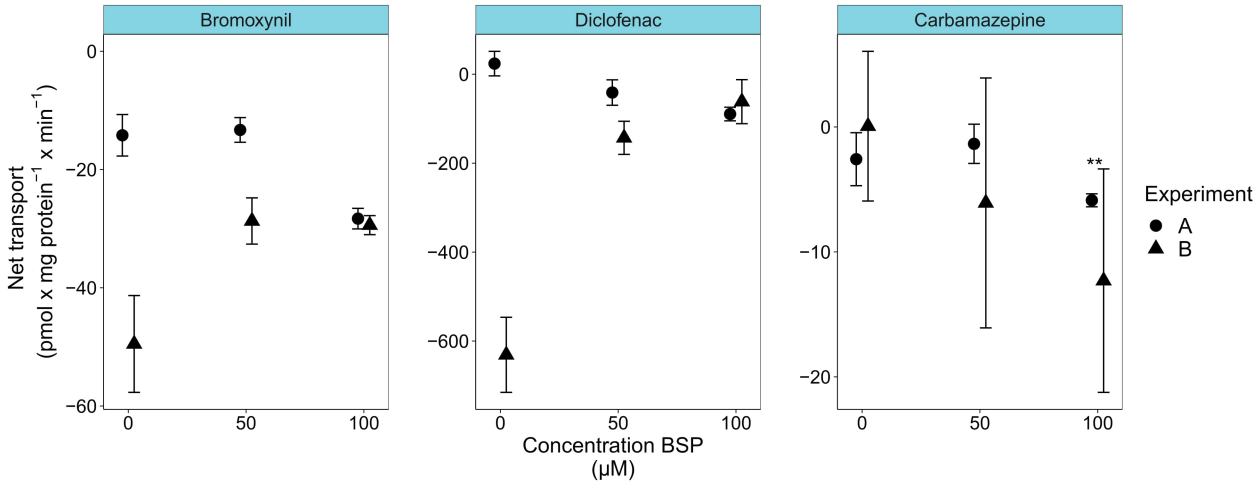

Figure S5. Oatp1d1-mediated transport of test compounds without or with 50 or 100 µM unlabeled BSP added. Test compounds were bromoxynil (100 µM incubation), diclofenac (100 µM incubation), and carbamazepine (100 µM incubation). The incubation period was 10 min. Net transport was calculated by subtracting the transport into HEK-Co cells from that into HEK-Oatp1d1 cells. The data of two independent experiments (A and B) are separately depicted; means ± SD of three replicates per concentration are shown. * indicates statistical significance (Manly's permutation test, *** $p < 0.001$). For net transport data upon incubation to test compounds at 10 µM, refer to Figure 4.

Addition of CsA

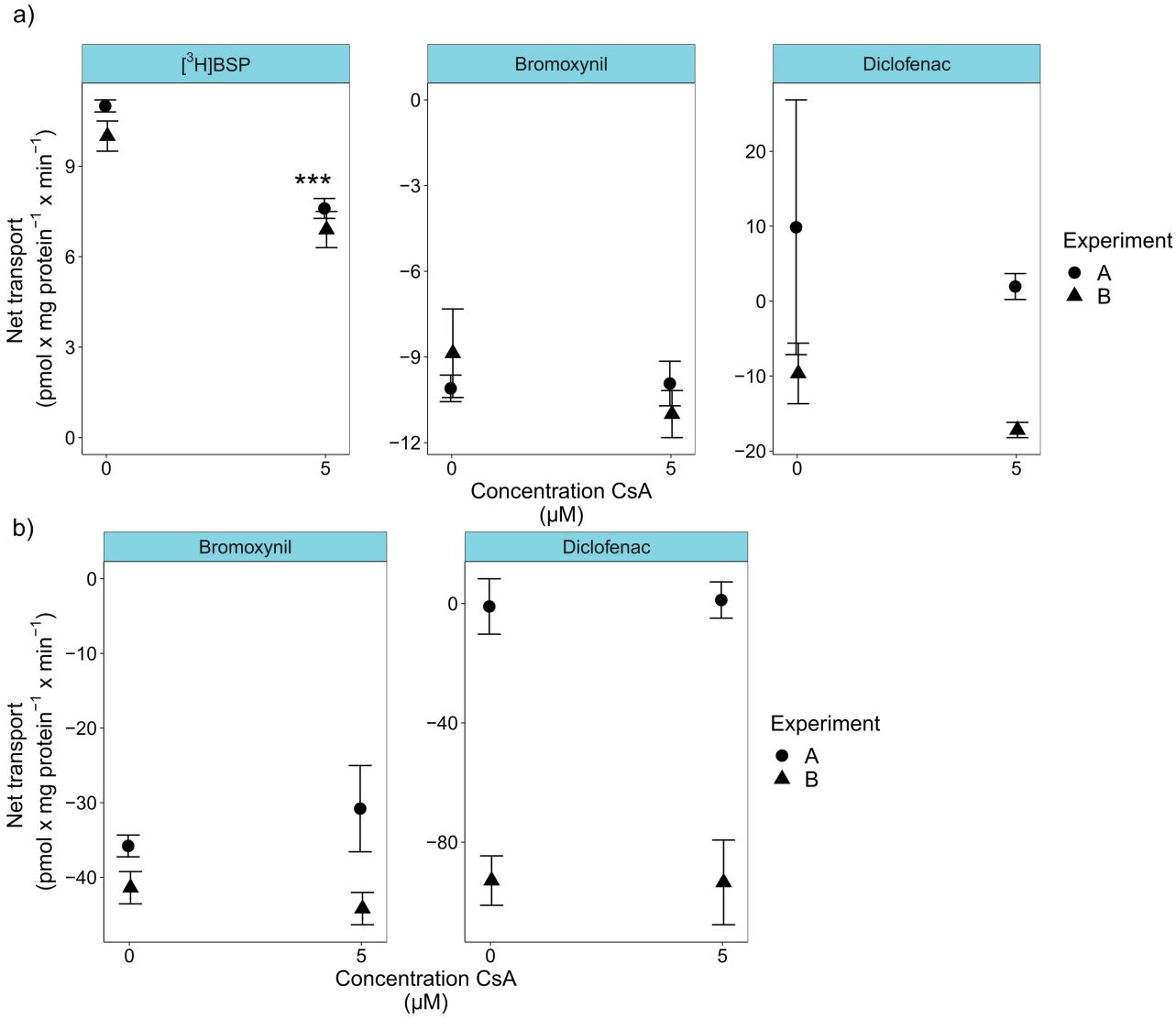

Figure S6. Effects of 5 µM cyclosporin A (CsA) on the uptake of (a) [3H]BSP at 1 µM and of bromoxynil and diclofenac, each at 10 µM and of (b) bromoxynil and diclofenac, each at 100 µM in Oatp1d1-transfected cells. Depicted are the net transport of [3H]BSP, bromoxynil, diclofenac, and carbamazepine when applied singly or in combination with CsA in a 10 min incubation. Net transport was calculated by subtracting the transport into Oatp1d1 cells from that into HEK-Co cells. Two independent experiments with three wells per concentration are presented as means ± SD, respectively. * indicates statistical significance (Manly's permutation test, *** $p < 0.001$).

Mixed incubation with bromoxynil and diclofenac

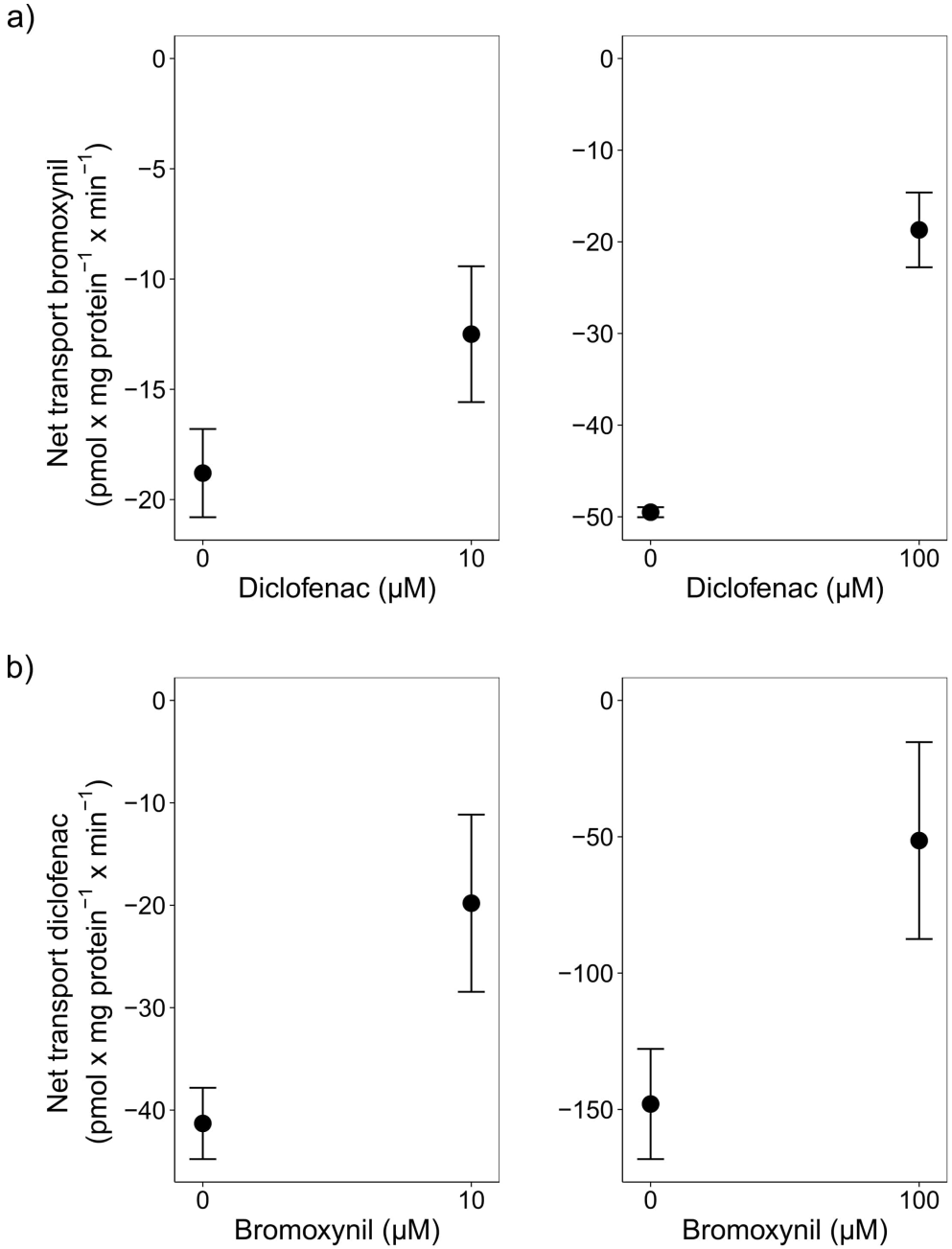

Figure S7. Effects of diclofenac and bromoxynil on the uptake of the respective other compound (expressed as net transport) in Oatp1d1-transfected cells. Depicted is the net transport of bromoxynil (a) and diclofenac (b) when applied singly or in combination with 10 (left)) or 100 µM (right)) of the respective other compound in a 10 min incubation. Net transport was calculated by subtracting the transport into Oatp1d1 cells from that into HEK-Co cells. Shown are means from three wells per concentration (circles) ± SD.

Results zebrafish embryo experiments

Effects on the phenotype of zebrafish embryos

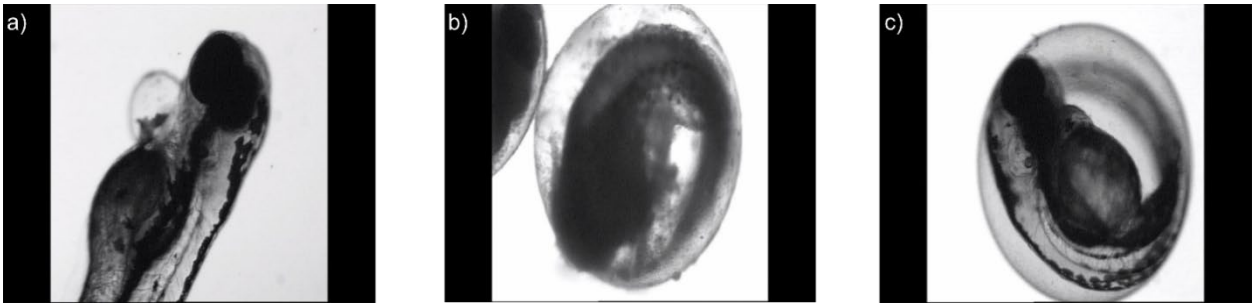

Figure S8. Microscopic pictures of zebrafish embryos exposed for 96 h at the a) EC25 of diclofenac with 50 µM BSP (edema pericard), b) EC25 of bromoxynil with 100 µM BSP (coagulation), and c) EC25 of carbamazepine with 100 µM BSP (no hatching).

Table S4. Observed toxicity on the phenotype in the exposure of 24 h (embryonic stage). k: coagulation; mtail: tail deformation; nodt: no detachment of tail; nosf: no formations of somites; ret: retardation

Substance A (exposure concentration)	Substance B (exposure concentration)	Total effects [%] Experiment 2	Total effects [%] Experiment 3	Effects
Control		0	0	
BSP (50 µM)		0	0	
BSP (100 µM)		0	0	
Bromoxynil (EC5)		0	0	
Bromoxynil (EC5)	BSP (50 µM)	0	0	
Bromoxynil (EC5)	BSP (100 µM)	8	0	k
Bromoxynil (EC25)		8	0	k
Bromoxynil (EC25)	BSP (50 µM)	0	8	ret, nodt, nosf
Bromoxynil (EC25)	BSP (100 µM)	0	0	
Diclofenac (EC5)		0	0	
Diclofenac (EC5)	BSP (50 µM)	0	17	k
Diclofenac (EC5)	BSP (100 µM)	8	0	k
Diclofenac (EC25)		0	17	k, ret, nodt, nosf
Diclofenac (EC25)	BSP (50 µM)	0	0	
Diclofenac (EC25)	BSP (100 µM)	0	0	
Carbamazepine (EC5)		0	0	
Carbamazepine (EC5)	BSP (50 µM)	17	0	k
Carbamazepine (EC5)	BSP (100 µM)	0	0	
Carbamazepine (EC25)		17	8	k, mtail
Carbamazepine (EC25)	BSP (50 µM)	0	0	
Carbamazepine (EC25)	BSP (100 µM)	0	0	

Table S5. Observed toxicity on the phenotype in the exposure of 24 h (larval stage). mtail: tail deformation; sco: scoliosis; (beh: observation of less movement)

Substance A (exposure concentration)	Substance B (exposure concentration)	Total effects [%] Experiment 2	Total effects [%] Experiment 3	Effects
Controls		0	0	
BSP (50 µM)		0	0	
BSP (100 µM)		0	0	
Bromoxynil (EC5)		0	0	
Bromoxynil (EC5)	BSP (50 µM)	17	0	sco
Bromoxynil (EC5)	BSP (100 µM)	0	0	
Bromoxynil (EC25)		0	0	
Bromoxynil (EC25)	BSP (50 µM)	0	0	
Bromoxynil (EC25)	BSP (100 µM)	0	0	
Diclofenac (EC5)		0	0	
Diclofenac (EC5)	BSP (50 µM)	0	0	
Diclofenac (EC5)	BSP (100 µM)	8	0	mtail
Diclofenac (EC25)		0	0	
Diclofenac (EC25)	BSP (50 µM)	0	0	
Diclofenac (EC25)	BSP (100 µM)	0	0	
Carbamazepine (EC5)		0	0	(beh)
Carbamazepine (EC5)	BSP (50 µM)	0	0	(beh)
Carbamazepine (EC5)	BSP (100 µM)	0	0	(beh)
Carbamazepine (EC25)		0	0	(beh)
Carbamazepine (EC25)	BSP (50 µM)	0	0	(beh)
Carbamazepine (EC25)	BSP (100 µM)	0	0	(beh)

Table S6. Observed toxicity on the phenotype in the mixed exposure to diclofenac and bromoxynil of 96 h. nohb: no heartbeat; nobc: no blood circulation; EdP: edema pericard; hf: heart frequency

Substance A (exposure concentration)	Substance B (exposure concentration)	Total effects [%] Experiment 1	Effects
Bromoxynil (EC5)		0	
Diclofenac (EC5)		27	EdP, no hatching
Bromoxynil (EC5)	Diclofenac (EC5)	71	hf, no hatching
Bromoxynil (EC25)		10	nohb, nobc
Diclofenac (EC25)		43	EdP
Bromoxynil (EC25)	Diclofenac (EC25)	93	EdP, nohb, no hatching

Internal concentration: mixed exposure to bromoxynil and diclofenac

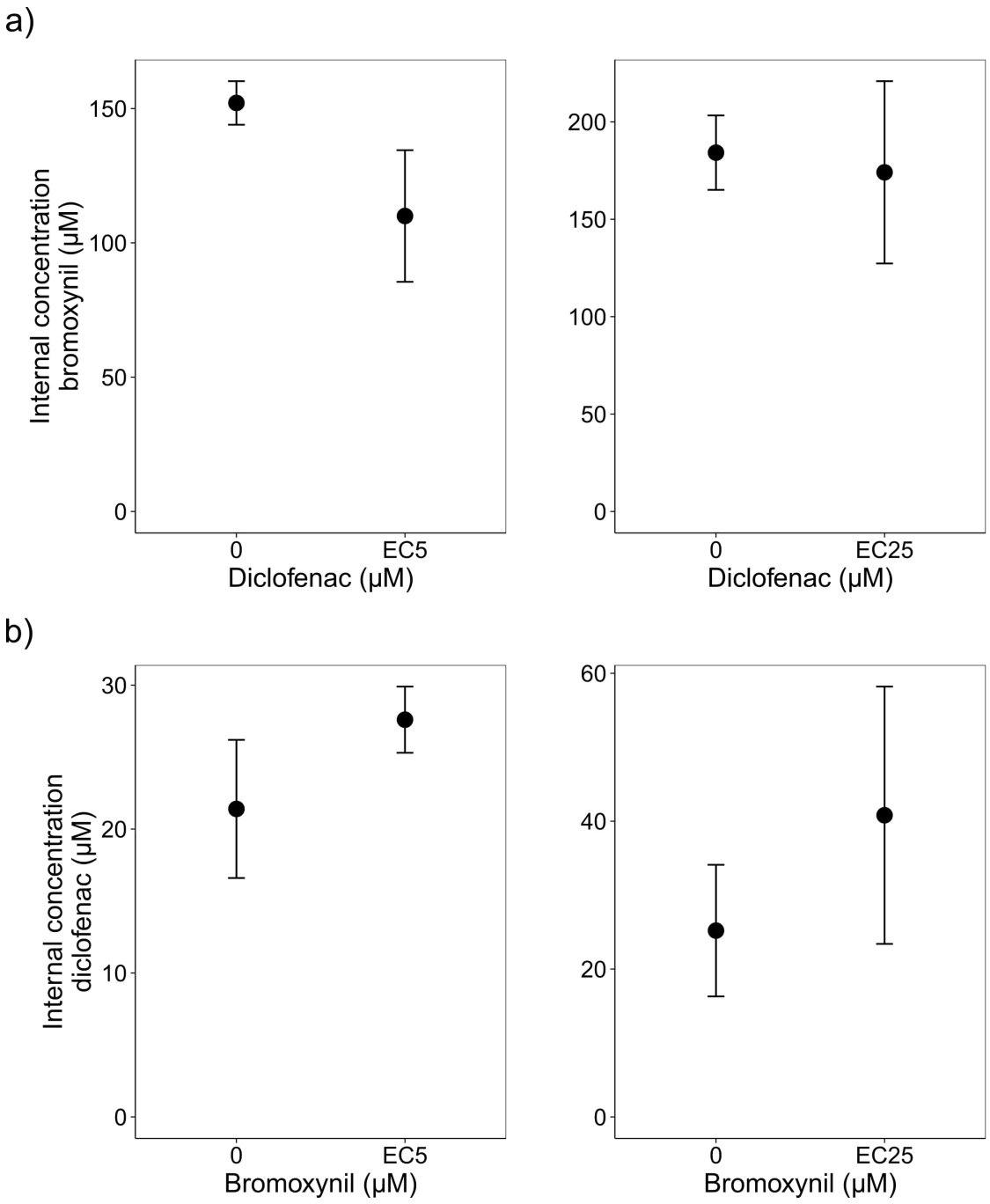

Figure S9. Effects of diclofenac and bromoxynil on the uptake of the respective other compound (expressed as internal concentration) in zebrafish embryos. Depicted is the internal concentration of bromoxynil (a) and diclofenac (b) when applied singly or in combination with EC5 (left) or EC25 (right) of the respective other compound. Shown are means from three replicates from one egg batch consisting of three pooled embryos (circles) ± SD.

MALDI-MS imaging: Bromoxynil isotopes peaks

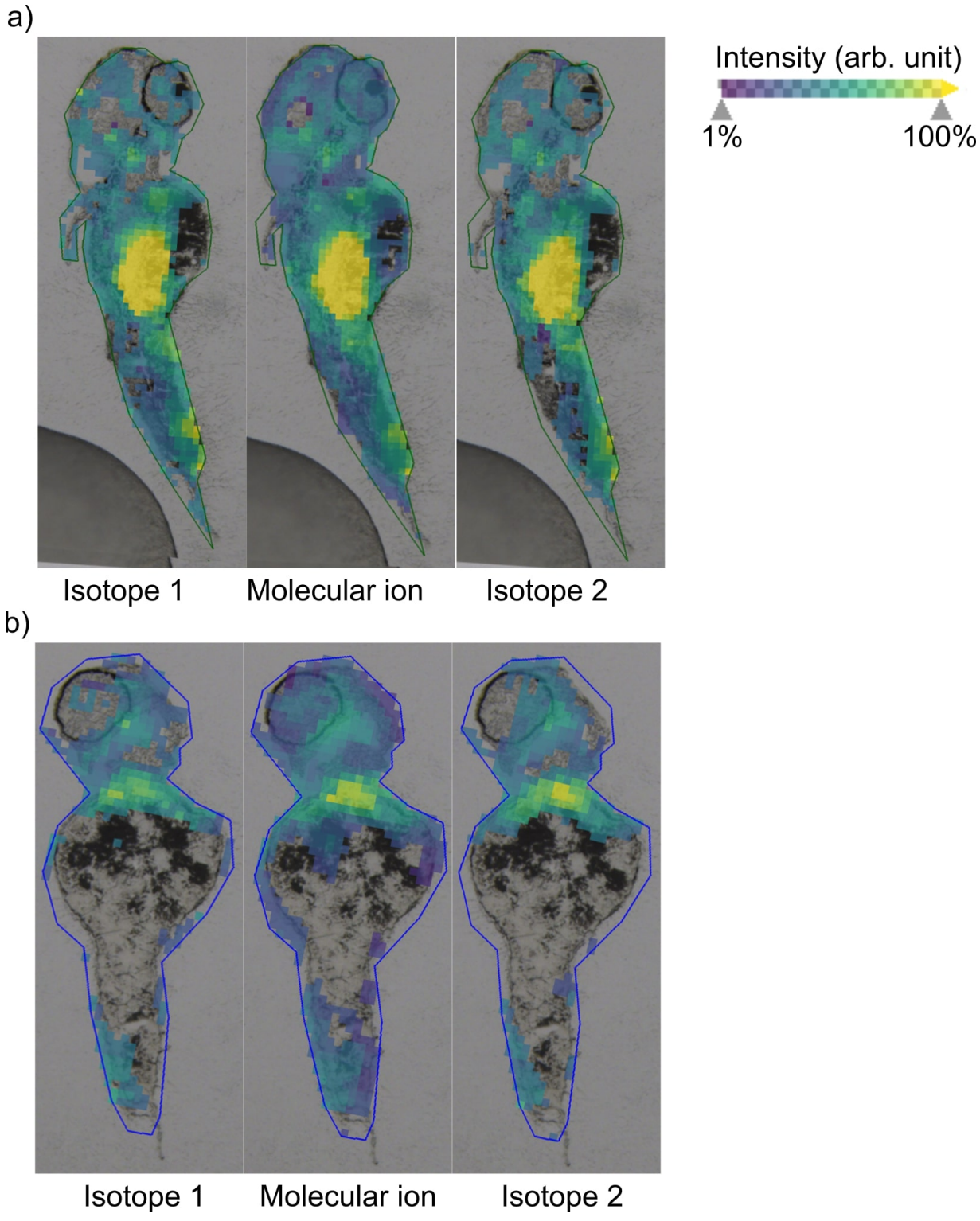

Figure S10. Distribution of bromoxynil isotopes: molecular ion (275.84671 m/z ± 0.19313 mDa) and the two most abundant isotopes 1 (273.84877 m/z ± 0.30818 mDa) and 2 (277.8447 m/z ± 0.27828 mDa) in two exposed zebrafish embryos (a and b). The colored line shows the measured area. The exposure duration was 72 h. The color bar shows the range from low (purple) to high bromoxynil intensity (yellow). Calculated theoretical relative (to the molecular ion) intensity ratios of the isotopes (1 and 2) are 51.3 and 49.0%. Measured relative intensity ratios were for a) 65.7 and 46.4%, b) 52.0 and 63.9%.

LA-ICP-MS negative control

a)

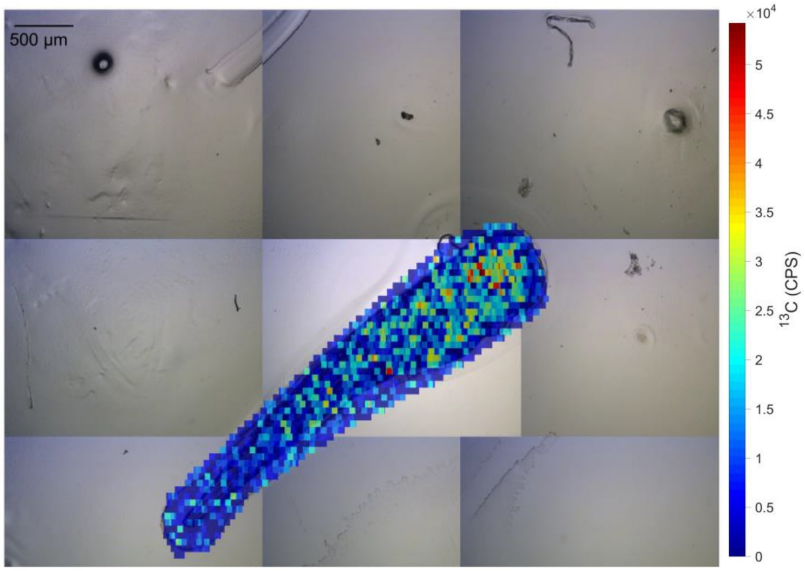

b)

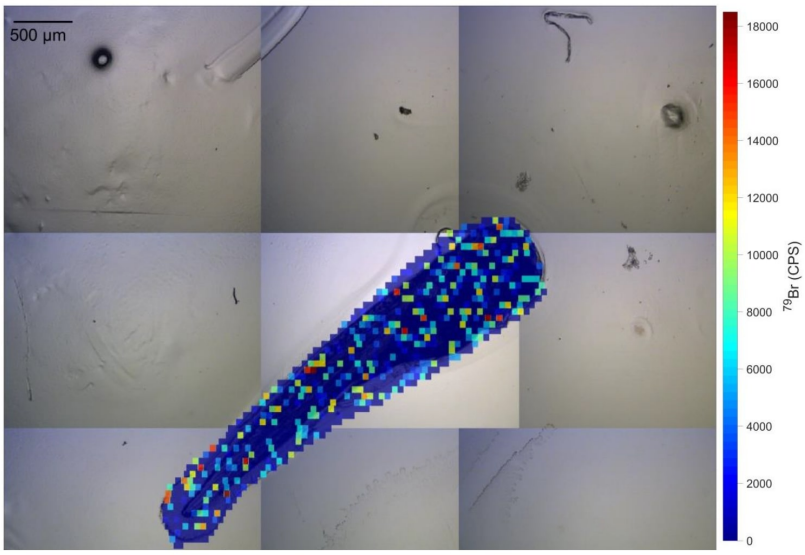

c)

Figure S11. LA-ICP-MS results of zebrafish embryo exposed for 96 h to ISO-water (negative control). The intensity of the 13C distribution (a), 79Br intensity (b), and microscopic picture before the ablation (c) are shown.

Chapter 6 Spatial distribution of biotransformation products and quantification of their contribution in the zebrafish embryo

Unpublished work

Introduction

The zebrafish embryo (*Danio rerio*) is an important model organism and used in various research fields such as ecotoxicology and toxicity testing of chemicals.[1,2] The zebrafish embryo is widely used as an alternative to animal testings because the European law does not protect the early developmental stages[3]. Toxicity measurements showed a similar sensitivity of the embryonic and early larva developmental stage with adult fish.[4,5] In some cases, the fish embryo toxicity test (FET) has replaced the acute fish toxicity (AFT) test, e.g., for the wastewater effluent tests in Germany.[6] The registration and authorization of new chemicals in the European Union (REACH) are still applying AFT tests because application and limitation domains of the FET are not sufficiently defined. Within the framework of FET, one uncertainty is the embryo's metabolic capacity.[7]

The metabolism of xenobiotics comprises phase I biotransformation (oxidative, reductive, or hydrolytic reaction) and phase II conjugation reactions, increasing the polarity of the xenobiotics.[8] Several studies have shown the expression of metabolic enzymes in the zebrafish embryo. Among them are the cytochrome P450 enzymes (CYP), glutathione-S-transferase (GST), sulfotransferase (SULT), and UDP- glucuronosyltransferase (UGT).[9–13] Furthermore, biotransformation of several xenobiotics, e.g., benz[a]anthracene[14], cocaine[15], valproic acid, benzocaine[16], clofibric acid[17] has been reported. The quantification of the transformation products is difficult because of unknown identity and missing analytical standards.

The present chapter investigates the spatial distribution of the 4-iodophenol, bromoxynil, diuron, and clofibric acid metabolites. The objective is to localize tissues involved in the biotransformation, estimate the quantitative amount of biotransformation, and determine whether the transformation products distribute within the zebrafish embryo. We combined mass spectrometry (MS) imaging techniques with bulk analysis of embryo extracts for this purpose. We studied the accumulation of the biotransformation products of 4-iodophenol, bromoxynil, and diuron between the embryonic body and the yolk to test the hypothesis of xenobiotics metabolism in the yolk. To complement the observations for 4-iodophenol laser ablation inductively coupled plasma-MS (LA-ICP-MS) was

used to study the spatial distribution of iodine-containing transformation products. We estimated the quantitative contributions of biotransformation of 4-iodophenol and bromoxynil with Nebulization-ICP-MS (Neb-ICP-MS) and LA-ICP-MS. Matrix-assisted laser desorption/ionization-(MALDI-) MS imaging explores the spatial distribution of the taurine metabolite of clofibric acid in comparison with the transforming enzyme.

The results can be used to answer (i) how quantitatively metabolism is affecting the steady-state concentration; (ii) are enzymes in the yolk also transforming chemicals; (iii) do metabolites localize in the transforming tissue.

Material & methods

Chemicals

The following chemicals have been used: clofibric acid (ICN Biomedicals Inc.), 4-iodophenol (Sigma-Aldrich (Seelze, Germany), trifluoroacetic acid (TFA, Sigma-Aldrich, Steinheim, Germany), NEG50 (Thermo Scientific, Schwerte, Germany).

Culture of Zebrafish and Collection of Eggs

We used the UFZ-OBI strain (generation F13−16), which was obtained initially from a local breeder and kept for several generations at the UFZ. Fish were cultured and used according to the German and European animal protection standards and approved by the Government of Saxony, Landesdirektion Leipzig, Germany (Aktenzeichen 75- 9185.64).[18] Embryos between 4-cell and 16-cell stage were separated on the day of spawning.

Exposure

Exposures are summarized in Figure 1. Exposure conditions for 4-iodophenol, bromoxynil, and diuron can be found in Chapter 4. Additionally, exposure to 4-iodophenol was performed for LA-ICP-MS measurements, and exposure conditions for clofibric acid are reported in the following.

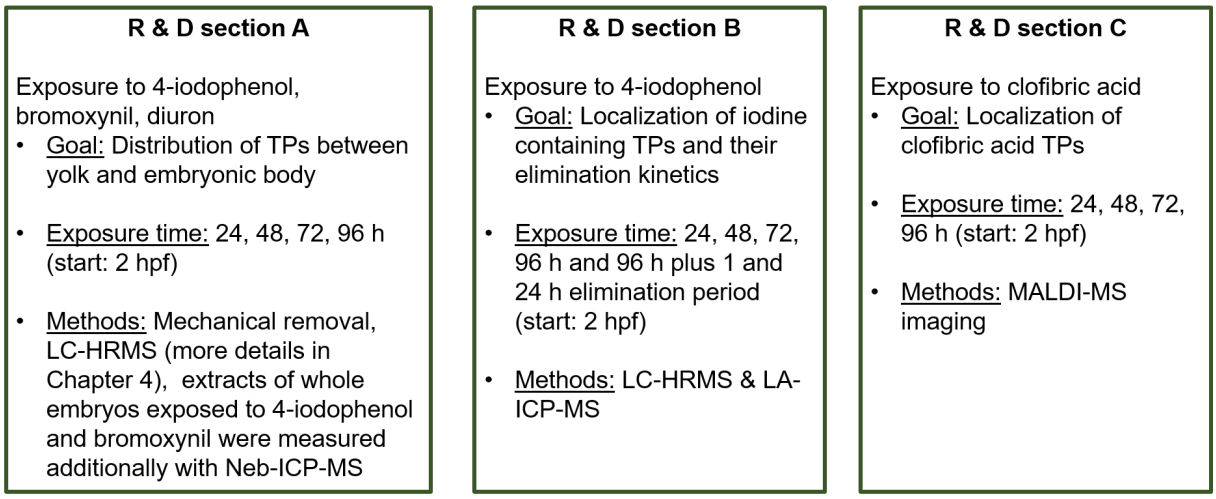

Figure 1. Overview of experiments discussed in this chapter and the applied analytical methods. (TP: transformation product)

The exposure experiments were performed according to the OECD 236.[19] Nine zebrafish embryos were transferred with 90 µL into a 20 mL glass vial containing 18 mL exposure solution or ISO-water[20] for control measurements. Vials were closed with metal lits and incubated in a climatic chamber (26 ± 1°C) and a light/dark cycle (14 h/10 h). Vials were horizontally shaken at 75 rpm. Exposure solutions without the embryos were run in parallel to control the stability of the substance. Three replicates per exposure duration were performed. At the beginning and end of the exposure, aliquot samples of the exposure solution were taken and stored at -20°C. Oxygen (VWRDO200, VWR Instruments) content and pH (pH 720, WTW Series, InoLab) were measured at the beginning and end of the experiment.

Exposure to 4-Iodophenol

4-Iodophenol was directly dissolved in ISO-water[20] at a measured exposure concentration of10.3 ± 2.6 µM. Embryos were exposed starting at 2±1 hours post fertilization (hpf) for 24, 48, 72, and 96 h.

Exposure to clofibric acid

Clofibric acid was directly dissolved in ISO-water[20], and the nominal exposure concentration was 0.23 mM (LC50 > 2.8 mM[17]). Embryos were exposed for 24, 48, 72, and 96 h.

Sample preparation

LC-HRMS of 4-iodophenol for R&D section B

At the end of the experiment, nine pooled embryos were pipetted into a FastPrep Tube (MP Biomedicals, Solon, OH, USA), washed twice with 1 mL Milli-Q water, snap-frozen in liquid

nitrogen, and stored at -20 °C. If the chorion was still present, it was carefully removed under the microscope before washing.

The stored embryo samples were extracted with 270 µL methanol. The samples were placed in a FastPrep®-24 instrument (MP Biomedicals, Solon, OH, USA) for 30 s at 6 U/S. Afterward, samples were placed in an ultrasonic bath for 15 min and centrifuged for 15 min at 13000 rpm (VWR Galaxy 14D microcentrifuge). The supernatant was taken and transferred to a 1.5 mL glass vial and diluted in methanol:Milli-Q water (1:1, v/v) for the LC analysis.

Calibration standards for the LC measurements were prepared in methanol:Milli-Q water (50:50, v/v) from 0.1 to 100 ng/mL.

Neb-ICP-MS

Embryo extracts of embryos exposed to 4-iodophenol and bromoxynil were diluted after LC-HRMS measurements. 75 µL of 4-iodophenol extracts were taken and diluted with 3 mL Milli-Q water. 75 µL bromoxynil extract and diluted with 5 mL 1% HNO_3.

LA-ICP-MS (4-iodophenol exposure)

For the LA-ICP-MS experiments, the chorion, if still present, was removed, the embryos were washed twice with 1 mL Milli-Q water in an Eppendorf tube and carefully placed on a glass slide. Water was removed, and embryos were dried at room temperature.

MALDI-MS imaging (clofibric acid exposure)

The chorion was removed, if still present, and embryos were washed twice with 1 mL Milli-Q water. The embryo was first carefully swiped with a plastic pipette through NEG50 in order to remove excess water and then transferred to a cryomold containing NEG50. The cryomolds were immediately placed on dry ice and frozen wrapped in aluminum foil. They were stored at -80 °C until cutting.

The cryomolds were placed into a microtome (Cryo-Star HM 560, Microm International, Walldorf, Germany) at -17 °C for 24 h prior to cutting. The embryos were cut into 12 µM slices and transferred to an ITO-coated glass slide (Bruker, Bremen, Germany). The slice was mounted on the slide by carefully placing the warm hand under the slide. The glass slides were dried and stored (maximum five days) until matrix application in a desiccator at 200-300 mbar.

On the day of analysis, teaching marks were drawn onto the glass slides with a white pen. Slides were weighed and scanned (OpticLab H580, Plustek, Ahrensfelde, Germany).

9-AA was chosen as a matrix and applied via sublimation. The sand bath was heated to 210 °C and kept at about 65 W. 300 mg 9-AA was placed in the sublimation device, the slides mounted with adhesive tape, and ice/water added. The vacuum was applied for 30 min with a pressure of 2 to 5 mbar. Afterward, the slides were weighed again. The average matrix amount per slide was 9.2 µg/cm^2.

LC-HRMS measurements

Liquid chromatography-high resolution MS (LC-HRMS) parameters for 4-iodophenol, bromoxynil, and diuron and molecular formulas for detected transformation products can be found in Chapter 4. Data were analyzed in OriginPro 2020. Peak areas of transformation products were normalized to the peak area of the internal standard.

Neb-ICP-MS

Nebulization (Neb-) ICP-MS was performed with an ICap-Q (ICap-Q, Thermo Scientific, Waltham, USA). Parameter settings are listed in Table 1.

Table 1. Neb-ICP-MS settings for the iodine and bromine measurement, respectively.

Parameter	Iodine	Bromine
RF power (W)	1550	1550
Cooling gas flow rate, Argon (L/min)	14	14
Auxiliary gas flow rate, Argon (L/min)	0.8	0.8
Nebulizer gas flow rate, Argon (L/min)	1.15	1.01
Dwell time (s)	1	0.1

The calibration of the instrument was performed with an iodide and bromide solution. The detection limit of the iodine measurement was 0.04 µg/L (limit of quantification 0.13 µg/L), and of the bromine 0.42 µg/L (limit of quantification 1.37 µg/L). In the negative control extracts of the bromoxynil exposure, a background level of bromine was detected; therefore, the quantification limit was set to 1.7 µg/L.

LA-ICP-MS measurements

LA-ICP-MS measurements were performed with an Analyte G2 (Teledyne CETAC Technologies Inc., Bozeman, MT, USA) coupled to a double-focusing sector field ICP-MS (Spectro, Ametek, Kleve, Germany). Zebrafish embryos were ablated in line scan mode. Parameters for the measurements are listed in Table 2. Quantification was performed with agarose gels spiked with iodide ICP-MS standard solution.[21] The standards were ablated under the same parameters as the zebrafish larvae (LOD 14 pg per 35 µm spot for ^{127}I and LOQ 24 pg). A calibration curve for the

iodine measurements can be found in Chapter 3. Data analysis was performed with Iolite 3.6 in Igor Pro 7.04. The workflow included a baseline subtraction, a correction of drift in intensity over time measured with the agarose standards, and the quantification of counts per second to mass. Exported data were overlaid with the optical photograph in MATLAB R2015b.

Table 2. LA-ICP-MS parameters.

LA-ICP-MS parameters for measurements	
RF power (W)	1300
Cooling gas flow rate, Argon (L/min)	13.50
Auxiliary gas flow rate, Argon (L/min)	2.6
Carrier gas flow rate, Helium (L/min)	0.8
Integration time (s)	1
Base interval (ms)	100
Wavelength of ArF laser (nm)	193
Laser beam diameter (µm)	35
Laser scan speed (µm)	35
Repetition frequency (Hz)	125
Laser fluence (J/cm^2)	1.77 (25% laser output at energy setpoint of 4.5 mJ)

MALDI-FT-ICR-MS imaging measurement

MS imaging measurements were carried out with a MALDI ion source (1kHz Laser of 335 nm, Smartbeam II, Bruker Daltonics, Bremen, Germany) coupled to an FT-ICR-MS (solarix XR 12T, Bruker Daltonics, Bremen, Germany). Parameter setting and measurement were conducted with ftms Control Software (Bruker Daltonics, Bremen, Germany) and teaching the position with Flex Imaging Software (Bruker Daltonics, Bremen, Germany). Clofibric acid exposed embryo sections were measured in negative mode with the following parameter settings: 14% laser power, 500 shots, 1000 Hz, minimum laser focus, 25 µM raster width.

MALDI-MS imaging data were imported to SCiLs Lab 2017; weak denoising, hotspot removal, and total ion count normalization were applied.

MS imaging data were scanned for clofibric acid and known transformation products. Only the taurine metabolite ($C_{12}H_{16}O_5NSCl$, m/z $[M-H]^-$ 320.0366) was detected. Peak identity was confirmed with the second most abundant isotope (m/z $[M-H]^-$ 322.0338). The theoretical abundances are 100% and 39%, and we measured 100% and 36% and 100% to 19%, depending on the section. Furthermore, the peaks were not visible in negative control embryo sections.

Results & discussion

A Distribution of transformation products of 4-iodophenol, bromoxynil, and diuron between yolk and embryonic body

In Chapter 4, we discuss the distribution of xenobiotics between the yolk and embryonic body. For the three substances 4-iodophenol, bromoxynil, and diuron, several transformation products were detected with LC-HRMS.[22] The peak areas of transformation products present within the first 72 h of exposure are shown and discussed in this chapter (Table 3). 4-Iodophenol and bromoxynil contained heteroelements (iodine and bromine) that are naturally not present in the zebrafish embryo; thus, quantifying the total elemental content was possible. Neb-ICP-MS was used to quantify the total elemental uptake. This was compared to the internal amount of 4-iodophenol and bromoxynil determined with LC-MS. By this, we could estimate the amount of biotransformation products (Figure 2). After 48 h, 56% of the total iodine content could be attributed to 4-iodophenol, after 72 h 36%, and after 96 h of exposure only 11% (Figure 2a). About 66% of the total bromine was assigned to the parent compound bromoxynil after 72 h of exposure and 28% after 96 h (Figure 2b). Furthermore, diuron has two transformation products (DCPU: 3,4-dichlorophenyl urea and DCPMU: 3-(3,4-dichlorophenyl)-1-methyl urea), which were available as analytical standard and thus allowing quantification. It was calculated that 70% of the summed diuron and the two transformation products were represented by diuron after 96(Figure 2c)

Table 3. Information on detected transformation products in zebrafish embryos and on their mass spectrometry data. For the complete data set, see the Supporting information of Chapter 4.

Transformation product	**m/z Molecular ion (Δppm)**	**Assigned elemental composition**	**Label**
Diuron			
N-didemethyldiuron (DCPU)	201.9470 (3.5 ppm)	$C_7H_2NO_2Cl_2$	
N-dimethyldiuron (DCPMU)	219.0090 (0.9)	$C_8H_9N_2OCl_2$	
di-hydroxydiuron	286.9960 (2.1 ppm)	$C_9H_{10}N_2O_3NaCl_2$	
hydroxydiuron	271.002 (1.1)	$C_9H_{10}N_2O_2NaCl_2$	
4-Iodophenol			
glucuronide	394.963 (0.5 ppm)	$C_{12}H_{12}O_7I$	TP1
sulfate	298.888 (1.7 ppm)	$C_6H_4O_4SI$	TP2
dimer sulfate	390.914 (0.8 ppm)	$C_{12}H_8O_5SI$	TP3
dimer hydroxyl sulfate	406.909 (1 ppm)	$C_{12}H_8O_6SI$	TP4
hydroxy sulfate	314.883 (1.9 ppm)	$C_6H_4O_5SI$	TP5
glucuronide sulfate	476.936 (1.7 ppm)	$C_{12}H_{14}O_{10}SI$	TP6
hydroxy methyl sulfate	344.893 (0 ppm)	$C_7H_6O_6SI$	TP7
hydroxy cysteine glucuronide	585.989	$C_{18}H_{21}NO_{11}SI$	TP8
Bromoxynil			
hydrolyzed bromoxynil	273.8504 (0.4 ppm)	$C_7O_2NH_5Br_2$	TP1
hydrolyzed bromoxynil	273.8504 (0.4 ppm)	$C_7O_2NH_5Br_2$	TP2
sulfate	371.817 (1.9 ppm)	$C_7H_2NO_5SBr_2$	TP3
sulfate	371.817 (1.9 ppm)	$C_7H_2NO_5SBr_2$	TP4
disulfate	453.03	$C_7HNO_8S_2Br_2Na$	TP5
N-acetylcysteine sulfate	505.8215 (2.8 ppm)	$C_{11}H_{10}NO_8S_2Br_2$	TP6
N-acetylcysteine sulfate, debrominated	427.9109 (2.1 ppm)	$C_{11}H_{11}NO_8S_2Br$	TP7

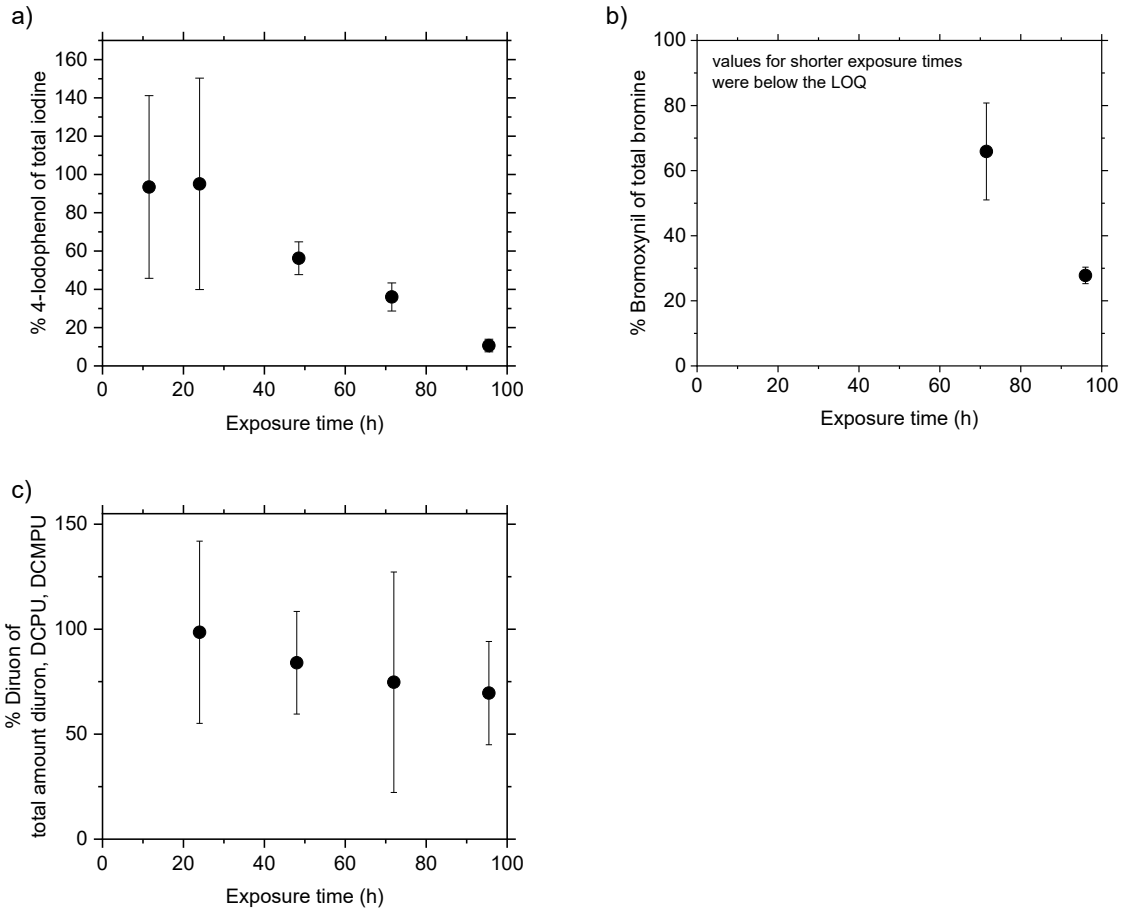

Figure 2. Percentage of parent compound (a) 4-iodophenol and (b) bromoxynil of total measured elemental iodine and bromine content, respectively. Parent compounds were quantified with LC-HRMS and elemental contents with Neb-ICP-MS. (c) Percentage of diuron of total quantified amounts of diuron, DCPU, DCMPU.

Among the detected transformation products of 4-iodophenol were hydroxylated, sulfated, methylated products and glutathione, and glucuronide conjugates (Figure 3a). For bromoxynil, hydroxylated and sulfated transformation products and N-Acetylcysteine conjugates were detected (Figure 3b). In the embryo extracts of the diuron exposure, hydroxy transformation products and the two previously reported[23] dehydroxylation and demethylation products, DCPU, and DCPMU were detected (Table 3).

For most of the detected transformation products of 4-iodophenol, bromoxynil, and diuron (Figure 4 to 6), the peak areas are larger in the whole embryo than in the embryonic body, suggesting that high fractions remain in the yolk. Two explanations can be postulated: biotransformation in the yolk and/or higher sorption of the transformation products to the yolk than the embryonic body. As previously shown, high proportions of neutral and especially hydrophobic chemicals accumulated in the yolk (Chapter 4). As transformation products are expected to be more polar, the sorption should be less to the yolk compartment. In addition, the yolk was shown to be actively involved in lipid metabolism.[24] Fraher et al.[25] discussed metabolic enzymes that are present in the yolk. Our

results indicate that the yolk can also biotransform xenobiotics as supported by the expression of several CYPs in the early zebrafish embryo. The CYPs likely originate from maternally derived transcripts. This fact may imply that the CYPs are at least in the first stages of the development inside the yolk. Furthermore, sulfotransferases sult2st1 expression was pronounced after labeling in the posterior of the yolk and the head.[26] The accumulation of diuron transformation product DCPMU in the yolk may be directly linked to its transforming enzyme CYP1.[23,27] CYP1 is expressed in the envelope of the yolk, intestine, and circulatory system.[28] In addition to the yolk, the yolk syncytial layer (YSL) also expresses metabolic enzymes[24] and may be involved in the biotransformation.

The results indicated the metabolism of xenobiotics inside the yolk. For future experiments, we recommend combining gene regulation, which can reflect enzymatic biotransformation, together with internal concentration measurements in the embryonic body and whole embryo. Furthermore, results of a later exposure start and shorter exposure time may better represent the site of transformation and exclude distribution within the zebrafish embryo.

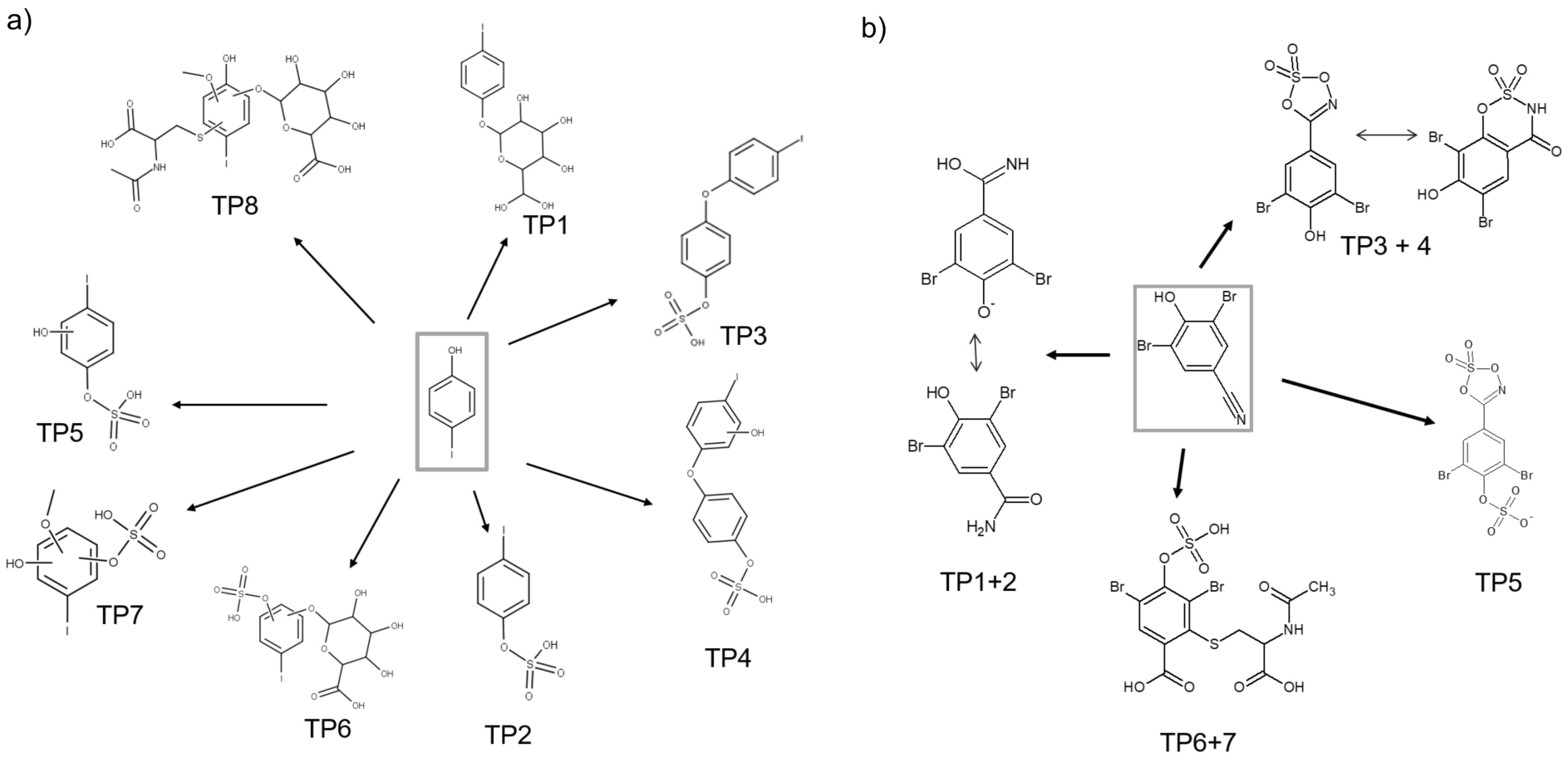

Figure 3. Proposed structures of transformation products (elemental formulas in Table 3) in zebrafish embryo extracts exposed to a) 4-iodophenol and b) bromoxynil.

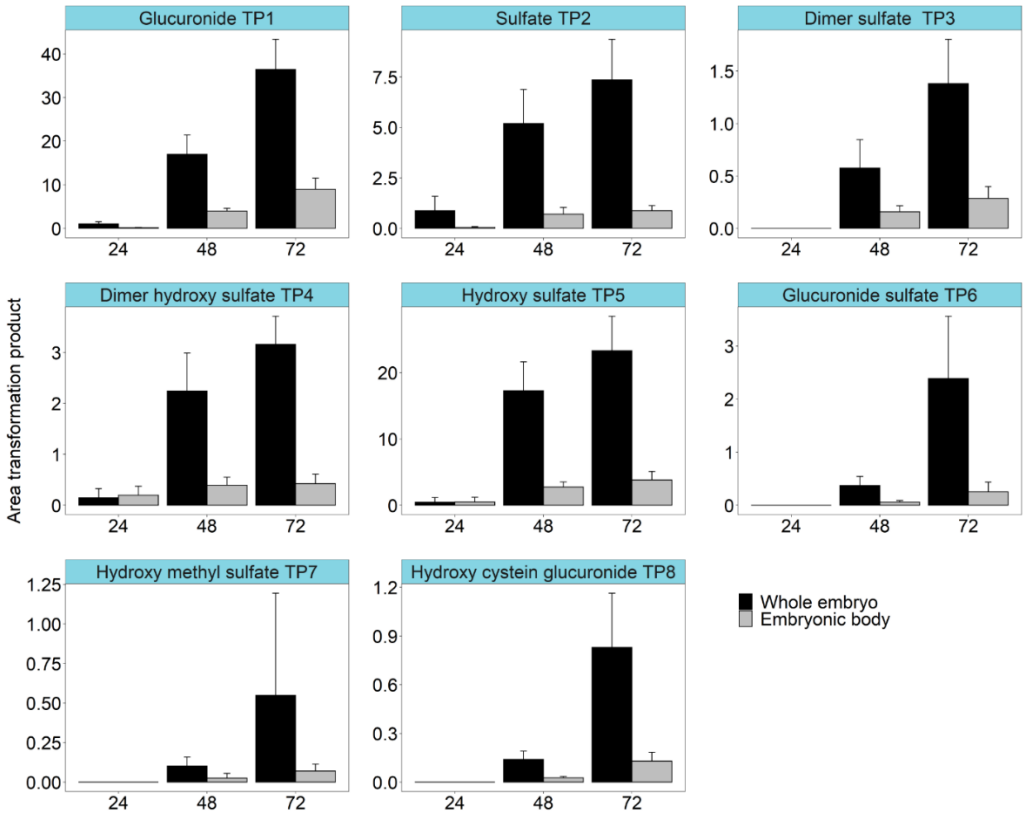

Figure 4. Peak area of transformation products of 4-iodophenol in the whole embryo and embryonic body. Embryos were exposed for 24, 48, and 72 h.

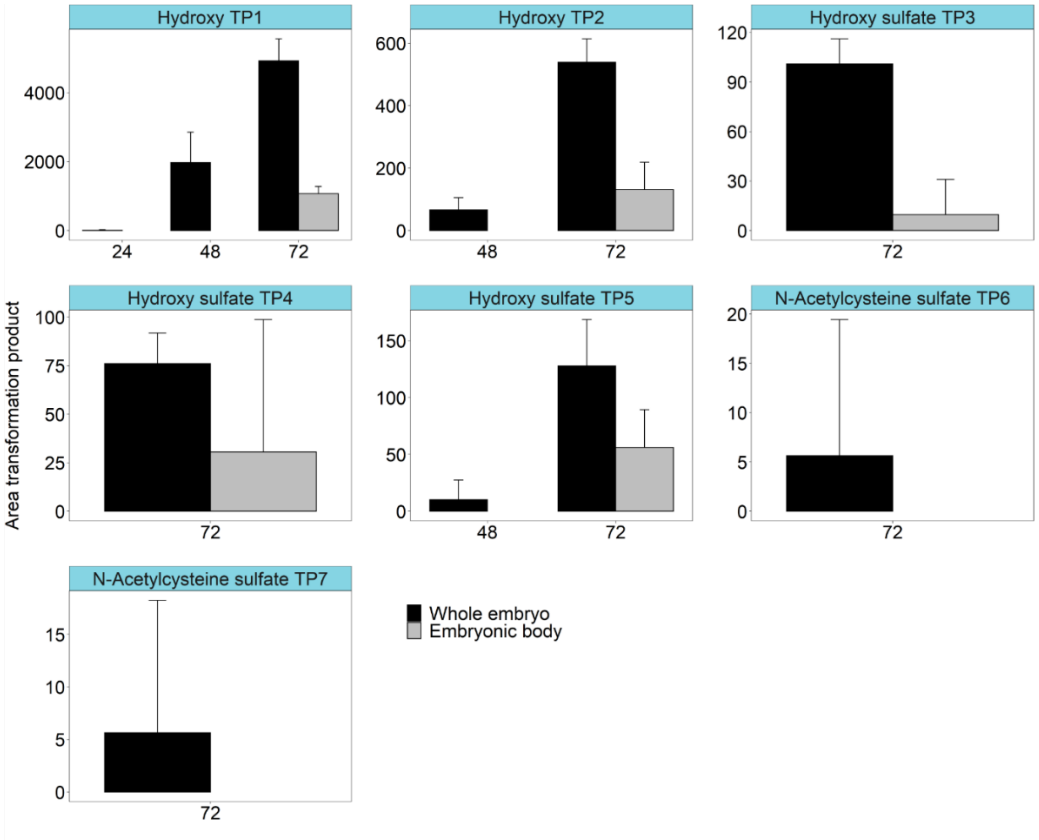

Figure 5. Peak area of transformation products of bromoxynil in the whole embryo and embryonic body. Embryos were exposed for 24, 48, and 72 h.

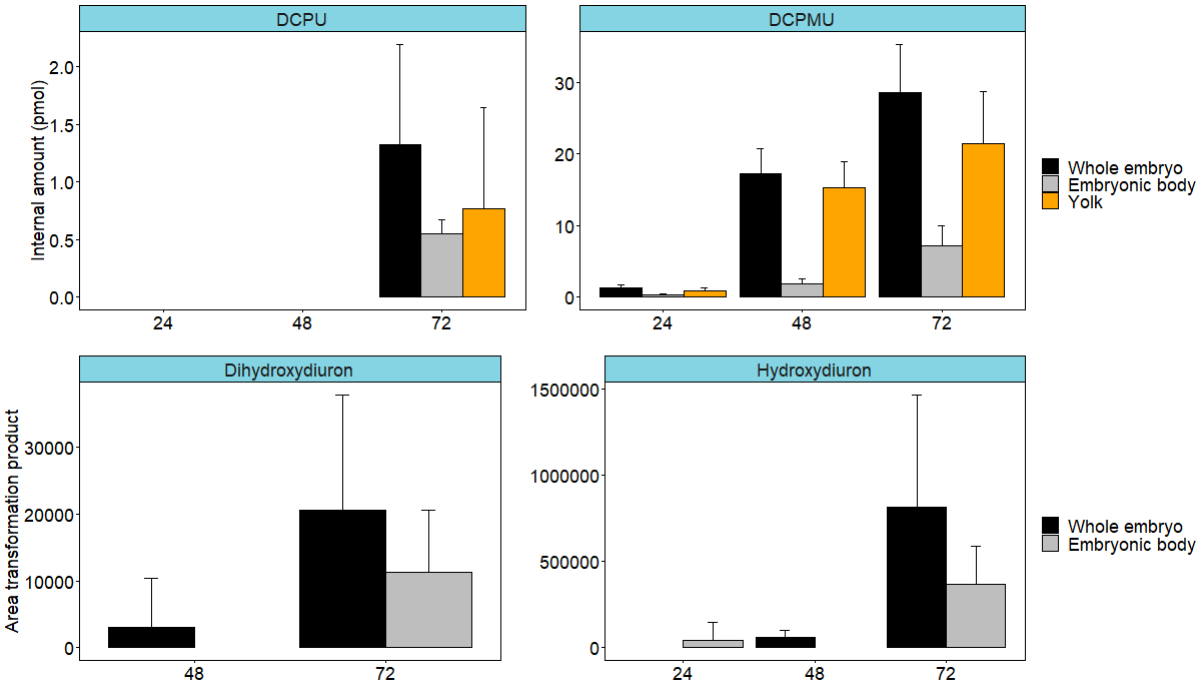

Figure 6. Quantified amount (DCPU: 3,4-dichlorophenyl urea, DCPMU: 3-(3,4-dichlorophenyl)-1-methyl urea) and peak area of transformation products of diuron in the whole embryo, embryonic body, and yolk. Embryos were exposed for 24, 48, and 72 h.

B Spatial distribution of iodine after 4-iodophenol exposure investigated with LA-ICP-MS

LA-ICP-MS was performed on embryos exposed to 4-iodophenol over 96 h, which were afterward placed in clean water for 24 h (elimination period). This allows following the accumulation of all iodine-containing substances (parent compound plus transformation products). LA-ICP-MS can support the previous results, and we can investigate older developmental stages (> 72 hpf) because the mechanical separation of the yolk was not possible in these stages.

The quantitative LA-ICP-MS results (Figure 8a) agreed with the previously determined iodine content in extracts by Neb-ICP-MS (Figure 2), demonstrating the successfully calibrated LA-ICP-MS data. The LA-ICP-MS results of the iodine to carbon ratio are displayed in Figure 7. This shows that the iodine intensity rises in the yolk with exposure duration. This supports previously reported sorption preferences of 4-iodophenol (Chapter 4). Already at 48 h of exposure, about 44% of the total iodine signal was associated with biotransformation products (Figure 2). The imaging data also indicate biotransformation in the yolk and/or preferred sorption of the transformation products to the yolk. Figure 7 underlines the findings of the mechanical separation of the yolk from the embryonic body in Figure 4. After 96 h of exposure, the iodine to carbon signal increased in the developing gastrointestinal (GI) tract. At this exposure duration, only 11% of the total iodine can be attributed to 4-iodophenol. The intestine contains many different enzymes involved in biotransformation, e.g., assays showing the activity of CYP1 and CYP2 enzymes (EROD, MCOD) showed increased activity in the intestine, liver, and anal pore at 104 hpf.[25,28]

Elimination kinetics showed that after 24 h, the parent compound was no longer present (Figure 8a). In contrast, several biotransformation products were detected in the extracts (Figure 8b), and the iodine signal was concentrated in the GI tract (Figure 7). This can likely be attributed to different sorption properties of the transformation products resulting in slower elimination than 4-iodophenol and ongoing glomerular filtration.[25]

Concluding, the GI tract is also an important body compartment for the accumulation of transformation products. This is presumably the result of the local expression of the transforming enzymes or the elimination route via the GI tract.

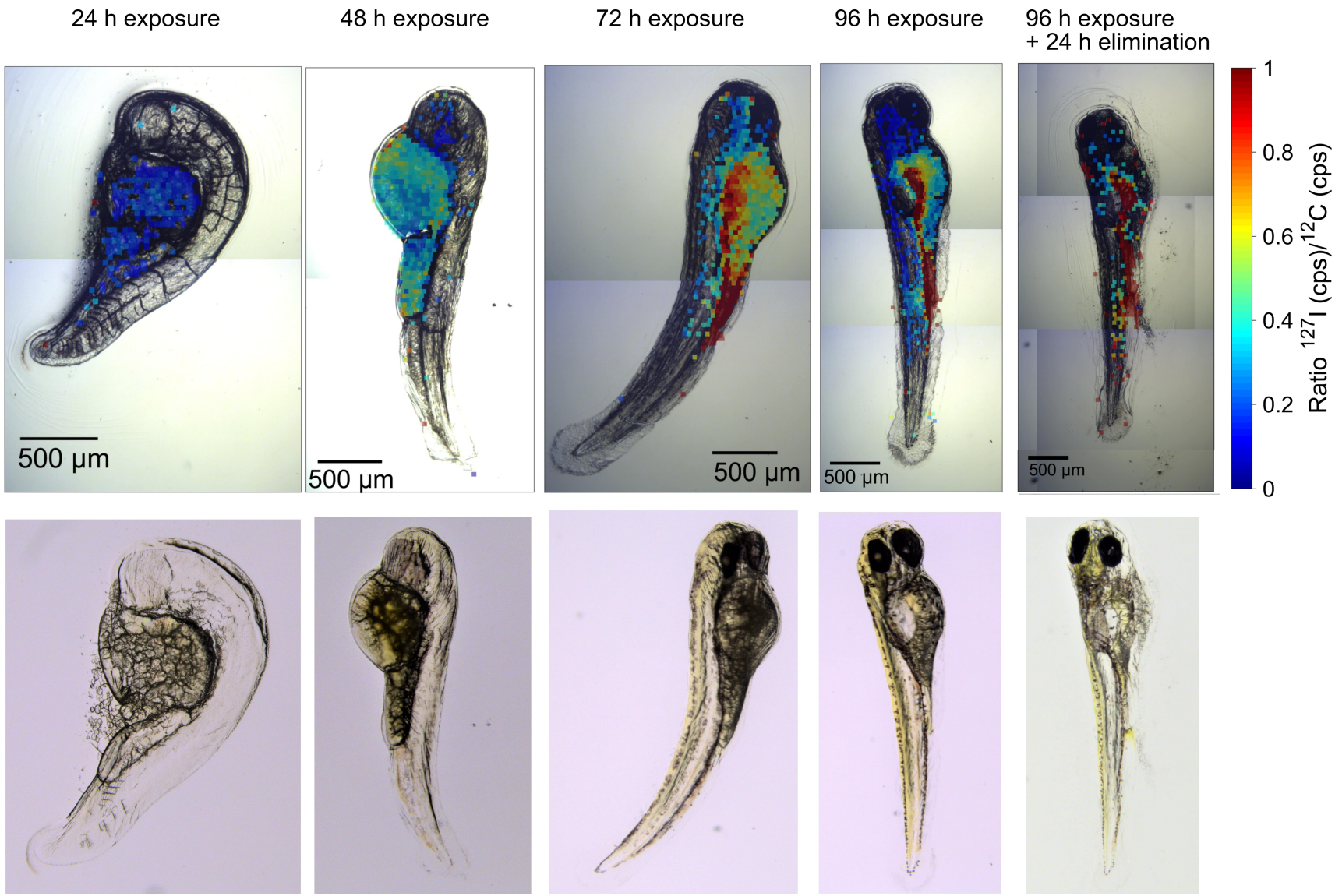

Figure 7. Ratios of iodine/carbon intensities (upper row) in zebrafish embryos exposed for 96 h to 4-iodophenol and afterward placed in clean water for 24 h. Measurements were performed with LA-ICP-MS. Corresponding microscopic images are displayed in the bottom row.

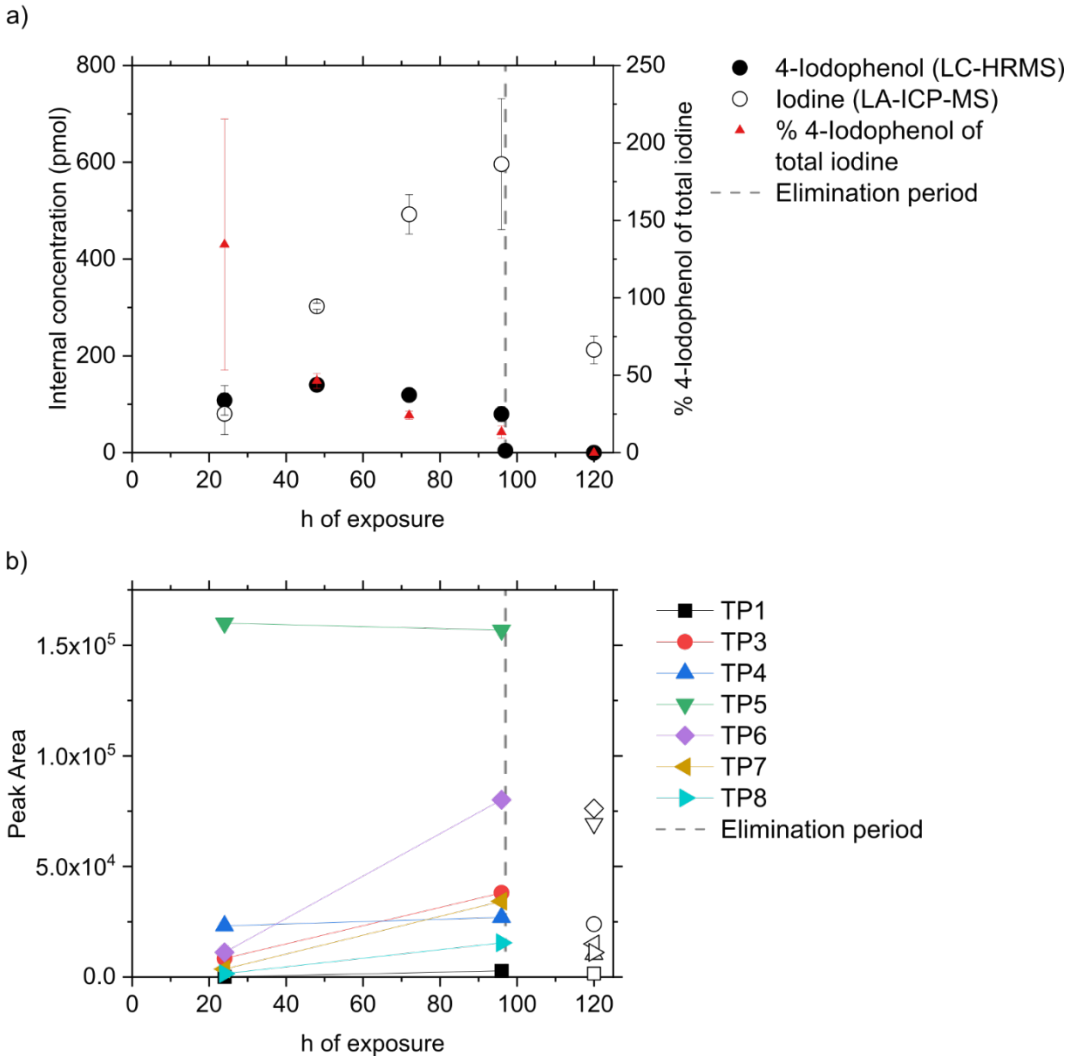

Figure 8. Time profiles of 4-iodophenol and transformation products in zebrafish embryos exposed for 96 h and afterward placed in clean water for 24 h. a) Internal concentration of 4-iodophenol measured with LC-HRMS and iodine measured quantitatively with LA-ICP-MS; b) Peak areas of transformation products of 4-iodophenol measured with LC-HRMS, for TP see explanation Table 3.

C MALDI-MS imaging of the clofibric acid taurine metabolite

The spatial distribution of clofibric acid and its transformation products was investigated with MALDI-MS imaging. Extensive biotransformation of clofibric acid was previously reported by Brox et al.[17] In our experiments, only one transformation product (taurine-conjugated clofibric acid, TP12 in Brox et al.[17]) was detected and not the parent compound because the method was not sensitive enough for the parent compound. An additional recrystallization step after sublimation may increase the extraction of the parent compound and improve the MALDI-MS imaging performance. The taurine metabolite was one of the transformation product also detected with large peak areas with LC-HRMS.[17]

The signal was apparent already after 48 h of exposure (Figure 9). The signal concentrated in a small spot above the yolk and around the yolk. At longer exposure durations, the signal was distributed in the whole GI tract (Figure 10). After 96 h of exposure, the high- and low-intensity areas varied up to one order of magnitude in their intensities. The taurine metabolite is formed by the N-acetyl transferase (NAT) and acyl-CoA synthetases (ACS) enzymes.[17] While the spatial expression of NAT is unknown yet, the expression of ACS was reported in the yolk syncytial layer (YSL) and the intestine (part of the GI tract) in the zebrafish embryo.[29] Hence, our results of the distribution of the transformation product corresponds to the tissue[29] expressing the transforming enzyme. Processes such as passive diffusion within the organism seem not to be quantitatively important for the taurine metabolite tissue distribution.

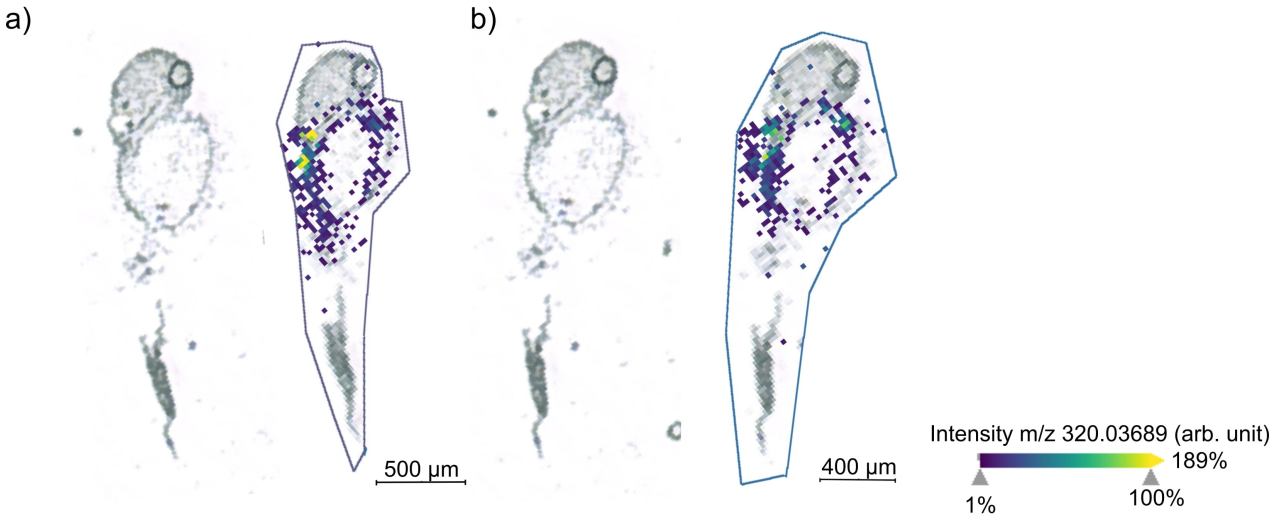

Figure 9. Spatial distribution of the clofibric acid taurine metabolite (m/z 320.03689 ± 1 mDa) in zebrafish embryo exposed for 48 h to clofibric acid (exposure start at 2 hpf).

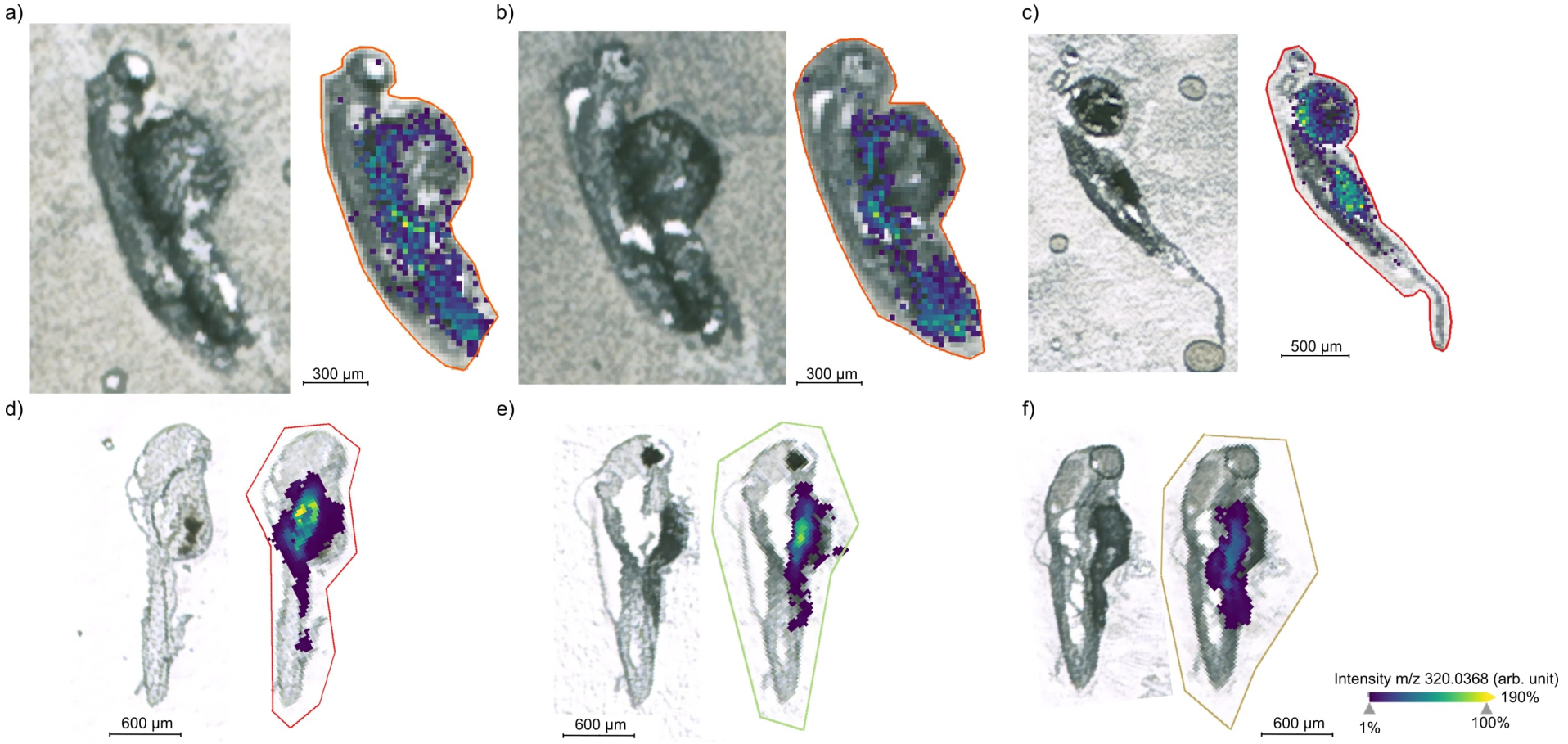

Figure 10. Spatial distribution of the clofibric acid taurine metabolite (m/z 320.0368 ± 1.3 mDa) in zebrafish embryo exposed for 72 h (a to c) and for 96°h (d to f) to clofibric acid (exposure start at 2 hpf).

Conclusion

In this study, we were able to quantify biotransformation products of 4-iodophenol, bromoxynil, and diuron. Amounts of transformation products clearly can extent their parent compounds. This is important for the toxicity evaluation as the transformation products can contribute to the effects in the zebrafish embryo. Furthermore, our data can be used to calculate steady-state kinetics, including the parameter, biotransformation rate, for the test compounds. We demonstrate that the transformation products of the three compounds accumulated to a major fraction in the yolk. Therefore, we assume that the yolk is active in xenobiotic metabolism, which has not been shown before. Additionally, the whole GI tract seems to be involved in the biotransformation and elimination of the transformation products of 4-iodophenol.

Moreover, our experiments showed that the clofibric acid taurine metabolite was localized in the tissue surrounding the yolk (likely the YSL) and in the GI tract, which agrees with the tissue expression of transforming enzymes. Surprisingly, the metabolite did not quantitatively distribute between the transforming and surrounding tissue in the organism. This has implications for the estimation of the potential toxicity of transformation products in target tissues:

(i) the target tissue is also the transforming tissue– the concentration at the target site may be much higher than the total internal concentration, enhancing the toxicity;

(ii) the target tissue is not the transforming tissue– the transformation product may not be able to reach the target site. Exposure experiments are also used to assess the toxicity of transformation products and expose the zebrafish embryo only to the transformation product dissolved in water. In this case, these exposure experiments could overestimate the toxicity of the transformation product.

Acknowledgments

The students Marta Muniz, Marion Lecluse, and Nina Morlet were involved in the experiments. Bettina Seiwert helped with the LC-HRMS measurements and the construction of possible transformation pathways. Josephine Karte performed Neb-ICP-MS measurements.

References

(1) Knöbel, M.; Busser, F. J. M.; Rico-Rico, Á.; Kramer, N. I.; Hermens, J. L. M.; Hafner, C.; Tanneberger, K.; Schirmer, K.; Scholz, S. Predicting Adult Fish Acute Lethality with the Zebrafish Embryo: Relevance of Test Duration, Endpoints, Compound Properties, and Exposure Concentration Analysis. *Environ. Sci. Technol.* **2012**. https://doi.org/10.1021/es301729q.

(2) Paparella, M.; Scholz, S.; Belanger, S.; Braunbeck, T.; Bicherel, P.; Connors, K.; Faßbender, C.; Halder, M.; Lillicrap, A.; Liska, R.; et al. Limitations and Uncertainties of Acute Fish Toxicity Assessments Can Be Reduced Using Alternative Methods. *ALTEX* **2020**, No. 2. https://doi.org/10.14573/altex.2006051.

(3) Strähle, U.; Scholz, S.; Geisler, R.; Greiner, P.; Hollert, H.; Rastegar, S.; Schumacher, A.; Selderslaghs, I.; Weiss, C.; Witters, H.; et al. Zebrafish Embryos as an Alternative to Animal Experiments-A Commentary on the Definition of the Onset of Protected Life Stages in Animal Welfare Regulations. *Reprod. Toxicol.* **2012**, *33* (2), 128–132. https://doi.org/10.1016/j.reprotox.2011.06.121.

(4) Lammer, E.; Carr, G. J.; Wendler, K.; Rawlings, J. M.; Belanger, S. E.; Braunbeck, T. Is the Fish Embryo Toxicity Test (FET) with the Zebrafish (Danio Rerio) a Potential Alternative for the Fish Acute Toxicity Test? *Comp. Biochem. Physiol. - C Toxicol. Pharmacol.* **2009**, *149* (2), 196–209. https://doi.org/10.1016/j.cbpc.2008.11.006.

(5) Belanger, S. E.; Rawlings, J. M.; Carr, G. J. Use of Fish Embryo Toxicity Tests for the Prediction of Acute Fish Toxicity to Chemicals. *Environ. Toxicol. Chem.* **2013**, *32* (8), 1768–1783. https://doi.org/10.1002/etc.2244.

(6) DIN. German Standard Methods for the Examination of Water, Waste Water and Sludge – Subanimal Testing (Group T) – Part 6: Toxicity to Fish. Determination of the Non-Acute-Poisonous Effect of Waste Water to Fish Eggs by Dilution Limits (T 6). *German Standardization Organization. DIN 38415-6*. 2003.

(7) Joint Report ECHA and UBA: Expert Workshop on the Potential Regulatory Application of the Fish Embryo Acute Toxicity (FET) Test under REACH, CLP and the BPR; European Chemical Agency, Umweltbundesamt: Helsinki, 2017.

(8) Beiras, R. Biotransformation. In *Marine Pollution*; Elsevier, 2018; pp 205–214.

https://doi.org/10.1016/b978-0-12-813736-9.00012-x.

(9) Jones, H. S.; Panter, G. H.; Hutchinson, T. H.; Chipman, J. K. Oxidative and Conjugative Xenobiotic Metabolism in Zebrafish Larvae in Vivo. *Zebrafish* **2010**, *7* (1), 23–30. https://doi.org/10.1089/zeb.2009.0630.

(10) Saad, M.; Cavanaugh, K.; Verbueken, E.; Pype, C.; Casteleyn, C.; Van Ginneken, C.; Van Cruchten, S. Xenobiotic Metabolism in the Zebrafish: A Review of the Spatiotemporal Distribution, Modulation and Activity of Cytochrome P450 Families 1 to 3. *J. Toxicol. Sci.* **2016**, *41* (1), 1–11. https://doi.org/10.2131/jts.41.1.

(11) Christen, V.; Fent, K. Tissue-, Sex- and Development-Specific Transcription Profiles of Eight UDP-Glucuronosyltransferase Genes in Zebrafish (Danio Rerio) and Their Regulation by Activator of Aryl Hydrocarbon Receptor. *Aquat. Toxicol.* **2014**, *150*, 93–102. https://doi.org/10.1016/j.aquatox.2014.02.019.

(12) Rastogi, A.; Clark, C.; Timme-Laragy, A. Mapping Glutathione Utilization in the Developing Zebrafish Embryo. *Free Radic. Biol. Med.* **2018**, *128*, S119. https://doi.org/10.1016/j.freeradbiomed.2018.10.291.

(13) Verbueken, E.; Bars, C.; Ball, J. S.; Periz-Stanacev, J.; Marei, W. F. A.; Tochwin, A.; Gabriëls, I. J.; Michiels, E. D. G.; Stinckens, E.; Vergauwen, L.; et al. From MRNA Expression of Drug Disposition Genes to in Vivo Assessment of CYP-Mediated Biotransformation during Zebrafish Embryonic and Larval Development. *Int. J. Mol. Sci.* **2018**, *19* (12), 1–30. https://doi.org/10.3390/ijms19123976.

(14) Kühnert, A.; Vogs, C.; Altenburger, R.; Küster, E. The Internal Concentration of Organic Substances in Fish Embryos-A Toxicokinetic Approach. *Environ. Toxicol. Chem.* **2013**, *32* (8), 1819–1827. https://doi.org/10.1002/etc.2239.

(15) Kirla, K. T.; Groh, K. J.; Steuer, A. E.; Poetzsch, M.; Banote, R. K.; Stadnicka-Michalak, J.; Eggen, R. I. L.; Schirmer, K.; Kraemer, T. Zebrafish Larvae Are Insensitive to Stimulation by Cocaine: Importance of Exposure Route and Toxicokinetics. *Toxicol. Sci.* **2016**, *154* (1), 183–193. https://doi.org/10.1093/toxsci/kfw156.

(16) Brox, S.; Seiwert, B.; Küster, E.; Reemtsma, T. Toxicokinetics of Polar Chemicals in Zebrafish Embryo (Danio Rerio): Influence of Physicochemical Properties and of Biological Processes. *Environ. Sci. Technol.* **2016**, *50* (18), 10264–10272.

https://doi.org/10.1021/acs.est.6b04325.

(17) Brox, S.; Seiwert, B.; Haase, N.; Küster, E.; Reemtsma, T. Metabolism of Clofibric Acid in Zebrafish Embryos (Danio Rerio) as Determined by Liquid Chromatography-High Resolution-Mass Spectrometry. *Comp. Biochem. Physiol. Part - C Toxicol. Pharmacol.* **2016**, *185–186*, 20–28. https://doi.org/10.1016/j.cbpc.2016.02.007.

(18) Fetter, E.; Smetanová, S.; Baldauf, L.; Lidzba, A.; Altenburger, R.; Schüttler, A.; Scholz, S. Identification and Characterization of Androgen-Responsive Genes in Zebrafish Embryos. *Environ. Sci. Technol.* **2015**, *49* (19), 11789–11798. https://doi.org/10.1021/acs.est.5b01034.

(19) OECD Guidelines for the Testing of Chemicals - Fish Embryo Acute Toxicity (FET) Test. *OECD 236* **2013**.

(20) ISO. Water Quality - Determination of the Acute Lethal Toxicity of Substances to a Freshwater Fish. *ISO 7346-1* **1996**.

(21) Stärk, H.-J.; Wennrich, R. A New Approach for Calibration of Laser Ablation Inductively Coupled Plasma Mass Spectrometry Using Thin Layers of Spiked Agarose Gels as References. *Anal Bioanal Chem* **2011**, *399*, 2211–2217. https://doi.org/10.1007/s00216-010-4413-1.

(22) Halbach, K.; Ulrich, N.; Goss, K.-U.; Seiwert, B.; Wagner, S.; Scholz, S.; Luckenbach, T.; Bauer, C.; Schweiger, N.; Reemtsma, T. Yolk Sac of Zebrafish Embryos as Backpack for Chemicals? *Environ. Sci. Technol.* **2020**, *54* (16), 10159–10169. https://doi.org/10.1021/acs.est.0c02068.

(23) Mohammed, A. M.; Karttunen, V.; Huuskonen, P.; Huovinen, M.; Auriola, S.; Vähäkangas, K. Transplacental Transfer and Metabolism of Diuron in Human Placenta. *Toxicol. Lett.* **2018**, *295*, 307–313. https://doi.org/10.1016/j.toxlet.2018.07.012.

(24) Fraher, D.; Sanigorski, A.; Mellett, N. A.; Meikle, P. J.; Sinclair, A. J.; Gibert, Y. Zebrafish Embryonic Lipidomic Analysis Reveals That the Yolk Cell Is Metabolically Active in Processing Lipid. *Cell Rep.* **2016**, *14* (6), 1317–1329. https://doi.org/10.1016/j.celrep.2016.01.016.

(25) Loerracher, A. K.; Grethlein, M.; Braunbeck, T. In Vivo Fluorescence-Based Characterization of Cytochrome P450 Activity during Embryonic Development of Zebrafish

(Danio Rerio). *Ecotoxicol. Environ. Saf.* **2020**, *192* (November 2019), 110330. https://doi.org/10.1016/j.ecoenv.2020.110330.

(26) Kudoh, T.; Tsang, M.; Hukriede, N. A.; Chen, X.; Dedekian, M.; Clarke, C. J.; Kiang, A.; Schultz, S.; Epstein, J. A.; Toyama, R.; et al. A Gene Expression Screen in Zebrafish Embryogenesis. *ZFIN Direct Data Submiss.* **2001**, http://zfin.org.

(27) Schüttler, A.; Altenburger, R.; Ammar, M.; Bader-Blukott, M.; Jakobs, G.; Knapp, J.; Krüger, J.; Reiche, K.; Wu, G. M.; Busch, W. Map and Model-Moving from Observation to Prediction in Toxicogenomics. *Gigascience* **2019**, *8* (6), 1–22. https://doi.org/10.1093/gigascience/giz057.

(28) Otte, J. C.; Schmidt, A. D.; Hollert, H.; Braunbeck, T. Spatio-Temporal Development of CYP1 Activity in Early Life-Stages of Zebrafish (Danio Rerio). *Aquat. Toxicol.* **2010**, *100* (1), 38–50. https://doi.org/10.1016/j.aquatox.2010.07.006.

(29) Quinlivan, V. H.; Farber, S. A. Lipid Uptake, Metabolism, and Transport in the Larval Zebrafish. *Front. Endocrinol. (Lausanne).* **2017**, *8* (NOV), 1–11. https://doi.org/10.3389/fendo.2017.00319.

Curriculum vitae Katharina Halbach

Born December 14, 1990 in Remscheid, Germany

Education and professional experience

Since Sept. 2016	**PhD Student at the Department of Analytical Chemistry, Helmholtz-Centre for Environmental Research – UFZ, Leipzig, Germany** Thesis: "Fate of xenobiotics inside the zebrafish embryo – mass spectrometry imaging for toxicokinetic studies"
Nov. 2019 – Nov. 2020	**Scientist in the project "Kleingewässermonitoring" at the department of Analytical Chemistry, Helmholtz-Centre for Environmental Research – UFZ, Leipzig, Germany**
Aug. 2014 – June 2016	**Master of Science in Environmental Chemistry, NTNU Trondheim, Norway** Master's thesis: "Study of mercury and selected trace elements in soil in the Norwegian Arctic, Svalbard" Final degree: A
Jan. – May 2015	Exchange semester at the University Centre in Svalbard, Norway
Oct. 2013 – July 2014	**Studies in Biology, RWTH Aachen University** Successful completion of several courses in fundamental biology and the specialization "Environmental Sciences"
Oct. 2010 – Sept. 2013	**Bachelor of Science in Chemistry, RWTH Aachen University** Bachelor thesis: "Synthesis of multifunctional ligands for gold nanoparticles" (Ø 1.3) Final degree: 2.0
Aug. 2001 – June 2010	**Abitur** Ernst-Moritz-Arndt-Gymnasium, Remscheid Final degree: 1.9

Scientific contributions

Publications

Halbach, K., Holbrook, T., Reemtsma, T., Wagner, S. (2021) Effective processing and evaluation of chemical imaging data with respect to morphological features of the zebrafish embryo. Anal. Bioanal. Chem. 413 (6), 1675–1687.

Halbach, K., Ulrich, N., Goss, K.-U., Seiwert, B., Wagner, S., Scholz, S., Luckenbach, T., Bauer, C., Schweiger, N., Reemtsma, T. (2020) Yolk sac of zebrafish embryos as backpack for chemicals? Environ. Sci. Technol. 54 (16), 10159 – 10169.

Halbach, K., Wagner, S., Scholz, S., Luckenbach, T., Reemtsma, T., (2019) Elemental imaging (LA-ICP-MS) of zebrafish embryos to study the toxicokinetics of the acetylcholinesterase inhibitor naled. Anal. Bioanal. Chem. 411 (3), 617 – 627.

Publications in preparation

Halbach, K., Aulhorn, S., Lechtenfeld, O., Lecluse, M., Leippe, S., Seiwert, B., Wagner, S., Reemtsma, T., König, J., Luckenbach, T. (2021) Spatial distribution of bromoxynil in zebrafish embryos and the role of the organic anion transporting polypeptide Oatp1d1. *in preparation.*

Muniz, M. S.; Halbach, K.; Araruna, I. C. A.; Martins, R. X.; Seiwert, B.; Lechtenfeld, O.; Reemtsma, T.; Farias, D. F. (2020) Moxidectin toxicity to zebrafish embryos: bioaccumulation and biomarker responses. *submitted.*

Oral presentations

Halbach, K., Ulrich, N. Goss, K.-U., Seiwert, B., Wagner, S., Scholz, S., Luckenbach, T., Bauer, C., Schweiger, N., Reemtsma, T. The yolk sac as backpack for chemicals? - Distribution of chemicals between the yolk and the embryonic body in the zebrafish embryo, SETAC SciCon, Dublin (online conference), May 03-07, 2020, Ireland

Halbach, K. Mass spectrometry imaging in the zebrafish embryo for mechanistic studies in (eco)toxicology, Institute Seminar of the Institute for Medical Physics and Biophysics, University Leipzig, Nov 08, 2019, Leipzig, Germany.

Halbach, K., Wagner, S., Luckenbach, T., Scholz, S., Seiwert, B., Reemtsma, T. An analytical platform to study uptake, spatial distribution, and metabolism of organic compounds in zebrafish embryos, ANAKON, March 25-28, 2019 in Münster, Germany.

Halbach, K. Complementary analytical techniques to study toxicokinetics of chemicals in the zebrafish embryo, BioGeo Colloquium of the Institute of Geosciences, Institute of Microbiology, Institute of Biodiversity ,University Jena, Feb 05, 2019, Jena, Germany.

Halbach, K., Scholz, S., Luckenbach, T., Reemtsma, T., Wagner, S. Uptake and Transformation of the AChE Inhibitor Naled in the Zebrafish Embryo Investigated with LA-ICPMS, BI(MS)2 2018 – First Workshop on Laser Bioimaging Mass Spectrometry 2018, May 24-25, 2018 in Münster/Germany.

Halbach, K., Wagner, S., Luckenbach, T., Scholz, S., Lechtenfeld, O., Reemtsma, T. Mass Spectrometry Imaging of Chemicals in Zebrafish Embryos, JungchemikerForum Frühjahrssyposium, March 21-24, 2018, Konstanz, Germany.

Poster presentations

Halbach, K., Wagner, S., Luckenbach, T., Scholz, S., Seiwert, B., Reemtsma, T. Toxicokinetic investigations on µm-scale in the zebrafish embryo, HIGRADE conference, Helmholtz Centre for Environmental Research, May 08, 2019, Leipzig, Germany.

Halbach, K., Wagner, S., Luckenbach, T., Scholz, S., Seiwert, B., Reemtsma, T. An analytical platform to study uptake, spatial distribution, and metabolism of organic compounds in zebrafish embryos, JungchemikerForum Frühjahrssyposium, March 20-23, 2019, Bremen, Germany.

Halbach, K., Wagner, S., Luckenbach, T., Scholz, S., Seiwert, B., Lecluse, M., Morlet, N., Reemtsma, T. Dynamics of the spatial distribution of 4-iodophenol in the zebrafish embryo investigated with LA-ICP-MS, Fish and amphibian embryos as alternative models in toxicology and teratology, December 29-30, 2018, Aulnay-sous-Bois/Paris, France.

Halbach, K., Wagner, S., Luckenbach, T., Scholz, S., Reemtsma, T. Uptake and transformation of the AChE inhibitor naled in the zebrafish embryo investigated with LA-ICP-MS, OurCon, September 25-28, 2017, Doorn, Netherlands

PHD DISSERTATION 8 | 2021

ISSN 1860-0387

Helmholtz Centre for
Environmental Research – UFZ
Permoserstraße 15
04318 Leipzig I Germany
www.ufz.de

Katharina Halbach | Fate of xenobiotics inside the zebrafish embryo – mass spectrometry ...